Design and Implementation of Nonlinear Time Series Analysis Techniques for Biophysical Signals and Systems

THESIS SUBMITTED FOR THE DEGREE OF

DOCTOR OF PHILOSOPHY (ENGINEERING)

JADAVPUR UNIVERSITY

2023

Submitted by:

Debanjan Parbat

Registration No.: D7/ISLM/70/16

School of Bioscience & Engineering

Jadavpur University

Kolkata: 700032

Thesis Details

1. **Title of the Thesis:** Design and Implementation of Nonlinear Time Series Analysis Techniques for Biophysical Signals and Systems
2. **Index No.** and **Date of registration:** D7/ISLM/70/16 registered on 12th September,2016
3. **Name, Designation and Institution of the Supervisor:**
   Prof. (Dr.) Monisha Chakraborty

   Professor

   School of Bioscience & Engineering
   Jadavpur University
   Kolkata: 32, India

4. **Email ID of the Supervisor**: monisha.chakraborty@jadavpuruniversity.in
5. **List of publications**

(a) *Publications related to Thesis Work*

[1] **D. Parbat** and M. Chakraborty, 'A novel methodology to study the cognitive load induced EEG complexity changes: Chaos, fractal and entropy based approach', *Biomedical Signal Processing and Control*, vol. 64, p. 102277, 2021.

[2] **D. Parbat** and M. Chakraborty, 'Multiscale entropy analysis of single lead ECG and ECG derived respiration for AI based prediction of sleep apnea events', *Biomedical Signal Processing and Control*, vol. 87, p. 105444, 2024.

[3] **D. Parbat** and M. Chakraborty, 'A python based support vector regression model for prediction of COVID19 cases in India', Chaos, Solitons & Fractals, vol. 138, p. 109942, 2020.

[4] **D. Parbat** and M. Chakraborty, 'A novel methodology to measure the Corticomuscular coherence using multifractal correlation and information theory approach during weight lifting exercise', Submitted to Computer Methods and Programs in Biomedicine, Elsevier.

(b) *List of National/International Conference/Workshops*

[5] **D. Parbat** and M. Chakraborty, 'Multi-Scale Entropy Analysis of surface Electromyography signals during biceps muscle contraction under varying loads'. Computational Science Symposium, IISc, Bangalore,2017. (Poster Presentation)

(c) Other publications during the period of Doctoral Research

[1] M. Chakraborty and **D. Parbat**, 'Fractals, chaos and entropy analysis to obtain parametric features of surface electromyography signals during dynamic contraction of biceps muscles under varying load', in *2017 2nd International Conference for Convergence in Technology (I2CT)*, 2017, pp. 222–229.

[2] A. Biswas, **D. Parbat**, and M. Chakraborty, 'Establishment of EMG-Force relationship obtained during Simultaneous Voluntary Contraction of Biceps and Flexor Digitorum Profundus Muscles', in *2019 IEEE 5th International Conference for Convergence in Technology (I2CT)*, 2019, pp. 1–6.

[3] G. Bala, **D. Parbat**, and M. Chakraborty, 'HRV Parameters as a Bio-marker of Preterm Infant and Normal Sinus Rhythm ECG', *International Journal of Computer Engineering and Applications*, vol. 12, no. IV, pp. 364–371, 2018.

[4] **D. Parbat**, U. Bhattacharjee, S. Paria, N. Das, and M. Chakraborty, 'Fractal Dimension and lacunarity based microscopic image texture characterization of coated and non-coated metallic substrates', *Advances in Materials and Processing Technologies*, vol. 8, no. 2, pp. 2244–2258, 2022.

[5] S. Parui, **D. Parbat**, and M. Chakraborty, 'A Deep Learning Paradigm for Computer Aided Diagnosis of Emphysema from Lung HRCT Images', in *International Conference on Computing in Engineering & Technology*, 2022, pp. 198–207.

STATEMENT OF ORIGINALITY

I…**DEBANJAN PARBAT**……registered on …**12th September, 2016....**do hereby declare that this thesis entitled **"… Design and Implementation of Nonlinear Time Series Analysis Techniques for Biophysical Signals and Systems …."** contains literature survey and original research work done by the undersigned candidate as part of Doctoral studies. All information in this thesis have been obtained and presented in accordance with existing academic rules and ethical conduct. I declare that, as required by these rules and conduct, I have fully cited and referred all materials and results that are not original to this work. I also declare that I have checked this thesis as per the "Policy on Anti Plagiarism, Jadavpur University, 2019", and the level of similarity as checked by Turnitin software is _____%.

Signature of Candidate:

Date:

Certified by Supervisor:

(Signature & Seal)

CERTIFICATE FROM THE SUPERVISOR

This is to certify that the thesis entitled " ***Design and Implementation of Nonlinear Time Series Analysis Techniques for Biophysical Signals and Systems*** " submitted by Shri ***Debanjan Parbat***, who got his/her name registered on ***12th September, 2016 with registration number D-7/ISLM/70/16 of 2016-2017*** for the award of ***Ph. D. (Engineering)*** degree of Jadavpur University is absolutely based upon his/her own work under the supervision of ***Prof. (Dr.) Monisha Chakraborty*** and that neither his/her thesis nor any part of the thesis has been submitted for any degree/diploma or any other academic award anywhere before.

_____

(Signature of the Supervisor and date with Office Seal)

Prof. (Dr.) Monisha Chakraborty

Professor

School of Bioscience & Engineering

Jadavpur University

Kolkata:32

DECLARATION

I do hereby declare that the thesis entitled "Design and Implementation of Nonlinear Time Series Analysis Techniques for Biophysical Signals & Systems" submitted by me for the fulfillment of continuous assessment of Ph. D. degree course in Engineering, from Jadavpur University, Kolkata, India under the supervision of Prof. (Dr.) Monisha Chakraborty, Professor, School of Bioscience & Engineering, Jadavpur University, Kolkata, India. Neither this nor any part of it has been submitted for either any degree/diploma or any other academic award anywhere before.

_____

Debanjan Parbat

Reg. No. D-7/FISLM/70/16

School of Bioscience & Engineering

Jadavpur University

Kolkata, India

Acknowledgements

I would like to express my deepest gratitude and I am indebted to my sole supervisor, Prof. (Dr.) Monisha Chakraborty, Professor, School of Bioscience & Engineering, Jadavpur University for her invaluable mentorship, unwavering encouragement, and insightful feedback that shaped this thesis.

I am grateful to the participants for their willing involvement as subjects in my experiments conducted in Biomedical Instrumentation Laboratory, School of Bioscience & Engineering, Jadavpur University under the expert supervision of Prof. (Dr.) Monisha Chakraborty and her active participation during the entire tenure of my PhD research work motivated me to carry out so many experiments.

My heartfelt thanks extend to my family and friends for their unending support and understanding during this challenging endeavor.

I would like to acknowledge my alma mater Jadavpur University for all kind of support and affiliation and would like to thank the State Government Research Fellowship Scheme provided by Department of Higher Education, Government of West Bengal, India under which I worked as a Senior Research Fellow.

Debanjan Parbat

Dedicated to my mother

"Maa"

Abstract

In the ever-evolving landscape of healthcare, the convergence of biomedical engineering and technological innovation stands as a beacon of progress. This thesis is a testament to the fusion of engineering principles with the intricacies of medical science, particularly in the realm of biomedical signal analysis. The human body, an amalgamation of interconnected systems, embodies a symphony of functions orchestrated by the cardiovascular, Musculo-skeletal, and nervous systems. Our exploration delves deep into the significance of understanding these systems through the lens of biomedical signals—key conduits revealing the body's nuanced physiological processes and early indicators of potential ailments.

Advancements catalyzed by the 4th Industrial Revolution have heralded a new era in healthcare. Technologies like AI, IoT, wearable devices, telemedicine, and 3D printing are reshaping the landscape, rendering healthcare more personalized and accessible. Amidst the burgeoning global population and the surge in communicable and non-communicable diseases, these innovations stand as stalwarts in addressing the challenges faced by the healthcare domain.

Within this context, signal processing emerges as a linchpin in interpreting biomedical signals—ECG, EEG, and EMG—signals that, despite their pivotal insights, present challenges due to their complex and non-stationary nature.

This thesis sets out with a clear objective: to traverse the domains of biomedical signals, shedding light on their quintessence in healthcare science and technology. We aim to bridge the gap between established methodologies, rooted in electrical engineering and statistical analyses, and a deeper comprehension of the underlying scientific principles governing these signals. Our journey unfolds through the exploration of nonlinear dynamics—Chaos, Fractals, and Entropy—as potent tools for modeling the intricacies within cardiovascular, nervous, and musculoskeletal systems. The complexities inherent in these signals demand methodologies beyond conventional linear approaches, prompting our foray into nonlinear time series analysis.

Methodologically, this thesis charts a course encompassing signal acquisition, meticulous denoising, and the deployment of Nonlinear Discrete Dynamical Systems to dissect the essence of ECG, EEG, and EMG signals—treating them as dynamic, nonstationary time series of discrete samples. Throughout our odyssey, Chaos analysis, leveraging the Largest Lyapunov Exponent, endeavors to measure the divergence rate of phase space trajectories. Concurrently, Fractal Dimension estimation discerns signal complexity through scaling behavior, while Entropy becomes our compass in navigating information transfer and unpredictability within these signals. The culmination of these analyses yields parameters serving as veritable descriptors of dynamic system states. These descriptors, meticulously extracted, are then harnessed to fuel machine learning models—Artificial Neural Networks, Support Vector Machines, Random Forests, and Decision Trees—for classification, regression, and predictive analytics.

Our voyage extends into experimental terrains, encompassing cardiovascular, neurological, muscular, and neuromuscular systems. Rigorous experiments involving EMG and EEG signal analyses unfold, capturing the essence of Motor Unit Action Potentials and neural dynamics associated with cognitive actions.

Ethical tenets stand as our guiding light in human subject experiments, ensuring the sanctity and integrity of our scientific pursuits. Notably, our contributions manifest in the formulation of an algorithm—a beacon of innovation—dedicated to the detection of sleep apnea from single-channel ECG signals. This algorithm intricately leverages Multiscale Entropy analysis during apnea events, a testament to our commitment to actionable applications rooted in robust scientific principles.

In summation, this thesis embarks on an expedition into the frontiers of Chaos, Fractal Dimension, and Entropy, aiming to decode the enigmatic language of physiological signals. Our endeavors are poised to amplify the understanding of system dynamics, laying the groundwork for these analyses to serve as indispensable features in diverse healthcare applications.

- Debanjan Parbat

Contents

List of Figures

List of Tables

Chapter 2

Chapter 3

Chapter 4

Chapter 1 Introduction

A brief overview of the relevant background information along with a statement of the research question and the objectives of the research. A brief overview of the research paper, including the methodology, findings, and conclusions is presented in this chapter.

1.1 Background

A human body is made up of many systems which are accompanied by various subsystems that work together in carrying out various physiological processes. The major systems of our human body can be classified as the Cardiovascular system, Musculo-skeletal system and Nervous system. These systems carry out specific functions of the human body under normal healthy conditions. Recent scientific and technological developments allow us to better understand the underlying processes that govern the functionalities of the human body system. These tools and techniques help us in disease diagnosis and treatment for making human lives better and increasing the overall life expectancy.

One of the areas where engineering principles are applied in providing effective healthcare in tandem with medical science is known as Biomedical Engineering. In Biomedical Engineering, we explore various tools and techniques that can be applied to make patient care and monitoring an efficient and cost-effective solution driven approach. The technological advancement in the 21st century is mainly driven by the silicon industry and experts call it The Industrial Revolution 4.0. The industrial revolution 4.0 is driving change in the global healthcare technology scenario making healthcare accessible to all in a very cost effective and customised approach. The applications of engineering and technology principles to address the various physiological processes is growing day by day and it is expected to further increase from 2021 due to the effects of Covid19 pandemic that ravaged the healthcare systems around the world. In a recent analysis report published by Deloitte, have thrown some light on global healthcare outlook post pandemic. The report mentions that during the tenure 2020 to 2024 the compound annual growth rate in global health spending is expected to be around 3.9 % which is a substantial rise from 2.8 % for the year 2015 to 2019. The report further elucidates that the Global health care spending with respect to GDP is projected to be around 10.3% during 2021 to 2022. The global population growth and ageing are important factors in assessing the impact of healthcare services and since the global population is estimated

to be around 8 billion by the year 2023. Most of the ageing and diminishing of population will be observed in Europe, Japan and Venezuela, whereas Asia and Africa will notice a substantial rise in population. The above facts suggest that the world is going to face severe healthcare related challenges amidst the rising population and increasing cases of communicable as well as non-communicable diseases. To address these challenges, technology has an important role to play in assisting medical professionals carrying out their work smoothly and efficiently. Modern healthcare is not limited to only treatment and cure but also in well-being and early diagnosis with a consumer centric approach. The consumers of modern healthcare look for solutions providing healthy lifestyle, vitality, well-being, early disease diagnosis and prevention along with care and treatment. Some technological innovations that are going to guide the future healthcare market are as follows:

> *Artificial Intelligence* and *Predictive analytics*, *Internet of Things* (IoT) and *Wearable technology*, *Telemedicine*, *3D Printing*, *Mobile Health*, *Nanotechnology*, *Cloud Computing*.

One of the promising areas of Biomedical Engineering that can contribute in early disease diagnosis, condition monitoring of vital organs, prevention using predictive analytics and cure, is the Biomedical Signals. Biomedical Signals and Systems is the subject that addresses the principles of generation, acquisition, processing and interpretation of physiological signals that emanate from the cellular interactions and excitations unique to a particular human body system. Most of the physiological processes going inside a human body emanate as signals that carry the information of the underlying system dynamics. The transient change in potential across the cell membrane of nerve and muscle cells due to the repolarization and depolarization of the cell membrane from its resting state potential, emanates on the surface of the body and can be collected as biophysical signals namely Electrocardiogram (ECG), Electroencephalogram (EEG) and Electromyogram (EMG). The ECG, EEG and EMG is generated due to the mechanical contraction of the muscle cells and neurons due to the propagation of the action potential. ECG, EMG and EEG are bioelectric in nature but the electrical potential generation scheme actually originated due to physical disturbance of the cell membrane in response to a stimulus. This is the reason we sometimes refer to the biomedical signals like EEG, ECG and EMG as Biophysical Signals representing Nervous, Cardiovascular and Musculo-skeletal systems of the human body.

The physiological information carried by these signals are of immense importance for early disease diagnosis and treatment. It is to note that diseases or any abnormalities in a human body system leads to alterations in normal physiological processes causing pathological processes to start which affects our well-being and health. The signals generated during the pathological process are relatively different from the normal signals with no pathology. The observation of the signal gives us a fundamental idea about the state of the system and any abnormalities associated with it. Biomedical Signals & Systems provide us with adequate knowledge about a particular system of interest and guides us in proper assessment of the ongoing state of the system either normal or pathological. Now, let us discuss a basic biomedical signal processing scheme that is followed throughout in analysis and interpretation of bio-signals collected from specific locations over the human body in a non-invasive manner. The various stages involved in biomedical signals analysis is shown as follows:

1. **Signal Acquisition**
    - *Sensors / Electrodes*
    - *Preamplification*
    - *Filters*
    - *Analog to Digital Conversion*
2. **Signal Processing**
    - *Artefact removal and denoising*
    - *Event Detection*
3. **Signal Analysis**
    - *Feature Extraction*
    - *Analysis of waveshape and waveform complexity'*
    - *Frequency Domain Characterization*
    - *Time-Frequency Domain characterization using Wavelet Transforms*
    - Non-linear Discrete Dynamical system modelling and analysis: *Fractals, Chaos and Entropy.*
4. **Classification, Pattern Recognition and Decision Making**
    - *Artificial Intelligence and Machine Learning*

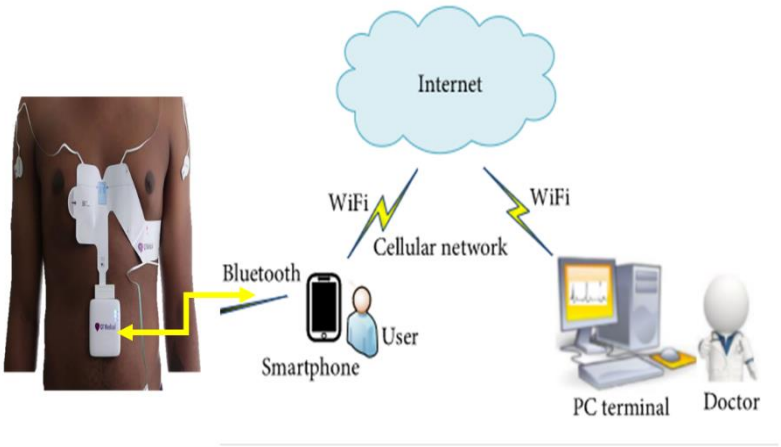

Figure 1. Schematic representation of a wireless ECG acquisition scheme

The steps of the entire signal processing scheme start with signal acquisition through signal processing and analysis ends with proper interpretation of the causative factors arising due to pathological abnormalities. With the advent of technology, the era of computer aided diagnosis has just begun and has a long way to go. Artificial Intelligence and Machine Learning are driving the future algorithms that are responsible for decision making and analysis of the physiological condition of the patient. In a typical automated diagnosis scheme, the signal is first acquired through electrodes placed at strategic positions and transmitted wirelessly over Bluetooth or Wi-fi to a nearby receiver, usually a smartphone or PC which is connected with the cloud. The backend server in the cloud collects the signals and further processing is done to carry out information retrieval from the signal about the state of the system under scrutiny. The results of the analysis are then sent to the receiver, patient party or medical professional for further treatment planning and cure. The schematic representation of the aforementioned technical scheme for a wireless ECG system is shown in fig.1. All the above application suggests that there is a need for design and development of robust Signal Detection, Processing and Analysis strategies so as to implement in computer aided diagnosis measures adopted by the industry inc. in compliance with Medical Device Regulations ISO 13485 and Quality Management Systems.

The signal acquisition is one of the significant steps in the overall Biomedical Signal Processing and Analysis domain. The signal acquisition involves Biomedical Instrumentation systems specifically designed to meet different signal generation schemes. A generalised version of a Biomedical Instrumentation components that are mainly responsible for accurate acquisition and measurement of bio-signals is shown in fig.2. Electrodes are attached at strategic positions to measure the biopotential at the skin surface, which is amplified using a biopotential amplifier with differential amplification technique. A signal conditioning circuit arrangement is made consisting of filters and converters that sends the filtered output to recorders, display units, alarm systems and storage systems. A basic control system is employed for smooth and robust functioning of the different stages of the signal acquisition system.

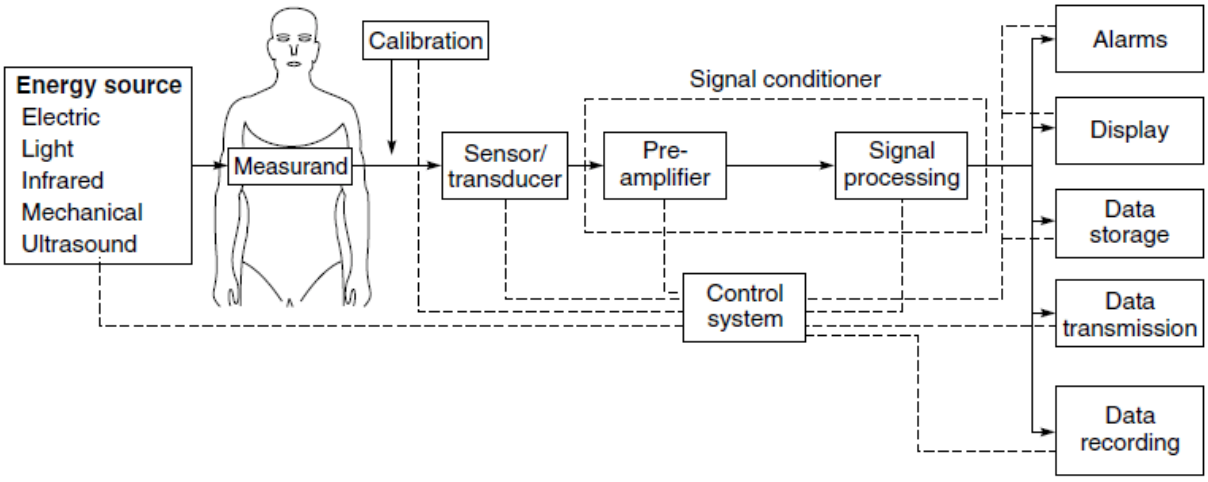

Figure 2. A generalised Biomedical Instrumentation System

ECG, EEG and EMG reveal the underlying system dynamics of the Heart, Brain and Muscles respectively. These three signals are generated due to the excitability of the cells under a specific stimulus that are collected non-invasively over the surface of the skin and scalp respectively. The signals are non-stationary with a high degree of nonlinearity making it rather impossible to analyse using basic signal processing schemes. The signals have very low amplitude and are fully embedded with noise making it a challenging task to denoise and remove the artefacts. A substantial amount of information loss is expected if we simply go for Fourier transform based

filtering techniques over the signal for noise removal. So specialised tools and techniques are needed for filtering and denoising of bioelectric signals like ECG, EEG and EMG. To address this issue, we went for the design and development of Non-Linear Time Series Analysis techniques best suited for analysing bioelectric signals like ECG, EEG and EMG. The Signal is assumed to be a discrete function of time or a Time Series with amplitudes in millivolt range for developing analysis techniques. The overall methodologies from signal acquisition to denoising to analysis and interpretation is presented in the form of various experimental studies conducted during the full tenure of the research.

1.2 Objective

Biomedical Signals was one of the first natural indicators of the normal physiological processes of the human body that attracted the medical professionals. Our human body is full of different sorts of bio signals, and an understanding of bio signals is not possible without a proper idea about the cause-and-effect relationship involving various physiological processes. An understanding of the biophysical signals and systems is very important from the point of view of our present-day healthcare science and technology.

It is often believed that there is no scope for further development in this branch of engineering but this is far from the actual scenario. It is true that many researchers are working in this domain since long and substantial knowledge has been developed regarding biomedical signal processing and analysis. Mainly electrical engineering and statistical analysis principles have been employed to find out the signal processing and analysis methodologies for Bio signals, but most often without a deeper understanding of the science hidden behind the rules. Most engineering and scientific applications of the biomedical signals and systems often do not require such an extreme effort as suggested in our work. We have presented some deeper aspects of the modelling of biophysical signals and systems with a lot of practical significance as well. The idea of Nonlinear Dynamics in modelling the functionalities of cardiovascular, nervous and musculoskeletal systems is explored to provide better insight into the underlying system dynamics related to various physiological processes. Development of algorithms based on nonlinear dynamics techniques is of significant importance in the field of computer aided diagnosis and post processing of signals. We are very much familiar with the importance of ECG, EEG and EMG in the field of medical

diagnostics and treatment, but most of the recent analysis techniques in application do not take into account the high degree of nonlinearity and non-stationarity of these biosignals. Moreover, there is utter scarcity of accurate and robust methodologies that can monitor and help in visualisation of the underlying changes of the system dynamics in case of long-term monitoring of physiological signals. To address the above challenges, we have proposed some methodologies based on Nonlinear discrete dynamical systems analysis like Chaos, Fractals and Entropy measures on ECG, EEG and EMG.

The machine learning and deep learning applications for automated computer aided diagnosis based on biomedical signals as indicators of the physical state of the system is a widely explored field. Development of accurate and robust models that can be deployed in real life scenarios is a difficult task to achieve considering the high volume of data associated with biophysical signals. To address these issues proper feature extraction techniques and dimensionality reduction techniques are needed for faster, efficient and robust Artificial Intelligence (AI) modules. AI based predictive analytics and classification in case of biomedical signals can only be achieved if the data preprocessing and feature extraction steps are improved to handle nonlinearity, multiresolution and nonstationary nature of biomedical signals and their signal generation scheme. Therefore, to make AI models accurate one can employ our proposed methodologies for feature extraction and dimensionality reduction. We have proposed our methods with an objective of providing better features for faster and accurate training of the AI models for deployment in real life conditions.

1.3 Brief Outline

A summarised overview of the contents of this thesis is presented in a lucid manner in the preceding section. As discussed in the prevailing sections, there is utter need in developing signal processing and analysis models to assess the underlying system dynamics associated with different physiological processes. There are many algorithms or methods present that deal with Biomedical Signal Processing and Analysis and hence a proper goal, objective and characteristics of the signal can only lead to optimum solutions.

In our work, we have performed extensive literature surveys and conducted background research on Biomedical Signals and Systems. We have chosen ECG, EEG and EMG as our signal of interest to understand the underlying system dynamics of Heart, Brain and Body. We have discussed the related works that have been done in application of nonlinear dynamics tools and techniques in modelling of the biomedical signals and systems. Fractals, Chaos and Entropy are the primary estimators for measuring the complexity of the bioelectric signals during dynamic tasks. The signal processing using Wavelet Transforms is also employed for artefact removal and denoising to address the non-stationarity and multiresolution characteristics of the bioelectric signals viz. ECG, EEG and EMG.[1]

After signal acquisition and denoising using Wavelet Transform, we have employed Nonlinear Discrete dynamical systems modelling using Chaos, Fractal Dimension and Entropy as proponents or bio markers of complexity variations in signal.[2]

As discussed above ECG, EEG and EMG measures the potential at a specific location on the body can be represented as x that changes over time t or **x(t)** which is a continuous time signal of variation of the potential with time. In digital measurements we represent **x(t)** as **x(nT)** or **x(n)** discrete points of amplitude over time, where n is index or measurements of the sample value and T represents the uniform interval in between the time instances of the measurement. In our work we have considered all these discrete time signals of ECG, EEG and EMG as nonstationary time series of samples at uniform time instances based on the sampling rate of the acquired signals.

The time series generated from a dynamical nonlinear system (Heart, Brain & Arm Muscle) can be tested for Chaos by the estimation of Largest Lyapunov Exponent. The exponential rate of divergence of the initial phase space trajectories depicting the evolution of the state of the system with time is quantified by Largest Lyapunov Exponent. Measurement of deterministic chaos gives us an insight into the predictability of the system having chaos and its initial sensitivity towards any kind of perturbations.

Estimation of fractal dimension from time series helps us measure the complexity of the signal in time and space based on the scale invariant patterns of bio signals. The scaling behaviour of the signal patterns helps in direct estimation of the fractal dimension that explains the system behaviour beyond the Euclidean dimension. The complexity of the signal depends on the intermittent fluctuations that occur within the time series for the entire acquired session. Several

types of fractal analysis are done, including box counting, lacunarity measures and multi-fractal analysis. When a single exponent of Fractal Dimension is not enough to understand the dynamics of the system then we can accommodate the system dynamics in the form of a spectrum of dimensional parameters exhibited by a multifractal system. A multifractal system is a generalised version of a fractal system and most biological systems in nature exhibit multifractal characteristics.[3]

Entropy, as it relates to dynamical systems, represents the rate of information transfer over different states of the system. The uncertainty or unpredictability of information content within a system can be measured using Entropy. It is basically a thermodynamic quantity describing the amount of disorder in the system but can be generalised to characterise the amount of information stored in more general probability distributions. When we apply Entropy methods for time series analysis, we take into account the concepts provided in Information theory about entropy measures as a predictor of information content. We can estimate the amount of past information required to have better predictions of the future based on Information theory concepts.

We have performed an experiment to study the cortico-muscular coherence (EEG-EMG) where we have employed two distinctive nonlinear dynamical cross correlation methods like Multifractal Detrended Cross-correlation Analysis (MFDXA) and Kraskov Mutual Information (MI). MFDXA is a multifractal systems analysis method and MI is an Information Theory concept based on information exchange using probability distributions between two time series under observation. The above experiment studies the mind and body inter-relationship while performing arm flexion and extension using different loads.

The above parameters are considered as descriptors of the dynamic state of the systems under observation. These parameters are used to describe the states of the systems and hence have immense potential to serve as features for supervised learning of Machine learning models. Artificial Intelligence and Machine learning models have been employed in our study for various uses like testing of significance, classification and predictive analytics using regression. Applications of deep learning models like Artificial Neural Network and 1D Convolution Neural Network for classification has also been employed and compared. The machine learning models employed in our study includes Support Vector Machines, Random Forest and Decision Tree for classification based on nonlinear dynamics features.

We have employed the previously mentioned tools and techniques in understanding the underlying dynamics of the Cardiovascular, Neurological, Muscular and Neuromuscular system of our body. We have performed some experiments on EMG and EEG signal acquisitions to test our methodologies. We have also analysed our models using ECG signals from Physionet online database for classification using deep learning techniques. In addition to this, during the Covid19 situation when we were all facing tough times due to the ongoing global pandemic, we were compelled to stay at home. During this time we took on the opportunity to work on preparing a time series prediction model for the total number of Covid19 cases in India including daily deaths and the estimated time for its decline. We employed artificial intelligence techniques to carry out regression methods using Support Vector Machines.

We have studied:

- EEG during cognitive loading of the brain (cognitive neurodynamics)
- ECG based classification of sleep apnea syndrome
- EMG during dynamic contraction of human arm under varying loads,
- EEG-EMG coherence (Cortico-muscular Coherence) while lifting varied loads with arm
- Prediction of Covid19 cases in India using Non Linear Time Series based prediction

The above experimental procedures have been discussed in the successive chapters with substantial explanation about the detailed methodology employed and obtained results with observations. EEG and EMG experiments were carried out on human subjects in our lab after taking their informed consent. We have followed the recommendations of the ethical committee guidelines for noninvasive experiments on human subjects.

References

[1] 'Biomedical Signal Analysis | IEEE eBooks | IEEE Xplore'. Accessed: Nov. 17, 2023. [Online]. Available: https://ieeexplore.ieee.org/book/7111421

[2] 'Nonlinear Biomedical Signal Processing, Fuzzy Logic, Neural Networks, and New Algorithms | IEEE eBooks | IEEE Xplore'. Accessed: Nov. 17, 2023. [Online]. Available: https://ieeexplore.ieee.org/book/5263178

[3] 'Time Frequency and Wavelets in Biomedical Signal Processing | IEEE eBooks | IEEE Xplore'. Accessed: Nov. 17, 2023. [Online]. Available: https://ieeexplore.ieee.org/book/5263548

Chapter 2 Literature Review

This section discusses the detailed review of scientific and technical literature collected from reputed scientific publications repositories like *IEEE Xplore©*, *Science Direct©*, *PubMed©*, *arXiv©*, *Google Scholar©*. Only papers that were published in peer reviewed Journals and conferences indexed in *SCI, SCIE, Scopus* and *Web of Science* were considered for review. The literature review section is classified under five subsections viz. Biomedical Signals and Systems, Cardiovascular dynamics, Muscle dynamics, Cognitive Neuro-dynamics and Neuromuscular dynamics. We have tried to include as many articles as possible having direct relevance to our proposed work and namely those works which helped us in conceptualization, design and evaluation of our proposed models.

A comprehensive and highly specialized field of study that explores the complex dynamics of biological and biophysical systems through the lens of nonlinear time series analysis. In this field, researchers delve into the intricate behaviours and patterns exhibited by biological data, such as Electrocardiograms (ECG), Electroencephalograms (EEG), and other physiological signals, to gain a deeper understanding of these systems. The key focus of this research is to uncover hidden relationships, identify nonlinear dependencies, and unveil the underlying mechanisms that traditional linear analysis methods may overlook. By employing advanced mathematical and statistical tools, researchers aim to extract valuable information from these signals that can aid in diagnosis, treatment, and prediction in various biomedical and biophysical applications. Non-linear time series analysis encompasses a wide range of techniques, including chaos theory, fractal analysis, recurrence plots, and entropy measures, among others. These methods allow researchers to detect complex patterns, irregularities, and self-organizing behaviors within biophysical data, providing critical insights into the dynamic nature of biological systems. Ultimately, the field of non-linear time series analysis for biophysical signals and systems plays a pivotal role in advancing the knowledge of complex physiological processes and has applications in fields such as cardiology, neuroscience, and bioinformatics, where understanding the nonlinear dynamics of data is paramount for better-informed decision-making and the development of improved healthcare practices.

2.1. Biomedical Signals and Systems

It is a well-known fact that biosignals are time-space recordings of a biological event occurring inside the body like beating of heart, contraction of muscles or blinking of eyes. The conglomeration of electrical, chemical and mechanical activity induces changes occurring inside our body denoted as specific events and these changes often produce signals that can be analysed. The functional state of an organ can be monitored by collecting the specific biosignals emanating at the surface of the body and can be analysed to reveal underlying information. Each organ system together creates the human body system and each organ system exhibits different kinds of biosignals like ECG monitors the cardiac activity and EEG measures the brain activity. Likewise, muscle activity of contraction due to flexion and extension can be measured by EMG. In a poly-parametric patient condition monitoring instrument, simultaneous acquisition of various signals is facilitated for real time monitoring of patient conditions like ECG, Respiration, Blood Pressure and SpO2. Biosignals are classified based on different characteristics of the signal like waveform shape, statistical properties, spatial-temporal variations, origin of source and type. Biosignals can also be classified based on the basis of their physiological origin like bioelectric signals like ECG, EEG and EMG which emanate from nerve and muscle cells respectively. Other forms of origin lead to the formation of Biomagnetic signals, Biochemical signals, Biomechanical signals, Bioacoustics signal and Biooptics signal which together encompasses the field of Biomedical Signals and Systems. In a certain real-life condition, the summation of most of these signals are produced simultaneously like in the case of a man doing sprint across a paved street would generate biomechanical signals due to the external forces as applied on the leg, simultaneously bioelectric signals will be generated due to muscle contraction and the metabolic activity of the muscle tissue will produce biochemical signals.

Biosignals are mostly random or stochastic and non-stationary in nature whose statistical properties vary with time. There is a high degree of uncertainty in the parameters that describe the biosignals. Biosignals are contaminated with random noise and are subjected to impulsive changes in the parameters owing to certain interference. These properties make the signal analysis task very sensitive towards different methodical approaches other than normal or linear deterministic signal processing and analysis tools. It is a challenging task to extract meaningful information from the contaminated low amplitude bioelectric signals which are highly susceptible to surrounding noise

and artefacts. These challenges can be overcome with the design of sophisticated state of the art medical signal acquisition instruments and devices along with powerful signal processing and analysis algorithms with high computational efficiency and accuracy.

The various avenues for Biomedical signals and systems analysis are widespread starting from the earlier Frequency domain techniques to very recent Artificial Intelligence algorithms. Biosignals have been represented by various frequency domain techniques primarily based on Fourier series representation.

Biomedical signals are represented in Frequency domain via methods that were derived fundamentally from Fourier Transforms and Fourier series representation of continuous discrete signals. Estimation of Power Spectral Density (PSD) and subsequent parameters from it like band power, mean frequency, median frequency, Low Frequency to High Frequency ratio, etc. are obtained for feature extraction. The Discrete Fourier Transform (DFT) is calculated for discrete sequences using the Fast Fourier Transform (FFT) algorithm. The squared magnitude spectrum of DFT gives a power spectrum known as Periodogram. A more robust estimate of PSD can be obtained by Welch's method. Other non-parametric approaches for estimation of Spectral Density are Least Square Method and Bartlett's method.

Another estimate of PSD can be obtained from the time domain analysis function known as Autoregressive function (AR). When we generate PSD using AR modelling, we get a robust estimate of PSD of Biosignals which are contaminated by noise. The few algorithms that calculate PSD based on AR modelling are based on solutions of the Yule-Walker equation and the maximum entropy based on Burg's method. AR model is basically a set of Auto Correlation Function (ACF) computed over the complete time period of the discrete sequence.

In frequency domain representation, one of the most used systems for biomedical signals and systems have been the Filter systems, Analog and Digital Filters. Analog filters are realised using Resistances and Capacitors arranged in a specific way to discard the unwanted frequency components of the analog input signal before its sampled into discrete samples using ADC converters. Digital filters can be of two types Infinite Impulse Response (IIR) or Finite Impulse Response (FIR) based on their output sequence of the impulse response of the transfer function. Filters are used for noise elimination and artefact removal of contaminated biosignals. Some of the types of Analog filters are Butterworth, Chebyshev, Bessel, Gaussian, Linkwitz-Riley, and

Legendre. In case of Digital filters, the process or different forms of realisation of the filter function determines it type such as Direct Form I and II, Lattice and Ladder, ARMA, State space structures, Gold Rader, Chamberlin, Kingsbury, Modified State Space, Agarwal-Burns, Harris-Brooking, ND-TDL. Other than filtering, signal averaging is also a kind of denoising technique often employed in case of multiple observations of a given state of the system.

In frequency domain analysis, the time domain information is lost and hence other avenues of biomedical signal analysis come to existence like Short Time Fourier Transform (STFT) and Wavelet Transform (WT). STFT and WT help in 2D representation of the dynamic characteristics of nonstationary biomedical signals in the joint Time-Frequency domain. The spectral representation of the signal varying in time is called a spectrogram of the signal that can be obtained by STFT and WT analysis. In case of STFT the width of the window/segment is fixed throughout the signal length and sinusoidal approximation is done whereas WT analysis liberates us from these constraints. In a wavelet analysis the signal is decomposed into shifted and scaled versions of the original or "mother" wavelet. Therefore, we can say that Wavelets are the most suitable tool in biomedical signal analysis that have varying shapes and resolutions and exhibit different characteristics at different scales. Other methods based on Time Frequency representation of the dynamic characteristics of the Biomedical signals are Wigner-Ville distribution and Choi-William's methods. Wigner-Ville displays very good localization properties and Choi-Williams can reduce the effects of interference. Although the popularity of Wavelets has diminished the use Of Wigner-Ville and Choi-William's methods of joint Time Frequency distributions.

Other than this Biomedical Signal analysis can also be done using Artificial Intelligence and Machine Learning methods based on Artificial Neural Network (ANN) and 1D Convolutional Neural Networks (CNN). Machine learning algorithms for classification based on supervised learning like Naïve Bayes, Linear Discriminant Analysis (LDA), Support Vector Machines (SVM), Random Forest (RF), Decision Tree (DT) are quite popular and has been used extensively in Biomedical signal analysis.

Previous studies have been mostly done using the methods as described till now, but a wide number of researchers and scientists recommended using Nonlinear Discrete Dynamical Systems Theory (NDDST) for modelling and analysis of Biomedical Signals and Systems. In NDDST the phase space representation of the signal is generated and based on the phase space plot different

parameters are calculated. The phase space portrait and bifurcation diagrams have long been used in ECG signal analysis to characterise different states and microstates of the system over the elapsed time. Since Biomedical signals are inherently nonlinear and non-stationary in nature the NDDST based methods are found to be reliable and suitable. Biomedical systems exhibit complex self-regulating physiological phenomena with irregular fluctuations over the length of the signal.

The methods that are based on studying the fluctuations and self-similarity of the patterns of the signal at different scales are Chaos estimation, Fractal Dimension (FD) and Entropy estimates. The Lyapunov exponent is an effective measure of Chaos in a system, whereas Highuchi's, Katz or Hurst's methods are employed for Fractal Dimension calculation. Entropies can be calculated using Approximate entropy, Sample Entropy, Fuzzy Entropy, Permutation Entropy, etc. All the above methods consider single scale approximations, whereas the above methods can be extended for Multiscale and Multifractal operations that characterise the signal observations in multiple scales. The phenomenon of self-similarity where scale invariant patterns are observed for small scale to large scales advocates the use of FD for characterization of the biosignals. The detrended fluctuation analysis (DFA) and multifractal detrended fluctuation analysis (MFDFA) are employed in case of biomedical signal analysis for detrending and multiscale observations to find the statistical self-similarity. Mutual Information and Multifractal Detrended cross-correlation analysis are often employed to study inter relationship between any two, time synchronised biosignals.

Although NDDST tools and techniques are found to be theoretically more suitable for biomedical signals and systems, practical implementation of the above techniques has not been widely explored. There is a gap in the intellectual contribution towards enrichment of biomedical signals analysis using NDDST methodologies and this gives us the opportunity to foray into the world of nonlinear dynamics.

This section describes the previous studies of various authors based on biomedical signals and system.

Khanna et al., (2023) [1] offered a novel framework for healthcare disease diagnosis (loTDL-HDD) based on ECG data collected from connected devices. With the use of DL models, the suggested loTDL-HDD model can analyze biological ECG data for signs of CVDs. Artificial Flora Optimization (AFO) is used as a hyperparameter optimizer to boost the performance of the

BILSTM method. To further ensure that the ECG signals are classified correctly, a Fuzzy Deep Neural Network (FDNN) classifier is used. On biological ECG signals and evaluate the loTDL-HDD model and look at the results from many angles.

Selvarajan et al., (2022) [2] employed Hadoop-based technologies to develop a four-tier approach, which allows it to deal with physical infrastructure concerns. Data transfers in these levels are performed using reference health data acquired from a variety of treatment facilities, and the whole thing is tied together utilizing a low-robustness Fuzzy Interface System Algorithm (FISA). In a simulation of the suggested model carried out in MATLAB with the aid of a biomedical signal processing toolkit, FISA is shown to operate superior about of signal strength, distance, and cost.

Kora P. et al., (2020) [3] presented a technique based on Convolutional Neural Networks (CNNs) to recognize cardiac problems. CNN, unlike other types of neural networks, include several layers. The CNN architecture was created to make the most of the input's anatomical structure, whether it 1D (signal) or 2D (picture). Convolution and Pooling are the two primary CNN procedures. Using a wavelet transform, and were able to isolate the most useful characteristics of the data and categorize them. Arrhythmia (ARR), Congestive Heart Failure (CHF), and Normal Sinus Rhythm (NSR) signals were all categorized by the suggested system. The experimental concludes on ARR signals from the MIT-BIH arrhythmia, CHF signals from the BIDMC congestive heart failure, and NSR signals from the MIT-BIH normal sinus rhythm databases demonstrated that the suggested structure is an accurate detector, vastly outperforming several previously methods.

Balan O. et al., (2019) [4] evaluated a comparative analysis of various Machine Learning (ML) and DL techniques, both with and without the application of feature selection. The goal is to perform binary classification of the six fundamental emotions - anger, disgust, fear, joy, sadness, and surprise - into two distinct categorical classes: one representing the presence of an emotion and the other indicating the absence of an emotion. They utilize physiological recordings and subjective ratings of valence, arousal, and dominance from the DEAP (Dataset for Emotion Analysis using EEG, Physiological, and Video Signals) database for this analysis. The results of this study reveal that the highest classification accuracies achieved for each emotion are as follows: anger - 98.02%, joy - 100%, surprise - 96%, disgust - 95%, fear - 90.75%, and sadness - 90.08%.

Notably, for four of the emotions (anger, disgust, fear, and sadness), the classification accuracies were superior when feature selection was not applied.

Hirai Y. et al., (2019) [5] indicated a revolutionary Analog-Frontend (AFE) IC and error correction by ML in a high-precision biological sensor system. For even less power consumption, the suggested system calibrates the ADC error on a remote PC with the help of a ML technique. An AFE IC's design complexity could be reduced by employing these methods due to the system's adaptability. For handle a wide range of biopotential signals, an 18-bit resolution and a bandwidth of about 5 kHz (without a digital low-pass filter) are desirable. The design runs on a 1.2 V supply and is manufactured using a 130 nm CMOS technology. The built ADC, when calibrated utilizing the suggested methods, produces an SNDR of 88 dB at a sample frequency of 250 kHz. With a gain of 28.5 dB and input-referred noise of just 2.52μVrms, the high-resolution ADC really shines.

Celin S. et al., (2018) [6] suggested an approach for classifying ECG signals using a classification methodology. In order to get rid of the high-frequency noise, the input signal is filtered first using a low pass, high pass, or Butterworth filter. Butterworth filters are used to clean up distorted signals. Once the signal has been preprocessed, it could use a peak detection technique to locate its peaks, and then use statistical parameters to extract its characteristics. Finally, the collected features are categorized into normal or pathological ECG signals using a mixture of SVM, Adaboost, ANN, and Naive Bayes classifiers. An analysis of empirical data reveals that the SVM, Adaboost, ANN, and Naive Bayes classifiers each achieve accuracy of 87.5%, 93.0%, 94.0%, and 99.7%, respectively. When compared to other classifiers, the naive bayes classifier has superior accuracy.

Belo D. et al., (2017) [7] created a DL network model that can learn and synthesize bio signals, with the synthesized signals being checked against the original signals for morphological similarity. This study investigates Gated Recurrent Units (GRU) used for Respiratory (RESP), Muscular (EMG), and Cardiac (ECG) training. Before being input into the model, each signal is pre-processed, segmented, and quantized into a fixed number of classes based on the amplitude of each sample. The model then consists of an embedded matrix, three GRU blocks, and a SoftMax function. As the model progresses through the learning process, it first learns to recognize the signal's general morphological features and then its periodic ones. The RESP and ECG are two signals whose predictions improve after training with these algorithms. This process for synthesis

has shown useful findings, which motivate its use to characterizing signals from various physiological sources. Table 1 below summarizes the summary of the Review of Literature and the authors' process used in their studies.

Table 1. Summarize the table of reviewed literature based on biomedical signals and system.

Authors	Year	Techniques Used	Outcomes
Khanna et al., (2023) [1]	2023	loT-DL-HDD	The highest accuracy achieved by the IoT DL-HDD model in the experiments was 93.452%, demonstrating the model's superiority.
Selvarajan et al., [2]	2022	FISA	The suggested approach outperforms the state-of-the-art techniques by an average of 78% under realistic time constraints.
Kora P. et al., [3]	2020	CNN	The CNN-optimized model efficiently learns relevant features and performs automatic classification, resulting in a commendable classification accuracy of 90.63%. This achievement represents a substantial improvement compared to the results of previous work.
Balan O. et al., [4]	2019	ML and DL	The best findings for rage classification have been achieved using SVM and no feature selection, utilizing the Petrosian and Higuchi fractal dimensions. Applying raw EEG measurements, LDA and SFS have reached a classification accuracy of 100%, which is cause for celebration. SVM and SFS using raw EEG values for detecting surprise (96%) and disgust

			(95%), kNN using Petrosian values for detecting disgust (95%), kNN using raw EEG values for detecting fear (90.75%), and SVM using Higuchi fractal dimensions for detecting melancholy (90.8%).
Hirai Y. et al., [5]	2019	ML	The AFE's efficiency was also boosted by ML mistake correction. The planned AFE's ADC has an SNDR of 88 dB at 250 kHz sampling and 20.5 Hz full-scale input.
Celin S. et al., [6]	2018	SVM, ANN, NB, Adaboost	The experimental findings show that the SVM, Adaboost, ANN, and Naive Bayes classifiers have respective accuracy levels of 87.5%, 93%, 94.5%, and 99.7%. The Naive Bayes classifier outperforms all others in terms of accuracy.
Belo D. et al., [7]	2017	DNN	Additionally, it's worth noting that these models require only a minimal amount of signal data for training, with ECG and EMG data requiring approximately 175 seconds and RESP data requiring 350 seconds. This efficient utilization of data for training underscores the model's effectiveness. Furthermore, the low error rates observed in RESP and ECG data classification demonstrate the potential for employing this model to accurately identify the sources of these signals.

2.2. Cardiovascular Dynamics: ECG

In order to study cardiovascular dynamics, Electrocardiography (ECG) has often been employed by researchers, medical practitioners and diagnostic experts as a reliable signature of the electrical activity of the heart. Back in 1902, when W. Einthoven first recorded ECG using a string galvanometer, since then we made substantial progress in ECG signal acquisition, transmission and interpretation. In the next 100 years, we made significant progress related to signal acquisition technology as well as in developing a set of algorithms and system developments backed by advanced information technologies.

It is a well-known fact that ECG is one of the primary sources of cardiac diagnosis but it involves a lot of challenges in signal analysis and interpretation. The engineers have utmost interest in solving the challenges related to signals acquisition, processing and analysis. The doctors are more interested in obtaining proper diagnostic information out of it. ECG signals have been widely studied all over the world by different interdisciplinary research groups comprising doctors, engineers, scientists and experts in order to address the challenges associated with ECG signal processing and analysis. ECG signal is highly non-stationary and corrupted by noise due to motion artefacts, instrumentation overhead, muscle contraction and twitching, and various other intrinsic factors. The high degree of nonlinearity in ECG signals makes it a difficult task for conventional signal processing models to achieve the desired results. The reproducibility and reliability of these techniques is often questioned in real life scenarios. We have conducted a survey of the various techniques which were adopted by researchers to effectively model the cardiovascular dynamics using ECG so as to be used for gathering relevant diagnostic information.

This section describes the previous studies of various authors based on cardiovascular dynamics.

Ashoor M. et al., (2023) [8] explored of the cardiovascular system often involves the utilization of mathematical modeling and descriptive-analytical approaches. These methods encompass the incorporation of a wide array of physiological, geometric, and functional parameters to comprehensively study the system. For evaluating the impact of the ADC emitted from the capillary bed on the other parameters of the cardiovascular system, it is recommended to use a complicated Fermi function as pseudo-pressure (RADC) expressed in mmHg sec ml^{-1}. For the unregulated, non-pulsatile cardiovascular system, the RADC function over time is included in a

framework of differential equations that is the subject of the baroreflex-feedback process. The simulation outcomes were presented with a decrease in RADC, while the other parameters (including heart rate, mean arterial and venous pressure) were raised in a non-linear way.

Xia Y. et al., (2023) [9] aims to evaluate the impacts of daily temperature on death rates in Chengdu, China between 2016 and 2020, focusing on total non-accidental, CVD, respiratory, CVA, and IHD. The average daily temperatures and deaths from 2016 to 2020 were collected. This study employed a Poisson regression approach and a distributed-lag nonlinear model to analyze the correlation between temperature and daily mortality. They looked at how factors like age, education, marital status, and sex played into the equation. This study showed that persons over the age of 85, as well as women, those with lower levels of education, and those who are widowed, divorced, or never married, are more susceptible to the effects of heat and cold.

Konar S. et al., (2022) [10] established AI models using non-linear time-series data of blood pressure and heart rate to forecast a patient's duration in the intensive care unit, length of hospital stays, and chance of survival after cardiac surgery. Each minute of their cardiac operations, 6064 patients at a single tertiary care hospital had their heart rates and blood pressures monitored. After cleaning the data, it was divided into a "train" set consisting of 781 patients and a "test" set consisting of 296 patients. The train data set underwent feature engineering and data balancing. The balanced train data set was used to train a variety of survival outcome classification and ICU/hospital stay regression models. Area Under the Curve (AUC), accuracy, F1-score, Root Mean Squared Error (RMSE), and correlation (R2) were used to assess the predictive power of these models when applied to the test data set.

Shinya Y. et al., (2022) [11] evaluated the effects of providing babies aged 3 months with aural feedback to their own spontaneous limb motions on their heart rates and movements. There was a correlation between the newborns' greater frequency of limb movements eliciting auditory input and their more regular rhythm of limb movements. In addition, prolonged attention to the auditory stimuli was likely reflected in an initial inhibition of the heart rate rise linked with the limb movement shortly after the time of the auditory input. Later, through auditory-motor learning, the peak strength of the heart rate rise was dampened by inhibiting the increase in heart rate even before the auditory feedback. These results imply that newborns learn to control their heart rate and movement patterns in preparation for auditory input.

Kazdagli H. et al., (2022) [12] focused on measuring HRV parameters in mice under two common anesthetics to see how they differ. Using the Pan-Tompkins real-time QRS detection technique, R waves were identified, and from this information the tachogram of RR intervals was derived. The HRV was analyzed in the frequency domain, the time domain, and using nonlinear methods. When compared to both group P and group P+F, both SD1 and SD2 were larger in the K+X group ($p<0.001$), but the SD2/SD1 ratio was less in the K+X group ($p<0.05$) for both sets of data. Groups did not vary from one another in terms of entropy.

Konstantonis et al., (2022) [13] introduces an innovative ML approach for detecting cardiovascular disease (CVD) in individuals with medium to high cardiovascular risk. The ML classifiers were meticulously evaluated for their performance. Within this cohort, which included a total of 46 CVD risk factors (covariates) integrated into an online cardiovascular framework, the calculations were executed swiftly, taking less than 1 second per patient. The results were highly promising, with an average accuracy of 98.40% and an area-under-the-curve (AUC) of 0.98 ($p<0.0001$) achieved for the detection of CVD presence during the first visit. Remarkably, during the second visit, the model maintained similar high performance, with an accuracy of 98.39% and an AUC of 0.98 ($p<0.0001$). Notably, the performance of this cardiovascular framework significantly outperformed traditional CVD risk scoring methods. These findings underscore the robustness of the ML paradigm for predicting CVD in individuals with medium to high cardiovascular risk.

Abubaker et al., (2022) [14] implemented the prowess of DL to the public ECG pictures collection of cardiac patients to forecast the four main cardiac abnormalities: abnormal heartbeat, myocardial infarction, history of myocardial infarction, and normal person classes. First, they investigated the transfer learning method; second, they suggested a novel structure for CNNs; and third, used the previously mentioned pretrained models alongside the own CNN model. These models included the Support Vector Machine (SVM), K-Nearest Neighbors (K-NN), Decision Tree (DT), Random Forest (RF), and Naive Bayes (NB). The empirical findings show that the suggested CNN model outperforms the state-of-the-art in terms of accuracy (98.23%), recall (98.22%), precision (98.31%), and F1 score (98.21%). The suggested CNN model also outperforms state-of-the-art methods like the NB algorithm by a significant margin when it comes to feature extraction, with an optimal score of 99.79%.

Alqahtani et al., (2022) [15] employs a combination of ML and DL models to estimate the probability that a given individual would acquire cardiovascular disease. The authors use six different categorization systems to predict cardiovascular disease. They use a publicly accessible dataset of cardiovascular disease patients to train the models. In this study, they employ RF to determine which aspects of cardiovascular illness are most informative. The experimental findings show that the ML ensemble model is most effective at predicting the onset of illness with an accuracy of 88.70%.

Abdalrada et al., (2022) [16] create a two-stage ML model to assess the probability of DM and CVD occurring together. The Diabetes Complications Screening Research Initiative (DiScRi) dataset was used, which included over two thousand subjects and over two hundred variables. First, they utilized the correlation matrix to eliminate unnecessary variables and inferred the major shared risk factors for DM and CVD using two ML models (logistic regression and Evimp functions) implemented in a multivariate adaptive regression splines model. When it came time to refine the model, and turned to a combination of classification and regression algorithms. Accuracy, sensitivity, and specificity were used to measure the effectiveness of the prediction models.

Nadakinamani et al., (2021) [17] suggest a reliable CVD prediction system that makes use of ML. Classifying well-known cardiovascular datasets, on the other hand, is a job for state-of-the-art ML techniques like REP Tree, M5P Tree, Random Tree, Linear Regression, Naive Bayes, J48, and JRIP. In order to determine which ML model is most effective for the proposed CDPS, its performance was measured in a number of ways. The Random Tree model excelled in predicting patients with cardiovascular illness, with the best combination of accuracy, MAE, RMSE, and prediction speed.

Apostolopoulos et al., (2021) [18] examined the diagnosis accuracy of medical specialists against that of ML and DL techniques. Although highly precise identification of coronary artery disease is unlikely even from professionals at the current time, progress has been made toward a state-of-the-art Computer-Aided Diagnostic system via the development of AI models that can compete with the human eye and knowledge. According to the findings, a hybrid multi-input network consisting of InceptionV3, and a RF is the best technique for competing with the accuracy of a medical expert. The 79.15% accuracy achieved by the expert is mirrored by this approach.

Sharifrazi et al., (2021) [19] improved the efficiency of detecting Hypertrophic cardiomyopathy (HCM) using a DL approach. The authors used Labeling the enhanced photos required a deep CNN. CNN has never been utilized for HCM diagnosis before, as far as everybody knows. When compared to human judgment, the method achieves recall of 97.0 percent, accuracy of 95.2 percent, and specificity of 93.1 percent on the original dataset. The authors have conducted more research on the proposed approach by experimenting with other optimizers (such as Adagrad and Adadelta) and other methods of data augmentation (such as height shift and rotation). For improve upon the greatest accuracy provided by any of the previously investigated data augmentation strategies, the authors used a data augmentation methodology.

Asif et al., (2021) [20] stated the various ML algorithms and conducts a comparative analysis for the prediction of CVD. The investigation encompassed the evaluation of twelve ML algorithms, considering their performance under Default Hyperparameters (DHP), Grid Search Cross-Validation (GSCV), and Random Search Cross-Validation (RSCV) methods. Impressively, both hard and soft voting ensemble classifiers (EVCH and EVCS) achieved a remarkable accuracy of 92%. However, a noteworthy observation was that the Ada-boost algorithm outperformed EVCH and EVCS in terms of precision and specificity, indicating its superior performance in these specific aspects.

Maji C. et al., (2020) [21] suggested Empirical Mode Decomposition (EMD) approach is a well-known nonlinear technique that is used to uncover previously concealed information in an ECG recording. Here, they conduct EMD on reports of ECGs separating arrhythmia from normal data from the popular MIT-BIH database to better understand the human heart as a dynamic model. The R/S method is used to calculate the well-known nonlinear parameter Hurst Exponent (H) for each IMF. They found a clear divide between healthy individuals and those with arrhythmia based on the H of 1st IMFs. By analyzing ECG signals alone, the model verifies with 94.92% confidence the existence of arrhythmia illness in patients without requiring additional, time-consuming, and costly procedures as the Holter test, echocardiography, and stress test.

Gospodinova E. et al., (2020) [22] presented the findings of a study focused on the examination of nonlinear dynamic characteristics within the time intervals between heartbeats (RR time series). The investigation involved the utilization of several nonlinear dynamic's methods, such as reconstructed phase space analysis, the computation of the largest Lyapunov exponent, and the

creation of Poincaré plots. The incorporation of nonlinear dynamics methods, alongside conventional linear ECG signal analysis techniques, underscores the importance of collaboration between information technology experts and cardiologists. This collaboration aims to seamlessly integrate these innovative methodologies into clinical practice, thereby enhancing the capabilities of physicians in diagnosing and detecting cardiovascular diseases at an early stage. The analysis of the examined signals was carried out through the application of a web-based tool utilizing a serverless architecture. It's important to note that this application is experimental in nature and not intended for commercial purposes.

Zheng L. et al., (2017) [23] investigated how different phases of sleep affect your heart rate. First, nocturnal polysomnography was used to extract Heart Rate Variability (HRV), Pulse Rate Variability (PRV), and Pulse Transit Time (PTT) from the electrical cardiac and pulmonary vascular responses of 10 healthy participants. Then they performed a linear and nonlinear feature extraction of HRV, PRV, and PTT. Nonlinear characteristics included approximation entropy (ApEn), sample entropy (SampEn), and fuzzy entropy (FuzzyEn), while linear features included mean intervals, the standard deviation of all normal interval (SDNN), and the coefficient of variation (CV). The findings showed that in HRV, PRV, and PTT, the SDNN and CV were bigger in REM sleep than in slow wave sleep (SWS; $p<0.05$). The REM ApEn was greater than the SWS ApEn in both HRV and PRV ($p<0.05$).

Table 2 below summarizes the summary of the Review of Literature and the authors' process used in their studies.

Table 2. Summarize the table of reviewed literature based on cardiovascular dynamics.

Authors [Reference]	**Year**	**Techniques Used**	**Outcomes**
Ashoor M. et al., [8]	2023	Fermi Function	The RADC's forecast of the other effective parameters was affected by the suggested value of b because of the shift in time during which these parameters were evaluated. Even though the minimum quantity (RADC) grew, the

			maximum quantities (Pa, Pv, and Hr) decreased in a nonlinear manner.
Xia Y. et al., [9]	2023	Poisson Regression	In this study, researchers found that persons over the age of 85, females, those with lower levels of education, and those who were single or never married were more likely to die after being exposed to extreme heat or cold in Chengdu.
Konar S. et al., [10]	2022	GNB+LR	The Gaussian Naive Bayes+Logistic Regression (GNB+LR) model emerges as the top choice for survival analysis, boasting an impressive AUC of 0.72, an accuracy rate of 83%, and an outstanding F1-score of 0.86. When it comes to analyzing hospital stay, the Gradient boosting (GB) model takes the lead, delivering the highest R2-score of 0.023. For the analysis of ICU stay, the XGBoost regressor shines as the superior model, showcasing the highest R2-score of 0.125.
Shinya Y. et al., [11]	2022	ML	These results indicate that newborns' developing auditory-motor interactions entail the anticipatory control of the cardiovascular system with corresponding changes in movement and attention.

Kazdagli H. et al., [12]	2022	ML	Analyses of heart rate variability (HRV), using nonlinear approaches, showed that the K+X combination results in less imbalance and disorder in the regulation of the ANS compared to pentobarbital and the P+F combination.
Konstantonis et al., [13]	**(2022)**	ML	In the CVD-CR system, the mean accuracy and AUC were recorded as 98.40% and 0.98 ($p<0.0001$), respectively. Similarly, in the case of the CVD-3YFU, the mean accuracy and AUC were very close, at 98.39% and 0.98 ($p<0.0001$).
Abubaker et al., [14]	**(2022)**	CNN	The suggested CNN model outperforms the state-of-the-art in terms of accuracy, recall, precision, and F1 score, all of which are 98.23 or higher.
Alqahtani et al., [15]	**2022**	ML Ensemble	The suggested method, which employed a majority voting strategy to develop an ML Ensemble model, outperformed the baseline findings in terms of accuracy. A total of 88.70% of predictions were correct using the ML Ensemble model.
Abdalrada et al., [16]	**2022**	ML	The ML model has a 94.09% prediction accuracy, 93.50% sensitivity, and 958.2% specificity for identifying cases of combined DM and CVD.

Nadakinamani et al., [17]	**2021**	RT	The RT model excelled in predicting patients with cardiovascular illness, with 100% accuracy, the lowest Mean Absolute Error (MAE), the lowest Root Mean Square Error (RMSE), and the shortest prediction time (in seconds) of 0.01.
Apostolopoulos et al., [18]	**(2021)**	ML and DL	In this data set, the approach achieves the same 79.15% accuracy as the expert.
Sharifrazi et al., [19]	**2021**	Deep CNN	A precision of 98.53% was achieved, which is higher than the greatest precision achieved by any of the previous data augmentation methods (95.83%).
Asif et al., [20]	**2021**	ML and Ensemble classifier	The Ada-boost algorithm stands out as a promising approach among the various models, demonstrating the highest precision with a value of 0.938 and a remarkable specificity of 0.926.
Maji C. et al., [21]	**2020**	EMD	The study shows that a probability of 94.92% was expected towards the predictability of arrhythmia disease in a patient.
Gospodinova E. et al., [22]	**2020**	CNN	The findings demonstrate that the approaches used could distinguish between healthy and ill people, which can aid in the diagnostic process.

Zheng L. et al., [23]	**2017**	SDNN	SDNN and CV exhibited significantly larger values during REM compared to SWS ($p<0.05$), and the CV was also notably greater in REM compared to LS ($p<0.05$). However, there were no statistically significant differences observed in ApEn, SampEn, and FuzzyEn across various sleep stages.

2.3. Muscle Dynamics: EMG

In order to understand the causes and relationship of different muscle groups in action, and how it influences the physical activities of daily human life, we perform Electromyography (EMG) analysis. Electromyography is an effective bioelectric signal that emanates on the skin surface and reveals significant information about the strength and condition of the underlying muscles. EMG signals have been widely used for studies related to Physiotherapy, Rehabilitation and Sports medicine. It is very challenging to obtain diagnostic information from raw EMG data collected over skin surface, hence very few studies have been done in this regard. Some significant studies related to EMG signal analysis models for detecting muscular dystrophy, sarcopenia and rehabilitation of paralytic patients have been reported here.

This section describes the previous studies of various authors based on muscle dynamics.

Zhang J. et al., (2022) [24] introduced physics-based domain information into the data-driven model as soft constraints to penalize/regularize the model's predictions, thereby providing a physics-informed DL system for musculoskeletal modeling. As an example of how the suggested framework could be used, they look at the problem of predicting the forces exerted by muscles and the motion of joints using just surface sEMG. The suggested architecture executes the CNN is used as the DNN. Simultaneously, the soft constraint is based on the physics equation connecting

muscle forces to joint kinematics. One reference dataset and one dataset gathered independently from six healthy people are used for experimental validations. The empirical findings prove the efficiency and reliability of the suggested system.

Jagnesakova D. et al., (2022) [25] assessed the potential of ML models in predicting muscle glycogen utilization during exercise without invasive methods. To serve as a reference, a basic Linear Regressor model was employed, and its performance was compared to four alternative models: polynomial Support Vector Regressor (pSVR), Gradient Boosting Regressor (GBR), Random Forest Regressor (RFR), and Voting Regressor. The evaluation of these models involved a 3-fold cross-validation approach with respect to time bands. Across all time bands, the baseline glycogen level emerged as the most crucial factor influencing changes in glycogen. Notably, the top-performing models were pSVR in the first-time band, Voting Regressor in the second time band, GBR in the third time band, and both Linear and Voting Regressors in the fourth time band. It is worth noting that the model errors increased as the time bands progressed, starting with a Mean Absolute Error (MAE) of 41 mmol·kg-1 in the first band and reaching 55 mmol·kg-1 in the fourth band.

Sohane A. et al., (2022) [26] provided a ML based model that can estimate knee muscle force for therapeutic treatments using input parameters such as height, mass, and angle, while keeping costs to a minimum. In terms of Mean Square Error (MSE), coefficient of determination (R2), and correlation (r), the RF ML model is expected to perform better than the other specified models. There is no statistically significant difference between the conventional and AMS databases, as determined by the t-test. As a result, the suggested model would be useful in a wide variety of settings, including study and creation of lower limb exoskeletons, rehabilitation, clinical settings, etc.

Wimalasena L. et al., (2021) [27] suggested AutoLFADS, a massive, unsupervised DL strategy first developed to clean up cortical spiking data, to predict muscle activation from EMG signals including information from several muscles. Spatial and temporal regularities underpinning multi-muscle activation are modeled by AutoLFADS's 33 RNNs. In the initial experiments with AutoLFADS, they saw that it dynamically adapts its frequency response characteristics across distinct stages of behavior by analyzing muscle activity from the rat hindlimb as it was locomoting. Improved joint kinematics prediction was achieved comparing to low-pass or Bayesian filtering

due to the model's single-trial estimations of muscle activation. Furthermore, they used AutoLFADS to analyze isometric forearm muscle activity in monkeys to verify the method's generalizability. For identifying high-frequency oscillations in the EMG that low-pass and Bayesian filtering missed, AutoLFADS improved the connection between recorded force and EMG activity.

Nasr A. et al., (2021) [28] suggested as an alternate strategy to static optimization for fixing the redundant data problem in inverse muscle models. They optimized the setup, training, and testing of a Recurrent Neural Network (RNN) to predict the distribution of muscle activation data. When applied to empirical data, the resultant ML model normalizes the regression to a value between 88 and 91%, representing the predicted muscle activation. They performed a sensitivity analysis using a sequential backward selection approach to identify the less significant inputs. Joint angle, activation torque, joint velocity, and joint acceleration were first, second, third, and second, respectively, in importance among the signals measured. The temporal dynamics of muscle activation patterns were revealed by the RNN model, which only needed 0.06 s of historical biomechanical input data and 0.01 s of anticipated feedback EMG signals.

Rosa L. et al., (2021) [29] evaluated the efficacy of a method that utilizes both conventional ML models and B-mode ultrasound recordings to detect dynamic changes in the length of muscular fascicles in real time. To train ML models, they used conventional automated tracking software (UltraTrack) to extract muscle fascicle lengths and then matched those lengths, frame by frame, with the corresponding B-mode ultrasound images sent into the tracker. The findings open the way for future work that needs continuous, non-invasive monitoring of muscle function in living organisms. Although somewhat lower than values acquired using the most prevalent post-processing procedures described in the literature, the correlation and RMSE values obtained by comparing ML-tracked to ground truth produced using the UltraTrack program were similar.

Smirnov Y. et al., (2021) [30] presented ML algorithms were tasked with the challenge of approximating the relationships between posture-dependent moment arm and muscle length for the muscles of the human arm and hand. They employed two different algorithms-a Light Gradient Boosting (LGB) machine and a fully linked Artificial Neural Network (ANN)-to figure out the wrapping kinematics of 33 muscles, each of which has up to six DOFs in the arm and hand model. Accuracy in execution was satisfactory with both the ANN and LGB models, just as it was with

the original polynomial model. Computing muscle variables in 1.1 ms using the ANN model was 39 times quicker than using the LGB model, making it suitable for real-time control solutions.

Waasdorp et al., (2021) [31] suggested an innovative, non-invasive approach for simultaneously monitoring the propagation of electrical and mechanical waves within muscles. This is achieved through the utilization of high-density electromyography and ultrafast ultrasound imaging, capturing data at a rate of 5000 Frames Per Second (fps). The mechanical waves were extracted from the collected data using an axial tissue velocity estimation technique based on one-lag autocorrelation. The excitation wave, in other words, the Action Potential (AP), exhibited a velocity of 3.9 ± 0.5 meters per second, while the subsequent mechanical wave, representing muscle contraction, had a velocity of 3.5 ± 0.9 meters per second. The experimental findings provided evidence that contracting sarcomeres, already activated by the AP, exert a pulling force on sarcomeres that have not yet been reached by the AP. These results were further supported by simulations involving contractions of a newly developed multisegmented muscle fiber model, comprising 500 sarcomeres arranged in series.

Nuckols R. et al., (2019) [32] evaluated how the dynamics of muscles and tendons affects how people react to being helped by an exosuit. Soleus and medial gastrocnemius muscle contraction status was evaluated using B-mode ultrasonography while naive volunteers walked with exosuit support. The respondents that benefited the most from the assistance started contracting their soleus muscles before the help even started, which they discovered to be a 15% decrease in workload. Subjects that reacted poorly (a decrease of 2% overall) had soleus muscle contractions that started after assistance had begun. The medial gastrocnemius tended to extend at the commencement of assistance in poorly responding patients, which could provide insight on the role played by knee mechanics. Based on these results, it seems that exosuit support may alter the dynamics of energy exchange between muscles, tendons, joints, and the environment, all of which contribute to effective walking.

Driess D. et al., (2018) [33] explored the potential of ML techniques in acquiring controllers for these systems. The primary focus is to investigate whether the musculoskeletal structure possesses characteristics conducive to the learning process. Specifically, they are interested in developing a control policy that maps target positions to muscle stimulations. Given the considerable redundancy of actuators in biomechanical systems, the approach employs a neural network to learn

a forward model. They then utilize sequential quadratic programming to derive the control policy, enabling us to adjust the co-contraction level, modify the system's stiffness, and integrate optimization criteria such as minimizing muscle stimulations.

Table 3 below summarizes the summary of the Review of Literature and the authors' process used in their studies.

Table 3. Summarize the table of reviewed literature based on Muscle Dynamics

Authors [Reference]	**Year**	**Technique Used**	**Outcomes**
Zhang J. et al., [24]	2022	CNN	The suggested framework has been shown to be effective through extensive experimental testing on two sets of data for predicting muscle forces and joint angles.
Jagnesakova D. et al., [25]	2022	pSVR, RFR, GBR	According to the findings, modeling a complicated physiological system like glycogen dynamics during exercise necessitates several models for different activity durations, each of which has its own distinct factor relevance.
Sohane A. et al., [26]	2022	ML	For the test dataset, the MSE of the RF strategy predictions relative to the observed Biceps Femoris, Rectus Femoris, Vastus Medialis, and Vastus Lateralis muscle forces is 19.92, 9.06, 5.97, 5.46, the correlation is 0.94, 0.92, 0.94, and R2 is 0.88, 0.84, 0.84, and 0.89, and the R2 is 0.89.
Wimalasena L. et al., [27]	2021	RNNs	The estimates of muscle activation inferred by AutoLFADS exhibited a stronger correlation with motor cortical activity recorded

			simultaneously, surpassing the performance of other tested methods.
Nasr A. et al., [28]	2021	RNN	This method could improve future decision-support systems for functional rehabilitation by allowing for real-time estimate and monitoring of muscle activation or EMG signals.
Rosa L. et al., [29]	2021	ML and SVM	The SVM emerged as the top-performing model, achieving an average r-value of 0.70 ±0.34 and an average RMSE of 2.86 ±2.55 mm in all direct training conditions. When optimized for all cross-participant conditions, it maintained a notable performance, yielding an average r-value of 0.65 ±0.35 and an average RMSE of 3.28 ±2.64 mm
Smirnov Y. et al., [30]	2021	ANN and LGB	Both models produced comparable error rates; the ANN model's error rate was 0.08 0.05% for muscle lengths and the LGB model's error rate was 0.53 0.29% for moment arms. While ANN needed 106 training samples to acquire the same level of accuracy, LGB models only needed 103, while being around 39 times slower in the assessment.
Waasdorp et al., [31]	2021	Non-Invasive method	Both the experiment and simulation produced pre-contractile motion, which is likely attributed to the activation of sarcomeres occurring earlier, subsequently pulling on sarcomeres that had not been excited yet. It is conceivable that this effect

			was amplified in the experimental setup due to latency relaxation.
Nuckols R. et al., [32]	2019	ML	The hypothesis suggests that aiding prior to the initiation of contraction may lead to the extraction of energy from the Achilles tendon and potentially disrupt the typical muscle-tendon resonance.
Driess D. et al., [33]	2018	NN	Experimental results on a generated human arm's musculoskeletal model and a genuine biomimetic muscle-driven robot demonstrate that the method can train an accurate controller despite significant redundancy and nonlinearity while maintaining sampling efficiency.

2.4. Cognitive Neurodynamics: EEG

The dynamics of the human brain when studied with respect to various cognitive actions, gives rise to a complex network of systems neuroscience concepts for decoding the pieces of neural information. The decoding of the underlying neural dynamics during different cognitive actions related to acquiring knowledge, interpretation of knowledge and different behavioural response is like a dynamic puzzle to solve based on information. The complexity of the brain processes involved for one or more cognitive actions can be studied with the help of a specialised set of tools and techniques.

Many researchers have studied the activities of brain using Electroencephalography (EEG) along with other imaging techniques like Magnetic Resonance Imaging (MRI), Computed Tomography (CT) scan, Positron Emission Tomography (PET) scan and Magnetoencephalography (MEG).

Cognitive Neuro Dynamics is an interdisciplinary field of study that combines elements of cognitive science, neuroscience, and dynamics. It focuses on understanding the complex and dynamic processes underlying cognitive functions such as perception, memory, decision-making, and problem-solving by examining the interactions within the neural networks of the brain. This emerging field investigates the dynamic patterns of brain activity and their relationship to cognitive processes, seeking to unravel the underlying mechanisms that govern cognitive functions. Cognitive Neuro Dynamics employs various research techniques, including neuroimaging, EEG, and computational modeling, to explore the intricate connections between brain dynamics and cognitive phenomena. The goal is to provide insights into the fundamental principles of how the brains operate, paving the way for advancements in fields like artificial intelligence, psychology, and neurology while contributing to the understanding of the human mind.

This section describes the previous studies of various authors based on cognitive neuro dynamics.

Sethuraman S. et al., (2023) [34] described SVM and KNN are used to treat Alzheimer's disease. Secondly, leverage rs-fMRI datasets from ADNI organizations and the specialized Alexnet and Inception blocks. By experimenting with different settings and were able to get satisfactory results when using other ML and deep learning methods. Using just three bands and no further feature selection, the suggested model provides respectable results. The findings demonstrate that the system's accuracy (96.61%) and AUC (0.9663) are sufficient for distinguishing AD individuals from normal controls.

Velichko A. et al., (2023) [35] introduced a perceptron-based chaos sensor model for quantifying the disorderliness of neurodynamic systems, drawing inspiration from biological systems. After being trained, a sensor on perceptron with 50 neurons in the hidden layer and 1 neuron at the output may provide a close approximation of the fuzzy entropy of a small time series with a determination coefficient of R2~0.9. Training and testing datasets for the perceptron were generated using the time series of spike intervals generated by the Hindmarsh-Rose spike model. The K-block cross-validation technique was used for selecting the perceptron model's hyperparameters and estimating the sensor's accuracy. The model achieves respectable approximations of the fuzzy entropy and the metric R2~0.5/0.8 even for a hidden layer with a single neuron.

Sánchez C. et al., (2021) [36] investigated the impact of media professionalization on cognitive neurodynamic during audiovisual cuts, employing the Phase-Locking Value (PLV) approach. The

findings reveal a significant change in the behavior of media professionals after cuts. Specifically, media professionals exhibited a decrease in their blink rate, suggesting their enhanced ability to manage the loss of visual information that blinks typically involve, particularly when new visual content is being presented. Media professionals exhibited less activity in the medial and frontal cortices in response to cuts, but both groups' visual cortices were activated similarly. Better communication across cortical regions coordinated for deciphering new visual input following cuts may have contributed to the enhanced brain connection seen in media practitioners.

Hamed S. et al., (2021) [37] explore the results of the Neurodynamic Nerve Flossing Technique (NFT) on femoral neuropathy in hemophilia patients. Thirty children diagnosed with hemophilia and Femoral Neuropathy were randomly split into two groups. Before and after treatments, the patients' Motor Conduction Velocity (MCV) along the femoral nerve and their subjective experience of pain using a Visual Analog Scale (VAS) were measured. When the two groups were evaluated again after treatment, the study group was found to have significantly improved femoral nerve MCV and pain perception compared to the control group (p0.05).

Shao L. et al., (2021) [38] suggested classifying individuals with ASD using a graph-based CNN and Deep Feature Selection (DFS) combination. First, in the DFS procedure, a sparse one-to-one layer is inserted between the input and the first hidden layer of a multilayer perceptron, allowing for a weight to be assigned to each Functional Connection (FC) feature and the selection of a subset of FC characteristics. Using the input FC features' weights, the DFS successfully selects crucial features for classification, as shown in the experiments. The effectiveness of the GCN classifier could be vastly enhanced by using DFS. When applied to the cleaned and normalized ABIDE dataset, the suggested technique outperforms the state-of-the-art approaches with an accuracy of 79.5% and an AUC of 0.85.

Zheng H. et al., (2018) [39] offered using deep CNNs and deep residual learning to analyze EEG data and determine a driver's mental state. As a result, we've created two models for identifying mental states, which we've termed EEG-Conv and EEG-Conv-R. Both models outperform state-of-the-art LSTM- and SVM-based classifiers in the intra- and inter-subject evaluations. To summarize, the show that (1) both EEG-Conv and EEG-Conv-R provide extremely strong classification performance for mental state prediction; (2) EEG-Conv-R is better suited for inter-subject mental state prediction; and (3) EEG-Conv-R converges faster than EEG-Conv. In

conclusion, the suggested classifiers they have developed have higher predictive power and show great promise for use in real-world brain-computer interfaces.

Derakhshanrad S. et al., (2018) [40] stated an informing perspective that could contribute to a novel approach in the field of cognitive neuroscience. A concise questionnaire was developed to assess participants' cognitive neurodynamic processing capacity diversity, while three standardized questionnaires were utilized to collect data concerning manifestations of college adaptation. The data underwent analysis through partial correlation, one-way ANOVA, and two-way ANOVA tests. The partial correlation test revealed a strong and positive correlation ($r \geq 0.7$, $P<0.001$) among the components of the cognitive neurodynamic process, indicating that the interconnected relationships between intention, meaning, and perception were influenced by feedback loops. The one-way ANOVA test demonstrated that students with varying cognitive neurodynamic processing capacities exhibited a range of college adaptation manifestations. Furthermore, the two-way ANOVA exhibited a statistically significant primary effect for neurodynamic processing capacity ($F2, 178=8.1$, $P<0.001$).

Table 4 below summarizes the summary of the Review of Literature and the authors' process used in their studies.

Table 4. Summarize the table of reviewed literature based on cognitive neuro dynamics.

Authors [Reference]	Year	Techniques Used	Outcomes
Sethuraman S. et al., [34]	2023	SVM and KNN	The authors found that rs-fMRI's multi-band characteristics were more promising as biomarkers for AD than their single-band counterparts. Also, the suggested ensemble model performed 5-9% better than state-of-the-art ML algorithms.
Velichko A. et al., [35]	2023	Multilayer Perceptron Neural Network	It is recommended to use a perceptron model with 50 neurons in the hidden layer, which yields an R20.9 level of

		Model, Modeling the Hindmarsh-Rose System	agreement in terms of model similarity when comparing SFU and SPE.
Sánchez C. et al., [36]	2021	PLV	They calculated the mean Spontaneous Blink Rate (SBR) for the remaining stimuli. Across all participants, the mean SBR averaged 12.33 ± 7.61 blinks per minute. In the group of non-media professionals, the mean SBR was 15.79 ± 8.72 blinks per minute, while in the group of media professionals, it was 8.87 ± 4.23 blinks per minute. As expected, the identified statistically significant differences between these groups for the remaining stimuli (Mann-Whitney U Statistic = 79.5, T = 415.5, n = 18, p = 0.009, Mann-Whitney Rank Sum Test).
Hamed S. et al., [37]	2021	NFT	Post-treatment femoral MCV was significantly higher than pre-treatment MCV in both groups (control and study); the percentages of improvement were 33.78 and 42.11 percent, respectively, with a (p=0.0001) significance level.
Shao L. et al., [38]	2021	DL	According to the findings, the suggested strategy outperforms previously evaluated strategies by a wide margin, with state-of-the-art prediction accuracy

			of 79.5% and a high discriminating AUC of 0.85.
Zheng H. et al., [39]	2018	LSTM and SVM	The following conclusions could be drawn from the experimental data: Both EEGConv and EEG-Conv-R outperform classic classifiers like SVM and LSTM when it comes to intra-subject mental state detection; EEG-Conv-R outperforms EEG-Conv, LSTM, and SVM-based classifiers when it comes to inter-subject mental state detection; and EEG-Conv-R converges faster than EEG-Conv and requires less time for feature extraction during training.
Derakhshanrad S. et al., [40]	2018	ANOVA	The findings of this study suggest that 187 students at an Iranian college could have undergone a cognitive neurodynamic process associated with circular causality in their cognitive functioning.

2.5. Neuromuscular Dynamics: EEG-EMG

If we extend the concepts of cognitive neurodynamics to model the inter-relationship between Motor cortex in human brain and associated body muscles, then an interesting field of research is born. The mapping of the correlation between EEG and EMG is done to obtain descriptive parameters to model Neuromuscular Dynamics. One of such descriptors is qualitatively known as Corticomuscular Coherence (CMC). The quantification of CMC is a challenging task to achieve

and only few studies have been incorporated in this domain. Obtaining information that could be of diagnostic importance is the major focus while doing studies related to CMC.

Neuromuscular dynamics is a field of study that explores the intricate relationship between the nervous system and the muscular system in the human body. It delves into the complex interactions and communication between nerve cells (neurons) and muscle cells, seeking to understand how signals from the brain and spinal cord are transmitted to muscles to initiate and control movement. This interdisciplinary field combines elements of neuroscience, physiology, biomechanics, and motor control to unravel the mechanisms governing muscle contraction, coordination, and adaptation. Researchers in neuromuscular dynamics aim to decipher the neural pathways, motor unit recruitment, and feedback loops that govern both voluntary and involuntary muscle actions, shedding light on conditions like muscle disorders, paralysis, and motor skill development. This understanding is crucial in fields such as rehabilitation, sports science, and the development of assistive technologies for individuals with neuromuscular impairments.

This section describes the previous studies of various authors based on neuromuscular dynamics.

Gulrandhe P. et al., (2023) [41] evaluated the efficacy of the Dynamic Neuromuscular Stabilization (DNS) method on functional capacity in OW/OB patients and to contrast the results with those of the traditional approach. The participants in this research were all between the ages of twenty and twenty-five, since that was the minimum age requirement. Both the experimental and control groups showed statistically significant weight gain or loss as measured by the body mass index and the submaximal work test before and after treatment. Neither the experimental nor the control groups showed any statistically significant differences in body mass index (kg/m2) (t-value=-0.15, p=0.87). The SMW test (meter) also failed to show any statistically significant differences between the experimental and control groups (t-values of -0.15 and -0.22, respectively; ps > 0.22).

Noamani A. et al., (2022) [42] aimed to comprehensively characterize the neuromuscular stabilization mechanisms underlying human sitting. To achieve this, the research investigated both passive and active stabilization mechanisms during seated stability in ten able-bodied individuals when subjected to perturbations. To account for the complex, time-varying nature of these processes and measurement uncertainties, an adaptive unscented Kalman filter was employed to

create a nonlinear neuromechanical model with physiological significance. The findings revealed that the passive mechanism rapidly countered gravitational disturbances, while the active mechanism responded with a complementary phasic reaction to external disturbances, engaging the appropriate trunk muscles and displaying non-isometric behavior. Importantly, the model exhibited a high level of accuracy and correlation in predicting trunk sway behavior during perturbed sitting, with an average correlation of 0.0007 (rad2) and 86.77%.

Bao X. et al., (2022) [43] presented that the muscle-generated torques converge to the stabilizing values, they suggest a control framework consisting of a robust control module that generates stabilizing torques and a neural network-based mapping mechanism with an anatomy-based updating law. Assuming that the skeletal dynamics may be approximated by Euler-Lagrange equations with restricted disturbances allows for the extension of the control framework, a detailed analysis of the system stability of the suggested control approach was performed. They report simulation studies in which perturbations were given to a three-dimensional musculoskeletal model of the human trunk as it rotated anterior to posterior and lateral to medial. Positive simulation findings point to this control method's potential for use in everyday clinical settings for trunk tracking tasks.

Madle K. et al., (2022) [44] find out how different postural situations affect abdominal wall tension (AWT), initially uncorrected and then after being guided through a series of exercises and stretches based on the concepts of Dynamic Neuromuscular Stabilization (DNS). DNS instructions resulted in a significant increase in AWT compared to naturally occurring activation. Most of the positions monitored by the sensors showed statistically relevant improvements (p .01; Cohen's d = 1.13 to 2.06). There was no discernible difference in pressure rises between the sensors, and the uptick in activity happened at the same time on both. For both sensors, the bear posture was the most active. Both sensors were shown to be significantly more active when the subject was in the supine leg lift position, or the bear posture compared to when they were activated spontaneously when sitting ($p < .001$). No matter the setting, neither gender showed any statistically significant differences (for either sensor).

Xing Y. et al., (2021) [45] suggested a new hybrid-learning based timeseries model using deep learning networks is used to predict the steering intention. Long short-term memory (LSTM) cells and a Bidirectional Recurrent Neural Network (RNN) are used to construct a shared temporal

pattern extraction layer that both intention prediction networks use. In order to fully take advantage of the predictive power of the model, and test it using a wide range of past data and future projections. Twenty-one individuals of varying ages and levels of driving expertise comprise the experimental data. Prediction accuracy in both driving modes is about 95%, demonstrating the efficacy of the suggested strategy.

Mansori M. et al., (2021) [46] looked explored the impact that Dynamic Neuromuscular Stability (DNS) training has on seniors' ability to walk and balance. This research was a before-and-after affair. Thirty males between the ages of 60 and 70 from Qom Province, Iran, participated in quasi-experimental research that year. The acquired data were analyzed using the paired t test and the analysis of covariance (ANCOVA) technique. Dynamic balance, static balance (P=0.001), and gait function all improved significantly between the pre- and post-test in the EG, while in the CG, no such improvement was seen (P>0.05). In addition, EG outperformed the control group in the post-test, and there was a statistically significant difference (P0.05) in the groups' mean scores on the balance and gait tests.

Xing Y. et al., (2020) [47] examined the neuromuscular dynamics of the driver's upper limb under free-flowing driving conditions, focusing on pattern recognition. Electromyogram signals were used to assess the neuromuscular dynamics of the upper limb, and behavioral data, such as steering torque and steering angle, were also recorded. Muscle activity patterns were studied using data from experiments collected from real-world driving situations. Smoothness and regularity of the steering torque were addressed in addition to the correlations, amplitudes, and responsiveness of the electromyogram signals. The findings provide light on the neuromuscular dynamics of the driver's upper limb and lay the groundwork for the design of autonomous cars' HMIs of the future.

Valenciano L. et al., (2019) [48] established whether there are any sex-related variations in the correlation between the Y-Balance test's measures of unilateral dynamic balance and other measures of neuromuscular function. The parameters separately related with the performance of both sexes' balance were identified using a stepwise multivariate linear least square regression with backward elimination analysis. For men, the most significant characteristics that remained associated with dominant (R2 = 23.1) and non-dominant (R2 = 33.5) balance scores were ankle dorsiflexion with knee flexed ROM and passive hip flexion. Women's balance test results remained significantly correlated with measures of core stability (R2 = 38.2), hip abduction isometric peak

torque (R2 = 46.9), passive hip abduction (R2 = 46.9), and ankle dorsiflexion with knee flexed (R2 = 46.9).

Lv C. et al., (2018) [49] created a real-time model of the neuromuscular responses of drivers when they manipulate the wheel. They examine the systems' transfer functions and natural frequencies. Key parameters of the transfer function model are determined using the Gauss-Newton technique and the experimental findings. Once the estimated model with the specified parameters has been created, the characteristics of the system may be investigated. driving neuromuscular system features are examined and contrasted across a range of steering duties, hand locations, and driving postures. This experimental data, together with the indicated system attributes, may serve as a solid starting point for designing a haptic take-over control system for autonomous cars.

Table 5 below summarizes the summary of the Review of Literature and the authors' process used in their studies.

Table 5. Summarize the table of reviewed literature based on neuromuscular dynamics.

Authors [Reference]	Year	Techniques Used	Outcomes
Gulrandhe P. et al., [41]	**2023**	**DNS**	Neither the control nor the experimental group showed any statistically significant differences in their mean changes from pre- to post-test BMI or SMW.
Noamani A. et al., [42]	**2022**	**Kalman Filter**	The model's predictions of trunk sway behavior during perturbed sitting were very accurate and correlated (average: 0.0007 (rad2) and 86.77%).
Bao X. et al., [43]	**2022**	**FNS**	These outcomes point to a controller that is both effective and strong enough to dismiss unforeseen disturbances,

			indicating that the control job was completed successfully.
Madle K. et al., [44]	**2022**	**DNS**	The bear posture elicited the highest levels of abdominal wall stimulation, both on its own and in response to instructions.
Xing Y. et al., [45]	**2021**	**RNN and LSTM**	The suggested system has the potential to serve as an efficient and crucial element within the shared control and takeover performance assessment system for autonomous vehicles.
Mansori M. et al., [46]	**2021**	ANCOVA statistical method	The results of this research demonstrate that DNS exercises have a beneficial impact on aspects of balance function and gait performance in the elderly.
Xing Y. et al., [47]	**2020**	EMG	The findings uncover the intricacies of neuromuscular dynamics in the driver's upper limb, laying the groundwork for the theoretical basis upon which future human-machine interfaces for automated vehicles can be designed.
Valenciano L. et al., [48]	**2019**	Linear Least Square Regression	The primary results of the present research suggest that, although having equal unilateral dynamic balance scores, male and female professional football players seem to be influenced by distinct measures of neuromuscular efficiency.

Lv C. et al., [49]	**2018**	**Gauss Newton**	The test findings show that the stiffness coefficient has substantially bigger values in the passive steering modes compared to the active steering modes. Stiffness coefficient values for the participants fall mostly between 2.5 and 3.5 Hz while doing passive steering activities, and below 1 Hz when performing active steering tasks.

References

1. Khanna, Ashish, Pandiaraj Selvaraj, Deepak Gupta, Tariq Hussain Sheikh, Piyush Kumar Pareek, and Vishnu Shankar. "Internet of things and deep learning enabled healthcare disease diagnosis using biomedical electrocardiogram signals." *Expert Systems* 40, no. 4 (2023): e12864.
2. Selvarajan, Shitharth, Hariprasath Manoharan, Tawfiq Hasanin, Raed Alsini, Mueen Uddin, Mohammad Shorfuzzaman, and Abdulmajeed Alsufyani. "Biomedical signals for healthcare using Hadoop infrastructure with artificial intelligence and fuzzy logic interpretation." *Applied Sciences* 12, no. 10 (2022): 5097.
3. file:///C:/Users/rasha/Downloads/BBRC_ECG_Deep_Learning.pdf
4. Bălan, Oana, Gabriela Moise, Livia Petrescu, Alin Moldoveanu, Marius Leordeanu, and Florica Moldoveanu. "Emotion classification based on biophysical signals and machine learning techniques." *Symmetry* 12, no. 1 (2019): 21.
5. Hirai, Yusaku, Toshimasa Matsuoka, Sadahiro Tani, Shodai Isami, Keiji Tatsumi, Masayuki Ueda, and Takatsugu Kamata. "A biomedical sensor system with stochastic A/D conversion and error correction by machine learning." *IEEE Access* 7 (2019): 21990-22001.
6. Celin, S., and K. Vasanth. "ECG signal classification using various machine learning techniques." *Journal of medical systems* 42, no. 12 (2018): 241.

7. Belo, David, João Rodrigues, João R. Vaz, Pedro Pezarat-Correia, and Hugo Gamboa. "Biosignals learning and synthesis using deep neural networks." *Biomedical engineering online* 16 (2017): 1-17.

8. Ashoor, Mansour, and Abdollah Khorshidi. "Modelling cardiovascular system using Fermi functions on capillary bed." *Sādhanā* 48, no. 3 (2023): 151.

9. Xia, Yizhang, Chunli Shi, Yang Li, Xianyan Jiang, Shijuan Ruan, Xufang Gao, Yu Chen et al. "Effects of ambient temperature on mortality among elderly residents of Chengdu city in Southwest China, 2016–2020: a distributed-lag non-linear time series analysis." *BMC Public Health* 23, no. 1 (2023): 149.

10. Konar, Sushant, Nitin Auluck, Rajarajan Ganesan, Atul Kumar Goyal, Tarunpreet Kaur, Mansi Sahi, Tanvir Samra, Shyam Kumar Singh Thingnam, and Goverdhan Dutt Puri. "A non-linear time series based artificial intelligence model to predict outcome in cardiac surgery." *Health and Technology* 12, no. 6 (2022): 1169-1181.

11. Shinya, Yuta, Kensuke Oku, Hama Watanabe, Gentaro Taga, and Shinya Fujii. "Anticipatory regulation of cardiovascular system on the emergence of auditory-motor interaction in young infants." *Experimental Brain Research* 240, no. 6 (2022): 1661-1671.

12. KAZDAĞLI, HASAN, HASAN FEHMİ ÖZEL, Mustafa Özbek, Şüheda Alpay, and Mürüvvet Alenbey. "Classical heart rate variability and non-linear heart rate analysis in mice under Na-Pentobarbital and Ketamine/Xylazine anesthesia." *Turkish Journal of Medical Sciences* 52, no. 3 (2022): 858-869.

13. Konstantonis, George, Krishna V. Singh, Petros P. Sfikakis, Ankush D. Jamthikar, George D. Kitas, Suneet K. Gupta, Luca Saba et al. "cardiovascular disease detection using machine learning and carotid/femoral arterial imaging frameworks in rheumatoid arthritis patients." *Rheumatology International* 42, no. 2 (2022): 215-239.

14. Abubaker, Mohammed, and Bilal Babayigit. "Detection of Cardiovascular Diseases in ECG Images Using Machine Learning and Deep Learning Methods." *IEEE Transactions on Artificial Intelligence* (2022).

15. Alqahtani, Abdullah, Shtwai Alsubai, Mohemmed Sha, Lucia Vilcekova, and Talha Javed. "Cardiovascular disease detection using ensemble learning." *Computational Intelligence and Neuroscience* 2022 (2022).

16. Abdalrada, Ahmad Shaker, Jemal Abawajy, Tahsien Al-Quraishi, and Sheikh Mohammed Shariful Islam. "Machine learning models for prediction of co-occurrence of diabetes and cardiovascular diseases: a retrospective cohort study." *Journal of Diabetes & Metabolic Disorders* 21, no. 1 (2022): 251-261.

17. Nadakinamani, Rajkumar Gangappa, A. Reyana, Sandeep Kautish, A. S. Vibith, Yogita Gupta, Sayed F. Abdelwahab, and Ali Wagdy Mohamed. "Clinical data analysis for prediction of cardiovascular disease using machine learning techniques." *Computational intelligence and neuroscience* 2022 (2022).

18. Apostolopoulos, Ioannis D., Dimitris I. Apostolopoulos, Trifon I. Spyridonidis, Nikolaos D. Papathanasiou, and George S. Panayiotakis. "Multi-input deep learning approach for cardiovascular disease diagnosis using myocardial perfusion imaging and clinical data." *Physica Medica* 84 (2021): 168-177.

19. Sharifrazi, Danial, Roohallah Alizadehsani, Navid Hoseini Izadi, Mohamad Roshanzamir, Afshin Shoeibi, Fahime Khozeimeh, Fariba Alizadeh Sani, et al. "Hypertrophic cardiomyopathy diagnosis based on cardiovascular magnetic resonance using deep learning techniques." *Colour Filtering* (2021)

20. Asif, Md Asfi-Ar-Raihan, Mirza Muntasir Nishat, Fahim Faisal, Rezuanur Rahman Dip, Mahmudul Hasan Udoy, Md Fahim Shikder, and Ragib Ahsan. "Performance Evaluation and Comparative Analysis of Different Machine Learning Algorithms in Predicting Cardiovascular Disease." *Engineering Letters* 29, no. 2 (2021).

21. Maji, Chiranjit, Pratyay Sengupta, Anandi Batabyal, and Hirok Chaudhuri. "Nonlinear and statistical analysis of ECG signals from arrhythmia affected cardiac system through the EMD process." *arXiv preprint arXiv:2002.03840* (2020).

22. Gospodinova, Evgeniya, Mitko Gospodinov, and Maria Negreva. "Nonlinear dynamics methods for analysis of ECG signals." In *Proceedings of the 21st International Conference on Computer Systems and Technologies*, pp. 194-200. 2020.

23. Zheng, Lianrong, Yifan Li, Weifeng Pan, Kunyang Li, and Guanzheng Liu. "Linear and Nonlinear analysis of Cardiovascular Time Series during Different Sleep Stages." In *2016 4th International Conference on Machinery, Materials and Information Technology Applications*, pp. 790-794. Atlantis Press, 2017.

24. Zhang, Jie, Yihui Zhao, Fergus Shone, Zhenhong Li, Alejandro F. Frangi, Sheng Quan Xie, and Zhi-Qiang Zhang. "Physics-informed deep learning for musculoskeletal modeling: Predicting muscle forces and joint kinematics from surface EMG." *IEEE Transactions on Neural Systems and Rehabilitation Engineering* 31 (2022): 484-493.

25. Jagnesakova, Dorota, David M. Dunne, José L. Areta, Carmen E. Lefevre, Xiaoxi Yan, Rodrigo Mazorra, and Samuel Impey. "A Machine Learning Approach to Predicting Muscle Glycogen Use During Exercise." (2022).

26. Sohane, Anurag, and Ravinder Agarwal. "Knee muscle force estimating model using machine learning approach." *The Computer Journal* 65, no. 5 (2022): 1167-1177.

27. Wimalasena, Lahiru N., Jonas F. Braun, Mohammad Reza Keshtkaran, David Hofmann, Juan Álvaro Gallego, Cristiano Alessandro, Matthew C. Tresch, Lee E. Miller, and Chethan Pandarinath. "Estimating muscle activation from EMG using deep learning-based dynamical systems models." *Journal of neural engineering* 19, no. 3 (2022): 036013.

28. Nasr, Ali, Keaton A. Inkol, Sydney Bell, and John McPhee. "Inversemusclenet: Alternative machine learning solution to static optimization and inverse muscle modeling." *Frontiers in Computational Neuroscience* 15 (2021): 759489.

29. Rosa, Luis G., Jonathan S. Zia, Omer T. Inan, and Gregory S. Sawicki. "Machine learning to extract muscle fascicle length changes from dynamic ultrasound images in real-time." *PloS one* 16, no. 5 (2021): e0246611.

30. Smirnov, Yaroslav, Denys Smirnov, Anton Popov, and Sergiy Yakovenko. "Solving musculoskeletal biomechanics with machine learning." *PeerJ Computer Science* 7 (2021): e663.

31. Waasdorp, Rick, Winfred Mugge, Hendrik J. Vos, Jurriaan H. De Groot, Martin D. Verweij, Nico De Jong, Alfred C. Schouten, and Verya Daeichin. "Combining ultrafast ultrasound and

high-density EMG to assess local electromechanical muscle dynamics: a feasibility study." *IEEE access* 9 (2021): 45277-45288.

32. Nuckols, Richard W., Krithika Swaminathan, Sangjun Lee, Dheepak Arumukhom Revi, Conor J. Walsh, and Robert D. Howe. "Investigating the role of muscle dynamics in individual response to soft exosuit assistance."

33. Driess, Danny, Heiko Zimmermann, Simon Wolfen, Dan Suissa, Daniel Haeufle, Daniel Hennes, Marc Toussaint, and Syn Schmitt. "Learning to control redundant musculoskeletal systems with neural networks and SQP: exploiting muscle properties." In *2018 IEEE International Conference on robotics and automation (ICRA)*, pp. 6461-6468. IEEE, 2018.

34. Sethuraman, Sambath Kumar, Nandhini Malaiyappan, Rajakumar Ramalingam, Shakila Basheer, Mamoon Rashid, and Nazir Ahmad. "Predicting Alzheimer's Disease Using Deep Neuro-Functional Networks with Resting-State fMRI." *Electronics* 12, no. 4 (2023): 1031.

35. Velichko, Andrei, Petr Boriskov, Maksim Belyaev, and Vadim Putrolaynen. "A Bio-Inspired Chaos Sensor Model Based on the Perceptron Neural Network: Machine Learning Concept and Application for Computational Neuro-Science." *Sensors* 23, no. 16 (2023): 7137.

36. Andreu-Sánchez, Celia, Miguel Ángel Martín-Pascual, Agnès Gruart, and José María Delgado-García. "The effect of media professionalization on cognitive neurodynamics during audiovisual cuts." *Frontiers in systems neuroscience* 15 (2021): 598383.

37. Hamed, Somaia A., Ibrahim M. Zoheiry, Nevien Maher Waked, and Lama Saad El-Din Mahmoud. "Effect of Neurodynamics Nerve Flossing on Femoral Neuropathy in Haemophilic Patients: A randomized controlled study." *Journal of Musculoskeletal & Neuronal Interactions* 21, no. 3 (2021): 379.

38. Shao, Lizhen, Cong Fu, Yang You, and Dongmei Fu. "Classification of ASD based on fMRI data with deep learning." *Cognitive Neurodynamics* 15, no. 6 (2021): 961-974.

39. Zeng, Hong, Chen Yang, Guojun Dai, Feiwei Qin, Jianhai Zhang, and Wanzeng Kong. "EEG classification of driver mental states by deep learning." *Cognitive neurodynamics* 12 (2018): 597-606.

40. Derakhshanrad, Seyed Alireza, and Emily Piven. "A cognitive neurodynamic approach to prediction of students' adaptation to college: An ex-post facto study." *Basic and Clinical Neuroscience* 9, no. 3 (2018): 217.

41. Gulrandhe, Purva, Rakesh K. Kovela, Snehal Samal, and Rakesh K. Kovela Sr. "Effect of the Dynamic Neuromuscular Stabilization Technique on Functional Capacity in Overweight and Obese Individuals: A Randomized Controlled Trial." *Cureus* 15, no. 7 (2023).

42. Noamani, Alireza, Albert H. Vette, and Hossein Rouhani. "Nonlinear response of human trunk musculature explains neuromuscular stabilization mechanisms in sitting posture." *Journal of Neural Engineering* 19, no. 2 (2022): 026045.

43. Bao, Xuefeng, Musa L. Audu, Aidan R. Friederich, and Ronald J. Triolo. "Robust Control of the Human Trunk Posture Using Functional Neuromuscular Stimulation: A Simulation Study." *Journal of Biomechanical Engineering* 144, no. 9 (2022): 091002.

44. Madle, Katerina, Petr Svoboda, Martin Stribrny, Jakub Novak, Pavel Kolar, Andrew Busch, Alena Kobesova, and Petr Bitnar. "Abdominal wall tension increases using Dynamic Neuromuscular Stabilization principles in different postural positions." *Musculoskeletal Science and Practice* 62 (2022): 102655.

45. Xing, Yang, Chen Lv, Yahui Liu, Yifan Zhao, Dongpu Cao, and Sadahiro Kawahara. "Hybrid-learning-based driver steering intention prediction using neuromuscular dynamics." *IEEE Transactions on Industrial Electronics* 69, no. 2 (2021): 1750-1761.

46. Mansori, Mohammad Hani, Yousef Moghadas Tabrizi, and Kamal Mohammadkhani. "Evaluation of the Effectiveness of Dynamic Neuromuscular Stability Exercises on Balance and Walking Function in the Elderly." *Iranian Rehabilitation Journal* 19, no. 3 (2021): 279-288.

47. Xing, Yang, Chen Lv, Yifan Zhao, Yahui Liu, Dongpu Cao, and Sadahiro Kawahara. "Pattern recognition and characterization of upper limb neuromuscular dynamics during driver-vehicle interactions." *Iscience* 23, no. 9 (2020).

48. López-Valenciano, Alejandro, Francisco Ayala, M. De Ste Croix, D. Barbado, and F. J. Vera-Garcia. "Different neuromuscular parameters influence dynamic balance in male and female football players." *Knee Surgery, Sports Traumatology, Arthroscopy* 27 (2019): 962-970.

49. Lv, Chen, Huaji Wang, Dongpu Cao, Yifan Zhao, Daniel J. Auger, Mark Sullman, Rebecca Matthias, Lee Skrypchuk, and Alexandros Mouzakitis. "Characterization of driver neuromuscular dynamics for human–automation collaboration design of automated vehicles." *IEEE/ASME Transactions on Mechatronics* 23, no. 6 (2018): 2558-2567.

Chapter 3 Computational Methods

There is a wide variety of computational tools and techniques for analyzing Biomedical Signals and Systems starting from the classical Frequency domain techniques to the very recent Artificial Intelligence based techniques. The extent of Digital Signal Processing tools of Biomedical signals for both linear system and non-linear system based continuous and discrete representation of time series is discussed herewith. This chapter embarks on a comprehensive exploration of diverse domains, venturing into the realms of signal processing, chaos theory, machine learning, and statistical analysis. Each section unravels the intricacies of these fundamental concepts, providing technical definitions and practical applications that illuminate their significance in various fields.

3.1. Frequency Domain characterization

Frequency domain representation of Biomedical signals can be classified as:

- Periodic representation of biosignals using Trigonometric Fourier Series, given by the equation 3.1

$$x(t) = a_0 + \sum_{m=1}^{\infty}(a_m \, cos \, cos \, m\omega_0 t + \, b_m \, sin \, sin \, m\omega_0 t \,) \qquad eq.3.1$$

  Where x(t) is the periodic biosignal and $\omega_0 = \frac{3\pi}{T}$ or the fundamental frequency and the coefficients a_m and b_m are the magnitude of sine and cosine terms.
- Compact Fourier Series represents the above series expansion in a compact form as shown in eq.3.2

$$x(t) = \frac{A_0}{2} + \sum_{m=1}^{\infty} A_m \, cos \, cos \, (m\omega_0 t + \, \emptyset_m) \qquad eq.3.2$$

  Where $\emptyset_m$ is the phase constant given as $\emptyset_m = \left(\frac{-b_m}{a_m}\right)$
- Exponential Fourier Series is another form of representing trigonometric Fourier series into exponential forms as shown in eq.3.3.

$$x(t) = \sum_{m=-\infty}^{\infty} c_m e^{kj\omega_0 t} \qquad eq.3.3$$

Where $c_m = \frac{A_m}{2} e^{j\emptyset_m}$ a complex number related to the trigonometric Fourier coefficients.

- Fourier Transforms:

  In case of Fourier series representation of the signals we have to keep in mind that it is only suitable for periodic signals but in reality, most of the biomedical signals are not periodic in nature with no repeatability in time. To address this issue one can apply Fourier Transforms to continuous aperiodic signals and decompose them into subsequent frequency components. Fourier Transforms is represented by the formula as shown in eq.3.4 where $X(\omega)$ is the frequency domain representation of the signal $x(t)$ in the time domain.

$$X(\omega) = \int_{-\infty}^{\infty} x(t) e^{-j\omega t} \qquad eq.3.4$$

In digital signal processing applications, the biosignal is acquired and stored in terms of discrete values by sampling the continuous analog signal using an ADC. Therefore, the continuous Fourier transform method as discussed above is not applicable in case of discrete samples of the biomedical signals. The modified version of continuous Fourier transform is formulated as Discrete Fourier Transforms for decomposing the signal components into different discrete constituent frequencies. The Discrete Fourier Transform (DFT) is a frequency domain tool for analyzing discrete biomedical signals as given by the expression in eq.3.5.

$$X(m) = \sum_{k=0}^{N-1} x(k) e^{-j\frac{2\pi mk}{N}};\ m = 0,1,\ldots.N-1 \qquad eq.3.5$$

Here *m* represents the digital frequency index, *x(k)* is the sampled approximation of *x(t)*, k is the discrete time variable, N is an even number that represents the number of samples for *x(k)*, and *X(m)* is the DFT of *x(k)*. The DFT is an important tool in biomedical signal processing and analysis which is a digital version of Fourier Transforms. The algorithm used to compute DFT is Fast Fourier Transform or FFT algorithm which is much faster than DFT and yields the same result on execution. If N is a power of 2 like 1024 data samples, then FFT is around 10 times faster than original DFT.

Another tool for Frequency domain-based analysis of biomedical signals is z-transforms. This transform is basically an alternate variant of DFT but easier to calculate as it doesn't require direct estimation using complex numbers. It is to note that, z-transform can be directly obtained from DFT by the approximation of $N \to \infty$ and by replacing $z = e^{-j\frac{2\pi mk}{N}}$. The z-transform of the discrete sequence *x(k)* is given as eq.3.6.

$$X(z) = \sum_{k=0}^{\infty} x_k z^{-k} \qquad eq.\ 3.6$$

Frequency domain characterization of the biomedical signals is often carried out in real life scenarios as the signal could be represented better in frequency domain than time domain. Engineers have a better understanding of the frequency domain characterization than the time domain. For example, Alpha frequency of EEG signal is 11 Hz is more informative than its time period of 0.09 sec. Biosignals don't convey satisfactory information when viewed in time domain due the variability and aperiodic nature of the generated waveform. Fourier transforms actually facilitate the representation of biomedical signals and systems for analysis in the frequency domain. Power Spectral Density (PSD) which is the distribution of the energy or power of the biosignal into a wide band of frequencies is an effective tool for frequency domain analysis of the biosignal. In time domain generally auto correlation function or ACF is estimated which gives an idea about the stochasticity of the biosignal, but Fourier spectrum based PSD estimate in frequency domain gives a lot more parameters for distinguishing between normal and diseased signals. The formula for ACF of a random sequence and PSD is given in equation 3.7 and 3.8 respectively.

The autocorrelation function ACF, $\varphi_{xx}(t_1, t_1 + \tau)$,of random time series of discrete sequence *x(k)* is given

$$\varphi_{xx}(t_1, t_1 + \tau) = \frac{1}{N} \sum_{k=1}^{N} x_k(t_1) x_k(t_1 + \tau) \qquad eq.\ 3.7$$

The accurate PSD estimate is done by windowing and averaging the periodograms at each segment (k) of let us say M samples, and periodogram of each segment of length M is given as $S_i(\omega)$ in eq.3.8

$$S_i(\omega) = \frac{1}{M}\left|\sum_{n=0}^{M-1} x_i(n)e^{-j\omega n}\right|^2, 1 \le i \le k \qquad eq.3.8$$

If the windowing is done before estimation of the Fourier transforms for the PSD estimate, then we get what is known as Welch's averaged periodogram. The Welch method of estimating the PSD is thought to be a better and smoothened representation of the frequency spectrum for Biomedical signal analysis and characterization. One can use PSD parameters like band power, percentage power, peak frequency, mean frequency or median frequency for effective characterization of the signal after acquisition, or filtering and denoising and even distinguishing between normal and abnormal conditions.

Another estimate of PSD can be obtained from the time domain analysis function known as Autoregressive function (AR). The AR model is denoted as shown in eq.3.9 which can be extended to work as an AR synthesis filter that generates the frequency spectrum of the input time series based on squared variance estimate which is analogous to power in frequency domain. The advantage of using AR model for PSD estimate over DFT based PSD estimate is that AR model is more robust to noise contamination present in most biological signals.

$$x(n) = \sum_{i=1}^{M} a_i x(n-i) + \varepsilon(n) \qquad eq.3.9$$

Here $x(n)$ is present value of discrete time sequence, $a_i$or the prediction coefficient, $\varepsilon(n)$ is the error in predicting the next value. The AR model is basically a set of ACF functions.

Once the signal is represented in the Frequency domain using PSD to understand the signal characteristics and the dominant frequency bands and their effect in the signal waveform, the signal is passed through filters for noise elimination and artifact removal. Analog and digital filters are linear systems and its output is the result of convolution between the input signal and impulse response of the filter. Analog and digital filters eliminate the unwanted frequency bands from the

overall frequency spectrum and are of three types based on their design Low Pass, High Pass and Band Pass. Other than this, filters can be of Infinite Impulse Response (IIR) and Finite Impulse Response (FIR) based on the input and output function. It is to note that the cell membrane acts as a Low Pass filter that preserves the Low frequency components of the signal passing through it. The general form of digital filter can be represented by the deference equation as shown in eq.3.10.

$$y(k) = \sum_{m=0}^{M} b_m x(k-m) - \sum_{m=1}^{N} a_m y(k-m) \qquad eq.\,3.10$$

Where $y(k)$ and $x(k)$ are the output and input discrete sequence at time say k, and M and N represent the count of the samples that determines the convergence of the output sequence. Going by the definition we can say that if the impulse response of the filter has a finite number of non-zero points, then it is IIR and if sequence terminates at zero then its FIR. IIR filters are generally said to be more efficient than FIR filters owing to a smaller number of filter coefficients in IIR but output sequences of IIR filters are sensitive to distortion. In filter design also ideal performance can be obtained by designing and implementing Windowed FIR filters with various windowing functions such as Hamming, Hanning and Kaiser windows. [1]

3. 2 Joint Time Frequency Domain Characterization

Joint Time Frequency Domain Characterization (JTFDC) is a signal processing technique that combines the time and frequency domains to provide a comprehensive analysis of signals. It involves methods that allow simultaneous representation of signal characteristics in both time and frequency, enabling the exploration of dynamic behaviors that may vary over time.

JTFDC finds applications in various fields such as communication systems, biomedical signal processing, and radar systems. In communication systems, JTFDC can be employed to analyze signals affected by varying channel conditions, while in biomedical signal processing, it aids in understanding the time-frequency characteristics of physiological signals. [2]

3.3. Wavelet Denoising and Decomposition

Wavelet denoising is a signal processing technique that uses wavelet transformations to remove noise from signals. It involves decomposing a signal into its constituent wavelet components, selectively removing noise, and reconstructing the signal.

Wavelet denoising is widely used in image processing, audio signal processing, and vibration analysis. In image processing, it helps enhance image quality by eliminating noise, while in vibration analysis, it aids in identifying and isolating specific frequency components associated with mechanical faults. [3]–[5]

3.4 Nonlinear Discrete Dynamical Systems Theory

Nonlinear Discrete Dynamical Systems (NDDS) theory studies the behavior of discrete-time systems with nonlinear dynamics. It focuses on understanding the evolution of a system over discrete time steps, considering the impact of nonlinearity on system behavior.

NDDS theory is applied in chaos theory, cryptography, and population dynamics. In chaos theory, it helps analyze the behavior of chaotic systems, while in cryptography, it contributes to the design of secure encryption algorithms based on nonlinear dynamics. [1], [6]

3.4.1. Chaos

Chaos refers to the unpredictable and complex behavior exhibited by certain deterministic systems. These systems are highly sensitive to initial conditions, leading to seemingly random outcomes.

Technical Definitions:

- **Deterministic chaos:** A type of chaos in which a system evolves according to deterministic rules, yet exhibits unpredictable behavior due to its sensitivity to initial conditions.

- **Nondeterministic chaos:** A type of chaos in which a system is governed by stochastic rules, introducing an inherent element of randomness into its behavior.

- **Butterfly effect:** A hallmark of chaos, demonstrating the profound impact of minuscule changes in initial conditions on the system's future trajectory.

Chaos theory finds applications in fields such as weather prediction, economics, and cryptography. In weather prediction, chaos theory helps model the complex interactions of atmospheric variables, while in cryptography, chaotic systems are employed to generate random sequences for secure key generation. [7]–[9]

3.4.2. Fractals

Fractals are geometric structures with self-similarity at different scales. In mathematical terms, a fractal is a complex pattern formed by repeating a simple process.

Fractals find applications in image compression, terrain modeling, and the study of irregular structures. In image compression, fractal-based algorithms can represent complex images more efficiently, while in terrain modeling, fractals help simulate realistic landscapes. [7], [10]–[12]

Multifractal analysis is significant because it allows researchers to go beyond traditional analyses that assume uniform scaling behavior. It provides a more nuanced understanding of complex systems and their underlying structures, enabling better modeling, prediction, and decision-making in various scientific and applied domains. [7], [13]

In conclusion, multifractal analysis is a powerful tool for exploring the intricate and multifaceted nature of complex data sets, contributing to advancements in fields ranging from signal processing to finance. The ability to capture varying degrees of self-similarity across different scales makes multifractal analysis a valuable approach in understanding the rich structures present in diverse datasets.

3.4.3. Entropy and Mutual Information

Entropy measures the uncertainty or disorder in a system, while mutual information quantifies the dependence between two random variables. Entropy is a fundamental concept in information theory that measures the uncertainty or disorder in a system. It quantifies the randomness or

unpredictability of a system and is typically measured in bits (or shannons), representing the amount of information needed to encode a single symbol or message.

Entropy plays a crucial role in various fields, including information theory, image processing, and machine learning. In information theory, entropy is used to quantify the amount of information in a message or signal. In image processing, entropy is employed to measure the complexity of an image for tasks like filtering and segmentation. In machine learning, entropy is utilized for feature selection and decision tree construction.

There are several different types of entropy, each tailored to specific applications and scenarios. Here's a brief overview of some key types:

1. **Shannon's Entropy:** This is the most widely used and fundamental form of entropy, applicable to discrete random variables. It measures the average uncertainty involved in predicting the outcome of an event based on a probability distribution.
2. **Rényi's Entropy:** This generalization of Shannon's entropy extends the concept to non-negative real numbers and is particularly useful in situations where the cost of errors varies.
3. **Havrda-Charvat Entropy:** This family of entropies encompasses both Shannon's and Rényi's entropies, offering a broader range of choices for measuring uncertainty.
4. **Conditional Entropy:** This type of entropy measures the uncertainty remaining about one random variable given the knowledge of another variable. It quantifies the amount of information gained by knowing the value of one variable to reduce the uncertainty about the other.
5. **Joint Entropy:** This entropy measures the combined uncertainty of two or more random variables. It represents the total uncertainty present in the system considering all the variables together.

Mutual Information

Mutual information is a closely related concept to entropy that quantifies the dependence or correlation between two random variables. It measures how much knowing the value of one

variable reduces the uncertainty about the value of the other variable. Mutual information is also typically measured in bits.

Mutual information finds applications in various fields, including information theory, image registration, and feature selection in machine learning. In information theory, mutual information is used to measure the amount of information that one signal conveys about another signal. In image registration, mutual information is employed to align two images by maximizing their mutual information. In feature selection in machine learning, mutual information is utilized to select the most informative features for a given task.

Just like entropy, there are different types of mutual information, each tailored to specific scenarios and applications. Here are some of the main types:

1. **Shannon's Mutual Information:** This is the most common form of mutual information, applicable to discrete random variables. It measures the reduction in uncertainty about one variable achieved by knowing the value of another variable.
2. **Rényi's Mutual Information:** This generalization of Shannon's mutual information extends the concept to non-negative real numbers and is particularly useful in situations where the cost of errors varies.
3. **Total Correlation:** This type of mutual information provides a normalized measure of dependence between two random variables, ranging from 0 for complete independence to 1 for perfect correlation.
4. **Conditional Mutual Information:** This entropy measures the reduction in uncertainty about one variable given the knowledge of another variable, while conditioning on a third variable. It quantifies the additional information gained by knowing the value of one variable beyond what is already known from another variable.
5. **Joint Mutual Information:** This entropy measures the combined dependence or correlation among three or more random variables. It represents the total reduction in uncertainty achieved by knowing the values of all the variables compared to knowing only individual variables.

By understanding and employing these different types of entropies and mutual information, we can effectively analyze and model various systems, optimize data transmission and storage, and enhance the performance of machine learning algorithms. Entropy and mutual information are used in information theory, image processing, and machine learning. In information theory, entropy is used to quantify the amount of information in a message, while mutual information is employed in image registration and feature selection in machine learning. [14]

Table 1. The table summarizing the key differences between entropy and mutual information:

Feature	Entropy	Mutual Information
Definition	Measures the uncertainty or disorder in a system	Measures the dependence between two random variables
Unit of measurement	Bits	Bits
Applications	Information theory, image processing, machine learning	Information theory, image registration, feature selection in machine learning

3.5. Classification

Classification is a process of categorizing input data into predefined classes or categories based on certain features.

Classification techniques, such as Support Vector Machines (SVM), Decision Trees, Random Forests, and Artificial Neural Networks (ANN), are widely used in image recognition, spam filtering, and medical diagnosis. SVM excels in binary classification tasks, Decision Trees provide interpretable decision rules, Random Forests enhance decision tree robustness, and ANNs model complex relationships in large datasets. [15], [16]

3.5.1. Support Vector Machines (SVM)

Support Vector Machines (SVM) is a supervised machine learning algorithm used for classification and regression tasks. SVM works by finding the hyperplane that best separates data points into different classes in feature space. It is particularly effective in high-dimensional spaces and is versatile in handling both linear and non-linear relationships through the use of kernel functions.

SVM has applications in various domains, such as image classification, handwriting recognition, and bioinformatics. In image classification, SVM can be employed to distinguish between different objects or scenes within an image. Handwriting recognition systems use SVM to classify handwritten characters, and in bioinformatics, SVM aids in the identification of biological patterns in genetic data.

3.5.2. Decision Trees

A Decision Tree is a tree-like model where each node represents a decision or test on a specific feature, leading to branches that represent the outcomes of the decision. Decision Trees are widely used for classification and regression tasks, offering a clear and interpretable structure.

Decision Trees find applications in finance for credit scoring, in medicine for disease diagnosis, and in manufacturing for quality control. In credit scoring, Decision Trees help assess the creditworthiness of individuals based on various factors. In medicine, they assist in identifying diseases by analyzing patient data, and in manufacturing, they aid in classifying products based on quality attributes.

3.5.3. Random Forest

Random Forest is an ensemble learning method that constructs a multitude of Decision Trees during training and outputs the mode of the classes for classification tasks or the mean prediction for regression tasks. It mitigates overfitting and improves accuracy by combining the predictions of multiple trees.

Random Forest is widely used in finance for fraud detection, in ecology for species classification, and in remote sensing for land cover classification. In fraud detection, Random Forest can identify anomalous patterns in financial transactions. In ecology, it aids in the classification of species based on environmental data, and in remote sensing, it helps analyze satellite imagery for land cover mapping.

3.5.4 Artificial Neural Networks (ANN)

Artificial Neural Networks (ANN) are computational models inspired by the structure and function of biological neural networks. ANNs consist of interconnected nodes organized in layers,

including input, hidden, and output layers. They are capable of learning complex patterns and relationships from data.

ANNs find applications in image and speech recognition, natural language processing, and autonomous systems. In image recognition, ANNs can identify objects within images, while in natural language processing, they aid in language translation and sentiment analysis. Autonomous systems, such as self-driving cars, use ANNs for decision-making based on sensor inputs. [17]–[19]

3.6 Statistical Analysis

Statistical analysis involves a range of methods for collecting, analyzing, interpreting, presenting, and organizing data to extract meaningful insights. It provides a foundation for making informed decisions in the presence of uncertainty.

Statistical analysis is crucial in fields like economics for market research, in social sciences for studying human behavior, and in epidemiology for analyzing disease trends. In market research, statistical techniques help analyze consumer preferences and market trends. In social sciences, statistical methods assist in understanding patterns of human behavior, and in epidemiology, they are essential for studying the spread and impact of diseases.

3.6.1. Test of Significance using ANOVA

Analysis of Variance (ANOVA) is a statistical method used to assess whether the means of two or more groups are statistically different from each other. It decomposes the total variance in the data into variance between groups and variance within groups, allowing researchers to determine if group means are significantly different.

ANOVA is widely applied in experimental research, clinical trials, and quality control. In experimental research, ANOVA helps compare the effects of different treatments or conditions. In clinical trials, it is used to assess the impact of interventions on health outcomes, and in quality control, ANOVA aids in ensuring consistency and reliability in manufacturing processes.

3.6.2. The Friedman tests for level of significance

The Friedman test is a non-parametric statistical test used to determine if there are statistically significant differences between multiple related groups. It is an extension of the Wilcoxon signed-rank test for more than two groups. The test is particularly useful when the data do not meet the assumptions of normal distribution required for parametric tests. The Friedman test finds applications in various fields such as psychology, medicine, and environmental science. In psychology, it might be used to compare the performance of participants across different experimental conditions. In medicine, it could be employed to assess the effectiveness of various treatments in a clinical trial. In environmental science, it might be used to compare pollutant levels across different regions.

In summary, these advanced signal processing and analysis techniques, coupled with powerful classification algorithms and robust statistical methods, provide a comprehensive toolkit for researchers and practitioners in diverse fields. Their applications extend from understanding complex signal behaviors to making informed decisions based on data-driven insights. The continuous development and integration of these techniques contribute to the advancement of science, technology, and decision-making processes in various domains. The detailed mathematical description of the above tools and techniques is beyond the scope of this work, so not presented here to avoid complexity and overflow of information. Although it is encouraged to go for further reading, to have a good grasp of these advance tools and techniques for signal processing and analysis. The reference provided at the end of this chapter can provide you with enough detailed mathematical foundations as required. These mighty tools were used with their improvised versions for the research work undertaken herewith. The subsequent use of these set of tools and techniques can be found in next chapters dealing with the experimental validation of the developed biomedical signal analysis models with scope for automation and computer aided diagnosis.

References

[1] ‘Nonlinear Biomedical Signal Processing, Fuzzy Logic, Neural Networks, and New Algorithms | IEEE eBooks | IEEE Xplore’. Accessed: Nov. 17, 2023. [Online]. Available: https://ieeexplore.ieee.org/book/5263178

[2] ‘Biomedical Signal Analysis | IEEE eBooks | IEEE Xplore’. Accessed: Nov. 17, 2023. [Online]. Available: https://ieeexplore.ieee.org/book/7111421

[3] R. Moore, S. Ezekiel, and E. Blasch, ‘Denoising one-dimensional signals with curvelets and contourlets’, in *NAECON 2014 - IEEE National Aerospace and Electronics Conference*, Jun. 2014, pp. 189–194. doi: 10.1109/NAECON.2014.7045801.

[4] ‘Time Frequency and Wavelets in Biomedical Signal Processing | IEEE eBooks | IEEE Xplore’. Accessed: Nov. 17, 2023. [Online]. Available: https://ieeexplore.ieee.org/book/5263548

[5] H.-Y. Lin, S.-Y. Liang, Y.-L. Ho, Y.-H. Lin, and H.-P. Ma, ‘Discrete-wavelet-transform-based noise removal and feature extraction for ECG signals’, *IRBM*, vol. 35, no. 6, pp. 351–361, Dec. 2014, doi: 10.1016/j.irbm.2014.10.004.

[6] K. Antanavičius *et al.*, ‘Nonlinear dynamics analysis of electrocardiograms for detection of coronary artery disease’, *Comput. Methods Programs Biomed.*, vol. 92, no. 2, pp. 198–204, Nov. 2008, doi: 10.1016/j.cmpb.2008.07.002.

[7] D. Jiao, Z. Wang, J. Li, F. Feng, and F. Hou, ‘The chaotic characteristics detection based on multifractal detrended fluctuation analysis of the elderly 12-lead ECG signals’, *Phys. Stat. Mech. Its Appl.*, vol. 540, p. 123234, Feb. 2020, doi: 10.1016/j.physa.2019.123234.

[8] V. Gupta, M. Mittal, and V. Mittal, ‘R-Peak Detection Using Chaos Analysis in Standard and Real Time ECG Databases’, *IRBM*, vol. 40, no. 6, pp. 341–354, Dec. 2019, doi: 10.1016/j.irbm.2019.10.001.

[9] Y. Li, F. Li, S. Lyu, M. Xu, and S. Wang, ‘Blind extraction of ECG signals based on similarity in the phase space’, *Chaos Solitons Fractals*, vol. 147, p. 110950, Jun. 2021, doi: 10.1016/j.chaos.2021.110950.

[10] S. Agrawal and A. Gupta, ‘Fractal and EMD based removal of baseline wander and powerline interference from ECG signals’, *Comput. Biol. Med.*, vol. 43, no. 11, pp. 1889–1899, Nov. 2013, doi: 10.1016/j.compbiomed.2013.07.030.

[11] H. M. C. Mary and D. Singh, ‘Fractal dimension of electrocardiogram: distinguishing healthy and heart-failure patients’, *J. Electrocardiol.*, vol. 46, no. 4, p. e21, Jul. 2013, doi: 10.1016/j.jelectrocard.2013.05.078.

[12] A. K. Mishra and S. Raghav, ‘Local fractal dimension based ECG arrhythmia classification’, *Biomed. Signal Process. Control*, vol. 5, no. 2, pp. 114–123, Apr. 2010, doi: 10.1016/j.bspc.2010.01.002.

[13] X. Yang, Z. Wang, A. He, and J. Wang, 'Identification of healthy and pathological heartbeat dynamics based on ECG-waveform using multifractal spectrum', *Phys. Stat. Mech. Its Appl.*, vol. 559, p. 125021, Dec. 2020, doi: 10.1016/j.physa.2020.125021.

[14] M. Zbili and S. Rama, 'A Quick and Easy Way to Estimate Entropy and Mutual Information for Neuroscience', *Front. Neuroinformatics*, vol. 15, 2021, Accessed: Nov. 17, 2023. [Online]. Available: https://www.frontiersin.org/articles/10.3389/fninf.2021.596443

[15] 'Neural Networks and Artificial Intelligence for Biomedical Engineering | IEEE eBooks | IEEE Xplore'. Accessed: Nov. 17, 2023. [Online]. Available: https://ieeexplore.ieee.org/book/5263228

[16] M. K. Moridani, M. Abdi Zadeh, and Z. Shahiazar Mazraeh, 'An Efficient Automated Algorithm for Distinguishing Normal and Abnormal ECG Signal', *IRBM*, vol. 40, no. 6, pp. 332–340, Dec. 2019, doi: 10.1016/j.irbm.2019.09.002.

[17] H. Qu, X. Gao, and L. Pang, 'Classification of mental workload based on multiple features of ECG signals', *Inform. Med. Unlocked*, vol. 24, p. 100575, Jan. 2021, doi: 10.1016/j.imu.2021.100575.

[18] A. R. Hassan and Md. A. Haque, 'An expert system for automated identification of obstructive sleep apnea from single-lead ECG using random under sampling boosting', *Neurocomputing*, vol. 235, pp. 122–130, Apr. 2017, doi: 10.1016/j.neucom.2016.12.062.

[19] Y. Hagiwara *et al.*, 'Computer-aided diagnosis of atrial fibrillation based on ECG Signals: A review', *Inf. Sci.*, vol. 467, pp. 99–114, Oct. 2018, doi: 10.1016/j.ins.2018.07.063.

Chapter 4 Experimental Design & Analysis

This chapter presents the results obtained through the utilization of the proposed method's architecture. It not only covers the various components of the suggested system architecture but also delves into the crucial methods and algorithms employed. The discussion offers an in-depth look into the implementation procedures, the process of experimentation, a meticulous analysis of the results, and an exploration of how features are extracted, and images are retrieved in the context of the proposed model. This comprehensive discussion provides a holistic view of the model's structure and operation, highlighting the intricacies of its design and performance.

Cognitive Neurodynamic study of the whole brain, often conducted using Electroencephalography (EEG), is a multidisciplinary field of research that seeks to unravel the intricate workings of the human brain during cognitive processes. EEG is a non-invasive technique that measures the electrical activity of the brain through electrodes placed on the scalp. This method provides real-time information about the brain's electrical patterns, allowing researchers to investigate the neural dynamics associated with various cognitive functions, such as perception, attention, memory, and decision-making. By examining the temporal and spatial patterns of neural activity, researchers can gain insights into how different brain regions communicate and coordinate to support these cognitive processes. This approach has applications in neuroscience, psychology, and clinical fields, enabling a better understanding of the neural basis of cognition and potential implications for diagnosing and treating neurological and psychiatric disorders.

Cardiovascular dynamics, as assessed through the electrocardiogram (ECG), offer a vital window into the functioning of the human heart. The ECG is a non-invasive diagnostic tool that records the electrical activity of the heart over time, reflecting the depolarization and repolarization of cardiac muscle cells. This information provides valuable insights into various aspects of cardiovascular health, including heart rate, rhythm, and the presence of arrhythmias. Moreover, the ECG can pinpoint abnormalities in the heart's structure and conduction system, aiding in the diagnosis of conditions such as myocardial infarctions, atrial fibrillation, and ventricular hypertrophy. Interpreting ECG waveforms and intervals, healthcare professionals can make informed decisions regarding patient care, from assessing overall heart function to guiding treatment strategies, making it an indispensable tool in the realm of cardiovascular medicine.

Electromyography (EMG) is a valuable technique used to study the muscular dynamics of the human arm and understand its neuromuscular functioning. EMG involves the measurement and analysis of electrical activity produced by the contraction of skeletal muscles. In the human arm, this method allows researchers and clinicians to assess the activity of individual muscles and muscle groups during various movements and tasks. By placing electrodes on the skin or directly into the muscle tissue, EMG can provide insights into muscle activation patterns, the timing and coordination of muscle contractions, and the level of muscle force exerted. This information is essential for the diagnosis of neuromuscular disorders, the optimization of rehabilitation protocols, and the enhancement of athletic performance. Additionally, EMG research plays a crucial role in understanding the complex interplay between the nervous system and the musculature, shedding light on the intricate dynamics of human arm movement and function.

Cortico-muscular coherence, as observed in the human brain while lifting loads, refers to the synchronization and coordination between the cortical activity in the brain and the muscular activity in the arm, as measured by electroencephalography (EEG) and electromyography (EMG) respectively. This phenomenon provides valuable insights into the neural control of voluntary movements, particularly during tasks that involve lifting and manipulating objects. When an individual engages in lifting loads, the brain's motor cortex generates commands to activate specific muscle groups in the arm, and this intricate coordination is reflected in the coherence patterns between EEG signals from the brain and EMG signals from the muscles. Studying cortico-muscular coherence can help researchers and clinicians better understand the neural mechanisms underlying motor control, which is essential for tasks like lifting weights, and may have implications for rehabilitation and the development of advanced prosthetic devices that aim to restore natural movements by interfacing with the human brain.

Support vector machines (SVMs) have emerged as a promising tool for time series analysis, particularly in the context of COVID-19 prediction. SVMs are supervised learning algorithms that excel at identifying patterns and relationships in complex data sets, making them well-suited for analyzing the dynamic nature of COVID-19 transmission patterns. One of the key advantages of SVMs for COVID-19 prediction lies in their ability to handle nonlinear relationships between variables. Unlike traditional time series models that assume linear relationships, SVMs can effectively capture the intricate and often non-linear dynamics of COVID-19 spread. This capability is crucial for making accurate predictions in the face of the ever-evolving nature of the

pandemic. Moreover, SVMs offer robustness to outliers and noise, a common challenge in real-world time series data. COVID-19 data is often subject to fluctuations and inconsistencies due to reporting delays, testing capacity limitations, and other factors. SVMs' ability to filter out outliers and focus on the underlying patterns ensures that predictions remain reliable despite these challenges.

In addition to their technical strengths, SVMs provide flexibility in incorporating various factors that influence COVID-19 transmission. Researchers can incorporate data on population demographics, mobility patterns, public health interventions, and vaccination rates into SVM models to gain a more comprehensive understanding of the factors driving COVID-19 spread. This holistic approach leads to more informed and accurate predictions. The application of SVMs for COVID-19 prediction has demonstrated promising results in various studies. Researchers have successfully employed SVMs to forecast short-term and long-term trends in COVID-19 cases, hospitalizations, and fatalities. These predictions have proven valuable for informing public health decisions, resource allocation, and risk assessment strategies. As the COVID-19 pandemic continues to evolve, SVMs are likely to play an increasingly important role in predicting future trends and informing effective public health responses. Their ability to capture nonlinear relationships, handle outliers, and incorporate diverse factors makes them a powerful tool for time series analysis in the context of COVID-19.

4.1. A Novel Methodology to study the Cognitive Load Induced EEG Complexity Changes: Chaos, Fractal and Entropy based approach

The below section is published in the journal Biomedical Signal Processing and Control, Elsevier, which deals with Dynamic Systems Theory (DST) to provide both the conceptual framework and literal description of the underlying complexity dynamics associated with human cognition, specifically during information processing of the brain under the effect of an external stimuli.

To study the complexity changes during cognitive loading of the brain using Largest Lyapunov Exponent (LLE), Higuchi Fractal Dimension (HFD) and Sample Entropy (SampEn) as a multiparametric signature of cognitive processing. The proposed methodology demonstrates joint Time-Space representation of the various Brain Rhythms under four different classes of Cognitive Tasks (Emotion, Focus, Memory and Problem Solving) given to four subjects. The raw EEG signal is acquired using a 19 channel EEG machine, denoised using Wavelet packet decomposition technique. Brain waves are extracted using the scalogram plot. The parameters are calculated for each channel over a 2 min analysis window sliding through the whole length. These parameters were able to classify between different cognitive states, such as Emotion, Focus, Memory and Problem Solving with an accuracy of 99%.

Previous works haven't addressed complexity changes during cognitive processing using DST. Earlier studies explain average topographical map of the brain for a fixed time window whereas, we have presented the topographical map over a customizable fixed time sliding window. The cubic representation of the brain map containing non-linear parameters can prove to be a significant visualization tool for monitoring effects of cognitive loading using DST proponents as biomarker.

4.1.1. Introduction

Human cognition generally involves brain processes such as attention, creation of knowledge, memory and working memory, judgement and evaluation, reasoning and computation, problem solving and decision making. It is to note, that many of the most influential findings in neuroscience have been understood within the functional context of cognitive theory. In this

context it can be said according to [1] cognitive neuroscience serves as a pathway to link the latent cognitive processes with the neural mechanisms that generate them. Measures of cognitive load is highly important considering the nature of work, as it affects those working in a high risk and complex environment. In a recent study conducted by [2] measured the individual and overall cognitive load of the surgical team while performing surgical tasks using inter-beat intervals (HRV). Studies conducted by [3] revealed that the Electroencephalogram (EEG) frequency bands and activated brain regions that contribute to cognitive load differed depending on the learning state. Differences in EEG frequency bands at specific locations of the brain during cognitive loading while performing Human Computer Interaction based tasks was also reported by [4]. An EEG based approach was also proposed in quantifying the spatiotemporal brain responses to the action of sensory stimuli using multivariate Temporal Response Function [5]. Measures of cognitive decline in individuals with psychopathic traits have been studied using EEG and many authors have reported that it has significant capability in deciphering the underlying neurodynamics [6]. The authors of the review on EEG microstates [7] had provided an overview on the available methods for analysis, interpretation and the functional behavioral and clinical correlates of EEG while investigating their spatial temporal dynamics associated with different cognitive states and neurological disorders. In the review we also found that several studies have further demonstrated that any perturbations on the mental processes associated with neurological conditions manifest as changes in the temporal dynamics of specific microstates [8] [9]. These studies suggest that there is a need for methods and techniques that could detect the cognitive processes occurring inside the brain using non-invasive scalp EEG. The electrical activity during information processing by the brain is altogether an extremely complex behaving system with strong non-linear and dynamic properties. The dynamic systems theory has been applied to find both the conceptual framework and as a literal description of a dynamic system, associated with human cognition [10].

EEG is reliable and one of the most sensitive indicator of brain functions to assess mental workload due to cognitive processing [11].The quantification of the complexity of the EEG signal is essential as it provides us an insight into the mechanism and characteristic features in order to advance our understanding of the brain functions [12]. Non-linear parameters are very effective indicators in studying the event related complexity changes in the functional areas of the brain [13]. It is to note

that, Non-linear parameters are widely used for varied neurophysiological studies and applications using EEG signal [14] [15].

The complexity and non-stationarity of the EEG signal, makes it a challenging task to acquire, process and analyze. Substantial information about the neurophysiological conditions in the brain can be obtained, when one gives proper emphasis on data processing for feature extraction. Since data processing involves lots of redundant data reduction and transformations, one should be careful enough in choosing the suitable methodology to minimize information loss. Some of the EEG data processing techniques commonly used are discussed in the works of [16] [17] [18]. The authors in previously reported studies have looked for the changes in temporal dynamics of EEG signal under moderate to rigorous mental stimulation using proponents of non-linear discrete dynamical systems. The brain in most of these cases have been seen as a nested network of coupled dynamical systems that maintain spatial and temporal dynamics which can be labeled through nonlinear biomarkers of EEG signal [19] [20]. Most of the studies, to the best knowledge of the authors of this article, calculated the non-linear dynamical parameters over the entire range of the signal, but none of them showed the exact variation of these parameters with time. The joint time space representation may help us in understanding the variation of specific spatial information of the brain functions with time.

It is a well-known fact that the cognitive processing of human brain is chaotic in nature and hence EEG signals also exhibits chaotic characteristics. In dynamic systems no single factor is more important than any other, so it is illogical to consider any given factor in isolation. Proponents of DST emphasize an appreciation for mutual, bidirectional dependencies between brain and behavior. Changes in brain complexity have been reported in pathological states as well as in normal cognition [21]. So, attempts have been made in this work to explain the variation of complexity with time during cognitive loading of the brain using Chaos, Fractal Dimension and Sample Entropy as proponents of dynamical systems theory. 2-D spatiotemporal representation of complexity changes of continuous long duration (14 to 34 minutes) EEG signals collected during cognitive loading of the brain is presented here. The dynamical changes occurring at each microstate is captured by the non-linear parameters and the overall changes pre, during and post application of the stimulus is shown as the variation over time.

This paper presents a robust wavelet-based methodology in EEG signal acquisition and denoising using Wavelet Packet Decomposition. The denoised signal is then decomposed into different scales to extract the specific brain rhythms. The specific brain rhythms viz. beta, alpha, theta and delta are used as signals to calculate the Largest Lyapunov Exponent (LLE), Higuchis' Fractal Dimension (HFD) and Sample Entropy (SampEn) over an analysis window of 2 minutes. The variation of these non-linear parameters with time during cognitive loading of the brain is shown in the form of topographical representation. The four cognitive tasks taken into consideration are that of Focus, Emotion Recognition, Problem Solving and Working Memory of four different subjects. The overall methodology to do so is presented in detail in the preceding sections. The next section discusses about the methodology and moves over to results and discussion and ends with a conclusion of complexity variation during cognitive loading of the brain using DST proponents as biomarkers. The prospective of the above method for classification is also shown as scope of future work.

4.1.2. Methodology

The methodology proposed here is basically an implementation of the non-linear time series analysis techniques to detect the variation in complexity during cognitive loading of the brain [22]. To study the effects on Non-linear characteristics of EEG signal acquired during application of cognitive stimulus to the brain., a signal processing approach is followed starting from design of experiments to data acquisition and analysis described in the preceding section.

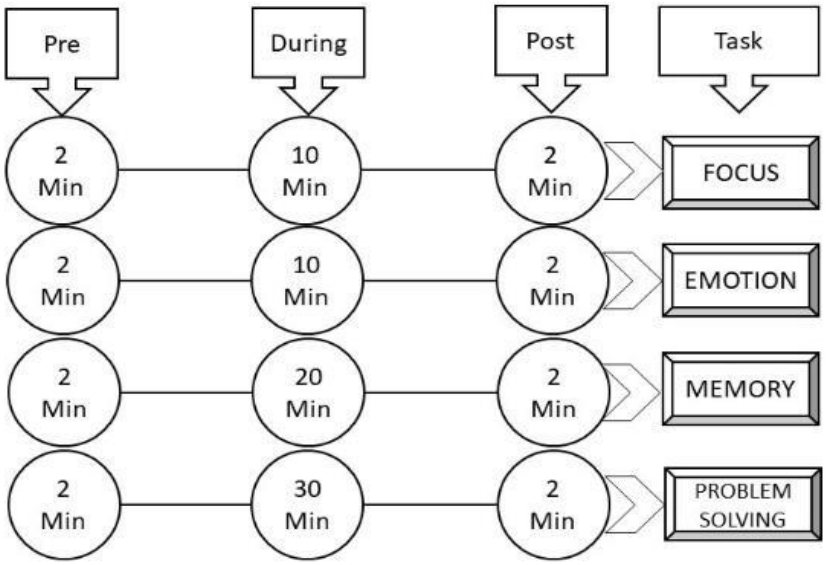

Fig. 1. Experimental protocol adopted for different task-based EEG sessions. In Pre and Post Sessions the subject was in normal relaxed condition. The subjects performed the specific task within a given time limit as shown above

Design of Experiment

This part explains about the manner in which a researcher organizes the manipulations and measurements of an EEG experiment. An inadequate EEG experiment design will lead to a lot of problems for a researcher since it could either fail to address the defined hypothesis or make things very difficult to interpret. In our experiment, we conducted continuous EEG signal data acquisition from a 19 channel EEG machine during four different cognitive tasks on four different subjects. Four different categories were selected from mobile phone-based brain training game, which are both scientifically designed based on the principles of cognitive neuroscience and simple fun to play, known as PEAK (http://www.peak.net/). The four categories under our study are selected on the basis of brain skills in Focus, Problem Solving, Memory and Emotion Recognition. Each subject was given the task for 10 repeated trials i.e. for example if one task takes 1 min time to complete, the subject was asked to perform the task continuously for 10 times or 10 minutes. This was done to ensure that the stimulus is strong enough to leave its footprint on the EEG signal response for better interpretation. Each EEG session was designed as shown in the Fig.1 with eyes open condition. The subjects were healthy male participants within the age group of 22 to 24

years, all pursuing masters in engineering. They were well aware about the experiment protocol and have some prior knowledge about EEG experiments. They were asked to choose their own skill training exercise based on their learning ability as provided in the mobile interface of the PEAK app. To assess the level of performance of each individual in completing their respective tasks, the scores were noted for each trial and separately plotted for ready reference as shown in Fig.3. The qualitative assessment about the amount of cognitive load the brain has to bear in executing the task has been carried out by marking on NASA Task Load Index sheet. Each subject was given the NASA Task Load Index sheet to mark, the amount of difficulty they faced in execution of the task, on a 10-point scale as shown in Fig.4 Screenshots of the mobile gaming interface are shown in Fig.2. for Focus, Memory, Problem Solving and Emotion Recognition.

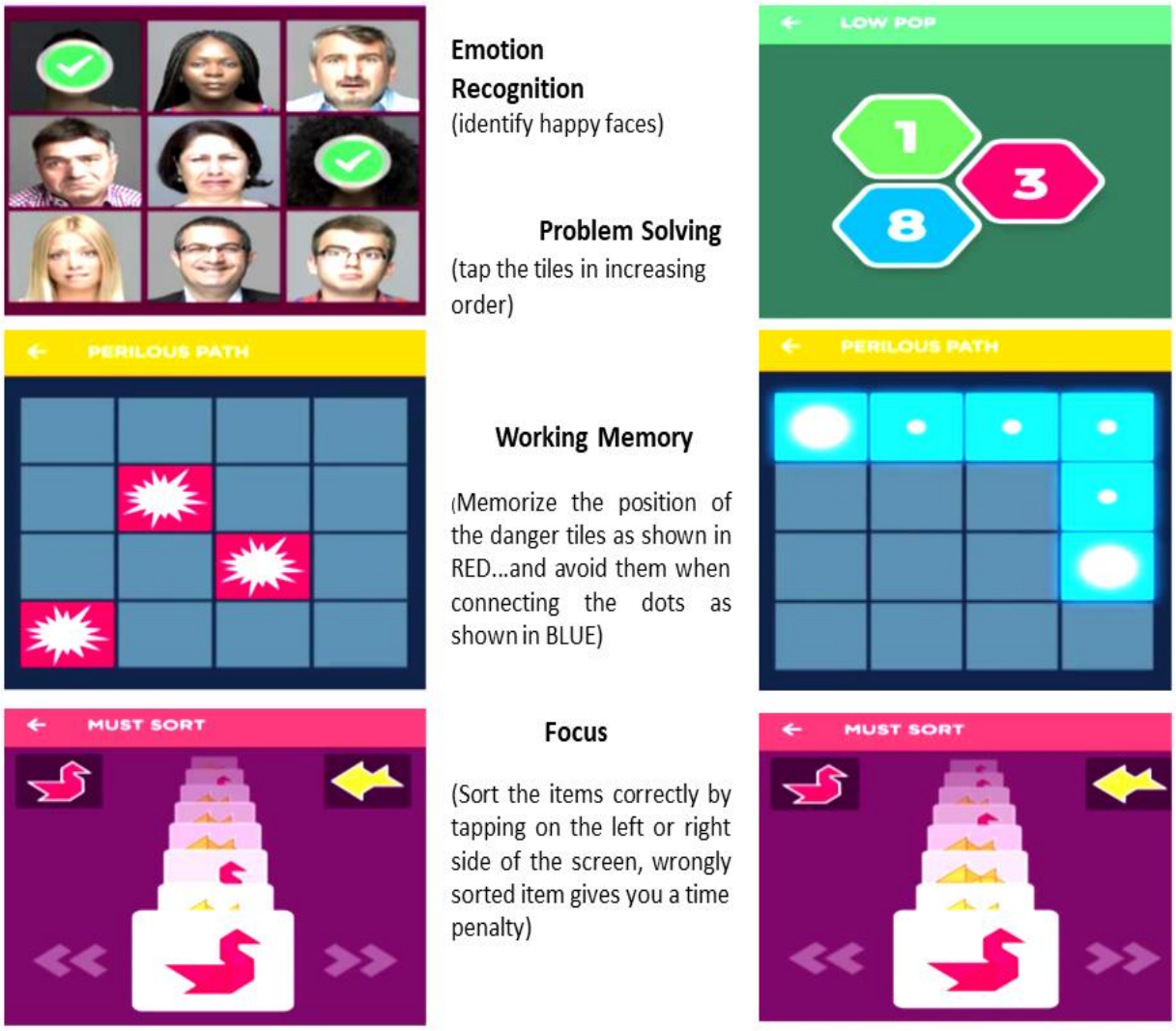

Fig. 2. Screenshots of the brain training application (PEAK), which was chosen as the cognitive task for the subjects under study. The Emotion recognition task was to identify happy faces among different facial expressions. The Problem-Solving task was to tap the polygonal shaped tiles with different colors having number in arbitrary order, and the subject needs to tap the tiles in increasing order within the given time limit. The second row of the Fig. matrix is about the Working memory task, where the subject is shown an image as shown in the left side. Red marks on the 3 different arbitrary positions in the grid are danger positions and then another image with two large white dots are shown for the subject to find a safe way to connect the dots avoiding the red ones. The last row is about Focus task, here the subject is asked to sort images by tapping left or right according to the given figures pre-determined sides. That is the red duck needs to be sent to the left and the Yellow Fish towards right.

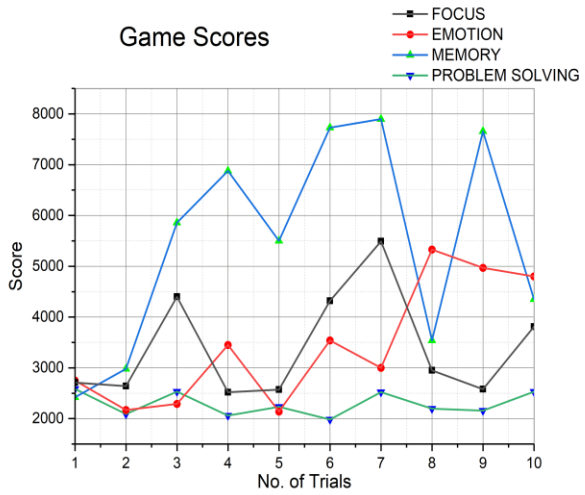

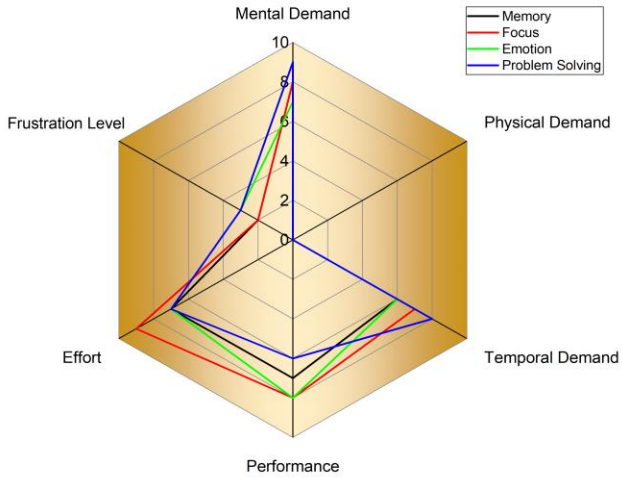

Fig. 3. The game scores of each individual with different number of trials Fig. 4. The Task Complexity chart

EEG signal acquisition

The electrical activity at the neuronal level can be traced and recorded from electrodes placed at specific positions on the scalp, which is familiarly known as Electroencephalogram or EEG. EEG signals are highly random, non-gaussian, non-stationary and non-linear. The cortical nerve cell inhibitory and excitatory postsynaptic potentials summate together to generate the EEG signals which are in turn extended to the scalp surface. The EEG signals have high temporal resolution and smaller spatial resolution.

EEG signal was collected from scalp electrodes placed at specific locations over the scalp covering the different functional areas of the brain. Electrodes were placed in accordance to the standardized international 10-20 system for EEG electrode placement (Fp1,Fp2,F3,F4,Fz,F7,F8,T3,T4,T5,T6,C3,C4,CZ,P3,P4,Pz,O1,O2). The spatial arrangement of the electrodes over the surface of the scalp is called montage, the electrical map as obtained from the referential montage (unipolar with common average reference) is used in our study [23]. The device used for EEG signal acquisition is a medical grade 19 channel PC based EEG data acquisition module (make: RMS Maximus®, India Pvt. Ltd). The signals are stored at 256 Hz sampling rate.

The impedance checks (<50kΩ) between the scalp and electrode surface was done to ensure good contact of the electrodes so as to reduce the chances of artefacts contaminating the EEG signal

response. The subjects were asked to sit in comfortable positions with restricted limb movements and were only made to focus in execution of the tasks, which required just the application of fingers. The signal acquisition was done while observing the band pass filtered (0.5Hz to 35Hz) output signal and an inbuilt EMG artefact removal filter (make: RMS Maximus®, India Pvt. Ltd) is applied to reduce the high frequency surface EMG contaminations. The mathematical details of artefact removal procedure at this stage are beyond the scope of this paper since we have used medical grade inbuilt digital filtering module provided with the software package. The artefact removal and feature extraction are further in this study with detailed explanation. The machine settings were as follows:**1.** Montage: Ref-Channel **2.** Filter (LF:0.5Hz to H.F: 35Hz, EMG Filter: ON, 50Hz Notch Filter: ON) **3.** Sweep: 30 mm/s **4.** Sensitivity: 20 µV/s. The continuous time series data of each channel w.r.t the common average reference is exported in **.csv** format for analysis in MATLAB®.

EEG signal processing

This section discusses about the signal processing methods adopted for representation of the fluctuations in the EEG signal response due to various events. Good number of studies have been performed using principal component analysis or independent component analysis (PCA/ICA) relating to removal of eye blink and muscle artefact from EEG signals [24] [25], but there remains a major concern in eliminating eye blinking and muscle artefacts without affecting the relevant EEG patterns. Thus, it is not ideal to directly apply PCA/ICA based methods for noise elimination, when prior knowledge about the EEG patters is not known. PCA and ICA have been reported as very good tool in case of feature extraction or dimensionality reduction of non-stationary physiological signals [26]. In EEG signal processing, Wavelet based methods have found a lot of attention in the recent decade primarily due to its ability to handle non-stationarity with significantly high computational efficiency [27] [28] [26].

In our case, we manually observed and applied Discrete Wavelet Transform based functions to preserve only those parts of the EEG signal that correlate well with the frequencies required to spot the changes due to cognitive loading of the brain. The signal is denoised using wavelet packet decomposition (WPD) technique to reduce the artefacts and make the signal ready for extraction of specific rhythms [29]. WPD is basically a generalized method of wavelet decomposition

techniques which provides a richer and robust signal analysis. The area of our interest is usually the low frequency oscillations which are supposed to carry information of the, cognitive load induced, changes occurring inside the brain. Selection of suitable wavelet and number of levels of decomposition is an important factor in denoising and extraction of sub-bands of EEG signal for further analysis.

The choice of wavelet and its order is chosen based on certain literature review on EEG signal denoising [27] [30]. The ideal choice of wavelet for our analysis was Daubechies'6^{th} order (Db6) having 6 vanishing moments out of the wavelet family comprising of Daubechies (Db), symlet (sym) and coiflet (coif). The level of decomposition for the WPD was set at 9. The level of decompositions was chosen based on the relation between level of decomposition and frequency estimate as shown in table 1. The thresholding techniques for decomposition used here is based on Shannon entropy to generate the frequency ordered coefficient matrix on analyzing the raw EEG signal using 1-D WPD technique. An optimized binary tree is selected for decomposition of raw EEG signals into different level. The depth of tree is actually the number of levels of decomposition as chosen for analysis.

Table1. The relation established between level of wavelet decomposition with Frequency is calculated as follows.

Level(N)	1	2	3	4	5	6	7	8	9
Freq($fs/2^N$) in Hz	128	64	32	16	8	4	2	1	0.5

The fluctuations occurring due to eye blinking and muscle artefacts are carefully observed and coefficient elimination was done at the relevant scales at different time instances. The coefficients of low frequency long range trends are preserved to obtain the specific features occurring due to

cognitive processing as shown in Fig.5 by thresholding the frequency ordered coefficients generated after WPD of the raw signal.

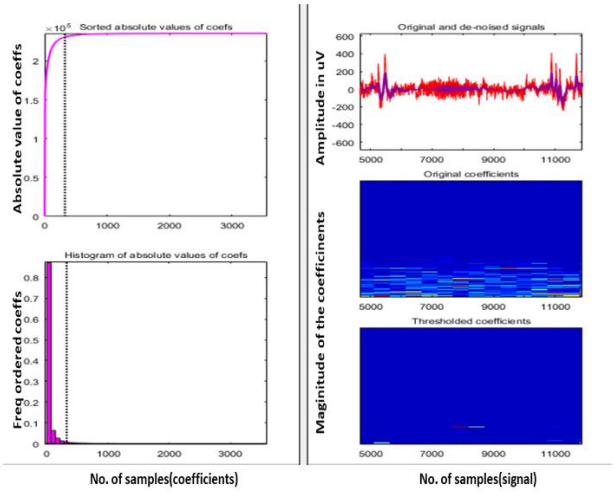

Fig. 5. WPD based denoising by coefficient thresholding

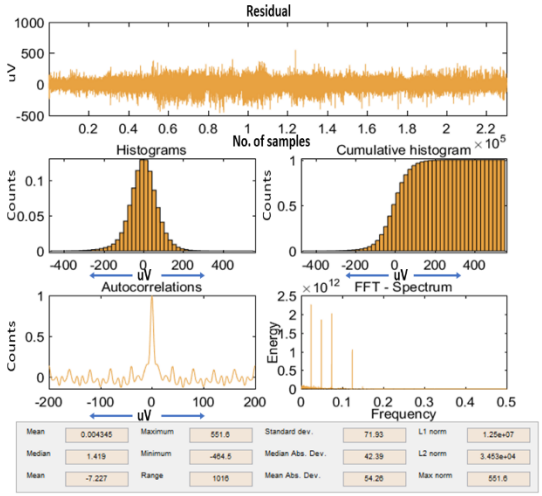

Fig. 6. Statistical measure of the residual of raw eeg signal

The Welch averaged periodogram power spectral density, based SNR and the respective band power of the signal in the range of 0.5 to 4 Hz, 4 to 8 Hz, 8 to 16 Hz and 13 to 30 Hz are calculated before and after denoising to ensure that the deterministic features in these bandwidths are increased after denoising. The residuals left after denoising is separately analyzed and found to be close correlates to white noise as shown in Fig.6. The denoised signals are considered as processed signals for further analysis as shown in Fig.7 in black color and the red one is the original signal.

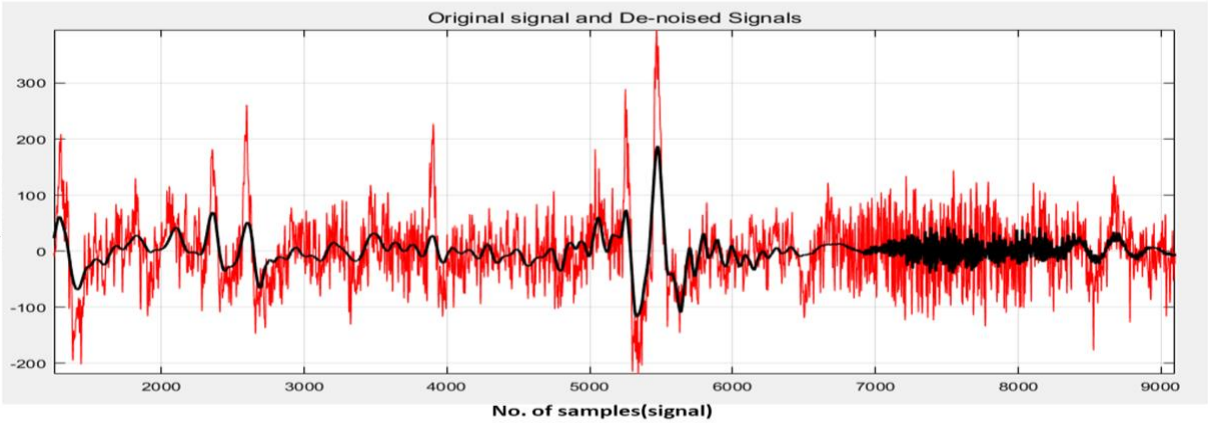

Fig. 7. A section of the denoised and raw EEG signal is shown after denoising using 1-D wavelet packet decomposition.

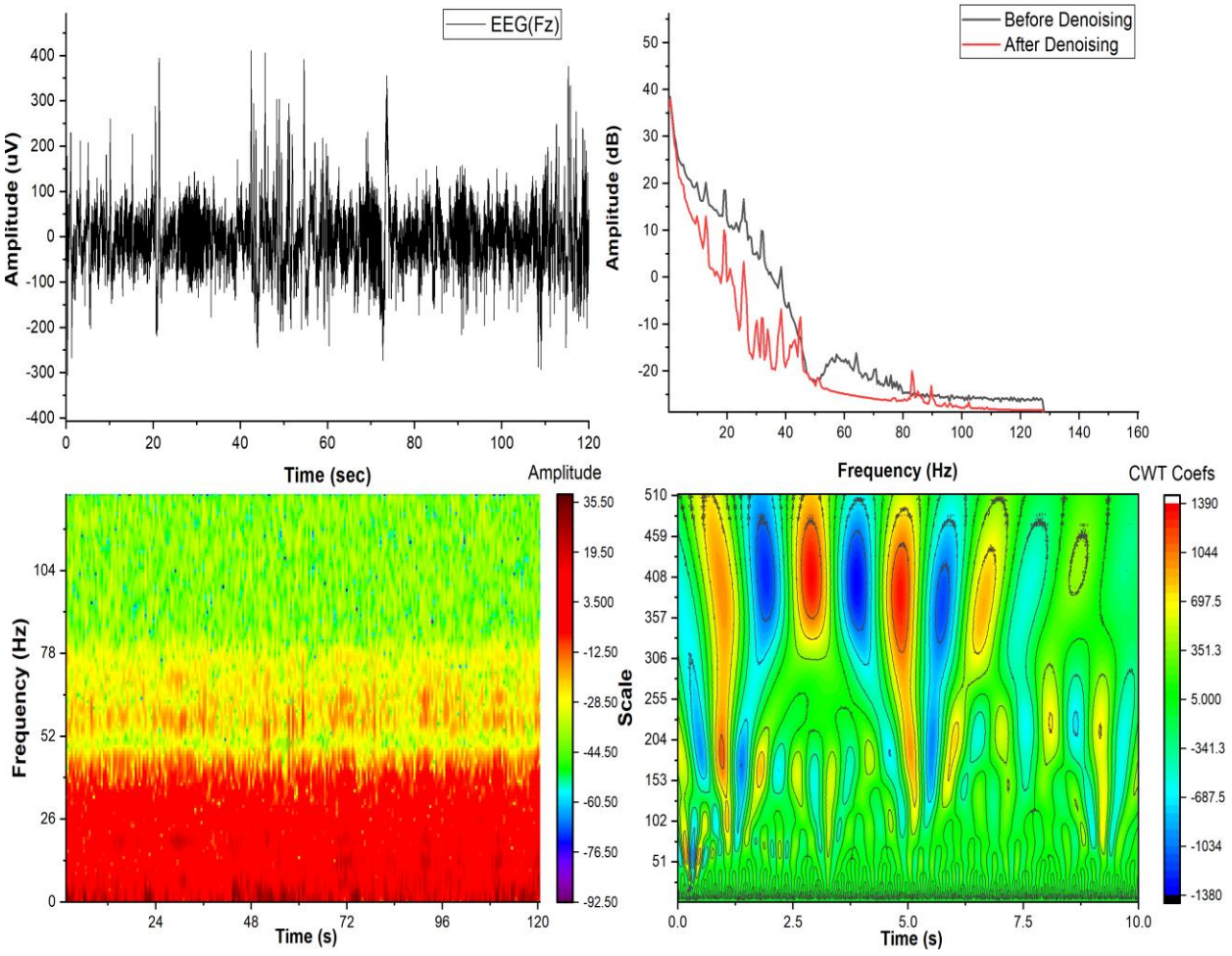

Fig. 8. The characteristics of EEG signal (Fz) is shown as Time-Amplitude, Frequency-Power, Time-Frequency and Time-Scale representation. In joint Time Frequency representation, we can see most of the energy band is in 0-30 Hz range shown in Red, the gamma activity can also be seen in yellow. [In CWT scalogram plot only 10s of the EEG is shown to present the scale invariant pattern of EEG and to locate the scales where the artefacts appear]

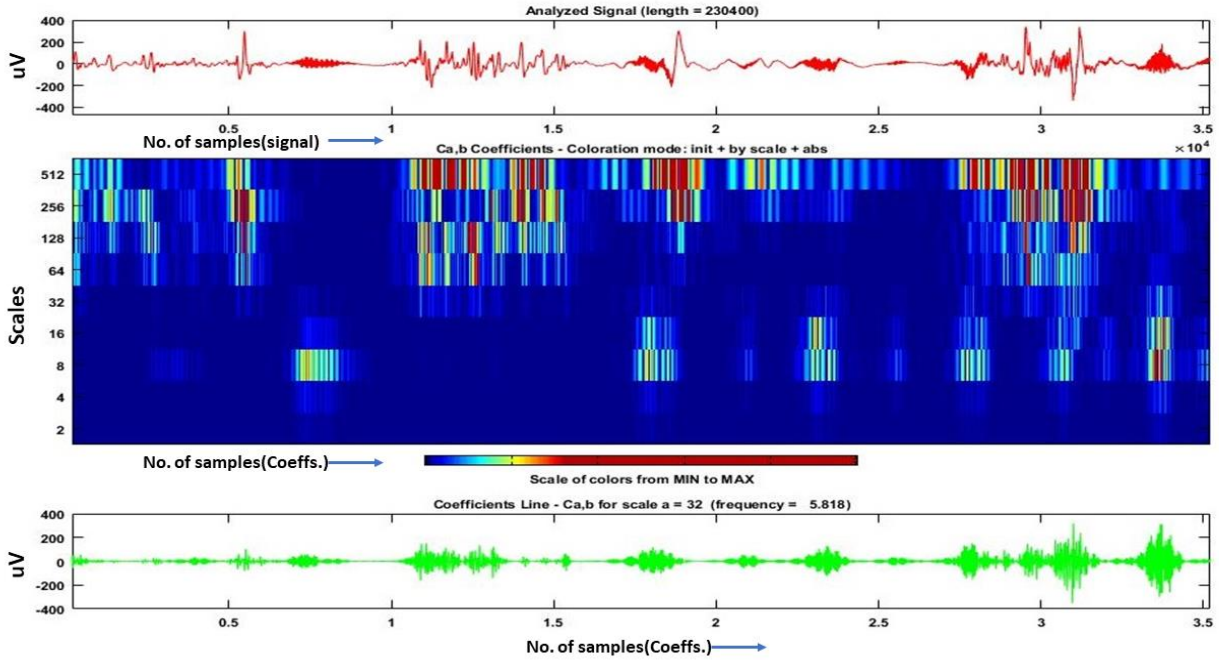

Fig. 9. Cwt scalogram plot used to extract low frequency brainwaves beta, alpha, theta and delta.

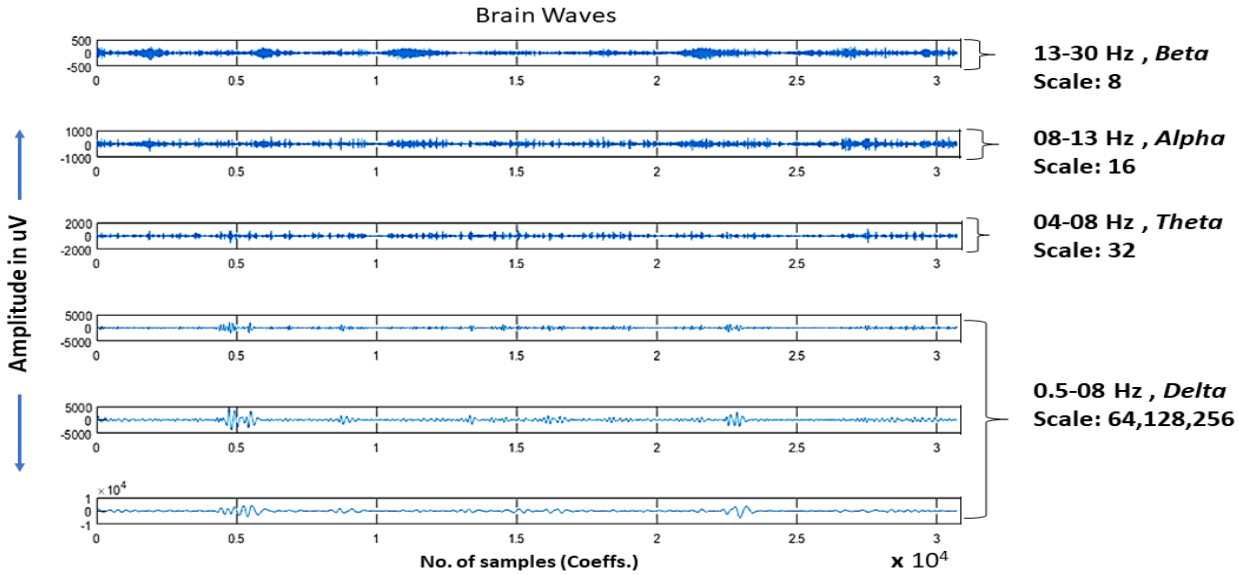

Fig. 10. Brainwaves after CWT extraction using dyadic scaling (8:256) for the frequency range 0.5-30Hz.

Denoised signal as obtained from WPD analysis is subjected to Continuous Wavelet Transforms to generate the scalogram or time scale representation of the amplitude of the denoised EEG signal. Db6 wavelet is used to generate the scalogram on a dyadic scale. The coefficients of the CWT at

different scales contain the relevant frequency bands as shown in Fig.9 and Fig.10. Using the scale to frequency conversion function in Matlab® by specifying the wavelet type and the sampling period, extraction of the low frequency brain waves was achieved. The extracted brainwave signals are free from the artefacts and are relatively smoother than the raw EEG signal as shown in Fig.10.

Here we can see that in the delta band we have three signals. Since, changes in fluctuations of the EEG wave occurs in low frequency band while cognitive processing, so we have preserved the coefficients at higher scales. These set of six signals are further analyzed separately for all the chosen non-linear dynamical parameters to detect the changes. Although to eliminate confusion, the average of parameters of all the three delta waves is presented in the results. The schematic representation of the overall methodology is presented in Fig.11. One EEG channel is selected and all parameters relevant to the study are separately obtained for topographic representation of the behavior of the underlying system dynamics.

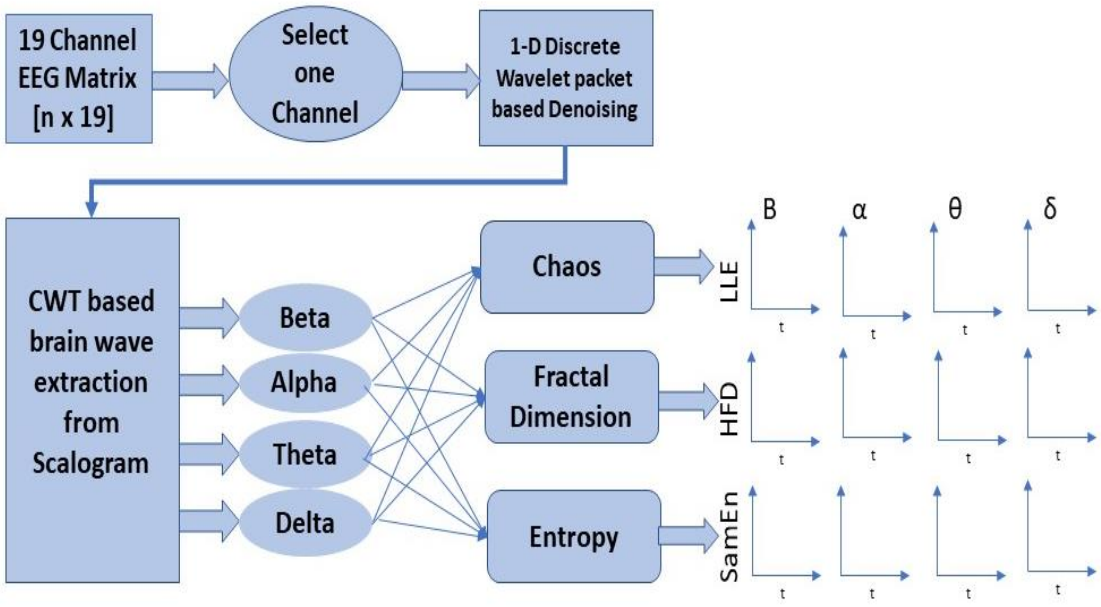

Fig. 11. The schematic representation of the proposed methodology

Data Analysis

There are various events such as sleep, epilepsy, reflexology, drugs, diabetes, meditation, music, noise/artefacts, etc. which have their influence on the EEG signal. The event in our case is the

cognitive load applied to the brain while performing tasks, which are designed by expert team of Peak® brain training application (www.peak.net), to specifically stimulate the Focus, Working Memory, Problem Solving and Emotion Recognition patterns of the brain. Biological time series analysis has long been recognized in the area of non-linear analysis methods. The non-linear dynamical techniques based on the concepts of Chaos, Fractals and Entropy has been applied to many areas of medicine and biology [31] [32] [33]. Previous studies have proposed to detect the hidden important dynamical properties of the physiological phenomenon based on the features of dynamical systems theory [34] [35]. A lot of researchers agree to the point that, completely relying on any one non-linear measure often proves to be ambiguous and hence it is advisable to test with two or more parameters since every one of them provides a different information about the system under study [36] [37]. EEG signals have very high temporal resolution and low spatial information and dynamical systems theory is very much advisable in case of such a non-stationary signal with high degree of non-linearity. The cognitive processes occurring inside the brain may be represented as non-linear discrete dynamical system which is obtained as EEG signal time series sampled at equal time intervals.

The experimental dataset covers the pre, during and post conditions along with 10 trials of the task conducted by each individual. The idea is to observe the variations occurring within the parameters while the functional state of the brain switches at fixed intervals. The changes in state of the brain while processing a certain task by an individual is modelled with the help of non-linear tools and techniques. So, in total we took 19 channel EEG data from a subject under pre, during and post conditions and decomposed each channel into six different waves Beta, Alpha, Theta, Delta1, Delta2 and Delta3. Therefore, for each individual we recorded 12 observations (Pre-1, During-10, Post-1). For simplicity we have obtained average Delta by averaging the values of the obtained nonlinear parameters of Delta1, Delta2 and Delta3. As a result, we can say that for each individual there is all total 19 x 4 i.e. 76 signals observed for 12 different states (Pre-1, During-10, Post-1) which generates 912 observations. We believe that this amount of data is sufficient for observing the changes in any particular human brain using 3 distinct nonlinear parameters in reaching a reliable conclusion

Chaos Analysis:

In general, we can say that a dynamical system is any system that evolves in time and our human brain exactly works the same way. We can assume that various brain processes occur through neural transmission of electrical discharges distributed over a volumetric surface, and this electrical activity of the brain can be traced over the scalp surface. Therefore, the signals collected through the EEG electrodes are a set of non-linear time series which contains information about the underlying causes of the dynamical behavior. Detection and quantification of chaos from non-linear time series is a widely explored process in the areas of neurophysiology to understand chaos in brain. The time series generated from a dynamical non-linear system can be tested for chaos by the estimation of Largest Lyapunov Exponent (LLE). Lyapunov exponents quantify the exponential divergence of initially close state-space trajectories, hence estimate the chaos in a system [38] [39]. A lot of algorithms exist for direct estimation of Lyapunov Exponents from Time Series like Wolf method [38], Rosenstein method [40], Kantz method [41], Synchronization method [42] [43], Benettin and the very recent Neural Network method proposed in reference [44]. We have chosen Rosenstein Algorithm due to its proven track record in the accuracy and reliability of feature extraction in case of chaos estimation of numerous biophysical signals and systems.

The steps of modified Rosenstein algorithm for estimation of largest Lyapunov exponent can be summarized as under:

1. Reconstruction of attractor dynamics from the non-linear time series by using the method of delays [45].
2. The reconstructed trajectory, **X**, can be expressed as a matrix where each row is a phase-space vector
3. $X = [X_1\ X_2\ X_3 \dots \dots X_M]$……[eq.1], Where, **X***i* is the state of the system at discrete time *i*. For an *N*-point time series, $\{x_1, x_{2,\dots}x_n\}$, each **X***i* is given by

$$X_i = \left[x_i\ x_{i+j} \dots \dots . x_{i+(m-1)\tau}\right] \text{……..[eq.2]}$$

Where, $\boldsymbol{\tau}$ is the *lag* or *reconstruction delay*, and *m* is the *embedding dimension*. Thus, **X** is an *M* × *m* matrix, and the constants *m*, *M*, τ, and *N* are related as

$$M = N-(m-1)\,\tau \quad \text{..... [eq.3]}$$

4. The embedding dimension is usually estimated in accordance with Takens' theorem. In our case we have used Cao's method [46] for estimation of minimum embedding dimension.
5. A good approximation of $\boldsymbol{\tau}$ can be done if we take the value equal the lag where the autocorrelation function drops to **63%** of its initial value. Calculation of this τ is accomplished using Fast Fourier Transform.
6. After reconstructing the dynamics, the algorithm locates the *nearest neighbor* of each point on the trajectory. The nearest neighbor, $X_{\hat{\jmath}}$, is found by searching for the point that minimizes the distance to the particular *reference point*, X_j

This is expressed as

$$d_j(0) = \left\| X_j - X_{\hat{\jmath}} \right\| \quad \text{..... [eq.4]}$$

Where, $d_j(0)$is the initial distance from the *j*th point to its nearest neighbor and $\left\| X_j - X_j \right\|$ denotes the Euclidean Norm. An additional constraint is imposed that nearest neighbors have a temporal separation greater than the mean period of the time series:

$$j - \hat{\jmath} > \widehat{mean\ period}. \quad \text{..... [eq.5]}$$

Here we have obtained the mean period as the reciprocal of median frequency calculated from Welch periodogram. The largest Lyapunov exponent λ_1 is then estimated as the mean rate of separation of the nearest neighbors. The basic principle of Rosenstein algorithm in calculating λ_1 is based on Sato's work [47]. Going by the definition of λ_1, we assume the *j*th pair of nearest neighbors diverge approximately at a rate given by the largest Lyapunov exponent

$$d_j(i) \approx C_j e^{\lambda_1 (i.\Delta t)} \quad \text{..... [eq.6]}$$

Where, *Cj* is the initial separation. By taking log on both sides of eq.6 we get a family of parallel lines for j=1, 2,…M and each with a slope roughly proportional to λ_1. The largest Lyapunov exponent is easily and accurately calculated using least-squares fit to the "average" line defined by

$$y(i) = \frac{1}{\nabla t}\langle \ln ln\, d_j(i)\rangle \quad \ldots\ldots\ldots\ldots \text{[eq.7]}$$

Where, $\langle \ln ln\, d_j(i)\rangle$ denotes average over all values of j. By avoiding the normalization, the current approach gains a slight computational advantage over the method by Sato *et al*. The proper fitting of the line is very much essential in accurate estimation of LLE using Rosenstein method, so we have ensured that, by limiting the number of iterations to 30. In doing so we have ensured that the line of best fit occurs when the iteration is kept at 30, since for higher iterations the nearest distance values attains saturation and it may result in unscrupulous estimation of the slope. The values of time delay and minimum embedding dimension are chosen from the plots as shown in fig.8 and fig.9. The reconstructed 3D phase space trajectory with 3 delay time coordinates is shown in fig.10(a). but it is to be noted that for EEG signal in our case the minimum embedding is chosen to be 4 as obtained from Cao's method. The small section of reconstructed signal with 4 delay time coordinates is shown as a time series in fig.10(b).

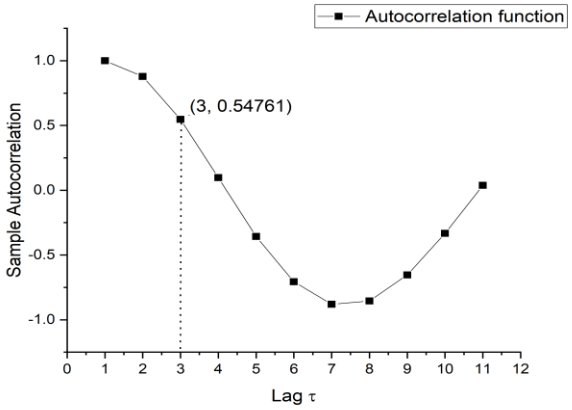

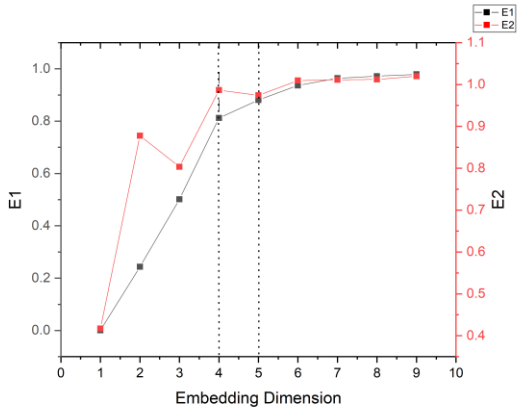

Fig. 12. Choice of delay time using Autocorrelation function Fig. 13. Choice of minimum embedding dimension

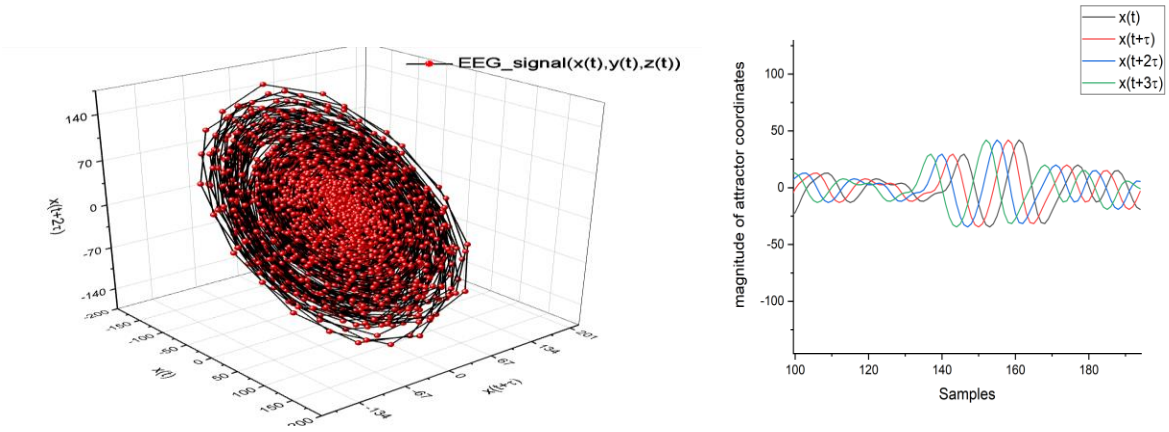

Fig. 14. In (a) we have shown the 3-D phase space attractor with three delay time coordinates and in (b) the reconstructed 4 -D attractor with 4 delay time coordinates of the taken EEG signal.

Fractal Analysis:

The complexity measure of physiological signals is well estimated by fractal dimension technique, which is an index for measuring the complexity of the signal and its governing system. Its applications are found in diverse fields like medical image and signal processing. Human brain is considered as a dynamical system., and EEG signal is the gateway towards estimating the complexity of the non-linear behavior of the brain [48]. Measuring the complexity in the EEG signal gives the state of the dynamical system [49]. Several algorithms have been developed in recent times to estimate Fractal Dimension of non-linear time series like Hurst's R/S, Katz, Petrosians, out of which Higuchi's method [50] is quite efficient and accurate in estimating fractal dimension of a non-linear EEG times series [51]. The general notion is that higher complexity and higher degree of self-similarity is accompanied with a higher value of Fractal Dimension.

In HFD method a given time series X(t) is converted into a new time series X_k^m;

$$\text{Where } X_k^m \text{ is X(m), X(m+k), X(m+2k),.....} X\left(m + \left[\frac{N-m}{k}\right].k\right) \qquad \text{(m=1,2,3,..k)}$$

Here $\left[\frac{N-m}{k}\right]$ denotes Gauss's notation, m and k are integers, which indicates the initial time and interval time respectively. Therefore, for a time interval, say k, we get k sets of new time series.

The length of the curve, generated from X_k^m is given by the following equation.8.

$$L_m(k) = \left\{ \left(\sum_{i=1}^{\left\lfloor \frac{N-m}{k} \right\rfloor} |X(m+ik) - X(m+(i-1)k)| \right) \frac{N-1}{\left\lfloor \frac{N-m}{k} \right\rfloor k} \right\} / k \quad \ldots\ldots\ldots \text{[eq.8]}$$

Here the term $\frac{N-1}{\left\lfloor \frac{N-m}{k} \right\rfloor k}$ represents the normalization factor for the curve length of subset time series.

Now, the length of the curve for the time interval k is calculated as the average value of k sets of $L_m(k)$ given as $\langle L(k) \rangle$. Now if the curve is fractal then it will follow the relation given in eq.9.

$$\langle L(k) \rangle \propto k^{-D} \ldots\ldots\ldots\ldots\ldots\ldots \text{[eq.9]}$$

The exponent D is the fractal dimension obtained from Higuchi's method or Higuchi's fractal dimension. In this method direct estimation of the fractal dimension is done by selecting a suitable value of K_{max}. The MATLAB script function for calculation of fractal dimension is called as hfd (x, K_{max}) which returns the FD value, when x (EEG signal) and K_{max} (no. of sets the original time series is divided into) is given as inputs. The value of K_{max} is chosen as the point after which the value of FD stops changing as shown in Fig.11.

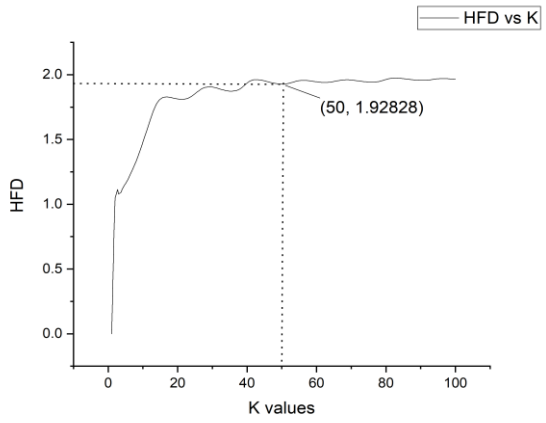

Fig. 15. HFD vs. K values to choose the optimized K value (K_{max}) for HFD estimation

Entropy Analysis

Entropy, as it relates to dynamical systems, is the rate of information production. Entropy is a measure of unpredictability of information content [52]. The idea that lies behind the estimation of entropy is in estimating the degree of randomness of a time series without any prior knowledge about the source from where it is generated. [53]. Some studies have been conducted, where the

utility of entropy based features are demonstrated for classification of epileptic EEG signal into normal, pre-ictal and ictal [54] [55] [56]. There are multiple entropy estimation techniques such as Approximate Entropy, Kolmogrov Entropy, Permutation Entropy, Fuzzy Entropy, Phase Entropy and Sample Entropy. Out of which we have chosen Sample Entropy as the effective, reliable and computationally efficient parametric method for direct estimation of entropy from the EEG signal time series [57]. The mathematical explanation of computing Sample Entropy is discussed in the preceding section.

SampEn (*m, r, N*) as proposed by [58] is precisely the negative natural logarithm of the conditional probability that two sequences similar for *m* points remain similar at the next point, where self-matches are not included in calculating the probability. Sample Entropy is basically derived from Approximate Entropy, with relatively same consistency and moreover SampEn is independent of the length of the data set and does not count self matches. Thus, a lower value of SampEn also indicates more self-similarity in the time series and less randomness with more predictability. The tolerance value for the distance estimation in the algorithm was typically set as 0.2 times the Standard Deviation.

Define $B_i^m(r)$ as $(N-m-1)^{-1}$ times the number of vectors X_j^m within r of X_i^m, where *j* ranges from 1 to N-m, and $j \neq i$ to exclude self-matches, and then define

$$B^m(r) = (N-m)^{-1} \sum_{i=1}^{N-m} B_i^m(r) \qquad \text{[eq.10]}$$

Similarly, define $A_i^m(r)$ as $(N-m-1)^{-1}$ times the number of vectors X_j^{m+1} within r of X_j^m, where *j* ranges from 1 to N-m $(j \neq 1)$, and set

$$A^m(r) = (N-m)^{-1} \sum_{i=1}^{N-m} A_i^m(r) \qquad \text{[eq.11]}$$

The parameter SampEn (m,r,N) is then defined as $\lim_{N\to\infty}\{-\ln[A^m(r)/B^m(r)]\}$, which can be estimated by the statistical form of the equation shown below.

$$SampEn(m,r,N) = -\ln\frac{A^m(r)}{B^m(r)} \qquad \text{[eq.12]}$$

Now set, $B = \left\{\frac{(N-m-1)(N-m)}{2}\right\} B^m(r)$ and $A = \left\{\frac{(N-m-1)(N-m)}{2}\right\} A^m(r)$, so that B is the total number of template matches of length m and A is the total number of forward matches of length m+1, and then SampEn can be expressed as $-\ln(A/B)$.

The required pseudo code is given in the appendix section with detailed and concise explanation of the steps involved in calculation of LLE, HFD and SampEn. The functions with user defined input arguments is individually defined in the Appendix section.

Statistical Significance Analysis:

One-way Analysis of Variance (ANOVA) test is carried out to check for the level of statistical significance of the generated dataset. The observed value of the non-linear parameters of respective electrodes over time are separately tested for statistically significant difference between groups and within group. The chosen groups are electrodes, which are distinct and independent of each other. The observed value of the Non-linear parameter over time window is the measurement variable. In table.3 we have shown an example of the ANOVA table as obtained. The level of significance α is set at 0.01 or 99% confidence interval. The p value is obtained based on F distribution statistics. The conditions of the null hypothesis (H_0) say, that there is no significant difference between the group means. Here we wish to reject the null hypothesis to accept the alternate hypothesis (H_A), suggesting that there is statistically significant difference in between the group means. If p value $\leq \alpha$ and $F \geq F_{crit}$; then we reject the null hypothesis and accept the alternate hypothesis. Here, $H_0 = \mu = \mu_{1\ldots N}$; $H_A = \mu \neq \mu_{1\ldots N.}$

Feature Classification:

This study employed and evaluated the Support Vector Machine, Random Forest and Decision Tree classification model based on supervised learning with nonlinear features [59] This study further includes systematic comparison of the performance of classification model over the defined feature space based on confusion matrix and accuracy score [60]. One feature vector X_1 is the frequency band beta, alpha, theta and delta set as categorical variables. The other vectors in the matrix of features X [799 x 17] is the fractal dimension, Lyapunov exponent and sample entropy

calculated for each EEG segment of 2min. The class or labels y is transformed to labels 1, 2, 3 and 4 using label encoder where **EMOTION'**: *'Label 1';* **'FOCUS'**: *'Label 2*'; **'MEMORY**': *'Label 3';* **'PROBLEM SOLVING':** *'Label 4'.* The steps of the classification algorithm implemented in *google colab*© Python IDE are discussed as follows:

- Loading the dataset in colab drive
- Import the libraries: numpy, matplotlib, pandas and scikit-learn
- Create the features [X_1, X_2,…..X_n] and labels [y] columns
- The missing values are replaced with mean
- The column string from the feature matrix is encoded into binary using OneHotEncoder
- The label column y is then encoded into 4 labels using LabelEncoder
- The dataset is then spilt into training and test set
- The columns of the training set and test set is transformed and scaled using normal standardization technique
- Training of the three classifier models
    - Support Vector Machine (SVM) ; kernel = rbf
    - Random Forest Classifier; n_estimators = 10, criterion = 'entropy'
    - Decision Tree Classifier, criterion = 'entropy'
- Performance metrics of the classifier models
    - Multi class Confusion Matrix
    - Classification accuracy score

The performance of the model is evaluated in accurate prediction of cognitive class labels from the input features obtained during each different 2 min segment. The training set is 60% and testing is 40% of the total dataset. [61].

4.1.3. Results and Discussion

The above analysis results in joint time space representation of the variation of non-linear dynamical parameters of EEG signal under the influence of cognitive load. The fluctuations in the values of different non-linear parameters provides insight on the functional abilities of the brain

during cognitive processing. The mental task load is considered as the stimulus for different subjects under study, and the response of the non-linear dynamical parameters under the stimulus is shown in the preceding section. In table 2. We provide with the general meaning and way of interpreting the three different Non-Linear Parameters chosen under our study. It would help the reader in understanding the plots and draw relevant interpretations from it. An attempt has been made to provide the reader with a visually enriching experience and enlightens in perceiving, how the effects of cognitive processes occurring inside our brain is reflected through the EEG signal fluctuations captured using non-linear dynamics parameters.

Table 2. Summary of the details of the Non-Linear parameters under study

PARAMETER	DEFINITION	INTERPRETATION	SIGNIFICANCE
LLE	The rate of exponential divergence of the nearby chaotic attractors in phase space.	• Indicator of a chaotic system (Deterministic Chaos) • Reveals the internal dynamics of a system • Measure of sensitivity to initial perturbations in the system	• High value of LLE corresponds to unpredictability and information loss • Positive LLE specifies the signal as deterministic
HFD	FD quantifies the complexity and self-similarity of a signal in the time domain.	• Measures the complexity of the signal.	• High Value of FD is associated with high amount of complexity in physiological signals • High value of FD corresponds to irregularity.
SAMPEN	Entropy is a measure of unpredictability of information content and irregularity in a dataset	• A mathematical measure of the level of randomness. • Measures the complexity of the signal in terms of degree of irregularity in the dataset.	• High entropy refers to higher complexity and unpredictability. • High entropy indicates greater irregularity and roughness in the signal pattern, cycles or trends.

Visualization

The data used to generate these plots are arranged as m x n matrix in a worksheet where m = Electrode/Channel position and n = time window. The elements in the matrix are the calculated nonlinear parameters. The steps involved in the algorithm for creating a contour from matrix (or virtual matrix) is as follows:

- Triangulation
- Linear interpolation.
- Drawing of contour lines.
- Connecting and smoothing of lines with color map

Chaos: Variation of Largest Lyapunov Exponent under four different cognitive tasks

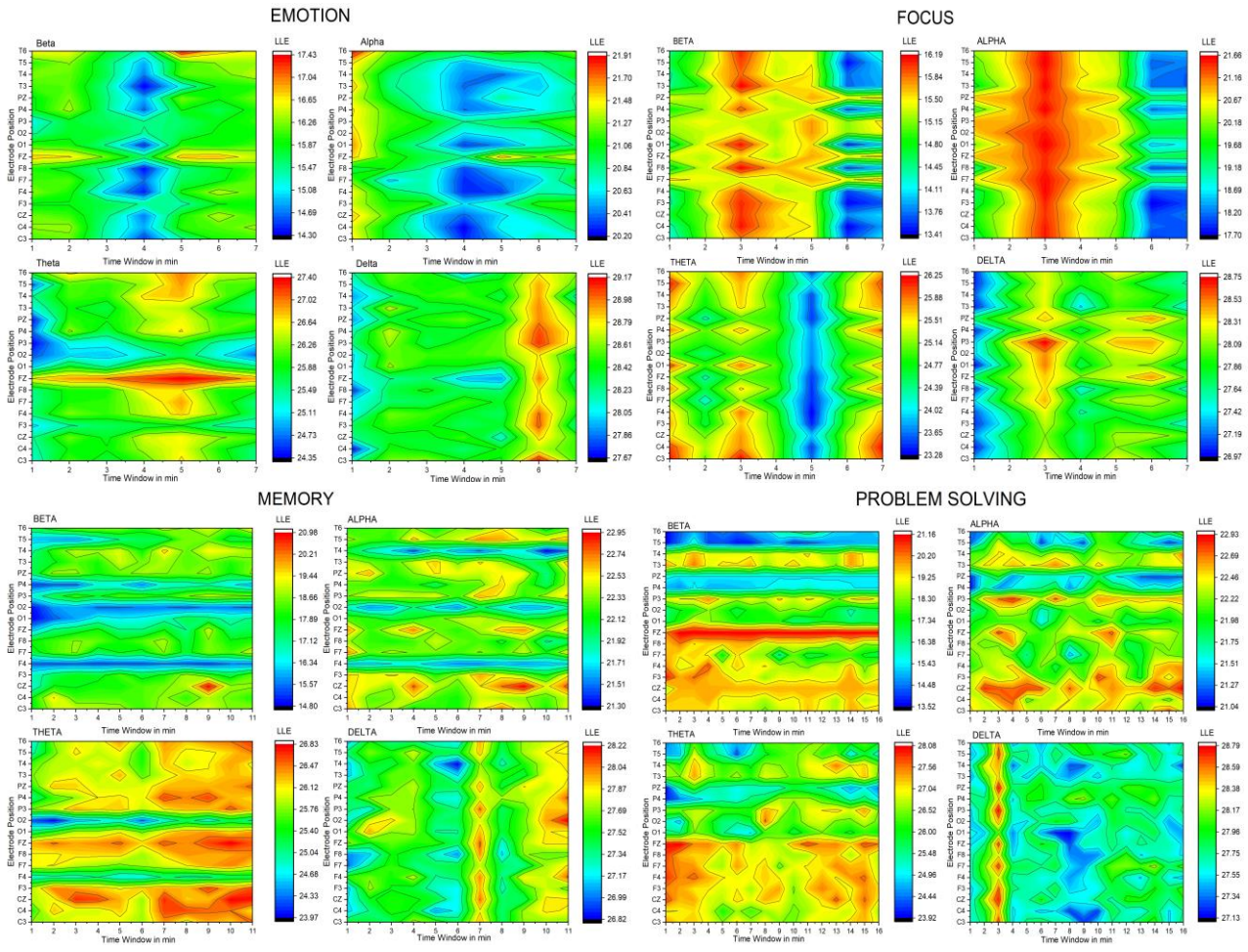

Fig. 16. Variation of Largest Lyapunov Exponent of beta, alpha, theta and delta rhythms under four different cognitive tasks

From the graphs in fig.16 we can see that the variations in LLE exponent follows a certain pattern, specifically in the beta and alpha rhythms. We can see that there are significant changes in the value of LLE during each time window and electrodes. The results suggest that the brain signals during cognitive processing have deterministic chaos and value of the LLE during different cognitive stimulus like Memory, Focus, Emotion and Problem Solving.

In Fig. 16 let's take the case of **Focus** task, where the subject was given the task which demands high focusing capability of the subject under study. We can very well spot the differences between three different stages viz. *Pre, During* and *Post* application of the task. LLE values are max during the task and minimum before the onset of task. The values of LLE again reduces post application of the task, indicating an innate desire to return back to its original state. The trend is observed in beta, alpha and delta band. Theta activity is observed to be of decreasing sensitivity to initial perturbations on application of the task marked in blue in the 5^{th} time window.

In case of **Emotion** recognition task, the subjects mental processing can be viewed as decreased beta and alpha activity (Time Window 3^{rd} to 5^{th}, Blue) during the task. The trends of theta and delta is complementing the actions of beta and alpha, since the former shows increased activity during the emotion recognition task.

Working **Memory** evaluation task shows significant non-uniform spatial variations over time, suggesting different location specific variations in trends. Fluctuations are observed in Parietal and Temporal region of the brain. The beta, alpha, theta and delta are found to have increased sensitivity to initial perturbations during and post application of the task. There is reduced activity in Occipital and Frontal lobes while memory processing by the brain.

The **Problem-Solving** task, which is a pretty long duration task with highest task load index among others. In this part it can be seen that there is wide spatial temporal variations and substantial activity is observed in Frontal and Central region. There is increased beta and alpha activity in these regions during the tasks, while there is decreased activity in theta and during the task. The blue mark over the time window 8^{th} to 10^{th} suggests reduced delta activity during the task. The theta activity lowers a bit during the task in synchronization with increased activity in Temporal and Parietal regions.

4.1.4. Fractal Dimension: Variation of Highuchi's Fractal Dimension for four different cognitive tasks.

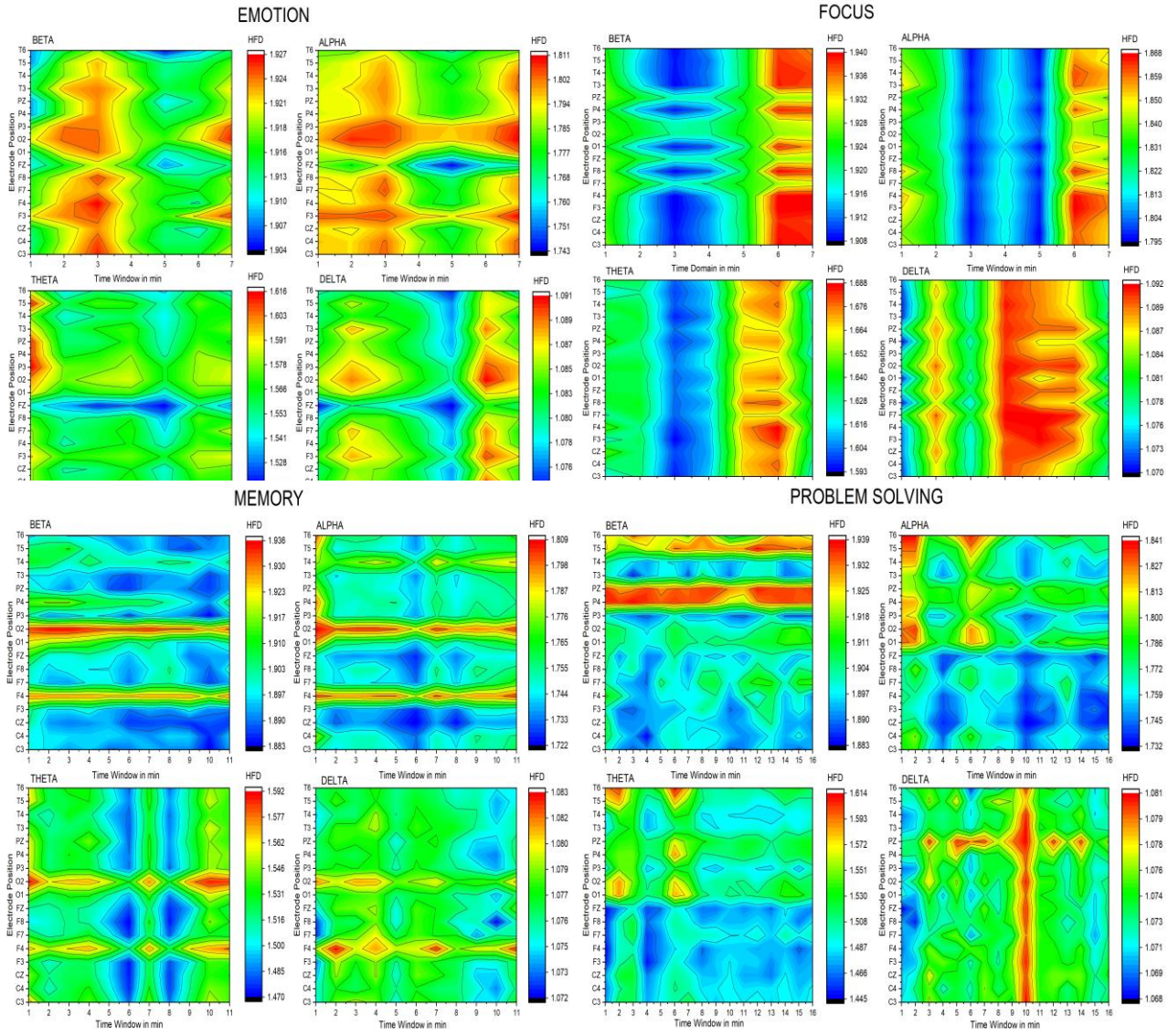

Fig. 17. Variation of Higuchi's Fractal Dimension of beta, alpha, theta and delta rhythms under four different cognitive tasks

The change in complexity of the signal can be estimated by fractal dimension. The plots in Fig.17 suggests that the changes in fractal dimension value is very much associated with changing complexities of the EEG rhythms during four different cognitive tasks. As we mentioned that, higher the fractal dimension higher is the complexity, so here we have observed higher complexity

patterns after the tasks. Fractal Dimension can easily distinguish between the different states of the brain while cognitive processing to complete the given tasks.

In case of **Emotion** recognition task, the trends in beta, alpha and delta activities suggest increased activity on initiation of the task and then a substantial dip observed during 5^{th} time window shown in blue. The after execution of the task there is significant increase in the task activity. The variation in complexity of the EEG signal with different spatial and temporal instances suggest activity of the brain in synchrony. The theta activity in case of Emotion recognition is found to be complementing the other three brain waves.

During the **Focus** task, there is decrease in complexity of the signal on application of the task as seen up to 4^{th} to 5^{th} time window from the 1^{st} window in beta, alpha and theta bands, whereas delta activity shows marginal increase within this segment. The results for post application of the task suggests that the complexity of the signal is higher than it was during the task as observed during the 6^{th} and 7^{th} window in red. Based on the observation it can be said that, cognitive processing of the brain in executing the Focus task involves high frequency fluctuations in brain rhythms after executing the task suggesting hysteresis effect induced while stimulating brain functions for focusing.

While working **Memory** evaluation task, spatial and temporal variations are observed in Fractal Dimension values. The Temporal and Parietal regions during beta, alpha, theta and delta activity are seen to be decreasing while execution of the task. The green shades turning blue over the time windows during the task is seen in beta and delta activities whereas there is marginal rise in complexity over 9^{th} to 11^{th} time window in alpha and theta activities. Delta activity follows similar patterns over Temporal, Central and Parietal regions, so it can be said that during memory processing delta activity is prevalent among most of the brain regions.

During the task of **Problem Solving**, which is a task of high temporal demand, likewise some spatial and temporal variations are observed. There are significant high frequency oscillations in beta activity from the lower Temporal and Parietal locations which does not change over time. In the frontal lobe channels, we see dormant theta and delta activity as shown in blue in 1^{st} time window, before initiation of the task but marginal activity in delta and alpha is observed. After initiation of the task (time window: 2^{nd} to 15^{th}) it can be seen that there are ups and downs in the magnitude of fractal dimension. The rise and fall can be related to the subject's perception of the

problem it solves at each time window. The complexity variations suggest frontal lobe activity in the form of fluctuations in beta, alpha, theta and delta rhythms while cognitive processing of the brain subjected to problem solving task.

Entropy: Variation of Sample Entropy for four different cognitive tasks.

Entropy as we know measures the rate of information transfer or one can say it as a quantitative measure of uncertainty in a system. It also measures the complexity or regularity of physiological signals. The results of the entropy variation among each subject is shown in Fig.18, which provides us some information on the amount of uncertainty in predicting the outcome. High entropy is also associated with more high frequency oscillations or intermittent fluctuations occurring within each time segment.

In case of **Emotion** recognition, marginal theta activity is observed in case of Temporal, Parietal and Central lobes. There are significant variations in complexity of beta, alpha and delta activity. During information processing of the brain while executing the memory recognition task, a rise in complexity is observed which reduces during the 4^{th} and 5^{th} time window. Post execution of the task in 7^{th} time window, entropy is found to reduce than the previous state, suggesting regularity and reduction in uncertainty of prediction.

When the subject is executing a **Focus** task, the Frontal, Occipital and Parietal lobes are found to show higher activity over the entire period with variations during and post execution of the task. The beta activity is seen to be moving from green shade to blue gradually over the time instance, suggesting reduction in uncertainty and increased regularity. The alpha and theta activity reduces to the minimum during 4^{th} and 5^{th} time window and found to increase after execution of the tasks in 7^{th} window. There is marginal change in delta activity, it can be seen that it increases during task and is maximum during 5^{th} and 6^{th} time window. The delta activity is minimum post execution of the task.

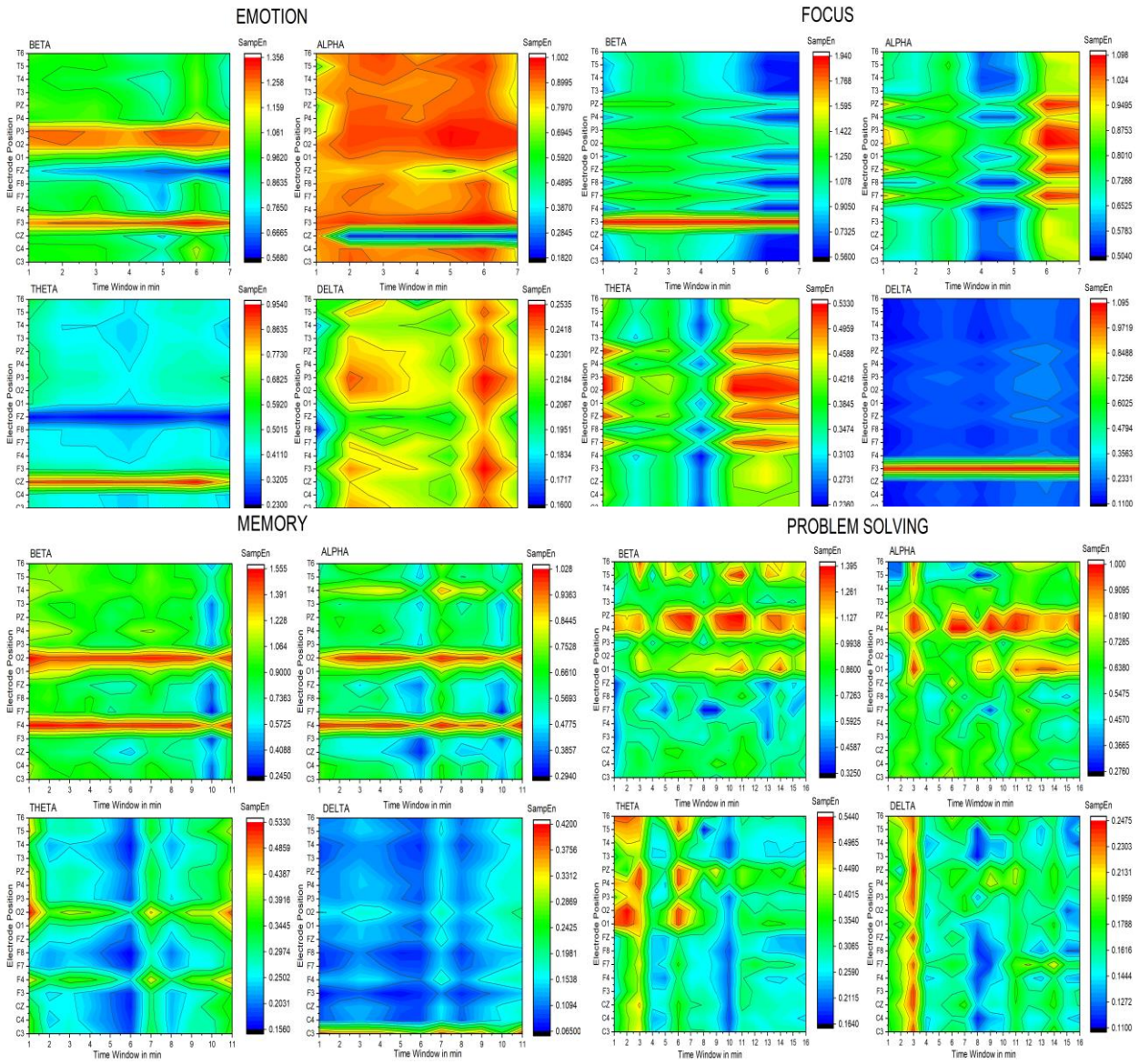

Fig. 18. Variation of Sample Entropy of beta, alpha, theta and delta rhythms under four different cognitive tasks

During working **Memory** evaluation task, the beta activity is found to decrease during time instances of 6th and 10th window, it is found to be higher elsewhere. The alpha activity is seen as a close correlate of beta activity showing minimum value during similar time windows. While in case of theta activity, there is reduction in complexity of the signal during execution of the task and is minimum during 5th and 6th time windows. The theta activity settles at higher complexity state post execution of the task as prevalent from the observation of 10th and 11th time windows.

The delta activity marginally increases during the initialization of the task but reduces to minimum during 5^{th} and 6^{th} window. There is marginal rise in delta wave complexity post execution of the task as seen in 10^{th} and 11^{th} window.

During the task of **Problem Solving**, spatial and temporal variations are observed. There is significant increase in beta, alpha, theta and delta activity during initialization of the task in 2^{nd} time window. The beta and alpha activity follow similar patterns of increasing and decreasing activity over different time windows. The subject's perception of the given problem during different time instances are unique, hence the intermittent fluctuations are observed. There are intermittent fluctuations in delta activity also. There is increased beta and alpha activity post execution of the task and comparatively lower theta and delta activity.

So, it can also be said that during cognitive loading of the brain the uncertainty in predicting the outcome reduces in most of the cases as observed in 2^{nd} time window, indicating the movement of the brain from normal disordered state to ordered state and again return to disorders. The beta and alpha fluctuations are clearly evident of the fact as discussed above. Therefore, the proposed methodology can distinctly differentiate not only the different brain rhythms and functional areas of the brain but also different cognitive processes.

Statistical Validation

The results are statistically validated using one-way ANOVA method to check for statistically significant difference between different groups. The observed *p-value* in all the cases is less than α and F statistic is greater than F_{crit}.as shown in table.3. Hence, we reject the null hypothesis and accept that there is statistically significant difference within the dataset at 99% confidence interval.

Table.3. ANOVA table example of LLE variations among different electrodes over time for beta activity during emotion recognition task. Likewise, other sets have been analyzed to test for significant difference.

ANOVA

Source of Variation	*SS*	*df*	*MS*	*F*	*P-value*	*F crit*
Between Groups	9.287838	16	0.58049	2.351267	0.004584	2.154893
Within Groups	29.37918	119	0.246884			
Total	38.66702	135				

Classification

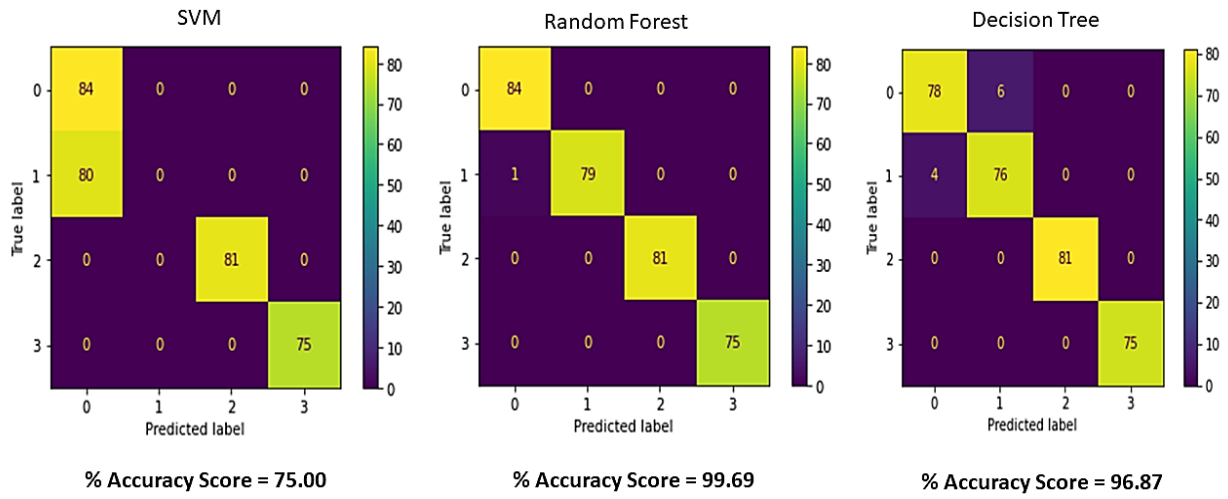

Fig. 19. Confusion matrix and % classification accuracy score of three classifier models based on features of chaos, fractal and entropy parameters of 4 classes of eeg waves.

The comparison of performance metrics of classification models SVM, random forest and decision tree classifier is shown in fig. 19. The number of false detections in case of Random Forest is much lower than that of SVM and Decision Tree classification models. The accuracy score of 99.69 % is also higher in case of Random Forest classifier model. Therefore, we can say that Random forest

classification model is best suited in predicting the class of cognitive process using the nonlinear features as obtained from feature extraction from eeg signals.

4.1.3. Conclusion

The major contribution of this research work presented here is associated in establishing a spatiotemporal descriptor of perceiving changes, in properties of the signal, subject to cognitive load. The effect of perturbation on the human brain with application of the stimulus generates variations in the characteristics of the EEG signal which is shown in the plots with different color scheme.

The change in values of LLE quantifies how much chaotic the system is and when does it move from uncertainty to certainty and vice versa. The changes in HFD represents the changing complexity of the signals and Entropy gives a measure of uncertainty in information content. Whenever the stimulus is applied, a change is observed, in values of the parameters under study. The three stages of the brain viz. pre, during and post application of the task has been found to be distinctive to each other. Moreover, we can see that there is synchrony among the three tested parameters, which helps in quantifying various electrophysiological states of the human brain subject to cognitive loading.

The results of classification models help us to conclude the fact that cognitive processing of the brain can be evaluated using LLE, HFD and SampEn as biomarkers or descriptors of micro and macro state variations of the brains and how it evolves with time. The joint time space representation of the non-linear parameters helps us to visualize the change in temporal characteristics of the EEG along with its electrode position placed at different functional areas of the brain. This joint distribution dataset serves as the feature space for classification output labels based on supervised learning method.

The cubic representation of the brain map containing non-linear parameters can prove to be a significant visualization tool in case of monitoring long range EEG. One can get analysis results in one single graph if the proposed method is incorporated for spatial-temporal non-linear analysis of EEG signals. In this way, we form a multi-parametric signature of cognitive processing and the methodology shall be extended in studying different aspects of the neurophysiological studies and applications.

5. Appendix

This program calculates the Lyapunov Exponent of an EEG signal

Input signal as *x;* Input minimum embedding dimension as *m;*

Input time delay as *τ*; Input mean period as *m*P;

Input number of iterations as *maxit*;

Define *N* as length of the signal x;

Define M = N – (m - 1) * τ ; *% M: Total number of reconstructed vectors*

Define Sub Function as PSR;

Begin PSR() *% Performs phase space reconstruction of the signal*

Pass In : x, m, τ; *% Arguments of the function*

Create a zeros matrix Y of dimension (M x m);

Repeat

for i = 1 to m;

Store values in each column of Y matrix obtained as x((1:M)+(i-1)*τ); % Delay shifting

end

Pass Out: Y

End PSR()

Define Main Function as LLE;

Begin LLE() % *Calculates Largest Lyapunov Exponent of signal x using Rosenstein method*

Call: PSR(x, m, τ)

Repeat

for i = 1 to M

Create a column vector x0 as output of column wise elemental multiplication of unit column matrix Mx1 and i^{th} row of matrix Y;

Calculate distance as square root of the square of the sum of the difference |Y|-|x0| and store as column vector;

Repeat

for j=1 to M

Check: If absolute value of (j – i) is less than equal to mean period mP then set distance as 1e10

end

end

Create variables nd and np as nearest distance and nearest position(index) by calculating the minimum value from the distance vector and row indices of each column;

end

Repeat

for k = 1 to maxit

Define max_index = M – k;

Set variable ev = 0 to store the values for the evolution vector;

Set variable p=0 and increment for each iteration of the loop;

Repeat

for j= 1 to M

Check: If j is less than equal to max_index and if np at j^{th} position is less than equal to max_index

Calculate the mean separation of the nearest neighbors as square root of the square of sum of difference

as Y(j+k) – Y(np(j)+k) and store as column vector

Check: If the mean separation is not equal to zero then increment ev as ev + log(mean separation);

and increment p as p + 1

end

end

end

Check: If p is greater than equal to zero, then store the divergence of nearest trajectories d as ev / p, as a column vector else set value of d = 0;

end

end

Calculate LLE as the slope of divergence of nearest trajectories verses no. of iterations using linear curve fitting

End Output: LLE

Hence the rate of divergence of the nearest trajectories is estimated which is familiarly known as Lyapunov Exponent

This program calculates the Higuchis' Fractal Dimension of an EEG signal

Input signal as *x*; Input max no. of new set of time series as *kmax*;

Define *N* as length of the signal x;

Define function as hfd();

Begin hfd()

Pass In: x, kmax;

Define Lmk as a zeros matrix of dimension (kmax, kmax);

Repeat

for k = 1 to kmax

for m = 1 to k

Define Lmki = 0;

Repeat

for i = 1 to ((N-m)/k) % [*take the value of i as integer nearest to zero*]

Update Lmki as Lmki+abs(x(m+i*k)-x(m+(i-1)*k));

end;

Set normalization factor Ng as $\frac{N-1}{\left[\frac{N-m}{k}\right]k}$;

Define Lmk as a matrix of dimension (m,k)= (Lmki*Ng)/k;

end;

end;

Define a row matrix of Lk of dimension (1, k);

Repeat

for k = 1 to kmax

Define Lk as a row matrix of dimension (1, k) = sum of row elements of Lmk from 1 to k and divide by k; % *gives the avg value for k sets of Lmk*

end

Define lnLk as logarithm of Lk;

Define lnk as logarithm of each element of array [1:kmax];

Calculate hfd as the slope of linear fit for the curve lnLk versus lnk;

End

Output: HFD

The above function is iterated for a range of values (0 to 100) of kmax and kmax is selected as 50. Hence we get the fractal dimension at kmax=50.

This program calculates the Entropy of an EEG signal based on sample entropy technique:

Input signal as *x*; Input minimum embedding dimension as *m*;

Define tolerance level for min distance r = 0.2 times the standard deviation of the signal;

Input delay time for down sampling as τ ;

Define time series data as data = downsampling x by τ no. of samples;

Define N as length of the signal;

Define function as SampleEntropy( )

Begin SampEntropy()

Pass In: data, r, m, τ ;

Create a zeros matrix C of dimension (1,2);

Create a data matrix of zeros dataMat of dimension (m+1, N-m);

Repeat

for i = 1 to m+1

Update rows of dataMat as samples of data from (i to N-m+i-1);

end

Repeat

for j = m to m+1

define zeros matrix count of dimension(1,N-m);

define template matrix tempMat = row elements of dataMat from (1 to j);

Repeat

for i = 1 to N-m

Calculate Chebyshev distance dist while excluding self-matching case = maximum of **{**absolute value of **[**column elements of tempMat from (i+1 to N-m) – repeat copies of elements of matrix (tempMat) for every i^{th} column in row 1 and N-m-i column**]}**;

Calculate Heaviside function of the distance as D with the condition if dist is < r then out 1 and if dist is not < than r then out 0);

define an array and store as count at every i^{th} iteration = sum of(D)divided by(N-m);

end

Store in $(j-m+1)^{th}$ element of C = sum of(count)divided by(N-dim);

end

Define output SampEn = log of (1^{st} element of C by 2^{nd} element of C);

End Output: SampEn

Hence the rate of information transfer or uncertainty in information content is measured by the SampEn value.

References

[1] M. J. Frank and D. Badre, "How cognitive theory guides neuroscience," *Cognition,* vol. 135, pp. 14-20, 2015.

[2] R. D. Dias, M. A. Zenati, R. Stevens, J. M. Gabany and S. J. Yule, "Physiological synchronization and entropy as measures of team cognitive load," *Journal of Biomedical Informatics,* vol. 96, no. 103250, 2019.

[3] M. Mazher, A. A. Aziz and A. S. Malik, "An EEG-Based Cognitive Load Assessment in Multimedia Learning Using Feature Extraction and Partial Directed Coherence," *IEEE Access,* vol. 5, pp. 14819-14829, 2017.

[4] N. Kumar and J. Kumar, "Measurement of Cognitive Load in HCI Systems Using EEG Power Spectrum: An Experimental Study," in *Procedia Computer Science 84* , New Delhi, 2016.

[5] G. V. Tcheslavski, M. Vasefi and F. F. Gonen, "Response of a human visual system to continuous color variation: An EEG-based approach," *Biomedical Signal Processing and Control,* vol. 43, p. 130–137, 2018.

[6] A. P. Clark, A. P. Bontemps, B. D. Batky, E. K. Watts and R. T. Salekin, "Psychopathy and neurodynamic brain functioning: A review of EEG research," *Neuroscience and Biobehavioral Reviews,* vol. 103, p. 352–373, 2019.

[7] C. M. Michel and T. Koenig, "EEG microstates as a tool for studying the temporal dynamics of whole-brain neuronal networks: A review," *NeuroImage,* vol. 180, pp. 577-593, 2018.

[8] J. Cabral, M. L. Kringelbach and G. Deco, "Exploring the network dynamics underlying brain activity during rest," *Prog. Neurobiol,* vol. 114, pp. 102-131, 2014.

[9] B. L. Foster, B. J. He, C. J. Honey, K. Jerbi, A. Maier and Y. B. Saalmann, "Spontaneous neural dynamics and multi-scale network organization," *Front. Syst. Neurosci.,* vol. 10, p. 7, 2016.

[10] S. Perone and V. R. Simmering, "Applications of Dynamic Systems Theory to Cognition and Development: New Frontiers," in *Advanves in Child Development and Behavior,* Elesevier, 2017, pp. 43-80.

[11] K. Yufeng, H. Qi, L. Zhang, S. Chen, X. Jiao, P. Zhou, X. Zhao, BaikunWan and D. Ming, "Towards an effective cross-task mental workload recognition model using electroencephalography based on feature selection and support vector machine regression," *International Journal of Psychophysiology,* vol. 98, no. 2, p. 157–166, 2015.

[12] Y. Chen and T. D. Pham, "Sample entropy and regularity dimension in complexity analysis of cortical surface structure in early Alzheimer's disease and aging," *Journal of Neuroscience Methods,* vol. 215, no. 2, pp. 210-217, 2013.

[13] S. Kesic´ and S. Z. Spasic´, "Application of Higuchi's fractal dimension from basic to clinical neurophysiology: A review," *Computer methods and programs in Biomedicine,* pp. 55-70, 2016.

[14] W. Xingyuan and L. Chao, "Researches on chaos phenomenon of EEG dynamics model," *Applied Mathematics and Computation,* vol. 215, no. 2, pp. 30-41, 2006.

[15] R. Acharya, O. Fausta, N. Kannathala, T. Chuaa and S. Laxminarayan, "Non-linear analysis of EEG signals at various sleep stages," *Computer Methods and Programs in Biomedicine,* vol. 80, no. 1, pp. 37-45, 2005.

[16] G. Yina, G. R.Naik, H. Shuhua, A. Ajith and H. T.Nguyen, "Nonlinear multiscale maximal Lyapunov exponent for accurate myoelectric signal classification," *Applied Soft Computing* , vol. 36, pp. 633-640, 2015.

[17] R. Chai, S. H. Ling, P. P. San, G. R. Naik, T. N. Nguyen, Y. Tran, A. Craig and H. T. Nguyen, "Improving EEG-based driver fatigue classification using sparse-deep belief networks," *Frontiers in neuroscience,* vol. 7, p. 103, 2017.

[18] A. Al-Ani, I. Koprinska and G. Naik, "Dynamically identifying relevant EEG channels by utilizing channels classification behaviour," *Expert Systems with Applications,* vol. 83, pp. 273-282, 2017.

[19] C. J. Stam, "Nonlinear dynamical analysis of EEG and MEG: Review of an emerging field," *Clinical Neurophysiology,* vol. 116, no. 10, p. 2266–2301, 2005.

[20] W. Klonowski, "Fractal analysis of electroencephalographic time series (EEG signals).," *The fractal geometry of the brain,* p. Springer413–429, 2016.

[21] E. Ruiz-Padial and A. J. Ibáñez-Molina, "Fractal dimension of EEG signals and heart dynamics in discrete emotional states," *Biological Pshycology,* pp. 42-48, 2018.

[22] L. Tang, H. Lv, F. Yang and L. Yu, "Complexity testing techniques for time series data : A comprehensive literaturer eview," *Chaos, Solitons and Fractals,* vol. 81, pp. 117-135, 2015.

[23] P. L. G. S. R. D. M. T. Thomas C Ferree, "Scalp elctrode impedance, infection risk, and EEG data quality," *Clinical Neurophysiology,* vol. 112, no. 3, pp. 536-544, 2001.

[24] S. Bhardwaj, P. Jadhav, B. Adapa, A. Acharyya and G. R. Naik, "Online and automated reliable system design to remove blink and muscle artifact in EEG," in *Conf Proc IEEE Eng. Med Biol Soc*, Milan, 2015.

[25] P. N. Jadhav, D. Shanamugan, A. Chourasia, A. R. Ghole, A. Acharyya and G. Naik, "Automated detection and correction of eye blink and muscular artifacts in EEG signal for analysis of Autism Spectrum Disorder," in *Conf Proc IEEE Eng Med Biol Soc.*, 2014.

[26] A. Subasi and M. I. Gursoy, "EEG signal classification using PCA, ICA, LDA and support vector machines," *Expert Systems with Applications,* vol. 37, no. 12, pp. 8659-66, 2010.

[27] H. Adelia, Z. Zhou and N. Dadmehr, "Analysis of EEG records in an epileptic patient using wavelet tranform," *Journal of Neuroscience Methods,* vol. 123, no. 1, pp. 69-87, 2003.

[28] A. Subasi, "EEG signal classification using wavelet feature extraction and a mixture of expert model," *Expert Systems with Applications,* vol. 32, no. 4, pp. 1084-93, 2007.

[29] M. Misiti, Y. Misiti, G. Oppenheim and J.-M. Poggi, Wavelet Toolbox MATLAB User's Guide, The MathWorks Inc., 1996.

[30] B. P. Marchant, "Time-Frequency analysis for biosystem engineering," *Biosystems Engineering,* vol. 85, no. 3, pp. 261-281, 2003.

[31] S. N. Sarbadhikari and K. Chakrabarty, "Chaos in the brain: a short review alluding to epilepsy, depression, exercise and lateralization," *Medical Engineering & Physics,* vol. 23, no. 7, pp. 445-455, 2001.

[32] M. H. Díaza, F. M.Córdova, L. Cañete, F. Palominos, F. Cifuentes, C. Sánchez and M. Herrera, "Order and Chaos in the Brain: Fractal Time Series Analysis of the EEG Activity During a Cognitive Problem Solving Task," in *Procedia Computer Science*, Rio de Janeiro, Brazil, 2015.

[33] M. Chakraborty and D. Parbat, "Fractals, chaos and entropy analysis to obtain parametric features of surface electromyography signals during dynamic contraction of biceps muscles under varying load," in *2nd International Conference for Convergence in Technology (I2CT)*, Mumbai, 2017.

[34] D. P. Subha, P. K. Joseph, R. Acharya and C. M. Lim, "EEG Signal Analysis: A Survey," *Journal of Medical Systems,* vol. 34, pp. 195-212, 2010.

[35] Y. Ma, W. Shi, C.-K. Peng and A. C.Yang, "Nonlinear dynamical analysis of sleep electroencephalography using fractal and entropy approaches," *Sleep Medicine Reviews,* vol. 37, pp. 1-9, 2017.

[36] T. F. Burns and R. Rajan, "Combining complexity measures of EEG data: multiplying measures reveal previously hidden information," *F1000Research,* vol. 4, p. 137, 2015.

[37] L. Zhenhu, W. Yinghua, S. Xue, L. Duan, V. L. J., S. J. W., H. Satoshi and L. Xiaoli, "EEG entropy measures in anesthesia," *Frontiers in Computational Neuroscience,* vol. 9, pp. 9-16, 2015.

[38] A. Wolf, J. B. Swift, H. L. Swinney and J. A. Vastano, "DETERMINING LYAPUNOV EXPONENTS FROM A TIME SERIES," *Physica D,* vol. 16, no. 3, pp. 285-317, 1985.

[39] J. C. Sprott, Chaoa and Time-Series Analysis, Oxford University Press, 2003.

[40] M. T. Rosenstein, J. J. Collins and C. J. D. Luca, "A practical method for calculating largest Lyapunov exponents," *Physica D Nonlinear Phenomenon,* vol. 65, no. 1-2, pp. 117-134, 1993.

[41] H. Kantz, "A robust method to estimate the maximal Lyapunov exponent of a time series," *Physics Letter A,* vol. 185, no. 1, pp. 77-87, 1994.

[42] A. Stefanski, "Estimation of the largest Lyapunov exponent in systems with impacts," *Chaos Solition Fractals,* vol. 78, p. 2443–2451, 2000.

[43] A. Stefanski and T. Kapitaniak, "Estimation of the dominant Lyapunov exponent of non-smooth systems on the basis of maps synchronization," *Chaos Solition Fractals,* vol. 15, no. 2, p. 233–244, 2003.

[44] J. Awrejcewicz, A. V. Krysko, N. P. Erofeev, V. Dobriyan, M. A. Barulina and V. A. Krysko, "Quantifying Chaos by Various Computational Methods. Part 1: Simple Systems," *Entropy,* vol. 20, no. 3, pp. 1-28, 2018.

[45] F. Takens, "Detecting strange attractors in turbulence," *Lect. Notes in Math,* vol. 898, p. 366, 1981.

[46] L. Cao, "Practical Method for determining minimum embedding dimension from a scalar time series," *Physica D,* vol. 110, no. 1-2, pp. 43-50, 1997.

[47] S. Sato, M. Sano and Y. Sawada, "Practical methods of measuring the generalized dimension and the largest Lyapunov exponent in high dimensional chaotic systems," *Prog.Theor.Phys,* vol. 77, no. 1, pp. 1-5, 1987.

[48] P. Paramanathan and R. Uthayakumar, "Application of fractal theory in analysis of human electrophysiological signals," *Computers in Biology and Medicine,* vol. 38, no. 3, pp. 372-378, 2008.

[49] C. Tricot, Curves and Fractal Dimension, New York: Springer, 1995.

[50] T. Higuchi, "Approach to an irregular time series on the basis of the fractal theory.," *Physica D,* vol. 31, no. 2, p. 277–283, 1988.

[51] M. Čukić, D. Pokrajac, M. Stokić, S. Simić, V. Radivojević and M. Ljubisavljević, "EEG machine learning with Higuchi's fractal dimension and Sample Entropy as features for successful detection of depression," *arXiv:1803.05985,* 2018.

[52] S. M. Pincus, "Approximate entropy as a measure of system complexity," *Proc Natl Acad Sci USA,* vol. 88, no. 2297-3301, pp. 2297-2301, 1991.

[53] A. Delgado-Bonal and A. Marshak, "Approximate Entropy and Sample Entropy: A Comprehensive Tutorial," *Entropy,* vol. 21, no. 6, p. 541, 2019.

[54] U. R. Acharya, S. V. Sree, S. Chattopadhyay, W. Yu and P. C. A. Ang, "Application of recurrence quantification analysis for the automated identification of epileptic EEG signals," *International Journal of Neural Systems,* vol. 21, no. 3, pp. 119-211, 2011.

[55] U. R. Acharyaa, F. Molinari, S. V. Sree, S. Chattopadhyay, K.-H. Ng and J. S. Suri, "Automated diagnosis of epileptic EEG using entropies," *Biomedical Signal Processing and Control,* vol. 7, no. 4, pp. 401-408, 2012.

[56] M. Li, W. Chen and T. Zhang, "Automatic epileptic EEG detection using DT-CWT-based non-linear features," *Biomedical Signal Processing and Control,* vol. 34, pp. 114-125, 2017.

[57] W. Chena, J. Zhuang, W. Yu and Z. Wang, "Measuring Complexity using FuzzyEn, ApEn, and SampEn," *Medical Engineering & Physics,* vol. 31, no. 1, pp. 61-68, 2009.

[58] J. S. Richman and J. R. Moorman, "Physiological time-series analysis using approximate entropy and sample entropy," *American Journal of Physiology,* vol. 278, no. 6, p. H2039–H2049., 2000.

[59] M. M. Rahman and S. A. Fattah, "An efficient feature extraction scheme for classification of mental tasks based on inter-channel correlation in wavelet domain utilizing EEG signal," *Biomedical Signal Processing and Control,* vol. 61, 2020.

[60] Y.-P. Lin, C.-H. Wang, T.-P. Jung, T.-L. Wu, S.-K. Jeng, J.-R. Duann and J.-H. Chen, "EEG-Based Emotion Recognition in Music Listening," *IEEE Transactions on Biomedical Engineering,* vol. 57, no. 7, pp. 1798-1806, 2010.

[61] F. Pedregosa, G. Varoquaux and A. Gramfort, "Scikit-learn: Machine Learning in {P}ython," *Journal of Machine Learning Research,* vol. 12, pp. 2825--2830, 2011.

4.2. Multiscale Entropy Analysis of single lead ECG and ECG derived respiration for AI based prediction of Sleep Apnea events.

This study was published in Biomedical Signal Processing and Control, Elsevier which is about Sleep apnea (SA) which is a prevalent sleep disorder that affects a significant portion of the adult population. The proposed method involves coarse graining a signal at different scales, using the popular multiscale entropy algorithms to detect apnea and normal events from single lead Electrocardiography (ECG), Instantaneous Heart Rate and ECG derived respiration. The idea of nonlinear dynamical systems analysis for feature extraction along with machine learning approach, the authors present here a moderately accurate sleep apnea detection model with an accuracy ranging from 70% to 100% based on two different probabilistic thresholds of 50 % and 70% with reduction in false positive rate from 28% to 14 % for applications in development of AI based IoT connected smart wearable devices. The two thresholding modes offer a choice to do a trade-off between high training accuracy with high false positive rate and low accuracy with low false positive rate. The performance metrics of each model have been reported and choice is made for

best suitable model with prospectives of implementation for diagnostic purposes. The effectiveness of the proposed method in accurate detection of sleep apnea requires further validation of the models with out of distribution dataset.

4.2.1. Introduction

In the US, roughly 2% to 5% of the adult population and more than 30% of the elderly population suffer from sleep apnea (SA), one of the most prevalent sleep disorders that is defined by breathing disturbance while sleeping [1]. According to a systematic review and meta-analysis published in The Lancet Respiratory Medicine in 2019, the estimated global prevalence of obstructive sleep apnea (OSA) in adults was 936 million (10.9%) and moderate-to-severe OSA was 425 million (4.9%). However, the prevalence varied widely across different countries and regions. Here are a few examples of country-specific prevalence estimates from the same study: USA: 54 million (22%), China: 150 million (13%), India: 110 million (10%), Brazil: 49 million (33%), Germany: 20 million (14%). [2], [3]

Obstructive sleep apnea (OSA) [4], central sleep apnea (CSA) [5], and complex sleep apnea syndrome are the three main kinds of sleep apnea. The frequent pharyngeal collapse that results in shortness (hypopnea) or cessation (apnea) of breathing during sleep is what distinguishes OSA. The common definition of apnea is the stoppage of breathing for at least 10 seconds, while the definition of hypopnea is a marked reduction in airflow for at least 10 seconds that is followed by either a 4% desaturation of blood oxygen level or neurological symptoms.[6]

Recurrent apnoeic episodes and a lack of respiratory effort are characteristics of CSA because the brain does not provide any signals to the muscles that control breathing [7]. These disruptions frequently wake people up from their sleep, which makes them excessively tired and sleepy during the day. Patients who suffer from both OSA and CSA are said to have complex sleep apnea syndrome. Stroke, ischemic heart disease, and cardiovascular dysfunction are also possible

outcomes of severe forms of SA [8]. It is one of the main causes of hypertension and is associated with severe cardiovascular morbidity. In order to reduce risk, it is crucial to diagnose and treat sleep apnea accurately and quickly.[9]–[11]

Currently, polysomnography (PSG), which necessitates a person to spend one or two nights in a sleep laboratory under the supervision of sleep specialists, is thought to be the gold standard for apnea diagnosis. In order to capture diverse physiological data, the subject's body is typically fitted with numerous sensors and wires. Electroencephalogram, or EEG, eye movements, blood oxygen level, SpO2, heart rate, and rhythm are some examples of these signals (electrocardiogram, or ECG). The professionals must examine the recorded data in order to make the final diagnosis. The apnea-hypopnea index (AHI), which is defined as the number of apnea-hypopnea events per hour over the course of the entire sleep duration, evaluates the severity of the SA. The method is time-consuming, expensive, and uncomfortable for the subjects because several sensors and wires are attached. As a result, the researchers have worked hard to develop PSG substitutes that have less complicated schemes and quicker decision-making abilities [12]. The use of information and communication technologies, such as eHealth, can help improve treatment adherence for sleep apnea patients through patient education, real-time monitoring of symptoms and Continuous Positive Airflow Pressure (CPAP) usage, self-management, and early identification and intervention of device or treatment issues. However, the effectiveness of eHealth technologies in improving CPAP adherence has not been extensively studied.[13], [14]

Over the past few years, numerous techniques to find SA have been suggested. These approaches differ from one another in terms of the physiological signals used to identify SA and the classification techniques. Existing work in the area of detection of sleep apnea can be broadly classified into three categories: clinical assessments, physiological measurements, and machine learning-based methods. Machine learning-based methods have shown promise in the detection of sleep apnea [15]. These methods involve the analysis of various physiological signals, such as electroencephalogram (EEG), electrocardiogram (ECG), and respiratory signals [16]. Machine learning algorithms can be trained on large datasets to identify patterns in the data that are indicative of sleep apnea. Recent studies have also explored the use of wearable devices, such as

wristbands and chest straps, for the detection of sleep apnea [17]. These devices can monitor physiological parameters such as heart rate, respiration, and oxygen saturation, providing a non-invasive and cost-effective alternative to PSG. Recent studies have also been conducted to detect sleep apnea from snoring signals.[18]

To identify sleep apnea, many researchers suggested deriving many features from the electrocardiographic (ECG) signal [19]. Furthermore, such algorithms estimate respiration from the ECG rather than detecting the respiratory signal, and they subsequently extract a collection of features that may be applied in differentiating the class of apnea and non-apnea [20]. For SA detection, numerous rule-based methods have been developed. The machine learning-based approach has recently gained popularity as a method for SA identification and monitoring, and researchers now have access to a variety of machine learning models. Many researchers have used models such as Support Vector Machines (SVM) [21], K-nearest neighbours (KNN), and Decision Tree (DT) with success [22], [23]. There have been reports of SA detection systems that combined several classifiers. Deep learning methods for SA detection, like Convolutional Neural Network (CNN) [67] and Recurrent Neural Network (RNN), have recently come into prominence.[24]–[32]

In this context we propose Multiscale Entropy analysis of single lead ECG signals along with the respiration signal derived from ECG. The Multiscale Entropy analysis involves coarse graining procedure of a signal at different scales. The temporal information associated due to Sleep Apnea may not be present at single scale but in certain conditions the temporal information is mostly abundant at higher scales [33]. This phenomenon suggests that it is more accurate to predict cardiac events when a signal is viewed at higher scales [34]. The heart rate complexity dynamics has been found to be an effective biomarker in early-stage prognosis of patient outcome after sudden cardiac arrest [35]. The use of Multiscale analysis-based model training and evaluation for sleep apnea detection has not been attempted before. This motivated us to develop a unique methodology for automated detection of sleep apnea events from long term ECG recordings suitable for wearable device applications. The use of three signals along with informed nonlinear features makes our proposed methodology very unique in comparison with previous studies that employed similar techniques for detection of Sleep Apnea from ECG signals. The application of the proposed methodology is mainly directed towards development of methods for implementation of the

algorithm in IoT connected smart wearable devices for home based continuous monitoring and detection of sleep apnea events from single lead ECG. This would solve the problem of complexity involved in sleep apnea detection devices based on traditional Polysomnographic recordings.

In the proposed methodology, ECG signal is first segmented into 60 sec events and then denoised using 1D wavelet denoising and then based on we have generated two more signals for each individual ECG segments i.e ECG_rate and Respiration as derived from ECG. The effect of Respiratory Sinus Arrythmia (RSA) during Obstructive Sleep Apnea (OSA) has been proven to be present during each respiratory cycle. During each respiratory cycle the heart rate increases during inspiration and decreases during expiration, suggesting the effect of parasympathetic nervous system in regulating the heart during the respiratory cycle. The effect of RSA is still present during apnoeic and hypoxia events and must be considered during the analysis [58]. This effect of RSA necessitates the use of instantaneous heart rate (ECG_rate) and EDR signals both along with ECG signals for feature extraction and model training. We have calculated the optimal time delay($\boldsymbol{\tau}$) and minimum embedding dimension (m) as parameters for different Multiscale Entropy calculations. We have then created a feature space F containing the outputs of all the popular Multiscale Entropy algorithms like, Multiscale Sample Entropy(X1) [36], [37], Refined Composite Multiscale Sample Entropy(X2) [38], [39], Multiscale Permutation Entropy(X3) [40], [41], Multiscale Composite Permutation Entropy(X4) [40], [42], and Multiscale Fuzzy Sample Entropy(X5) [43]. Similarly, we have calculated the entropies for ECG rate and Respiration signals. We have used the overall feature set to train different ML models for performance analysis and validation of the same in detecting Apnea and Normal events. The entire coding was done using Python 3.9 Anaconda environment running in laptop with 2.8 GHz Intel Core i3 10th Gen processor with 4GB RAM and relevant links to the source code is provided in the appendix. The data was sourced from Physionet.org for ECG based Sleep Apnea studies.

In the next section (II) the methodology is explained in detail and then moving on to the results and discussion (III). The article is concluded (IV) in the end with future recommendations(V) on enhancing this research outcome.

4.2.2. Methodology:

This section explains the steps of the proposed algorithm for efficient and accurate detection of Sleep Apnea events using Machine Learning models trained with Multiscale Entropy Features. The section is divided into Data Sourcing, Data Preprocessing, Feature Extraction, Machine Learning and Performance Validation. The detailed flow chart of the proposed algorithm is shown in fig.20. In the proposed methodology ECG lead 1 signals are isolated into 1 min segments and then denoised using 1D discrete wavelet transforms. The denoised ECG signal is then used to locate R peaks, based on which the instantaneous heart rate signal and ECG derived respiration signal are obtained. Three signals viz. ECG, heart rate and EDR are simultaneously used to calculate delay embedding parameters for multiscale entropy calculation and this step is repeated throughout the signal vectors for feature extraction. The obtained feature set is used to train the classifier models and validate the model performance based on the test data from the feature set. The model then classifies whether the signal belongs to apnea or Non apnea class.

a. Data Sourcing

The proposed algorithm has been trained and tested using Apnea-ECG dataset downloaded from Physionet.org [68],[69]. The data are made up of 70 records, which may be obtained from this page. The records are broken down into a learning set of 35 records (a01 through a20, b01 through b05, and c01 through c10) and a test set of 35 records (x01 through x35). The length of each recording ranges from little under 7 hours to about 10 hours.

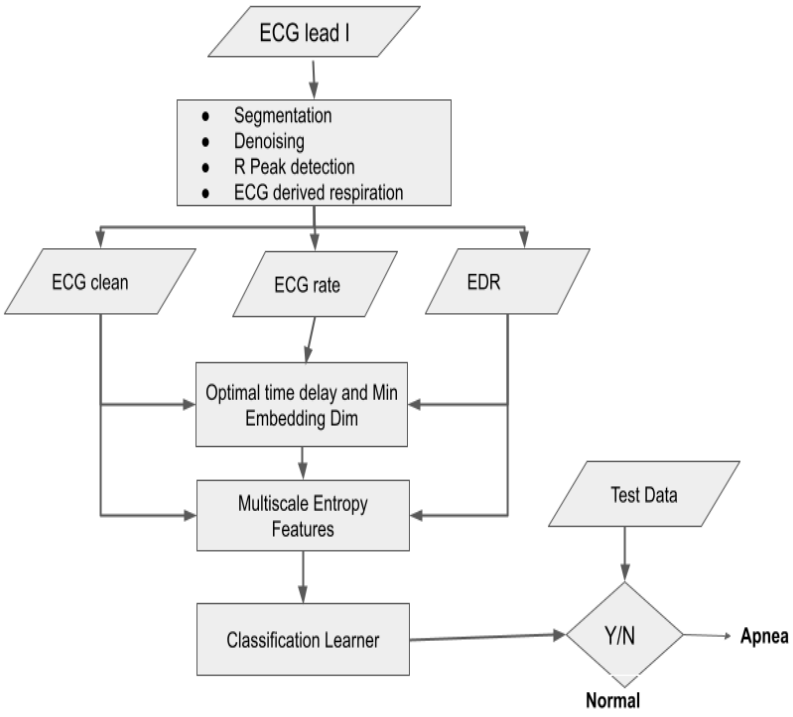

Fig.20 ECG Apnea detection flow chart

Each recording consists of a continuous digitised ECG signal, a collection of apnea annotations (determined by human experts based on simultaneously recorded respiration and related signals), and a set of machine-generated QRS annotations (in which all beats regardless of type have been classified normal). Digitised ECGs (16 bits per sample, least significant byte first in each pair, 100 samples per second, nominally 200 A/D units per millivolt) are stored in files with names of the kind rnn.dat. We have used the learning set of 35 ECG recordings viz. a01 through a20, b01 through b05 and c01 through c05.

b. Data Preprocessing

In this stage, we have downloaded the dataset from the PhysioNet repository and started preparing the dataset in order to meet our algorithm requirements. In the first stage we have segmented the dataset into 1 min segments since Apnea and Non-Apnea events are labelled for every 1 min interval. We have extracted the data from all the 35 recordings and combined them into a single pandas data frame. The segmented data is then cleaned using Wavelet based denoising, where the

choice of wavelet being Sym5 and level 1 to smoothen the signal without losing any relevant information from the ECG morphology. The cleaned ECG signal shown in Fig.21 is then used to determine the R peaks using the improved Pan Tompkins algorithm by Nabian et.al [44]. The ECG motion artifacts have been removed from the segments using the method as suggested by Lipponen & Tarvainen [45] based on the beat classification technique for HRV analysis. The R peaks were detected after removal of the motion artifacts. After the calculation of the R peaks based on the above algorithms, we have separately calculated the ECG rate and ECG Derived Respiration (EDR) from the Clean ECG signals as explained below.

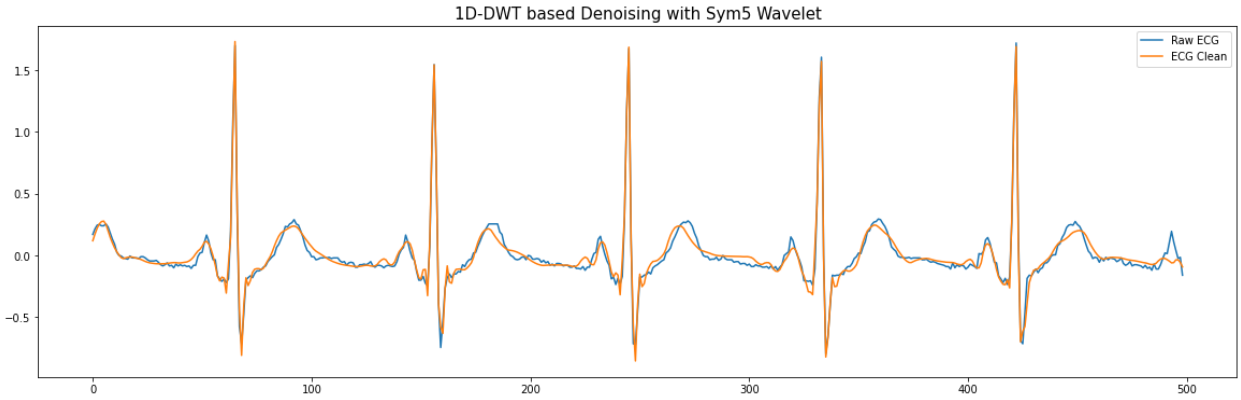

Fig.21 The clean ECG signal as obtained from the wavelet based denoising of raw ECG signal

ECG rate

The ECG rate is obtained by analysing a series of peaks to get the signal rate (per minute). It is a universal function that applies to any peak sequence (i.e., not specific to a particular type of signal). The calculation is 60 divided by the period, where the period is the interval between the peaks. The ECG rate with mean heart rate line is shown in fig.22

EDR

In order to identify and treat problems like stress and sleep disturbances, continuous monitoring of breathing is essential. Biomarkers for the detection of mental stress, anxiety, and sleep apnea occurrences include respiratory rate, breathing phases, and tidal volume. Additionally, the relationship between respiration and heart rate has been explored to investigate the interactions between the cardiac and respiratory systems as well as a biomarker for the aforementioned disorders.

ECG-derived respiration (EDR) is a non-invasive way to monitor respiration activity when respiratory signals are not recorded. EDR is the extraction of respiratory information from ECG. This offers ease in clinical settings since it enables simultaneous cardiac and respiratory signal monitoring from an ECG signal that has been collected.[19]

Numerous studies have demonstrated that respiration extracted from an ECG can approximate the respiratory rate and even the respiratory wave pattern (EDR). The morphological characteristics of the ECG, which are primarily impacted by respiration, characterise the derived signal. The respiratory-induced chest motions that alter the electrodes' position in relation to the cardiac vector can be used to explain this influence. Additionally, the electrical impedance of the chest changes as the lungs fills and empty. Respiration therefore influences the ECG's shape. The ECG derived respiration is calculated from the ECG_rate signal using the algorithm as suggested by Van Gent et al. [46], shown in Fig.23.

The proposed algorithm extracts the breathing patterns from the gathered heart rate data in addition to heart rate. Heart rate typically rises with breath and falls with exhale. As a result, it becomes possible to estimate the breathing rate from heart rate data. The Van Gent's method uses a single channel ECG signal and a bandpass filter with a cutoff frequency of around 0.16 Hz to extract the respiratory component from the ECG signal. The filtered signal is then rectified and low-pass filtered to obtain a smoothed respiration signal.

The following steps are involved in the Van Gent's method:

1. Preprocessing: The ECG signal is first pre-processed to remove any baseline wander and noise.
2. Bandpass Filtering: A bandpass filter with a cutoff frequency of around 0.16 Hz is applied to the pre-processed ECG signal to extract the respiratory component.
3. Rectification: The filtered signal is rectified to ensure that only positive amplitudes are considered.
4. Low-Pass Filtering: The rectified signal is then low-pass filtered with a cutoff frequency of around 0.05 Hz to obtain a smoothed respiration signal.
5. Peak Detection: The peaks of the respiration signal are detected, and the time difference between consecutive peaks is calculated.
6. Respiration Rate Calculation: The respiration rate is then calculated by dividing the number of peaks detected within a specified time period (usually 1 minute) by the time duration.

The respiration rate calculated using the Van Gent's method may not be as accurate as that obtained using more sophisticated methods such as impedance pneumography or respiratory belt measurement. However, it is a simple and non-invasive method that can be used in situations where other methods are not available or practical.

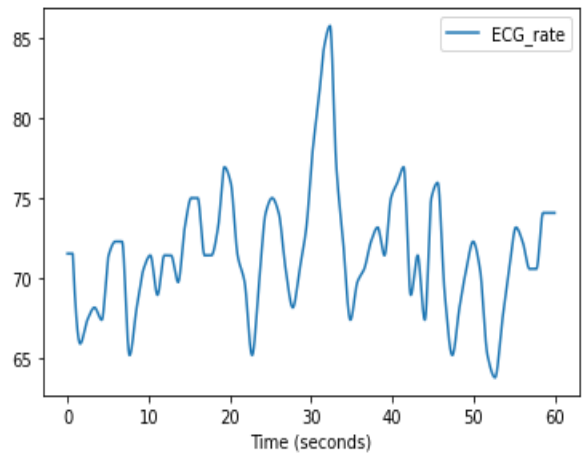

Fig.22. ECG rate or variation of heart rate per min.

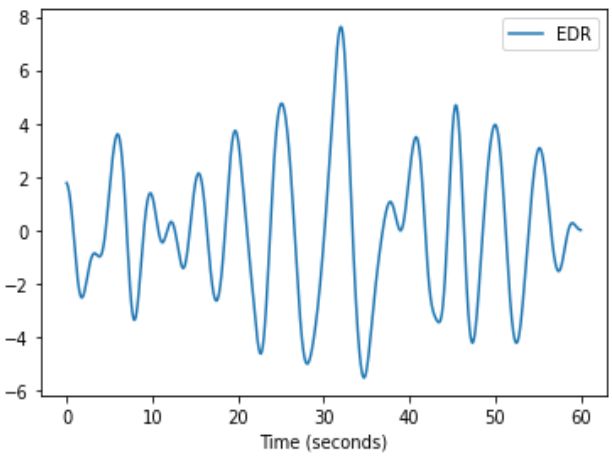

Fig.23. ECG derived Respiration or EDR

After calculating the ECG_rate and EDR signals a data frame is constructed in pandas with three signals for every raw ECG signal segment. The data frame keys include ECG_Clean, ECG_Rate and EDR which represent the pre-processed dataset to be used for feature extraction and subsequent AI model training to predict Sleep Apnea events.

c. Calculation of Time Delay and Minimum Embedding Dimension

One of the two crucial variables used in the creation of the time-delay embedding of a signal is the time delay (Tau, also known as Lag), together with the embedding dimension m. It reflects the time difference between the original signal and its delayed form as measured in samples (s). In other words, how many samples are taken into account between a signal's current state and its nearest previous condition. When Tau is less than the ideal theoretical value, the attractor is not adequately expanded and successive coordinates of the system's state are connected. On the other hand, when it is larger than it ought to be, subsequent coordinates become almost completely independent, creating an unrelated and chaotic cloud of dots. Different approaches were put forth by various authors to help in selecting the delay but while choosing we went for Rosenstien's time delay estimation using autocorrelation function and choosing the optimal delay when the magnitude of the autocorrelation function falls to (1/1-e) from the peak [47].

The second crucial factor (the first being the delay) in the creation of a time-delay embedding of a signal is the Embedding Dimension (m, also known as d or order). It relates to the quantity of delayed states (lagged-by versions of the signals) that we embed. Although values of 2 or 3 are frequently used in practice, multiple writers proposed several numerical techniques to direct the choice of m. In our case we have used the modified False Nearest Neighbours Algorithm by Cao [48] for calculation of minimum embedding dimension based on Average Nearest Neighbours. It averages all ratios of the distance in the m+1 to m dimension, specifies E1 and E2 as parameters, and utilises the maximum Euclidean distance to represent nearest neighbours. When E1 stops changing, the dimension is said to be optimal (reaches a plateau). If the signal originates from an attractor, E1 plateaus at dimension d0. The ideal minimum embedding dimension is then d0*+1.

To discriminate between deterministic and stochastic signals, E2 is a helpful parameter. Since the future values are unrelated to the previous values, a constant E2 close to 1 for any embedding dimension d suggests random data. The estimation of optimal time delay and optimal dimension is shown in Fig.24 and Fig.25 respectively, which has been used as the best choice of parameters for Entropy estimation in the next steps.

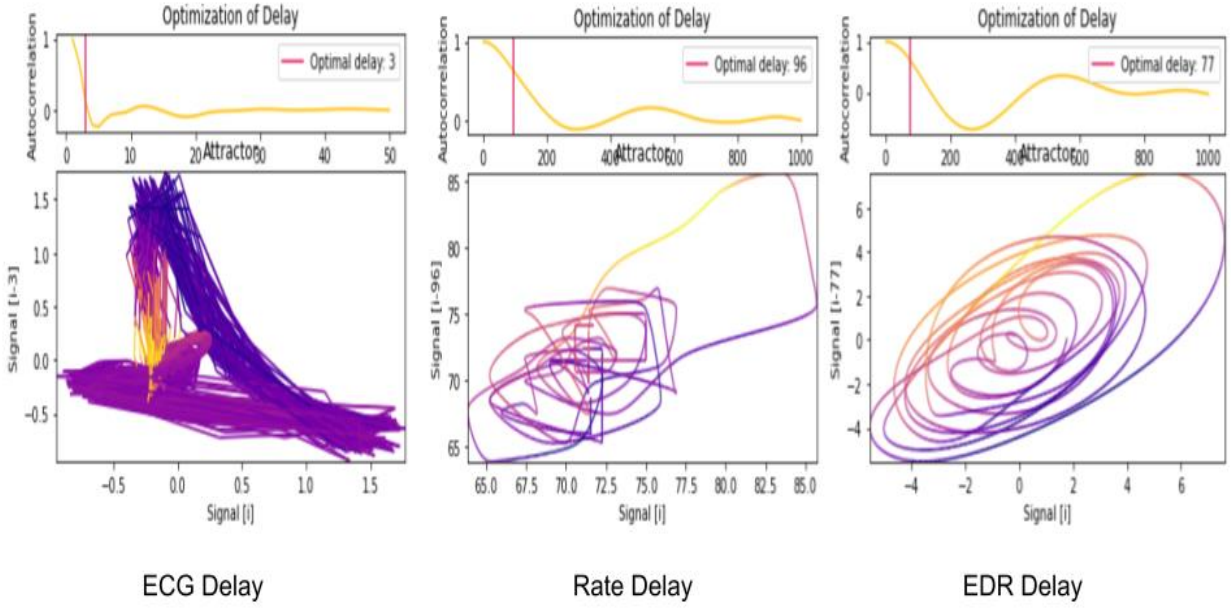

Fig.24. The optimal time delay estimation using Rosenstein autocorrelation method and and delay time attractors

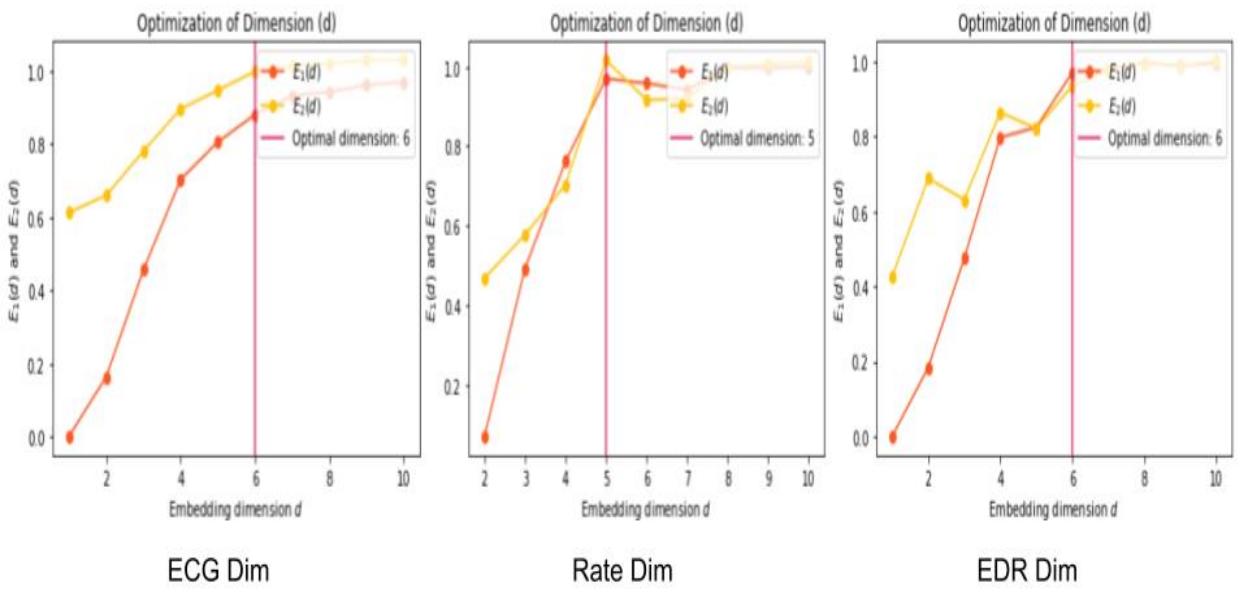

Fig.25. The optimal embedding dimension (d) as obtained by the Average Nearest Neighbour method suggested by Cao, to select the optimal dimension when both the Estimators E1 and E2 cross each other and stop changing.

A time delay of 3 and a minimum embedding dimension of 5 are typical values used for chaotic systems. Chaotic systems exhibit sensitive dependence on initial conditions and complex temporal behaviour, making them difficult to model using traditional mathematical approaches. The time delay embedding technique provides a way to reconstruct the dynamics of these systems in a phase space, making it possible to analyse and predict their behaviour.[49]

d. Multiscale Entropy Analysis

A variety of metrics, such as sample entropy and approximate entropy, can be used to analyse the complexity of time series. Some of these indicators do not, however, account for the many time scales present in physical systems. Costa et al. proposed the multiscale entropy technique to characterise signal complexity in the 2000s. The sample entropy algorithm is used in the MSE algorithm to evaluate coarse-grained time series, which describe the system dynamics on several scales. MSE relies on the computation of sample entropy over a variety of scales. Since its inception, MSE has gained popularity as a way for determining how complicated a signal is. It has been successfully employed in a variety of research domains, such as biological time series

The features for training the machine learning model for classification of sleep apnea events are obtained from the Multiscale Entropy Analysis using sample entropy and permutation entropy based multiscale estimators. Here, we propose to utilise the most advanced of these algorithms, which were developed to address some of the original MSE's drawbacks. The original MSE algorithm along with the various improvements which address several drawbacks are presented in the review paper by Anne Humeau-Heurtier. We have used a combination of a few selective algorithms to obtain MSE values at higher scales irrespective of the data length and sampling frequency.

The feature set is defined as a union U of the other three feature vectors as shown in eq.1. The overall feature set is computed as a set of all the different entropy calculations for each individual 1min segment of ECG, Heart Rate and EDR signals.

$$F_{all} = U\{Fecg(x1, x2, \ldots xi),\ Frate(x1, x2, \ldots xi),\ Fedr(x1, x2, \ldots xi)\};\ i = 1 \text{ to } 5 \qquad \text{Eq. [1]}$$

Here x_1 = Multiscale Sample Entropy, x_2 = Refined Composite Multiscale Sample Entropy, x_3 = Multiscale Permutation Entropy, x_4 = Multiscale Composite Permutation Entropy, x_5 = Multiscale Fuzzy Sample Entropy. Therefore, the overall set of features is of the size (5 x 3) 15 columns for each signal segment. The target variable is a binary column [1 = Apnea and 0 = non-Apnea] embedded with the feature matrix.

Multiscale Sample Entropy (MSE)

There are two steps in the MSE algorithm [37].

(1) a coarse-graining method to produce a collection of time series that depict the dynamics of the system on various time scales. The time series data are averaged inside successive but separate windows of length *i* to produce the coarse-graining method for scale *i*. Thus, the coarse-grained time series is computed as for a univariate discrete signal of length *N* $\{x_1, x_2, \ldots, x_N\}$ is given by the equation below:

$$y_j^{(\tau)} = \frac{1}{\tau}\sum_{i=(j-1)\tau+1}^{j\tau} x_i \ , \qquad 1 \le j \le \frac{N}{\tau} \qquad \text{Eq. [2]}$$

For scale one, the coarse-grained time series $\{y^{(1)}\}$ corresponds to the original signal. The length of the coarse-grained time series $\{y^{(\tau)}\}$ is N/τ.

(2) Calculating each coarse-grained time series' sample entropy.

A sequence of *m* consecutive data points that matches another sequence of the same length will likely still match the other sequence when their length (match with tolerance of r) is increased by one sample (sequences of m+1), according to the conditional probability measure sample entropy. *m* thus designates the length of the patterns that are being compared to one another. The biggest absolute difference of the respective scalar components of two vectors is determined in this definition to represent the distance between them. Sample Entropy is given by the equation below.

$$SampEn(m, r, N) = -ln\frac{A^{(m)}(r)}{B^{(m)}(r)} \qquad \text{Eq. [3]}$$

where $A^{(m)}(r)$ is the probability that two sequences will match for m + 1 points and $B^{(m)}(r)$ is the probability that two sequences will match for m points (with a tolerance of r), where self-matches

are excluded. Analytical representation of the sample entropy of a coarse-grained white noise time series, can be expressed as given in the equation below.

$$X = -ln \int_{-\infty}^{+\infty} ½ \sqrt{\frac{\tau}{2\pi}} \left[er\left(\frac{x+r}{\sqrt{\frac{2}{\tau}}}\right) - er\left(\frac{x-r}{\sqrt{\frac{2}{\tau}}}\right) \right] \exp\left(-\frac{x^2\tau}{2}\right) dx \qquad \text{Eq. [4]}$$

The overall expression in Eq. [4] calculates the negative natural logarithm of the integral of a complex function involving the error function, exponential function, and the square of x. This formula captures the complexity or irregularity in the white noise signal by considering the similarity between different patterns within the signal.

Multiscale Permutation Entropy (MPE)

PE or Permutation Entropy is based on the permutation patterns and order relations between signal value orders. In some well-known chaotic dynamical systems, such the noise-free logistic map, it is equivalent to the Lyapunov exponents; nevertheless, PE produces more significant results in the presence of both observational and dynamical noise. PE is computationally quick, has fewer parameters and is conceptually simpler than other entropies like Approximate Entropy and Fuzzy Entropy. It is also more resistant to artefacts and noise. Furthermore, both non-stationary and non-linear signals can be employed with the PE. Permutation Entropy (PEn), which extracts a probability distribution of the ordinal patterns in between values of a time series, is a reliable indicator of the complexity of a dynamic system. Utilising ordinal descriptors improves resistance to significant artefacts that occur infrequently. PEn has been used in the context of EEG, ECG, and stock market time series and is applicable to regular, chaotic, noisy, or real-world time series. It is equivalent to the Shannon entropy mathematically speaking after the signal has been discretized by examination of the permutations in the time-embedded space.

Let us assume an univariate discrete signal of length N be x = {x_1, x_2, …., x_N} and at each time t of x, a vector is created as: $X_t^{d,\tau} = \{x_t, x_{t+1}, \ldots\ldots x_{t+(d-2)\tau}, x_{t+(d-1)\tau}\}$ for t = 1,2,...*N-(d-1)*τ, where d is the minimum embedding dimension and τ is the time delay.. While calculating PE, the d values x_i are associated with numbers from 1 to d and arranged in ascending order as $\{x_{t+(j_1-1)\tau}, x_{t+(j_2-1)\tau}, \ldots\ldots x_{t+(j_{d-1}-1)\tau}, x_{t+(j_d-1)\tau}\}$. Now for each different sample, d! number of different ordinal patterns will be there known as 'motifs' and denoted by π. For each motif, the relative frequency is calculated as follows:

$$p(\pi_i^{d,\tau}) = \frac{C\{t|t \le N-d, type(X_t^{d,\tau}) = \pi_i^{d,\tau}\}}{N-d+1} \quad \text{Eq. [5]}$$

where C{} denotes the cardinality of the set. From this the PE is obtained as the following expression

$$H(x,d,\tau) = -\sum_{\pi_k=1}^{\pi_k=d!} p(\pi_k)\, ln\, p(\pi_k) \quad \text{Eq. [6]}$$

The highest value of PE is obtained when all motifs have equal probability and the lowest value of PE is obtained closer to zero in case of a completely regular signal. Like MSE, MPE consists of two primary phases. First, a time series is subjected to a "coarse graining" procedure. Take into account an N-length real-valued time series. By averaging the temporal data points inside non-overlapping frames of increasing duration, or scale factor, multiple subsequent coarse-grained versions are created. While in the second step PE is calculated for each coarse-grained time series. The obtained PE values are then plotted as a function of the scale factor.

Improved Versions of MSE and MSPE

MSE is a method that can be used with different types of entropic measures. The calculations of MSE and MSPE based on Sample Entropy and Permutation Entropy have certain drawbacks,

which were addressed in their improved versions. Many authors suggested different changes in the original way of calculating MSE either by changing the coarse graining procedure from sequential to time shifted and rolling average or by adopting methods to reduce the variance of entropy values computed at larger scales. In this regard many algorithms have been proposed such as Refined Multiscale Entropy, Composite Multiscale Entropy, Refined Composite Multiscale Entropy, Modified Multiscale Entropy, Intrinsic Mode Entropy, Hierarchical Entropy, Adaptive Entropy, etc. All the above-mentioned algorithms make use of SampEn or PE to obtain accurate results of entropy.

Fuzzy versions

In order to address the drawbacks of the above-mentioned algorithms for short time signals and non-deterministic signals, the Fuzzy version of the Multiscale SampEn has been realised. Therefore, it can be said that the Fuzzy version of SampEn can actually address all the drawbacks in estimation of entropy of nonstationary and nonlinear physiological signals and systems.

Fuzzy Sample Entropy (FSE) is a measure of complexity of a time series, based on the concept of fuzzy logic. It is a variation of sample entropy, which is a measure of regularity and complexity of signals. FSE is used to measure the complexity of a signal in the presence of noise and works better than sample entropy in the presence of non-stationary and noisy signals. FSE along with its Multiscale versions, has been used in a variety of applications including biomedical signal analysis, biomedical signal classification, and automatic speech recognition. Fuzzy Entropy is given by the following equation.

Fuzzy Entropy = -1 * (Sum of (Membership Degree * log (Membership Degree))) Eq. [7]

Where the Membership Degree is the degree of similarity between two time series in case of SampEn.

The choice of optimal **scale factor** for Multi Scale Entropy estimation is chosen as following

$$Scale = \frac{len(sig)}{m+10} \quad \text{Eq. [8]}$$

Where len(sig) denotes length of the signal and m is the minimum embedding dimension.

Machine Learning Model

Machine Learning models are algorithms used to build predictive and classification models from data. These models are used to identify patterns or underlying relationships in data, and can be used for a variety of tasks, including predicting future outcomes or classifying data points. They can also be used for anomaly detection or identifying outliers in a dataset, or for clustering data points into distinct categories. The types of Machine Learning models range from supervised learning algorithms like logistic regression and support vector machines, to unsupervised learning algorithms like k-means clustering. Machine Learning models are a powerful tool for understanding and leveraging data to make more informed decisions.

We have chosen the most popular ML models used in classification of real-world datasets and have a proven track record of delivering good performance. The models included in our study for automated classification of sleep apnea events from single lead ECG data are defined below.

1. Decision Trees (DT): Decision trees are a supervised learning algorithm used for both classification and regression problems. It uses a tree-like structure to make decisions based on certain conditions and it uses a set of if-then rules to classify a given data. [50]
   Model Parameters – [criterion: 'entropy', max_depth: 12, min_samples_split: 2, min_samples_leaf: 1, max_features: None (All features), splitter: best, minimum_impurity_decrease: 0.0]
2. Random Forest (RF): Random Forest is an ensemble learning algorithm. It is an extension of the decision trees algorithm. It creates a forest of decision trees from randomly selected subsets of the training set. It then averages the results from different decision trees to improve the accuracy of the predictions.[51]

Model Parameters –[n_estimators: 128, criterion: 'gini', max_depth: 10, min_samples_split: 2, min_samples_leaf: 1, max_features: 'auto', bootstrap: True]

3. Support Vector Machines (SVMs): SVMs are supervised learning algorithms used for both classification (SVC) and regression (SVR) problems. It is one of the most powerful machine learning algorithms and is based on the concept of finding a hyperplane that best separates the data points.[52]
   Model Parameters – [C: 1.0, kernel: 'rbf', degree: 3, gamma: "scale', coef0: 0.0, shrinking: True, probability: True, tol: 0.001, cache_size: 200, class_weight: None]

4. AdaBoosted Decision Trees (ADT): AdaBoost (Adaptive Boosting) is a machine learning algorithm that combines the predictions of multiple weak classifiers to create a strong classifier. In the case of decision trees, the AdaBoost algorithm is known as AdaBoosted Decision Trees (ADT). In ADT, the algorithm begins by training a decision tree on the training data. This tree is typically a small, shallow decision tree called a weak learner, which may have low accuracy on its own. The algorithm then evaluates the performance of this tree on the training data and assigns weights to each data point based on whether it was classified correctly or incorrectly. The algorithm then trains another decision tree, but this time it places greater emphasis on the misclassified data points from the previous tree, by assigning them higher weights. This process is repeated for a specified number of iterations, with each subsequent tree trying to correct the errors of the previous trees. Finally, the individual trees are combined into a single strong classifier, where each tree is weighted according to its performance during training.
   Model Parameters – [base_estimator: DecisionTreeClassifier, n_estimators: 50, learning_rate: 1.0, algorithm: 'SAMME.R', random_state: None

5. Voting Classification Model (VC): A voting classifier (VC) model is an ensemble model that combines multiple individual classification models and predicts the class based on the highest probability of the predictions of the individual models. In other words, the voting classifier model makes the final prediction by aggregating the outputs of several base

classifiers. There are two main types of voting classifier models i.e Hard Voting and Soft Voting of the predicted probabilities from the ensemble of base models. The architecture of the Voting Classification model used here is shown in fig. We have used RF, SVC and DT to create the ensemble model and a soft voting classifier model that predicts the outcome based on the predicted probabilities of the base models. [53] Model Parameters – [estimators: ['RF', 'SVC', 'DT'], voting: 'soft', weights: None, n_jobs: None, flatten_transform: True]

6. Stacked Classification Model (SC): A stacked classifier (SC) model is a type of ensemble learning model that combines multiple classifiers or base models to make more accurate predictions. In a stacked classifier model, the outputs of the base models are combined using a meta-classifier, which learns to make predictions based on the outputs of the base models. In our case we have used RF, SVC and ADT as base learning models and Multi-Layer Perceptron (MLP) neural network model as the Meta classifier. The detailed architecture of the stacking mechanism is shown in fig 26. [54], [55] Model Parameters – [estimators: ['RF', 'SVC', 'ADT'], final_estimator: MLP, cv: None, stack_method: 'predict_proba', n_jobs: None, passthrough: False]

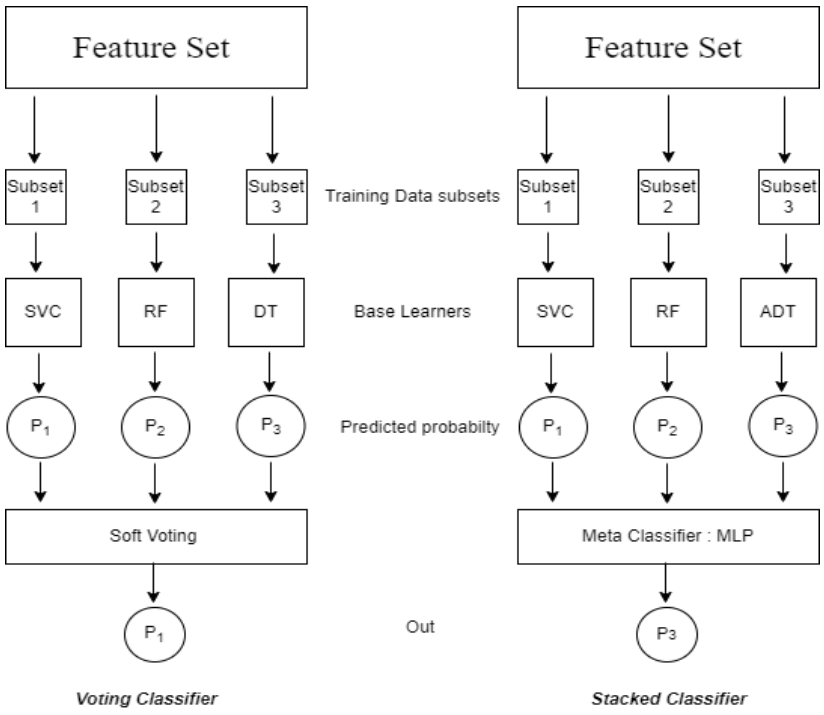

Fig.26 The block diagram representation of the voting classifier model and stacked classifier model incorporated here to create advanced models for classification of apnea events

The feature set is split as 70% training dataset and 30% test dataset with 5 folds validation for performance evaluation of the said ML models. The model performance is evaluated based on the below mentioned performance evaluation metrics.[56]

1. Accuracy Score: Accuracy is the number of correctly predicted results divided by the total number of predictions made.
2. Sensitivity: Precision is the ratio of correctly predicted positive results to the total number of predicted positive results.
3. Specificity: Recall is the ratio of correctly predicted positive results to the total number of actual positive results.
4. ROC Curve: ROC Curve is a graphical representation of the performance of a classification model at various thresholds.
5. AUC: AUC is the area under the ROC curve and it is used to measure the performance of a classification model.

Sensitivity and specificity are two important metrics for evaluating the performance of any algorithm as obtained from the Confusion Matrix. Sensitivity measures the proportion of true positives that are correctly identified, while specificity measures the proportion of true negatives that are correctly identified. To calculate sensitivity and specificity, we used the following formula:

$$\text{Sensitivity} = (\text{True Positives}) / (\text{True Positives} + \text{False Negatives}).$$

$$\text{Specificity} = (\text{True Negatives}) / (\text{True Negatives} + \text{False Positives}).$$

4.2.3. Results and Discussion

In this section, the results obtained for the procedure of MSE based feature extraction are presented along with the Machine Learning models performance metrics. The results are thoroughly discussed to make sense of the quantitative values associated with the underlying physiological phenomenon of cardiac activity. Multiscale entropy (MSE) features are an important tool in machine learning, as they can provide valuable insight into the complexity of data. MSE can provide a measure of the complexity of data by calculating the entropy of the data at multiple scales. This allows for the detection of subtle patterns that would otherwise be difficult to detect using traditional methods. MSE can also be used to detect anomalies in data, which can be used to improve accuracy in classification tasks. In addition, MSE can be used to reduce the dimensionality of data, allowing for more efficient and accurate training of machine learning algorithms. The estimation of MSE reduces the chance of misdetection of peaks or inter beat intervals, since it calculates the rate of information transfer among ordered samples. The estimation of entropy is generally independent of data length and sampling frequency; therefore, it can be used to measure interval related analysis or event-based analysis. We aimed to explore the possibility of MSE features in correctly classifying the diseased from the normal. The high degree of nonlinearity and nonstationary in ECG signals makes it advisable to work with Entropy features after proper estimation of its optimisation parameters like time delay and minimum embedded

dimension. Estimation of time delay was attempted for each segment of the signal and similarly for the minimum embedded dimension. The choice of time delay and minimum embedding dimension is crucial for accurate reconstruction of the dynamics of the system. In general, the time delay should be chosen to be greater than the correlation time of the system, while the minimum embedding dimension should be greater than or equal to the number of independent state variables of the system.

All the plots in Fig.27, contain the plots of different Multiscale Entropy Analysis Techniques used to calculate the feature set for training Machine Learning models for sleep apnea detection using single lead denoised ECG as per the proposed methodology. The plots for calculating the Multiscale Entropy analysis results of ECG rate and ECG derived Respiration are presented in Fig.28 and Fig.29 respectively.

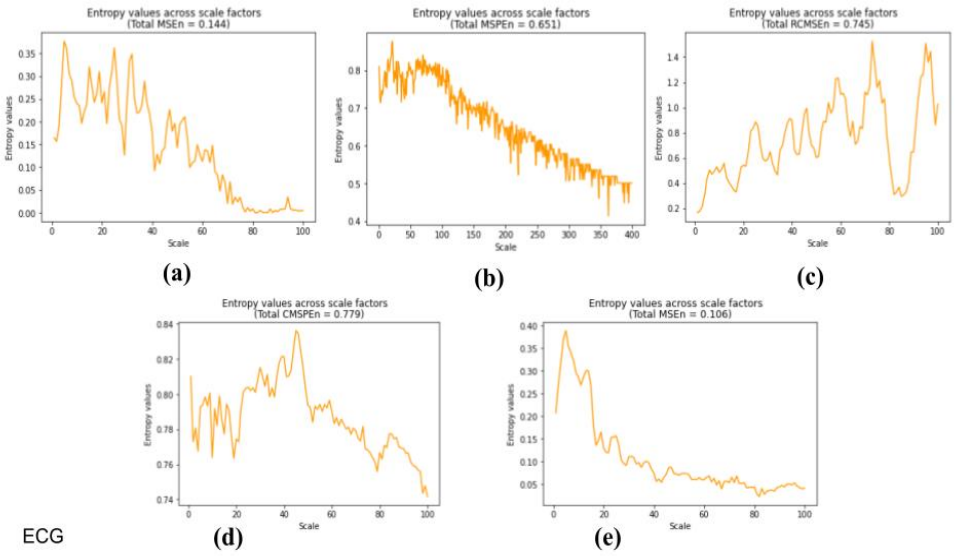

Fig.27. The multiscale entropy analysis results are shown where each figure corresponds to sample entropy and permutation entropy calculations with different techniques of coarse graining and windowing functions. Multiscale Analysis: (a)MS-SampEn, (b)MS-PEn; Refined Composite Multiscale Analysis: (c)RCMS-SampEn, (d)CMS-PEn; Fuzzy Multiscale Analysis: (e)FuzzyMS-SampEn

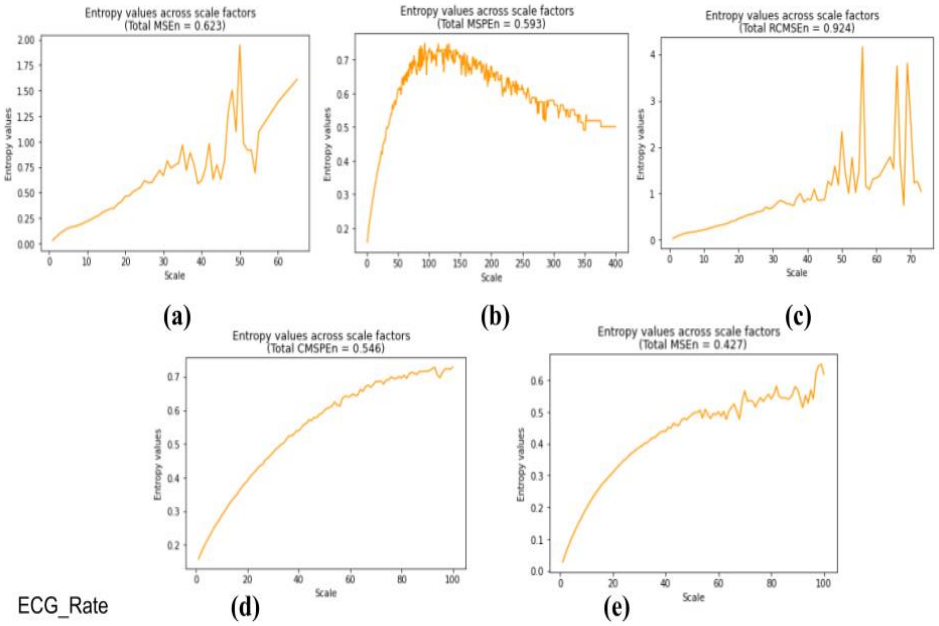

Fig.28. The Multiscale entropy plots as obtained from MSE analysis using different methods on ECG_Rate signal.Multiscale Analysis: (a)MS-SampEn, (b)MS-PEn; Refined Composite Multiscale Analysis: (c)RCMS-SampEn, (d)CMS-PEn; Fuzzy Multiscale Analysis: (e)FuzzyMS-SampEn

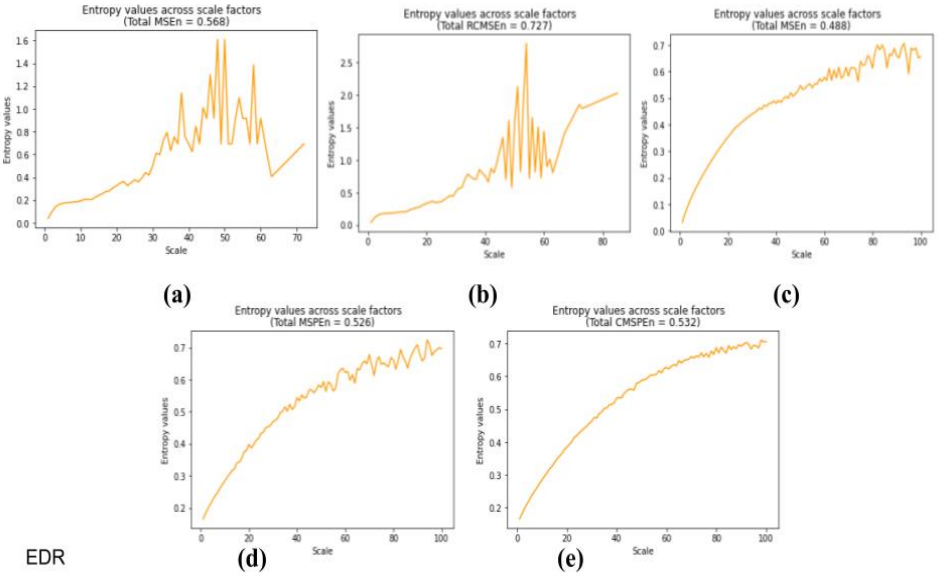

Fig.29. The Multiscale entropy plots as obtained from MSE analysis using different methods on ECG derived respiration signals. Multiscale Analysis: (a)MS-SampEn, (b)MS-PEn; Refined Composite Multiscale Analysis: (c)RCMS-SampEn, (d)CMS-PEn; Fuzzy Multiscale Analysis: (e)FuzzyMS-SampEn

In Fig.27 to Fig.29 the plots represent calculation of sample entropy and permutation entropy at multiple scales. From the figures it is very much clear that entropy values increase as we increase the scale factor, indicating that there is much more information content in the signal at higher scales than at single scale. The stochastic nature of the ECG signal is responsible for such a behaviour of the Entropy Plots. In ECG signals after scale 50 there is significant decrease of entropy values and the fluctuation reaches saturation. Increasing the scale factor beyond 100 can lead to even more accurate detection of Entropy Values but at a high computational cost. So we thought of calculating the area under the entropy vs. scale factor curve for scale factor up to 100. This approximation gave us an accurate estimate of entropy to be used as features for detecting Sleep Apnea events from single lead ECGs.

Feature Set Evaluation

The feature set serves as the multiparametric signature of the underlying patterns that represent a specific class, which is Sleep Apnea in our case. The multiple features change its magnitude based on the complexity of the patterns in segmented ECG channels. These features are the digital biomarkers of the said disease which identifies the abnormality based on estimation of the irregularity in patterns of ECG wave occurrence at each interval. These features have been found to be effective in discriminating between healthy individuals and those with sleep apnea, and may be useful in developing accurate and reliable diagnostic tools for this disorder. However, further research is needed to optimise the use of MSE features for sleep apnea detection and to validate their effectiveness in clinical settings.

Total number of ECG samples = 17039 [**A**: **38.23%** (6514 instances); **N**: **61.77%** (10525 instances)] Where A stands for Apnea which is the positive class and N is No-Apnea which is the negative class.

Total number of MSE features = 15(5:5:5) * 17039 = 255585

When two classes in a dataset are imbalanced, it means that one class has significantly fewer instances than the other. This can have several consequences on the performance of machine learning models trained on this dataset:

1. Bias: The imbalanced dataset can introduce a bias towards the majority class, which may lead to poor performance on the minority class. The model may predict the majority class most of the time, which can result in low accuracy, precision, recall, and F1 score for the minority class.
2. Overfitting: The model can overfit on the majority class, which can cause it to perform poorly on the minority class. Overfitting occurs when the model becomes too specialised on the training data and does not generalise well to new data.
3. Poor generalisation: The model may not be able to generalise well to new data, especially if the imbalance is extreme. This can be problematic when deploying the model in the real world where the distribution of the classes may be different from the training data.

There are several techniques that can be used to address the imbalance in the dataset, such as:

1. Resampling: This involves either under sampling the majority class or oversampling the minority class to balance the distribution.
2. Synthetic data generation: This involves generating new data points for the minority class using techniques such as data augmentation, SMOTE, etc.
3. Cost-sensitive learning: This involves assigning different misclassification costs to the different classes to account for the imbalance.
4. Ensemble learning: This involves combining multiple models to improve performance on the minority class.

This motivated us to try Ensemble learning since, generating synthetic abnormal diseased data, which is Sleep Apnea in our case needs proper expert validation and annotations, which may not agree with the algorithmic data labelling.

Table.4 The performance evaluation results of the different classification algorithms for finding the best_fit model

Prob Threshold= 50%	***Accuracy Score***	***Sensitivity***	***Specificity***	***False Positive Rate***	***AUC***
SVC	97.790	65.504	71.368	28.632	64.959
RF	100	52.574	71.281	28.719	62.082
DT	100	66.645	74.256	25.744	68.312
ADT	98.807	68.674	74.271	25.729	68.704
VC	100	65.197	72.815	27.185	66.529
SC	100	66.971	74.190	25.810	68.306
Prob Threshold= 70%	***Accuracy Score***	***Sensitivity***	***Specificity***	***False Positive Rate***	***AUC***
SVC	69.131	53.341	80.026	19.974	67.536
RF	66.569	51.679	85.377	14.622	68.205
DT	82.902	51.263	75.985	24.015	64.416
ADT	66.980	51.956	85.898	14.102	68.588
VC	67.410	51.905	83.459	16.541	67.813
SC	**74.315**	**53.799**	**82.740**	**17.260**	**68.960**

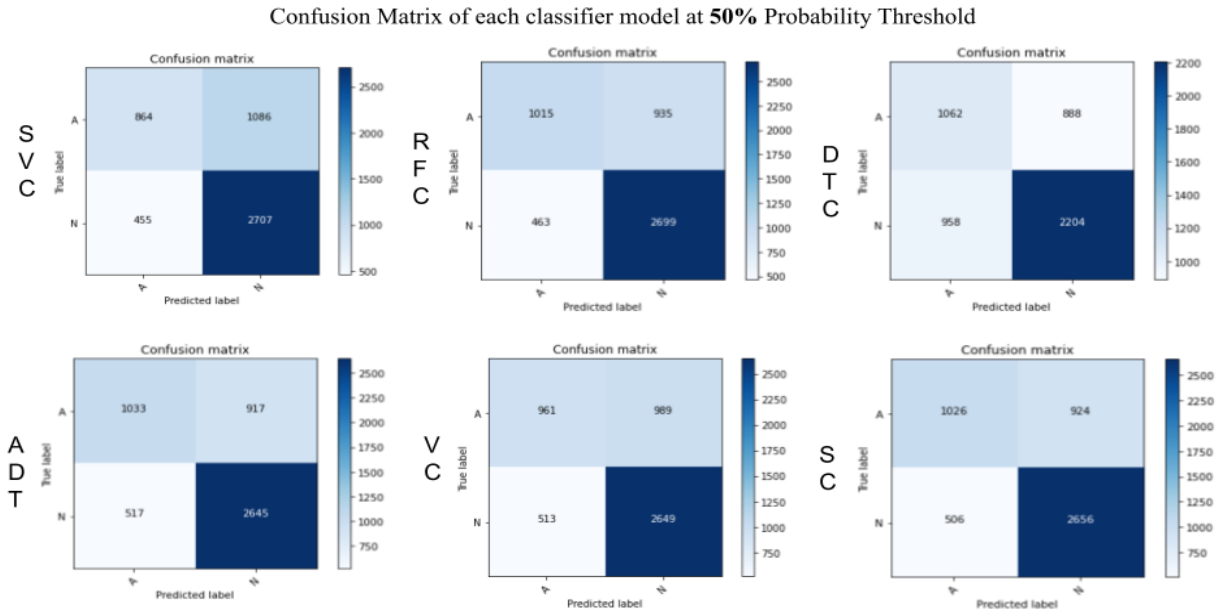

Fig.30. The figure showing Confusion Matrix of each classifier model at 50% Probability Threshold

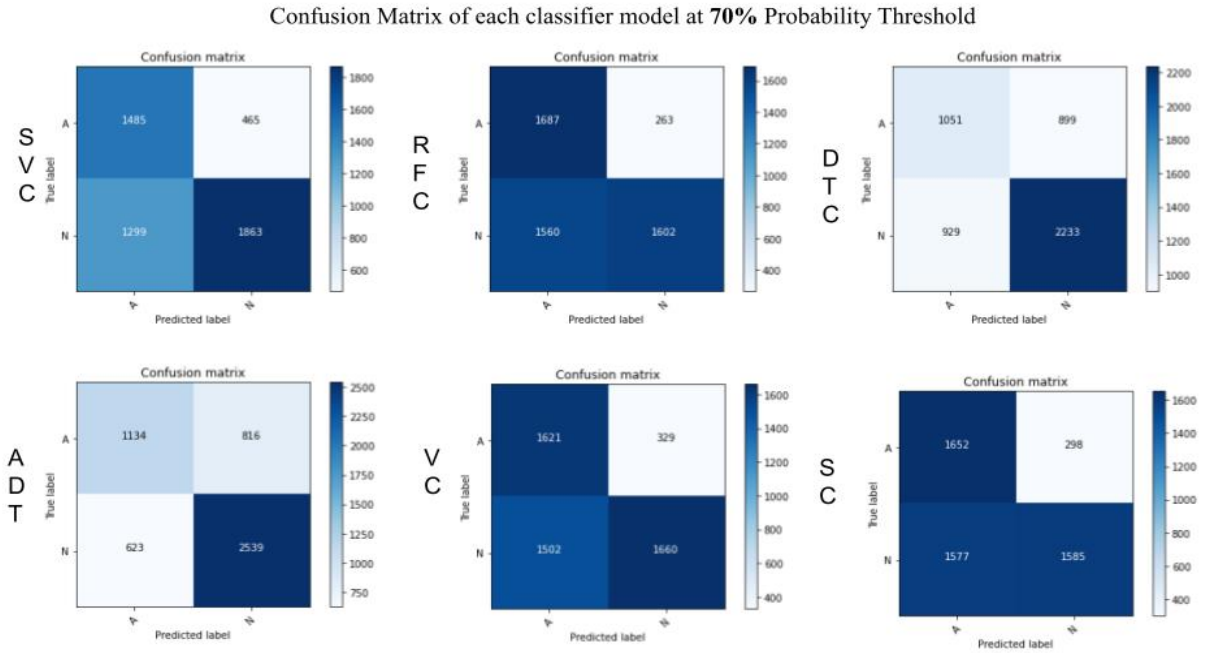

Fig.31. The figure showing Confusion Matrix of each classifier model at 70% Probability Threshold

In Fig.30 and Fig.31 the confusion matrix for each classifier model is shown at Probability Threshold of 50% and 70% respectively. In the 70% probability threshold we can see the significant reduction of false positives compared to the 50% threshold model in Fig. 30. The accuracy of the models' predictions is affected by the increase of probability threshold but a significant reduction is obtained in false positive cases.

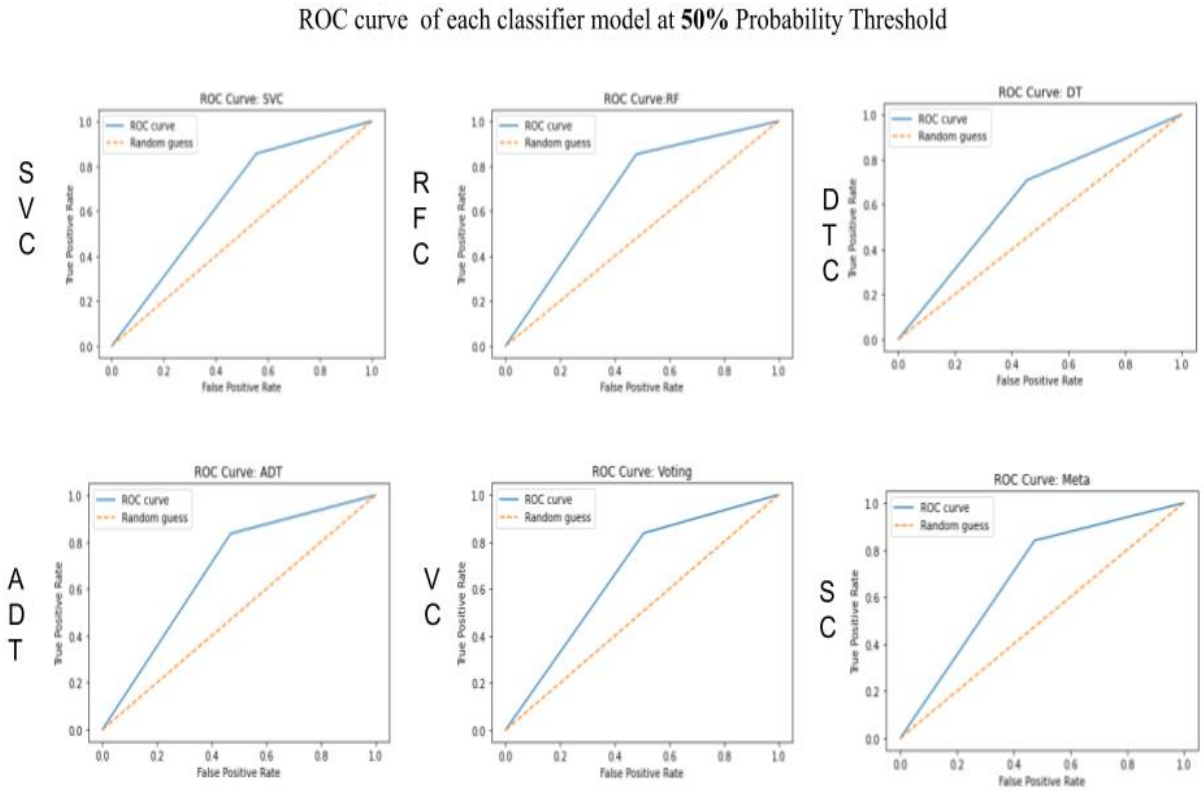

Fig.32. The figure depicts the ROC curve of each classifier model in comparison with a random guess scheme at 50% probability threshold.

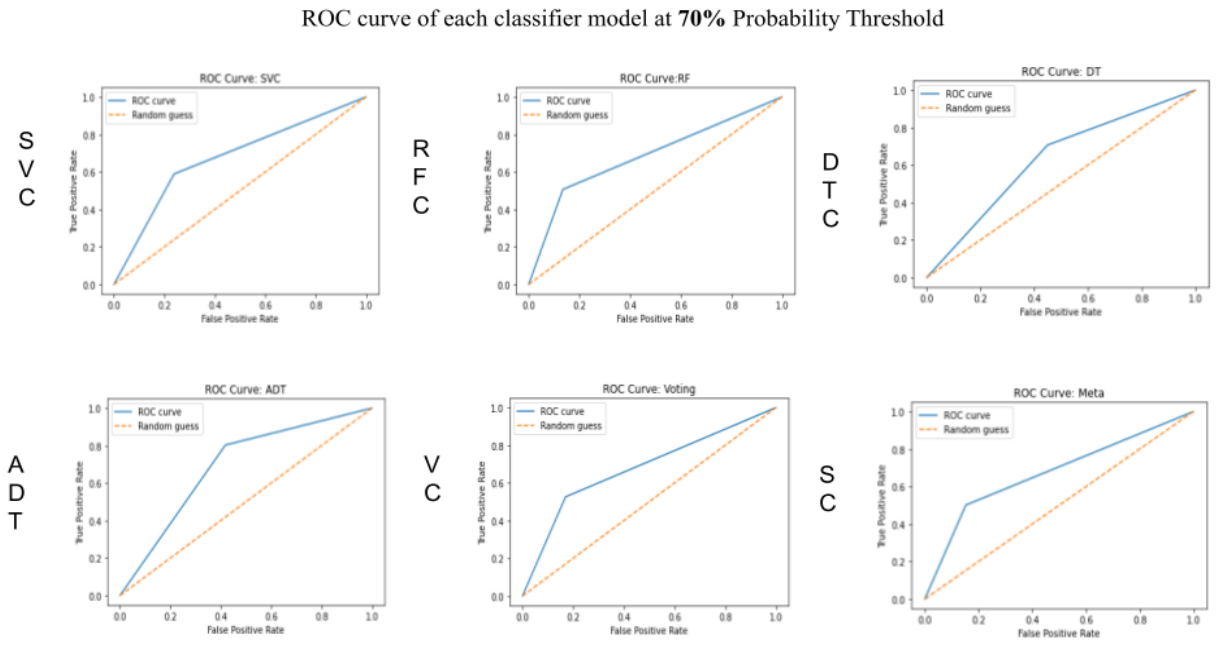

Fig.33. The figure depicts the ROC curve of each classifier model in comparison with a random guess scheme at 70% probability threshold.

In Fig.32 and Fig.33 The ROC curves for each classifier model are generated comparing the actual output labels in test set and predicted labels from the models, to identify the trade-off between false positives and true positive predictions made by the model on the test data. The AUC suggests that the predictions made by the models are better than random guess for each instance and hence the output is not a result of random guess rather it is deterministic with scope for improvement.

Based on the metrics provided in table.2, it appears that the models at 50% probability threshold have high accuracy but relatively low sensitivity and specificity. The false positive rate is also relatively high, indicating that the model may be incorrectly classifying a significant proportion of negatives as positives. The AUC is moderate, indicating that the model is better than random guessing, but not performing as well as it could be. A high specificity classifier model is useful when the goal is to minimize the number of false positive predictions, which are cases where the model incorrectly predicts a positive outcome when the true outcome is negative. In other words, a high specificity model is good at identifying true negative cases with a high degree of accuracy.

Applications of high specificity models include medical diagnosis, where a false positive prediction can lead to unnecessary treatment or interventions, and fraud detection, where a false positive prediction can lead to false accusations or unnecessary investigations. In these cases, it is important to have a model that can accurately identify negative cases and minimize the number of false positives.[57]

To address these issues, we increased the probability threshold to 70% and evaluated the performance of the models with an objective to reduce the false positives, since it is of utmost importance in the medical diagnostic applications.

Based on the performance metrics provided, the Stacked Classifier model with base learners and neural network based meta classifier has an accuracy score of 74.315%, which means that it correctly predicts the class label for about 74% of the samples in the dataset. The sensitivity of the model is 53.799%, which indicates that only around half of the actual positive samples are correctly identified by the model. On the other hand, the model has a relatively high specificity of 82.74%, which means that it correctly identifies a large proportion of the actual negative samples. The false positive rate is 17.26%, which indicates that the model misclassified around 17% of the actual negative samples as positive. The AUC score is 68.96%, which indicates that the model's performance is better than random guessing, but it is not very effective in distinguishing between the positive and negative classes. Overall, the model's performance is moderate, with a relatively high accuracy score and specificity but low sensitivity. The false positive rate is least in the Stacking ensemble method, which reduces the chances of incorrect predictions for some negative samples. Further analysis and improvements may be needed to improve the model's performance. In case of RF and ADT, the classification report suggests that the least false positive rate can be achieved by them but with a significant amount of reduction in the accuracy score relative to 50% probability threshold models and also Stacked Classification model. The ADT model's performance may also be considered to be moderate with very low false positives and satisfactory accuracy score. The ADT model is less prone to be overfitting the training dataset than the DT model, hence it can also be considered as a good model in detecting Sleep Apnea events from a single channel of ECG data.

The performance of the model can be improved if there is more amount of Apnea data compared to the Normal data. This data imbalance between the two classes results in lower test/validation accuracy compared to the overall accuracy of the model in predicting from the training dataset. The Entropy feature based training and testing of Sleep Apnea detection model has substantially reduced the hardware cost and computational cost as compared to traditional polysomnographic recordings and analysis. The algorithm can be retrained with a real-life dataset containing more instances of Apnea events, leading to a more accurate and robust performance of proposed mode based on multiscale entropy features.

In order to compare the performance of our proposed model with the existing methods, we have selected few papers on automated sleep apnea detection using traditional methods, machine learning and deep learning methods. The comparison report is presented in Table 3 containing information about the referred article, methods employed, the signals used, the limitations of the methods and performance metrics like Accuracy, Sensitivity and Specificity. We can understand from the table that, although a lot of studies have been reported on sleep apnea detection using machine learning approach, there is still enough limitations and constraints on their applicability in real life scenarios. Due to the limited availability of dataset on Sleep Apnea conditions, it is a challenging task to validate the models on real life scenario, although the articles have reported quite good training accuracy. The choice of robust features and probabilistic prediction with threshold for small dataset has been addressed in our study which was not attempted in any previous studies. Our proposed model is giving very high training accuracy, but on the validation set we had to do a trade-off between Specificity and Sensitivity of the model to reduce the false positive rate which is a primary area of concern in case of diagnostic applications. The limitations in this study are the unavailability of out of distribution dataset for validation of the model's performance with unseen data. The constraints of training a machine learning model with limited data has got its own challenges, which we have tried to overcome with our novel entropy features and data preprocessing techniques.

Table.5. Comparison of performance metrics and scheme employed by existing methods on automated detection of Sleep Apnea from ECG signals.[59]

Ref	Model	Signal	Drawbacks	Performance (%)		
				Accu-racy	Sensiti-vity	Speci fi-city
[60]	Deep neural neutral (DNN), 1D CNN, 2D CNN, (RNN), Long Short-term memory (LSTM), Gated recurring unit (GRU)	ECG	The classification of sleep apnea types is not possible with the available data since the PSG data was not cross-verified. The system is unable to determine the exact start or end time of apnea events; it can only identify their presence. Additionally, the ECG signals were not isolated from other signals like snoring movements. It is important to note that the study was conducted on a limited population.	99.0	99.0	NA
[61]	Ensemble subspace discriminators (ESD)	HRV	It is possible to rank the most prominent feature. By employing deep learning, the accuracy can be enhanced.	87.5	100	NA
[62]	SVM, Logistic Regression, RF, ADT, and Bagging classifier	ECG and HRV	The inability to adjust air pressure limits the effectiveness of utilizing an automatic mobile-based OSA monitoring system for controlling OSA.	88.57	90.32	90.25

[63]	ANN, SVM, Linear discriminant analysis (LDA), Partial least squares regression (PLS), and augmented naïve Bayes classifier (aNBC)	ECG, HRV, and EDR	The proposed model lacks a feature selection mechanism to achieve the highest level of accuracy in the system. However, it was observed that increasing the number of selected features actually resulted in a decrease in the classifier's accuracy.	82.12	88.41	72.29
[64]	Ensemble of Bagged Tree	ECG	Sleep onset latency was utilized as a classification measure for sleep apnea disorder in a specific age group, but its effectiveness for the elderly population has not been validated.	86.27	NA	NA
[65]	CNN	ECG	The current method is encountering an overfitting issue and necessitates additional validation using supplementary clinical dataset. However, it is important to note that the severity of sleep apnea cannot be accurately classified as the AHI (Apnea Hypopnea Index) was not derived from short term ECG recordings.	99.0	98.0 (f1-score)	NA
[66]	EDR extraction ECG variance and phase space reconstruction area	ECG and EDR	In this study, it is possible to perform feature selection in order to enhance accuracy.	90.9	89.6	NA

4.2.4. Conclusion

The proposed methodology involved detecting sleep apnea events from 60 sec long ECG segments using Multiscale Entropy based feature extraction algorithm and training several classification models like SVC, RF, DT, ADT, VC and SC. The automated diagnosis of sleep apnea events from single channel ECG has immense importance in home-based monitoring of sleep apnea patients using a wearable device, which can acquire continuous ECG signals overnight and alert the patient or caregiver whenever an anomaly is detected. The algorithm is computationally efficient and also provides satisfactory performance evaluation reports on training and testing dataset. The use of Voting classifiers and Meta classifiers gives a more robust estimation of the output compared to the single mode classifiers. The meta classification technique reduces bias and handles the pros and cons of each individual base model before making a prediction. This technique reduces the chances of overfitting and also reduces the error in identifying patterns in the dataset that lead to the desired output.

The proposed methodology can be extended further to validate the model performance on real life datasets after integrating it with wearable ECG acquisition devices and calibrate the model performance after each stage of new data ingestion into the system. The authors here try to provide an alternative algorithm using Multiscale Entropy analysis to detect the hidden patterns in ECG rhythms and ECG derived respiration. The validation of the algorithm with the benchmark device is due next to be incorporated to find the use case reports and real-world performance evaluation reports before its implementation, for the use of the general population.

4.2.5 Future Scope of Work

In the next stages, we need to retrain the model with enough Apnea class dataset and also include the other basic features like ECG intervals and characteristics related to the inter beat intervals in time domain. The accuracy of the said model may be increased by including those features along

with the Apnea class dataset. The limitations of this study can be resolved in future studies subject to availability of sleep apnea database with single lead ECGs. If a greater number of subjects with sleep apnea conditions are made available then the inter subject variability can also be incorporated based on ethnicity, age group, gender, etc. to improve the accuracy of the models.

References

[1] S. Garbarino, N. Magnavita, A. Sanna, and N. L. Bragazzi, 'Estimating the hidden burden of obstructive sleep apnoea: challenges and pitfalls', *Lancet Respir. Med.*, vol. 8, no. 1, p. e1, Jan. 2020, doi: 10.1016/S2213-2600(19)30416-3.

[2] L. Grote, 'The global burden of sleep apnoea', *Lancet Respir. Med.*, vol. 7, no. 8, pp. 645–647, Aug. 2019, doi: 10.1016/S2213-2600(19)30226-7.

[3] A. V. Benjafield *et al.*, 'Estimation of the global prevalence and burden of obstructive sleep apnoea: a literature-based analysis', *Lancet Respir. Med.*, vol. 7, no. 8, pp. 687–698, Aug. 2019, doi: 10.1016/S2213-2600(19)30198-5.

[4] W. P. Potsic, 'Obstructive sleep apnea', *Pediatr. Clin. North Am.*, vol. 36, no. 6, pp. 1435–1442, Dec. 1989, doi: 10.1016/s0031-3955(16)36798-0.

[5] C. Guilleminault and A. Robinson, 'Central sleep apnea', *Neurol. Clin.*, vol. 14, no. 3, pp. 611–628, Aug. 1996, doi: 10.1016/s0733-8619(05)70276-0.

[6] S. Lee, H. F. Chiu, and C. N. Chen, 'Sleep apnea--an overview', *Singapore Med. J.*, vol. 30, no. 1, pp. 24–27, Feb. 1989.

[7] J. Lin and M. Suurna, 'Sleep Apnea and Sleep-Disordered Breathing', *Otolaryngol. Clin. North Am.*, vol. 51, no. 4, pp. 827–833, Aug. 2018, doi: 10.1016/j.otc.2018.03.009.

[8] S. Javaheri *et al.*, 'Sleep Apnea: Types, Mechanisms, and Clinical Cardiovascular Consequences', *J. Am. Coll. Cardiol.*, vol. 69, no. 7, pp. 841–858, Feb. 2017, doi: 10.1016/j.jacc.2016.11.069.

[9] A. Culebras, 'Sleep apnea and stroke', *Curr. Neurol. Neurosci. Rep.*, vol. 15, no. 1, p. 503, Jan. 2015, doi: 10.1007/s11910-014-0503-3.

[10] T. Kasai, 'Sleep apnea and heart failure', *J. Cardiol.*, vol. 60, no. 2, pp. 78–85, Aug. 2012, doi: 10.1016/j.jjcc.2012.05.013.

[11] G. Seravalle and G. Grassi, 'Sleep Apnea and Hypertension', *High Blood Press. Cardiovasc. Prev. Off. J. Ital. Soc. Hypertens.*, vol. 29, no. 1, pp. 23–31, Jan. 2022, doi: 10.1007/s40292-021-00484-4.

[12] F. Ralls and L. Cutchen, 'A contemporary review of obstructive sleep apnea', *Curr. Opin.*

Pulm. Med., vol. 25, no. 6, pp. 578–593, Nov. 2019, doi: 10.1097/MCP.0000000000000623.

[13] S. Baillieul *et al.*, 'Sleep apnoea and ischaemic stroke: current knowledge and future directions', *Lancet Neurol.*, vol. 21, no. 1, pp. 78–88, Jan. 2022, doi: 10.1016/S1474-4422(21)00321-5.

[14] J. J. Aardoom, L. Loheide-Niesmann, H. C. Ossebaard, and H. Riper, 'Effectiveness of eHealth Interventions in Improving Treatment Adherence for Adults With Obstructive Sleep Apnea: Meta-Analytic Review', *J. Med. Internet Res.*, vol. 22, no. 2, p. e16972, Feb. 2020, doi: 10.2196/16972.

[15] N. Salari *et al.*, 'Detection of sleep apnea using Machine learning algorithms based on ECG Signals: A comprehensive systematic review', *Expert Syst. Appl.*, vol. 187, p. 115950, Jan. 2022, doi: 10.1016/j.eswa.2021.115950.

[16] A. Pinho, N. Pombo, B. M. C. Silva, K. Bousson, and N. Garcia, 'Towards an accurate sleep apnea detection based on ECG signal: The quintessential of a wise feature selection', *Appl. Soft Comput.*, vol. 83, p. 105568, Oct. 2019, doi: 10.1016/j.asoc.2019.105568.

[17] Z. Zhuang *et al.*, 'Accurate contactless sleep apnea detection framework with signal processing and machine learning methods', *Methods*, vol. 205, pp. 167–178, Sep. 2022, doi: 10.1016/j.ymeth.2022.06.013.

[18] S. Cheng *et al.*, 'Automated sleep apnea detection in snoring signal using long short-term memory neural networks', *Biomed. Signal Process. Control*, vol. 71, p. 103238, Jan. 2022, doi: 10.1016/j.bspc.2021.103238.

[19] C. Varon *et al.*, 'A Comparative Study of ECG-derived Respiration in Ambulatory Monitoring using the Single-lead ECG', *Sci. Rep.*, vol. 10, p. 5704, Mar. 2020, doi: 10.1038/s41598-020-62624-5.

[20] K. Cao and X. Lv, 'Multi-task feature fusion network for Obstructive Sleep Apnea detection using single-lead ECG signal', *Measurement*, vol. 202, p. 111787, Oct. 2022, doi: 10.1016/j.measurement.2022.111787.

[21] H. Singh, R. K. Tripathy, and R. B. Pachori, 'Detection of sleep apnea from heart beat interval and ECG derived respiration signals using sliding mode singular spectrum analysis', *Digit. Signal Process.*, vol. 104, p. 102796, Sep. 2020, doi: 10.1016/j.dsp.2020.102796.

[22] S. Xu *et al.*, 'A review of automated sleep disorder detection', *Comput. Biol. Med.*, vol. 150, p. 106100, Nov. 2022, doi: 10.1016/j.compbiomed.2022.106100.

[23] M. Balci, S. Tasdemir, G. Ozmen, and A. Golcuk, 'Machine Learning-Based Detection of Sleep-Disordered Breathing Type Using Time and Time-Frequency Features', *Biomed. Signal Process. Control*, vol. 73, p. 103402, Mar. 2022, doi: 10.1016/j.bspc.2021.103402.

[24] H. Almutairi, G. M. Hassan, and A. Datta, 'Classification of Obstructive Sleep Apnoea from single-lead ECG signals using convolutional neural and Long Short Term Memory networks', *Biomed. Signal Process. Control*, vol. 69, p. 102906, Aug. 2021, doi: 10.1016/j.bspc.2021.102906.

[25] K. Li, W. Pan, Y. Li, Q. Jiang, and G. Liu, 'A method to detect sleep apnea based on deep neural network and hidden Markov model using single-lead ECG signal', *Neurocomputing*, vol. 294, pp. 94–101, Jun. 2018, doi: 10.1016/j.neucom.2018.03.011.

[26] P. Kumar Tyagi and D. Agrawal, 'Automatic detection of sleep apnea from single-lead ECG signal using enhanced-deep belief network model', *Biomed. Signal Process. Control*, vol. 80, p. 104401, Feb. 2023, doi: 10.1016/j.bspc.2022.104401.

[27] U. Erdenebayar, Y. J. Kim, J.-U. Park, E. Y. Joo, and K.-J. Lee, 'Deep learning approaches for automatic detection of sleep apnea events from an electrocardiogram', *Comput. Methods Programs Biomed.*, vol. 180, p. 105001, Oct. 2019, doi: 10.1016/j.cmpb.2019.105001.

[28] F. Bozkurt, M. K. Uçar, M. R. Bozkurt, and C. Bilgin, 'Detection of Abnormal Respiratory Events with Single Channel ECG and Hybrid Machine Learning Model in Patients with Obstructive Sleep Apnea', *IRBM*, vol. 41, no. 5, pp. 241–251, Oct. 2020, doi: 10.1016/j.irbm.2020.05.006.

[29] H. Liu, S. Cui, X. Zhao, and F. Cong, 'Detection of obstructive sleep apnea from single-channel ECG signals using a CNN-transformer architecture', *Biomed. Signal Process. Control*, vol. 82, p. 104581, Apr. 2023, doi: 10.1016/j.bspc.2023.104581.

[30] A. Zarei, H. Beheshti, and B. M. Asl, 'Detection of sleep apnea using deep neural networks and single-lead ECG signals', *Biomed. Signal Process. Control*, vol. 71, p. 103125, Jan. 2022, doi: 10.1016/j.bspc.2021.103125.

[31] F. R. Mashrur, Md. S. Islam, D. K. Saha, S. M. R. Islam, and M. A. Moni, 'SCNN: Scalogram-based convolutional neural network to detect obstructive sleep apnea using single-lead electrocardiogram signals', *Comput. Biol. Med.*, vol. 134, p. 104532, Jul. 2021, doi: 10.1016/j.compbiomed.2021.104532.

[32] H. Pant, H. K. Dhanda, and S. Taran, 'Sleep apnea detection using electrocardiogram signal input to FAWT and optimise ensemble classifier', *Measurement*, vol. 189, p. 110485, Feb. 2022, doi: 10.1016/j.measurement.2021.110485.

[33] W.-Y. Pan, M.-C. Su, H.-T. Wu, T.-J. Su, M.-C. Lin, and C.-K. Sun, 'Multiscale entropic assessment of autonomic dysfunction in patients with obstructive sleep apnea and therapeutic impact of continuous positive airway pressure treatment', *Sleep Med.*, vol. 20, pp. 12–17, Apr. 2016, doi: 10.1016/j.sleep.2015.11.021.

[34] Z. Wang *et al.*, 'Single-lead ECG based multiscale neural network for obstructive sleep apnea

detection', *Internet Things*, vol. 20, p. 100613, Nov. 2022, doi: 10.1016/j.iot.2022.100613.

[35] F. Riganello, F. Zubler, M. Haenggi, and M. De Lucia, 'Heart rate complexity: An early prognostic marker of patient outcome after cardiac arrest', *Clin. Neurophysiol.*, vol. 134, pp. 27–33, Feb. 2022, doi: 10.1016/j.clinph.2021.10.019.

[36] M. Costa, A. L. Goldberger, and C.-K. Peng, 'Multiscale entropy analysis of biological signals', *Phys. Rev. E Stat. Nonlin. Soft Matter Phys.*, vol. 71, no. 2 Pt 1, p. 021906, Feb. 2005, doi: 10.1103/PhysRevE.71.021906.

[37] M. Costa, A. L. Goldberger, and C.-K. Peng, 'Multiscale Entropy Analysis of Complex Physiologic Time Series', *Phys. Rev. Lett.*, vol. 89, no. 6, p. 068102, Jul. 2002, doi: 10.1103/PhysRevLett.89.068102.

[38] S.-D. Wu, C.-W. Wu, S.-G. Lin, C.-C. Wang, and K.-Y. Lee, 'Time Series Analysis Using Composite Multiscale Entropy', *Entropy*, vol. 15, no. 3, Art. no. 3, Mar. 2013, doi: 10.3390/e15031069.

[39] S.-D. Wu, C.-W. Wu, S.-G. Lin, K.-Y. Lee, and C.-K. Peng, 'Analysis of complex time series using refined composite multiscale entropy', *Phys. Lett. A*, vol. 378, no. 20, pp. 1369–1374, Apr. 2014, doi: 10.1016/j.physleta.2014.03.034.

[40] T. Liu, W. Yao, M. Wu, Z. Shi, J. Wang, and X. Ning, 'Multiscale permutation entropy analysis of electrocardiogram', *Phys. Stat. Mech. Its Appl.*, vol. 471, pp. 492–498, Apr. 2017, doi: 10.1016/j.physa.2016.11.102.

[41] H. Azami and J. Escudero, 'Improved multiscale permutation entropy for biomedical signal analysis: Interpretation and application to electroencephalogram recordings', *Biomed. Signal Process. Control*, vol. 23, pp. 28–41, Jan. 2016, doi: 10.1016/j.bspc.2015.08.004.

[42] W. Ying, J. Tong, Z. Dong, H. Pan, Q. Liu, and J. Zheng, 'Composite Multivariate Multi-Scale Permutation Entropy and Laplacian Score Based Fault Diagnosis of Rolling Bearing', *Entropy*, vol. 24, no. 2, p. 160, Jan. 2022, doi: 10.3390/e24020160.

[43] H. Azami and J. Escudero, 'Refined composite multivariate generalized multiscale fuzzy entropy: A tool for complexity analysis of multichannel signals', *Phys. Stat. Mech. Its Appl.*, vol. 465, pp. 261–276, Jan. 2017, doi: 10.1016/j.physa.2016.07.077.

[44] 'An Open-Source Feature Extraction Tool for the Analysis of Peripheral Physiological Data', *IEEE J. Transl. Eng. Health Med.*, vol. 6, p. 2800711, Oct. 2018, doi: 10.1109/JTEHM.2018.2878000.

[45] J. A. Lipponen and M. P. Tarvainen, 'A robust algorithm for heart rate variability time series artefact correction using novel beat classification', *J. Med. Eng. Technol.*, vol. 43, no. 3, pp. 173–181, Apr. 2019, doi: 10.1080/03091902.2019.1640306.

[46] P. van Gent, H. Farah, N. van Nes, and B. van Arem, 'HeartPy: A novel heart rate algorithm for the analysis of noisy signals', *Transp. Res. Part F Traffic Psychol. Behav.*, vol. 66, pp. 368–378, Oct. 2019, doi: 10.1016/j.trf.2019.09.015.

[47] M. T. Rosenstein, J. J. Collins, and C. J. De Luca, 'A practical method for calculating largest Lyapunov exponents from small data sets', *Phys. Nonlinear Phenom.*, vol. 65, no. 1, pp. 117–134, May 1993, doi: 10.1016/0167-2789(93)90009-P.

[48] L. Cao, 'Practical method for determining the minimum embedding dimension of a scalar time series', *Phys. Nonlinear Phenom.*, vol. 110, no. 1, pp. 43–50, Dec. 1997, doi: 10.1016/S0167-2789(97)00118-8.

[49] D. Parbat and M. Chakraborty, 'A Novel Methodology to study the Cognitive Load Induced EEG Complexity Changes: Chaos, Fractal and Entropy based approach', *Biomed. Signal Process. Control*, vol. 64, p. 102277, Feb. 2021, doi: 10.1016/j.bspc.2020.102277.

[50] L. Breiman, *Classification and Regression Trees*. New York: Routledge, 2017. doi: 10.1201/9781315139470.

[51] L. Breiman, 'Random Forests', *Mach. Learn.*, vol. 45, no. 1, pp. 5–32, Oct. 2001, doi: 10.1023/A:1010933404324.

[52] S. R. Gunn, 'Support Vector Machines for Classification and Regression'.

[53] 'sklearn.ensemble.VotingClassifier',*scikit-learn*. https://scikit learn/stable/modules/generated/sklearn.ensemble.VotingClassifier.html (accessed Mar. 15, 2023).

[54] D. H. Wolpert, 'Stacked generalization', *Neural Netw.*, vol. 5, no. 2, pp. 241–259, Jan. 1992, doi: 10.1016/S0893-6080(05)80023-1.

[55] 'sklearn.ensemble.StackingClassifier', *scikit-learn*. https://scikit-learn/stable/modules/generated/sklearn.ensemble.StackingClassifier.html (accessed Mar. 15, 2023).

[56] Y. Liu, Y. Zhou, S. Wen, and C. Tang, 'A Strategy on Selecting Performance Metrics for Classifier Evaluation', *Int. J. Mob. Comput. Multimed. Commun. IJMCMC*, vol. 6, no. 4, pp. 20–35, 2014, doi: 10.4018/IJMCMC.2014100102.

[57] C. Ferri, J. Hernández-Orallo, and R. Modroiu, 'An experimental comparison of performance measures for classification', *Pattern Recognit. Lett.*, vol. 30, no. 1, pp. 27–38, Jan. 2009, doi: 10.1016/j.patrec.2008.08.010.

[58] M. R. Bonsignore, S. Romano, O. Marrone, and G. Insalaco, 'Respiratory sinus arrhythmia during obstructive sleep apnoeas in humans', *Journal of Sleep Research*, vol. 4, no. s1, pp. 68–70, 1995, doi: 10.1111/j.1365-2869.1995.tb00190.x.

[59] N. Singh and R. H. Talwekar, '"Comparison of machine learning and deep learning classifier to detect sleep apnea using single-channel ECG and HRV: A Systematic Literature Review"', *J. Phys.: Conf. Ser.*, vol. 2273, no. 1, p. 012015, May 2022, doi: 10.1088/1742-6596/2273/1/012015.

[60] E. Urtnasan, J.-U. Park, E.-Y. Joo, and K.-J. Lee, 'Automated Detection of Obstructive Sleep Apnea Events from a Single-Lead Electrocardiogram Using a Convolutional Neural Network', *J Med Syst*, vol. 42, no. 6, p. 104, Apr. 2018, doi: 10.1007/s10916-018-0963-0.

[61] M. J. Rahman, R. Mahajan, and B. I. Morshed, 'Severity classification of obstructive sleep apnea using only heart rate variability measures with an ensemble classifier', in *2018 IEEE EMBS International Conference on Biomedical & Health Informatics (BHI)*, Mar. 2018, pp. 33–36. doi: 10.1109/BHI.2018.8333363.

[62] G. Sannino, I. De Falco, and G. De Pietro, 'An automatic rules extraction approach to support OSA events detection in an mHealth system', *IEEE J Biomed Health Inform*, vol. 18, no. 5, pp. 1518–1524, Sep. 2014, doi: 10.1109/JBHI.2014.2311325.

[63] N. Pombo, B. M. C. Silva, A. M. Pinho, and N. Garcia, 'Classifier Precision Analysis for Sleep Apnea Detection Using ECG Signals', *IEEE Access*, vol. 8, pp. 200477–200485, 2020, doi: 10.1109/ACCESS.2020.3036024.

[64] E. R. Widasari, K. Tanno, and H. Tamura, 'Automatic Sleep Disorders Classification Using Ensemble of Bagged Tree Based on Sleep Quality Features', *Electronics*, vol. 9, no. 3, Art. no. 3, Mar. 2020, doi: 10.3390/electronics9030512.

[65] E. Urtnasan, J. U. Park, E. Y. Joo, and K. J. Lee, 'Identification of Sleep Apnea Severity Based on Deep Learning from a Short-term Normal ECG', *J Korean Med Sci*, vol. 35, no. 47, p. e399, Dec. 2020, doi: 10.3346/jkms.2020.35.e399.

[66] P. Janbakhshi and M. B. Shamsollahi, 'Sleep Apnea Detection from Single-Lead ECG Using Features Based on ECG-Derived Respiration (EDR) Signals', *IRBM*, vol. 39, no. 3, pp. 206–218, Jun. 2018, doi: 10.1016/j.irbm.2018.03.002.

[67] R. V. Sharan, S. Berkovsky, H. Xiong, and E. Coiera, 'ECG-Derived Heart Rate Variability Interpolation and 1-D Convolutional Neural Networks for Detecting Sleep Apnea', in *2020 42nd Annual International Conference of the IEEE Engineering in Medicine & Biology Society (EMBC)*, Jul. 2020, pp. 637–640. doi: 10.1109/EMBC44109.2020.9175998.

[68] T. Penzel, G. B. Moody, R. G. Mark, A. L. Goldberger, and J. H. Peter, 'Apnea-ECG Database'. *physionet.org*, 2000. doi: 10.13026/C23W2R.

[69]. T Penzel, GB Moody, RG Mark, AL Goldberger, JH Peter. The Apnea-ECG Database. *Computers in Cardiology 2000;* 27:255-258.

4.3. Multi-Scale Entropy Analysis of surface Electromyography signals during biceps muscle contraction under varying loads

This section delves into the multiscale analysis of Electromyography signals and led to the foundation for implementing multiscale analysis for musculoskeletal dynamic studies, the below methodology was presented in Computational Science Symposium, Centre for Data Science, IISc Bangalore.

4.3.1 Objective

It is a well-known fact that Voluntary body movement is due to the contraction of muscles, which moves the bones connected to the joints. The neuromuscular system controls the muscle movement, providing complex and regulatory operations, such as lifting a weight or kicking a ball, controlled by centers that are further up the nervous system. The above tasks occur by collecting information from certain sensory inputs, joint angle, muscle loading, and movements like extension or flexion which are transmitted to brain for computation and execution [1]. The activation of muscle fibres from the central nervous system gives rise to motor unit action potential (MUAP) trains depending on the recruitment pattern of the muscles. The association of these MUAP trains gives rise to the Electromyography or EMG signal. The factors affecting EMG signal constitutes the noise and artefacts pertaining to instrument and physiological factors. The EMG signal is highly non-stationary signal having inherent multi-scale characteristics [2]. It is to note that Physiologic systems are regulated by interacting and inter-related mechanisms that occurs at multiple spatial and temporal scales. The output variables of physiological systems often exhibit complex fluctuations that are not simply due to noise but contain information about the underlying system dynamics. Many studies have been done, in the field of EMG, related to fatigue estimation or feedback applications but to characterize the dynamic behaviour of EMG signal some non-linear techniques are needed to be tested. It can be modelled on the basis of a non-linear dynamic system and not a randomly distributed signal [3]. The Multi Scale Entropy based analysis methods have recently proved to be successful in measuring the complexity or regularity of physiological signals and are often accurate in establishing parameters to separate the diseased and normal conditions

[4]. We have found that MSE algorithms have been incorporated, prevalently on involuntary physiological signals like ECG and EEG studies but very few studies have been done on EMG. Therefore, we wish to determine the underlying system complexity during biceps muscle flexion and extension while lifting loads of various denominations by assessing the MSE parameters. Once the multi-scale phenomenon is established for dynamic contraction of muscles then it can be extended to capture the system dynamics under different exercise protocols and kinesiology studies.

4.3.2. Methods

Our primary investigations with EMG signal under biceps muscle flexion while lifting loads revealed a lot about the progressive nature of the recruitment patterns of the MUAP trains captured through an EMG signal acquisition circuitry with surface electrodes and differential amplification technology. The times series as obtained was analysed to determine the system dynamics using non-linear techniques like Fractals, Chaos and Entropy Analysis. We reported our findings in [6] [7] [8] based on Fractal Dimension, Multifractal behaviour, Chaotic behaviour and sample Entropy analysis. The Fractal Dimension revealed the non-linear characteristics of the EMG signal taken under arm flexion condition with an assumption of scale invariance being independent of time and space. From the physiologic point of view, during dynamic contraction of muscles, spatial and temporal variations are bound to exist so it advocates the use of multifractal structures to define the physiological significance. The Multifractal Detrended Fluctuation Analysis (MFDFA) method estimates fractal dimension at multiple scales and is a good estimator of multifractal characteristics of physiologic signals. The term complexity is usually attached to the Fractal dimension concept, Fractal Dimension or Complexity can be viewed as a scaling rule comparing how a patterns detail changes with the scale at which it is considered.

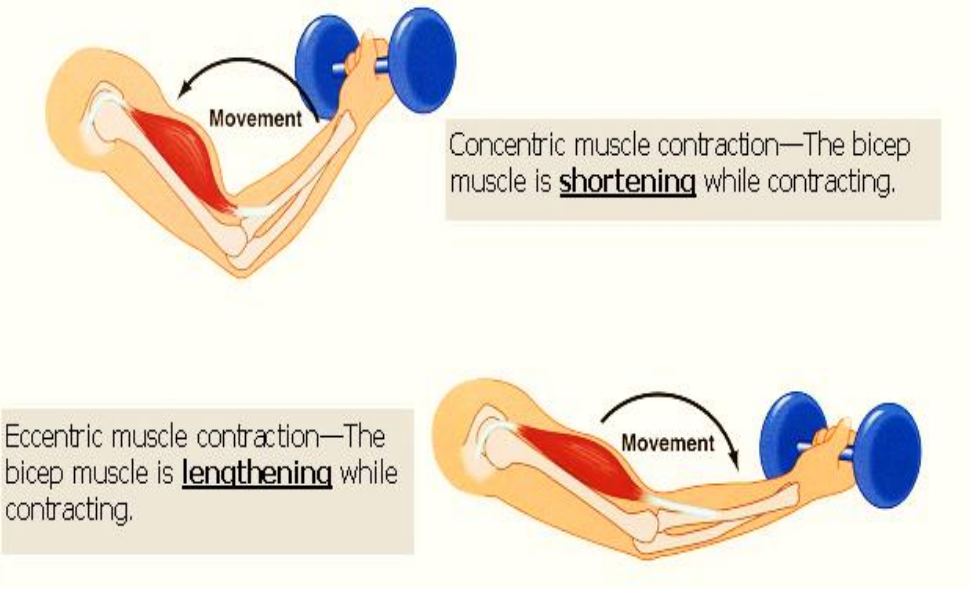

Fig.34. experimental protocol

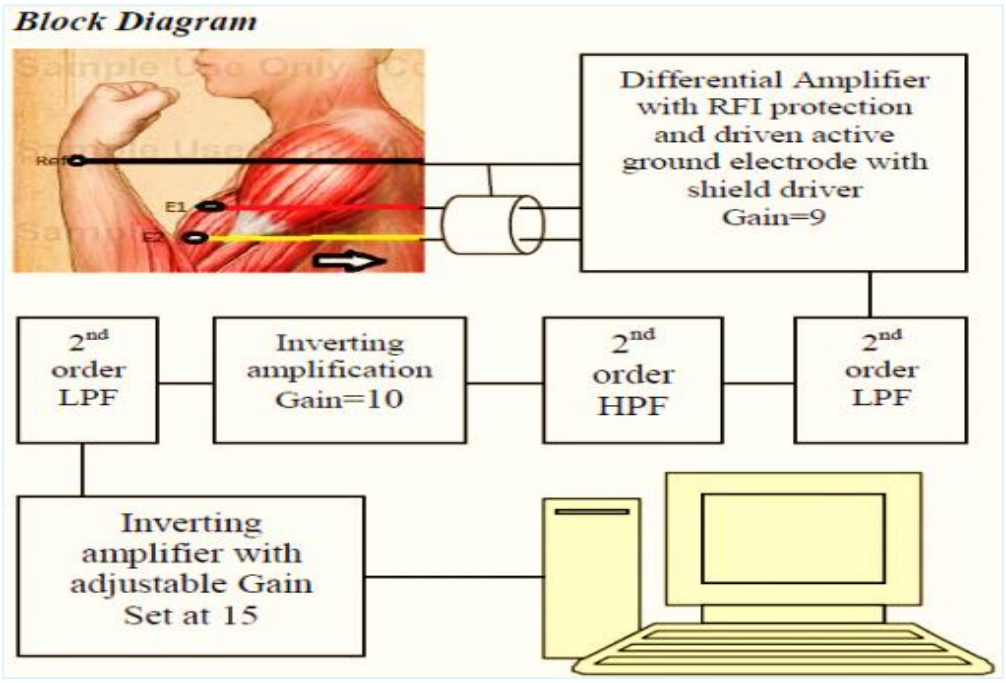

Fig.35. Block diagram of the Experimental setup

In 2005, Costa et. al. mentioned that traditional approaches to measuring the complexity of biological signals fail to account for the multiple time scales inherent in such time series [4][5]. These algorithms have yielded contradictory findings when applied to real-world datasets obtained in health and disease states, so they have advised the use of Multiscale Entropy Analysis for biomedical signals. Entropy, as it relates to dynamical systems, is the rate of information production. Entropy is a measure of *unpredictability* of *information content*. It is also said that Entropy basically does the characterization of creation of information in a dynamical system.

MSE analysis results on physiological signals supported the general theory of "Complexity Loss" due to aging and disease. MSE algorithms are primarily based on sample entropy technique where SampEn (m, r, N) is precisely the negative natural logarithm of the conditional probability that two sequences similar for m points remain similar at the next point, where self-matches are not included in calculating the probability. Therefore m defines the length of the patterns of the sequences that are compared to each other within the tolerance of r for N no. of samples. The lower value of SampEn indicates more self-similarity in the time series. Recent studies are more focused towards applications of MSE based algorithms since the results obtained are less ambiguous and quite often, they are successful in establishing direct correlations between the physiological reasons and computational results. MSE technique for analysing time series is based on comparing their degree of complexity and is not based on the classical approach of time series analysis related to deterministic and stochastic mechanisms. These specialities of the MSE method help it to address the biomedical signal complexities since it is designed on the basis of defining a quantitative measurement of complexity that assigns minimum values to both deterministic/predictable and uncorrelated random/unpredictable signals [9]. The MSE algorithms have evolved a lot in recent times due to the rise in computational science and technology and now various other improved version of it, all based on the sample entropy technique, is available in the literature such as permutation entropy, improved multiscale entropy, Refined Multiscale fuzzy entropy (based on standard deviation/based on mean/based on variance), etc [10][11]. Refined composite MSE algorithm has given better results in data representation of electrophysiological brain data while computing on resting-state Magnetoencephalograms (MEG) from 36 patients of Alzheimer's disease and 26 control subjects [12].

4.3.3. Significance:

The method consistently indicates a loss of complexity with aging, with an erratic cardiac arrhythmia atrial fibrillation, and with a life-threatening syndrome congestive heart failure. Further, these different conditions have distinct MSE curve profiles, suggesting diagnostic uses. The ability of the MSE to characterize brain dynamics in EEG and MEG signals has been demonstrated in several conditions. This method has not yet found any profound application in case myopathy related disorders where EMG signal analysis results are of quite significance. Effective characterization of EMG signal in order to obtain constructive diagnostic features is very essential hence we look forward in finding out the best possible representation of the physiologic state of the biceps muscles while lifting load with Multiscale Entropy based algorithms. The features could be helpful for automated classification of diseased and normal conditions or in classifying flexion-extension actions with machine learning algorithms. Therefore, a better representation of the muscles physiologic condition by Multiscale Entropy Analysis can extend its application towards computer aided diagnosis and muscle rehabilitation studies and application.

4.3.4. Results:

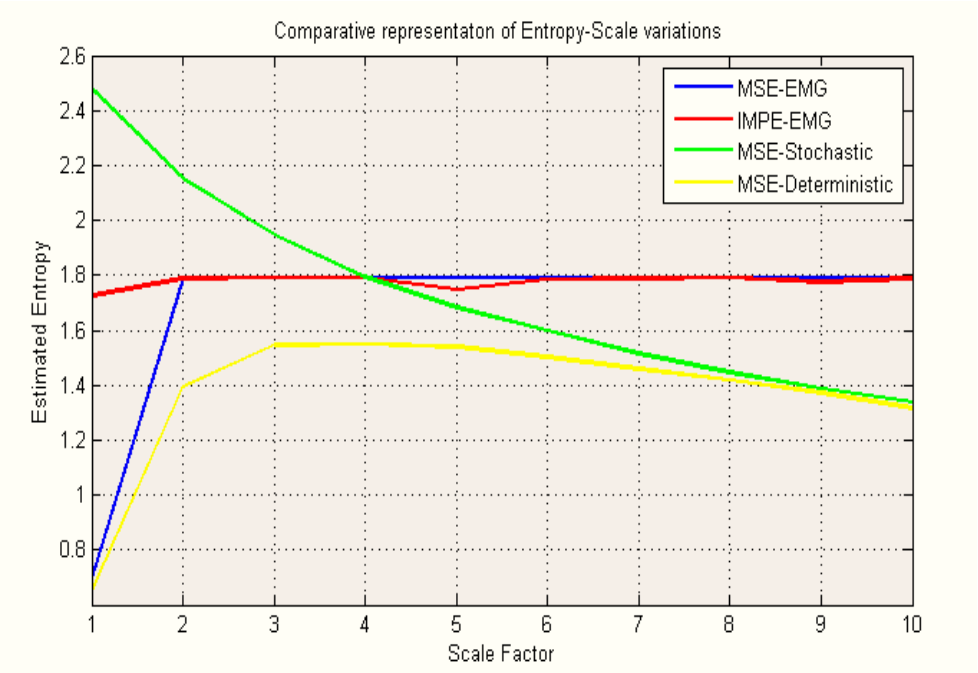

Fig.36 comparative representation of Entropy-Scale variation of EMG signal (by MSE and IMPE method), Stochastic signal and Deterministic signal at (a) no load contraction.

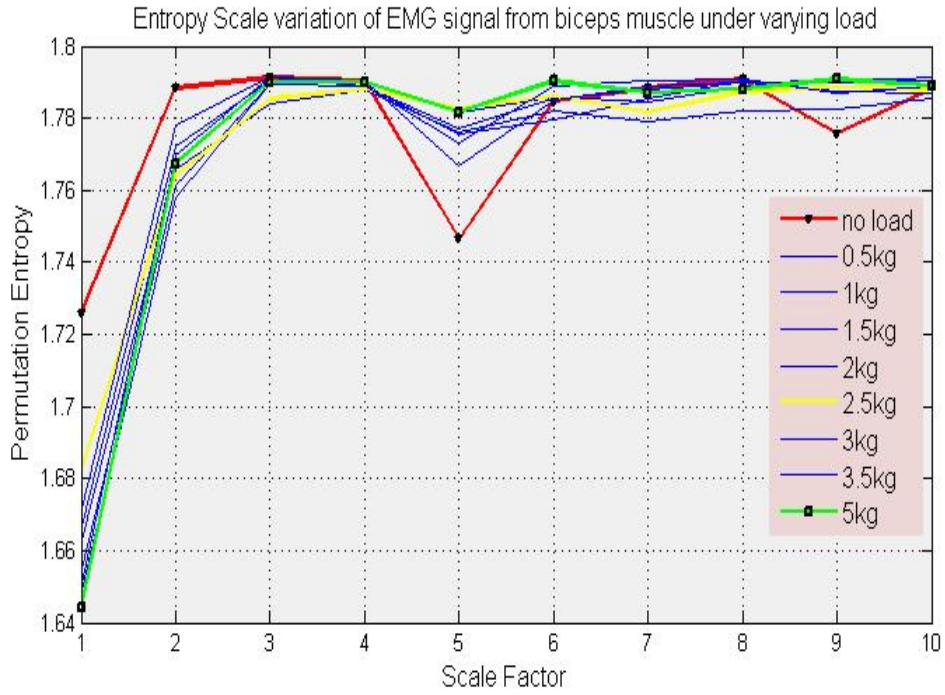

Fig.37. It represents the Entropy Scale variation for EMG signal collected from Biceps muscle during arm flexion-extension with different loads (weights).

4.3.5. Conclusion

A high degree of sensitivity is seen for the entropy values to the dynamical state of the system. Values are observed to change drastically when loads shift. Power fluctuation in percent better reflects the dynamic nature of the load. The computation of entropy may be useful for assessing the development of motor unit action potentials or firing rates of action potentials with loading of muscles because of its relationship to energy and chaos in determining the order or disorder states of systems. We find that as the load rises, the Entropy values fall, indicating that the system is becoming more regular and the firing pattern of the MUAP is becoming less unpredictable. Changes in Entropy largely determine the balance between order and disorder in a system. Thus, fluctuations in Entropy may be used to evaluate the physical complexity of weightlifting.

References:

[1]. J. D. Bronzino, '*The Biomedical Engineering Handbook: 2nd Edition*', Biomedical Engineering Fundamental, CRC Press LLC, 2000.

[2]. De Luca C.J. *Electromyography. Encyclopaedia of Medical Devices and Instrumentation,* (John G. Webster, Ed.) John Wiley Publisher,98-109,2006

[3]. Nieminen H, Takala EP. '*Evidence of deterministic chaos in the myoelectric signal'.* Electromyogr Clin Neurophysiol 1996;36(1):49–58.

[4]. Madalena Costa, Ary L. Goldberger, and C.-K. Peng, *Multiscale entropy analysis of biological signals*, PHYSICAL REVIEW E 71, 021906 (2005).

[5]. Madalena Costa, Ary L. Goldberger, and C.-K. Peng, *Multiscale Entropy Analysis of Complex Physiologic Time Series*, PHYSICAL REVIEW LETTERS, vol 89,no. 6, 068102-3 (2002).

[6]. M. Chakraborty, D. Parbat, '*Fractal analysis of sEMG signal under Varying Load Conditions* ', 2nd Int. Conf. on Control, Instrumentation, Energy& Communication,2016,IEEE.

[7]. M. Chakraborty, D. Parbat, *'Comparative study of MFDFA technique for Isometric and Isotonic muscle Contraction*', 3rd Int. Conf. on Recent Advances in Information Technology,2016,IEEE.

[8]. M. Chakraborty, D. Parbat, 'Fractals, Chaos and Entropy analysis to obtain Parametric Features of surface Electromyography signals during Dynamic Contraction of Biceps Muscles under Varying Load', 2017 2nd International Conference for Convergence in Technology (I2CT), 2017,IEEE (Accepted Manuscript)

[9]. B.-Y. Yaneer, *Dynamics of Complex Systems* sAddison-Wesley, Reading, Massachusetts, 1997

[10]. Hamed Azami, Javier Escudero, '*Improved multiscale permutation entropy for biomedical signal analysis: Interpretation and application to electroencephalogramrecordings*', Biomedical Signal Processing and Control 23 (2016) 28–

41. [11]. Hamed Azami, Alberto Fernández**,** Javier Escudero, '*Refined Multiscale Fuzzy Entropy based on Standard Deviation for Biomedical Signal Analysis',* arXiv.org.

[12]. Javier Escudero, Evrim Acar, Alberto Fernández, Rasmus Bro, *Multiscale entropy analysis of resting-state magnetoencephalogram with tensor factorisations in Alzheimer's disease,* Brain Research Bulletin 119 (2015) 136–144,Elsevier.

4.4. A novel methodology to measure the Corticomuscular coherence using multifractal correlation and information theory approach during weight lifting exercise

Corticomuscular coherence (CMC) is the synchronisation of brain activity with muscle activity, reflecting the coordination between neural oscillations in the cortex and muscle contractions. It is assessed using Electroencephalography (EEG) for cortical activity and Electromyography (EMG) for muscle activity. By analysing specific frequency bands, such as beta or gamma, coherence measures quantify the strength and consistency of the phase relationship between cortical and muscular oscillations in a given frequency range. This is study aimed to provide a methodology to measure corticomuscular coherence using nonlinear cross-correlation parameters. The study attempts to analyse the interrelationship between CMC and load on the arms, while performing flexion and extension in response to a visual cue. This study is submitted to Computer Methods and Programs in Biomedicine, Elsevier as an original research article.

The proposed methodology introduces an analysis technique based on nonlinear dynamical systems theory to quantify corticomuscular coherence during weight lifting. An in-house experiment was conducted to validate this technique using simultaneously acquired EEG and EMG data from different subjects. The experimental data was preprocessed and segmented, and several parameters including Multifractal Detrended Crosscorrelation Analysis (MFDXA), Mutual Information (MI), and Joint Entropy (JEn) were calculated to describe the underlying dynamics of neuromuscular coordination.

The results demonstrated that these parameters were highly statistically significant in distinguishing corticomuscular coherence at different weights with $p < 0.01$. This suggests that they are reliable descriptors of corticomuscular coherence and could potentially be used to assess neuromuscular disorders such as cerebral palsy, stroke rehabilitation, paralysis, or other conditions

associated with loss of neuromuscular coordination. The method offers a cost-effective and non-invasive way to quantify the degree of neuromuscular dysfunction in patients. It could serve as a measurement tool, and with the integration of Artificial Intelligence and Machine Learning techniques, it could provide automated detection of corticomuscular coherence. This approach has the potential to enhance diagnostic capabilities and facilitate treatment planning for individuals with neuromuscular disorders.

4.4.1 Introduction

Corticomuscular coherence (CMC) is a measure of the synchrony between the activity of the motor cortex, as measured by electroencephalography (EEG), and the activity of muscles, as measured by electromyography (EMG) [1], [2]. The measurement of CMC is important for understanding the neural control of movement and for developing new rehabilitation techniques for motor impairments [3]. Previous studies used various neuroimaging techniques such as positron emission tomography (PET), functional magnetic resonance imaging (fMRI), transcranial magnetic stimulation (TMS), and electroencephalogram (EEG) to investigate the mechanisms of the motor cortex in stroke patients. However, the specific role of the ipsilateral motor cortex and secondary motor areas in controlling muscle activity remains incompletely understood [4], [5]. To address this knowledge gap, researchers have employed a method called corticomuscular coherence, which involves simultaneous measurement of EEG signals and corresponding electromyography (EMG) signals. Corticomuscular coherence (CMC) was initially observed between magnetoencephalography (MEG) and EMG and has since been detected using techniques such as EEG, electrocorticography (ECoG), and surface electromyography (sEMG). This approach has been widely used and validated across different methods and species [6].

To measure CMC, EEG and EMG signals are simultaneously recorded from electrodes placed on the scalp and on the surface of the muscle, respectively. The EEG signal is typically recorded from electrodes placed over the motor cortex, which is responsible for controlling movement. The EMG signal is recorded from electrodes placed on the surface of the muscle that is involved in the movement of interest. The EEG and EMG signals are then preprocessed to remove noise and artefacts, such as muscle activity that is not related to the movement of interest [7]. After

preprocessing, spectral analysis is performed to identify the frequency bands that show coherence between the EEG and EMG signals. The most commonly used frequency band for measuring CMC is the beta band (13-30 Hz) [8], [9]. However, other frequency bands, such as the gamma band (30-100 Hz), have also been used [10], [11]. Coherence is calculated as the correlation between the EEG and EMG signals in the frequency band of interest, and is typically expressed as a coherence value between 0 and 1. Several techniques have been developed to analyse and interpret CMC, including time-frequency analysis, coherence phase analysis, and partial coherence analysis. These techniques provide information about the timing and directionality of the coherence, as well as the neural networks involved in the generation of the coherence. Some of the most commonly used methods for calculating CMC are discussed in the preceding section.

Fourier transform-based coherence is the most commonly used method for calculating CMC. It involves calculating the coherence between the EEG/MEG and EMG signals in the frequency domain using a Fourier transform [12]–[14]. The coherence value is calculated as the square of the cross-spectral density between the two signals divided by the product of their individual power spectral densities [15]. Wavelet transform-based coherence method involves using a wavelet transform to analyse the EEG and EMG signals in both the time and frequency domains [16], [17]. The coherence value is calculated in a similar way as with Fourier transform-based coherence. Time-frequency coherence method involves calculating the coherence between the EEG and EMG signals at different time points and in different frequency bands using a time-frequency analysis, such as the Morlet wavelet transform. This provides information about the temporal evolution of the coherence and its frequency distribution [18]. Coherence phase analysis: This method involves calculating the phase difference between the EEG and EMG signals in the frequency band of interest [19]. This provides information about the directionality of the coherence, i.e., whether the motor cortex is driving the muscle activity or vice versa. Partial coherence analysis: This method involves calculating the coherence between the EEG and EMG signals while controlling for the influence of other variables, such as joint angle or force [20], [21]. This provides information about the specific neural networks involved in the generation of the coherence. The study by Gray et al. [22] introduced a method for measuring correlations between local field potentials with high temporal resolution. However, this method lacked the ability to analyse correlations with respect

to frequency. Wavelet coherence, on the other hand, provides frequency information and adapts the integration window size to compute correlations, resulting in improved temporal resolution. Another algorithm called the impulse response function was presented in [23] but lacked statistical analysis and frequency information. A study in [24] proposed an estimation of coherence adapted to non-stationary signals using auto-regressive moving average modelling but did not mention statistical properties. Additionally, a method called generalised synchrony was suggested by [25], [26] to detect non-linear coupling between neural populations, complementing wavelet coherence by capturing non-linear interactions that may go unnoticed. Measures of non-linear couplings are less affected by spurious linear couplings due to limitations in spatial resolution or electrode reference choices in recordings, particularly in EEG.

CMC is a versatile tool that has widespread applications in the area of motor control research [7], [14], [27], assessment of motor disorders like Parkinson's [28], [29], cerebral palsy [30], poliomyelitis [11] and myoclonic epilepsy [31], neurorehabilitation after stroke [32]–[34], brain machine interface[35], [36] and sports science. In conclusion, the measurement of CMC using EEG and EMG signals is a valuable tool for studying the neural control of movement and developing new rehabilitation techniques for motor impairments.

In this regard we propose a novel methodology to measure the CMC using the Nonlinear dynamical systems theory approach to calculate the correlation between the respective EEG and EMG channels, moreover the rate of information transfer between the said variables is also studied using Information theory metrics. We have investigated the utilisation of Multifractal Detrended Fluctuation Cross-correlation Analysis (MFDXA) [37] to observe the correlation between the fluctuation functions of EEG and EMG. We also estimated the amount of shared information in between variables using Mutual Information (MI) [38] and Joint Entropy (JEn) [39] based individual probability density functions of EEG and EMG respectively. A high mutual information score indicates that the two variables are highly dependent, while a low score indicates that they are independent. Moreover, a high joint entropy estimate indicates that the two distributions have a lot of randomness or uncertainty, while a low joint entropy estimate indicates that the two distributions are highly correlated and have less randomness or uncertainty. Therefore, we have

selected these parameters to validate the overall performance of these parameters in accurately measuring the correlation between the EEG and EMG during dynamic muscle contraction under varying weights. The said parameters are investigated to capture the dynamics of the neuro-muscular coordination during lifting weights with the right arm as presented in the visual cue. We aim to quantify and model the underlying dynamics associated with the neuro-muscular coordination required for lifting various weights with one arm.

4.4.2. Methods

This section discusses the different steps involved in the estimation of CMC using quantitative parameters to efficiently measure the amount of correlation between the EEG and EMG signal during dynamic contraction of the elbow joint under varying loads. The first step involves design of the experiment protocol for simultaneous acquisition of EEG and EMG, then comes the data preprocessing stage where EEG and EMG signals are preprocessed to make them fit for analysis using the CMC calculation algorithm which is discussed in the final stage along with the statistical validation scheme. The block diagram representing the entire methodology from signal acquisition to statistical validation is shown in fig.40

Experiment Design

In order to validate our hypothesis, we have designed an experimental protocol for simultaneous acquisition of EEG and EMG while performing weight lifting tasks by 5 normal subjects, with no history of cognitive impairment. The mean age of the subjects is 26 ± 3 years and all right-handed male individuals. The subjects were asked to lift varying weights using their right arm based upon 60 sec visual cues. The visual cue instructed the subjects to do arm flexion, hold and arm extension. The arm was kept in an upright antigravity position and weight blocks were placed on the palm and then asked to perform 90-degree flexion and back to the neutral position by extension as shown in fig.38 and fig.39. EEG from cortical regions (C3, C4 & Cz) were acquired simultaneously with EMG signals from Biceps Bracchi(M1) and Flexor Carpi Radialis (M2) muscles of the right arm. The EEG electrodes were placed at the strategic position with conducting EEG paste and impedance check was performed to keep the skin-electrode impedance below 100 ohms. We used

metallic Ag/AgCl electrodes with circular cross-section and 10 mm dia for data acquisition. Skin preparation was done using ethyl alcohol to reduce any oily deposition on the skin before applying the EMG electrodes. EEG reference electrode was also used other than the linked ear electrodes and ground electrode for bipolar measurements. The instrument used to collect EEG was RMS Maximus 24 Channel Portable EEG machine and for EMG we have used a high sampling frequency Aleron 401 2/4 channel EMG machine by RMS. All subject specific data was saved in .csv format for offline analysis.

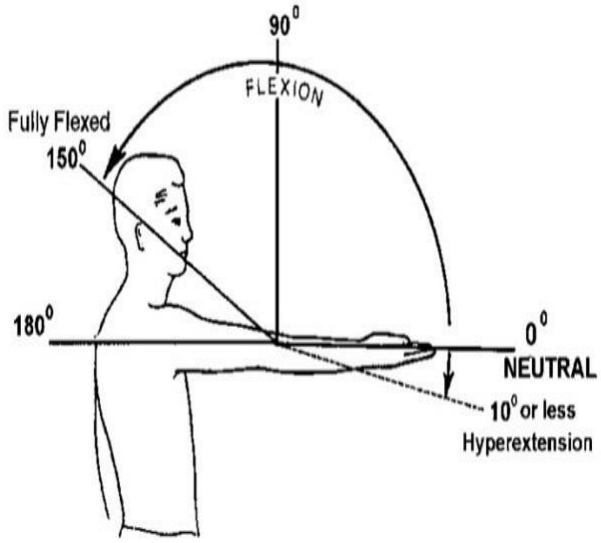

Fig.38 Elbow flexion-extension positions

Fig.39 Snapshot of the experiment protocol

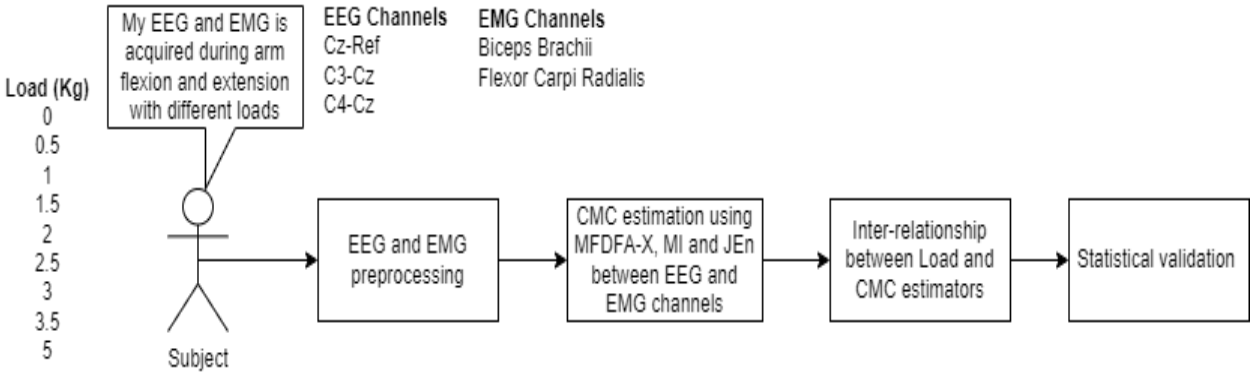

Fig.40 The block diagram representing the overall scheme of the proposed CMC estimator methodology

Data Preprocessing

In the data preparation stage, the EEG and EMG data have been processed separately as per their individual characteristics. The data preprocessing steps includes signal denoising, downsampling (in case of EMG), filtering, segmentation and data length matching.

In case of EEG data processing, three channels of bipolar EEG signals (C3-Cz, C4-Cz, Cz-Ref) are all denoised using 1D continuous wavelet transform method using Pywavelet python library. A specific denoising algorithm has been developed which includes creation of the wavelet filter and application of the wavelet filter to extract the EEG signal within the required frequency range of 0.5 to 80 Hz. We have used the Daubechies 6 wavelet filter function and decomposition of the signals up to level 8. To get the desired frequency bands we have calculated the scales corresponding to the target frequency band which is 0.5 Hz to 80 Hz and obtained the indices of the scales that are closest to the target scales. Then we have written the function for wavelet based denoising of a single EEG channel as the argument. The function is pretty straightforward, which decomposes the signals up to level 8 and stores the corresponding coefficients into 2D arrays. From the corresponding coefficients an if condition is applied to skip the coefficients that fall into the desired level else set the coefficients to zero. In our case preserving level 5,6 and 7 has given the best fit output after reconstructing the signal from the filtered coefficients. We have validated the output using the Welch Power Spectral Density plot to estimate the frequency band of the signal. After denoising we have applied a Butterworth filter of order 2 to extract the beta band (13-30) Hz from the denoised EEG signal. The beta band is the final choice for our CMC estimation owing to its significance in limb movements and various other cognitive actions.

Similarly, the EMG signal was also denoised and filtered but only after downsampling to match the sampling frequency of the EEG signal which is 256 Hz. The raw EMG signal was stored at a sampling frequency of 3500 Hz, but significant information can be obtained from the band of 20 to 100 Hz from arm muscles during dynamic contraction due flexion and extension. Therefore, we have downsampled the EMG signal to its target frequency of 256 Hz which very well suits our application since the highest frequency in the desired bandwidth is 100 Hz. The downsampling function removes the high frequency components using a 8th order Butterworth filter and

reconstructs the signal by adding all the downsampled factorth samples. A new time array is also defined to match the samples with the actual time of recording the signals.

The downsampled signal is denoised using a 1D discrete wavelet denoising method where we have used the Db6 wavelet and decomposed up to level 4 and reconstructed the signal using a hard thresholding method. The denoising algorithm for EMG is quite different from one used for EEG denoising since in EMG denoising we used thresholding based on a sigma estimator which is calculated as the mean absolute deviation of the signal. This is unlike the EEG signal denoising which includes the concept of scale to frequency conversion for selection of the coefficients, primarily because EEG signals are composed of delta, theta, alpha, beta and gamma bands whereas EMG signal doesn't contain any such specific bands. Therefore, to address this scenario two different schemes have been employed. The EMG signal is then filtered using a 2nd order Butterworth filter to obtain the signal in the 20 to 100 Hz range. The EMG signal denoising and filtering is validated using the Welch Power Spectral Density plot to see the energy contained within the desired bandwidth. The clean EMG signal is then used to calculate the CMC with respect to the EEG channels.

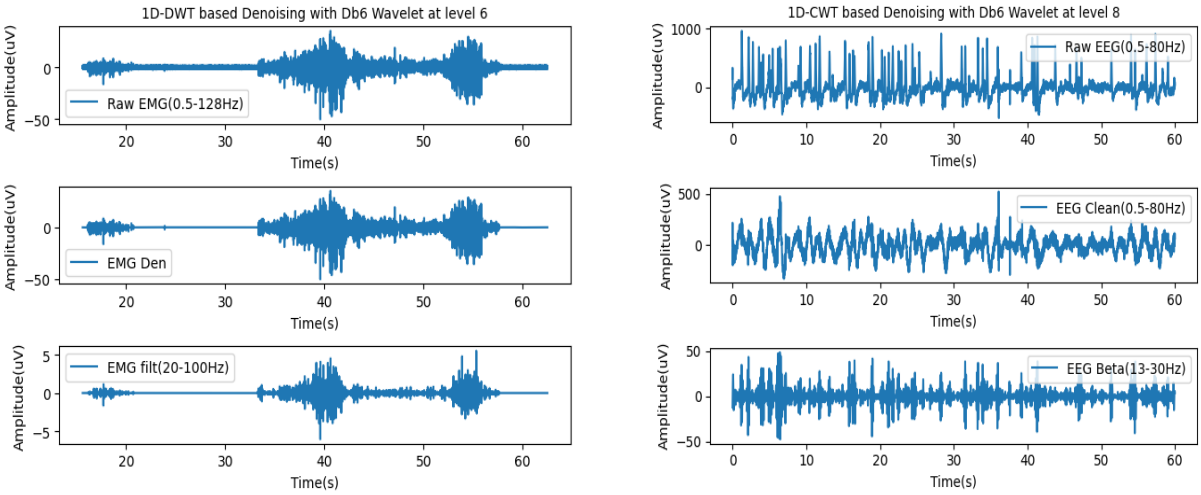

(a) (b)

Fig.41. Plot showing the steps of raw EMG (a) and raw EEG (b) signal denoising and filtering scheme for extraction of clean and filtered signals within the desirable frequency range.

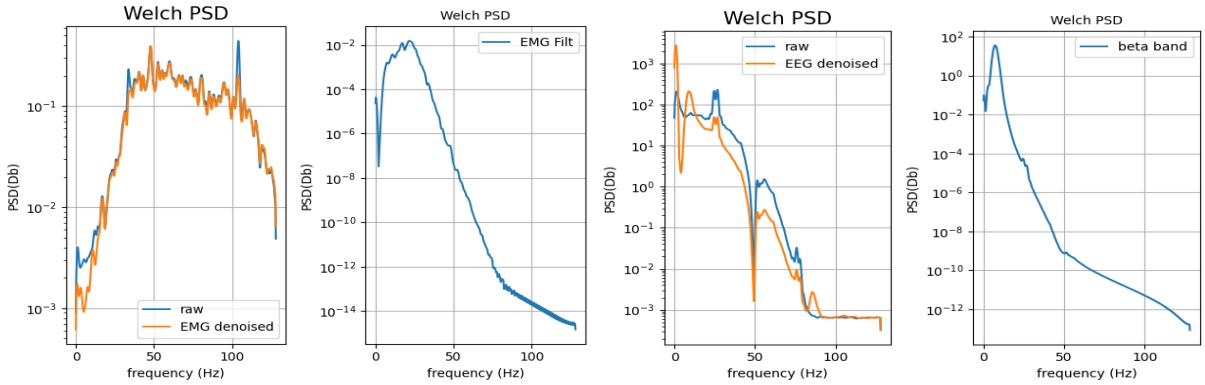

(a) (b)

Fig.42. The Welch PSD plots for EMG raw, denoised and filtered signals in (a) and for EEG raw, denoised and filtered EEG beta band (b) are shown in the figure.

Segmentation was performed from the whole EEG recording, to extract 60 sec of EEG segments that corresponds to specific 60 sec of EMG signal under varying weights. We have specially extracted the 9 segments from the overall EEG recording of respective individuals for every different event of arm extension and flexion with 9 different loads.

Corticomuscular Coherence estimation

In this section, the different parameters used for Corticomuscular Coherence have been explained in detail, and how they have been implemented in our proposed methodology have been discussed. Namely, three parameters were chosen to quantify the synchronicity of the brain and muscles while performing a cognitive action. These parameters help us to evaluate the cross correlation along with the rate of uncertainty between the EEG and EMG in estimating information about the effect of one variable onto the other in terms of uncertainty measurements. The effectiveness of these parameters in accurate estimation of the synchronicity between EEG and EMG and in explaining the underlying dynamics associated with the coherence of the neuromuscular system, has been studied thoroughly in this work.

MFDXA

Multifractal Detrended cross-correlation analysis (MFDXA) is a method used to analyse the correlation properties of two or more time series that have been recorded simultaneously. The method is based on the multifractal formalism, which is a mathematical framework used to analyse complex systems that exhibit scaling behaviour over a range of length scales [40]. The basic idea behind MFDXA is to quantify the degree of similarity between two time series by examining their cross-correlation function. The cross-correlation function measures the degree to which the two time series are synchronised or out of phase with each other over different time scales. MFDXA extends the traditional cross-correlation analysis by using the concept of multifractality to quantify the degree of correlation over a range of time scales. Multifractality refers to the property of a complex system where different parts of the system exhibit different degrees of scaling behaviour.

In MFDXA, the cross-correlation function is computed over a range of time scales, and the scaling behaviour of the function is analysed using the multifractal formalism. The resulting multifractal spectrum provides information about the degree of correlation between the two time series over different time scales. MFDXA has been applied in a wide range of fields, including finance, geophysics, and neuroscience, to analyse the correlation properties of complex systems. The method has the advantage of being able to capture the complex and non-linear nature of many real-world systems, and has the potential to provide valuable insights into the underlying dynamics of these systems. The steps of the algorithm used to compute the multifractal spectrum and to understand the nature of the cross-correlation coefficients varying across scales is described below.

Here are the steps for calculating the Multifractal Detrended Cross Correlation Analysis (MFDXA) between two variables:[41]

1. Choose the two variables that you want to analyse. Let's call them X and Y.

2. Divide the X and Y time series into non-overlapping windows of equal size.

3. Calculate the detrended fluctuation function (DFA) for each window of X and Y separately.

4. Calculate the cross-correlation function (CCF) between the detrended time series of X and Y for each window.

5. Apply the DFA to the CCF of each window to obtain the multifractal scaling exponents.

6. Calculate the qth-order correlation coefficient between the two variables as a function of the scale factor s.

7. Obtain the q-dependent scaling exponent h(q) from the slope of the log-log plot of the correlation coefficient versus s.

8. Calculate the generalised Hurst exponent H(q) from the scaling exponent h(q).

9. Obtain the singularity spectrum f(α) from the Legendre transform of the generalised Hurst exponent H(q).

10. Finally, analyse and interpret the singularity spectrum f(α) to understand the multifractal nature of the cross-correlation between the two variables.

The singularity spectrum describes the relationship between the singularity strength (alpha) and the scaling exponent (H(q)) or f(α). It provides insights into the distribution and strength of singularities in the data at different intensity ranges. The singularity spectrum can be plotted to visualise the multifractal properties of the data. The above algorithm has been implemented using the *fathon* Python library in Google collab.

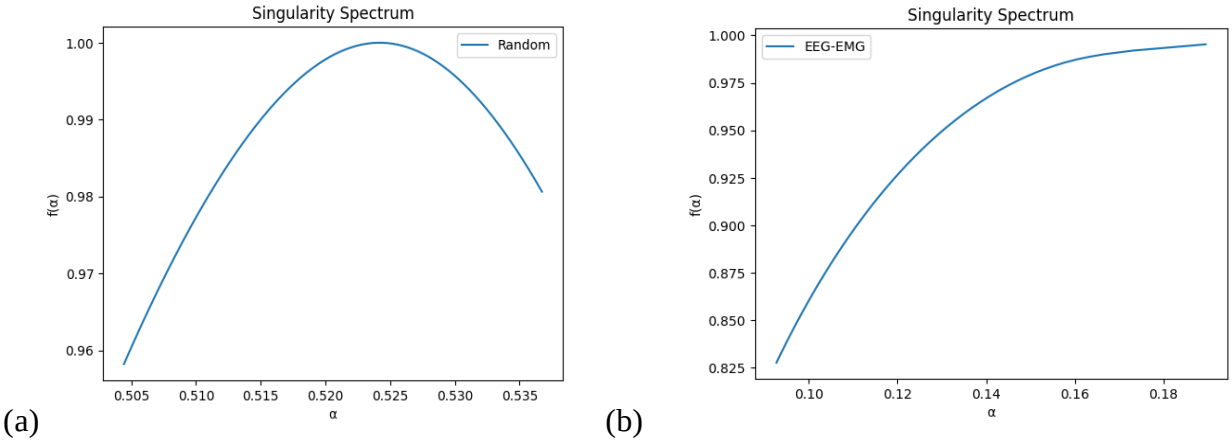

(a) (b)

Fig.43 (a) and (b) depicts the multifractal spectrum of corresponding correlation coefficient between two random variables in (a) and EEG - EMG cross correlation in (b). The multifractal spectrum is represented graphically as a plot with the scaling exponents on the y-axis and the corresponding measure of the segments on the x-axis. This exponent characterises the rate of change of the fractal dimension as the scale decreases.

The multifractal spectrum is a mathematical concept used to analyse and characterise complex systems or datasets that exhibit fractal properties at multiple scales. Fractals are geometric objects that exhibit self-similarity, meaning they possess similar structures or patterns regardless of the scale at which they are observed. A multifractal spectrum provides a quantitative measure of the scaling behaviour of different components or regions within a fractal or multifractal system. It describes how the fractal dimensions vary across the dataset, revealing the degree of heterogeneity or non-uniformity in the distribution of fractal properties. The shape of the spectrum reveals important information about the structure and organisation of the system. For instance, a concave spectrum suggests a hierarchical organisation, as seen in Fig.43(a), while a convex spectrum indicates a more homogeneous or self-similar distribution of fractal dimensions.

If the multifractal spectrum is exponential, as seen in Fig.43(b), it means that the scaling exponents follow an exponential function. In other words, the rate of change of the fractal dimensions varies exponentially as the scale decreases. An exponential multifractal spectrum suggests that the system under study has a high degree of complexity and heterogeneity. It implies that the fractal dimensions of different components or regions within the system change rapidly as the scale is reduced. This indicates the presence of intricate and diverse structures at various scales. Exponential multifractal spectra are often observed in complex systems where multiple underlying processes or mechanisms interact and contribute to the overall structure. Examples can be found in areas such as turbulence in fluid dynamics, certain types of financial markets, or the distribution of natural resources in ecological systems. In summary, an exponential multifractal spectrum indicates a highly complex and heterogeneous system with intricate structures at multiple scales. It suggests rapid changes in the fractal dimensions as the scale decreases and provides insights into the underlying processes and interactions within the system.

For cross correlation analysis, as shown in Fig.44, the Pearson’s product-moment correlation coefficient between the fluctuation functions of the two time-series is calculated for different segment lengths. The Pearson product-moment correlation coefficient, often referred to as Pearson's correlation coefficient or simply Pearson's correlation, is a statistical measure that quantifies the linear relationship between two variables [42]. It assesses how well the relationship between the variables can be described by a straight line This cross-correlation coefficient is used to identify the magnitude of corticomuscular coherence and observe the change in its value during arm flexion and extension with varying loads.

Pearson's correlation coefficient is denoted by the symbol "r" and takes values between -1 and +1. The sign of the correlation coefficient indicates the direction of the relationship, while the magnitude represents the strength of the relationship. Pearson's correlation coefficient is based on the covariance between the variables, normalised by the product of their standard deviations.

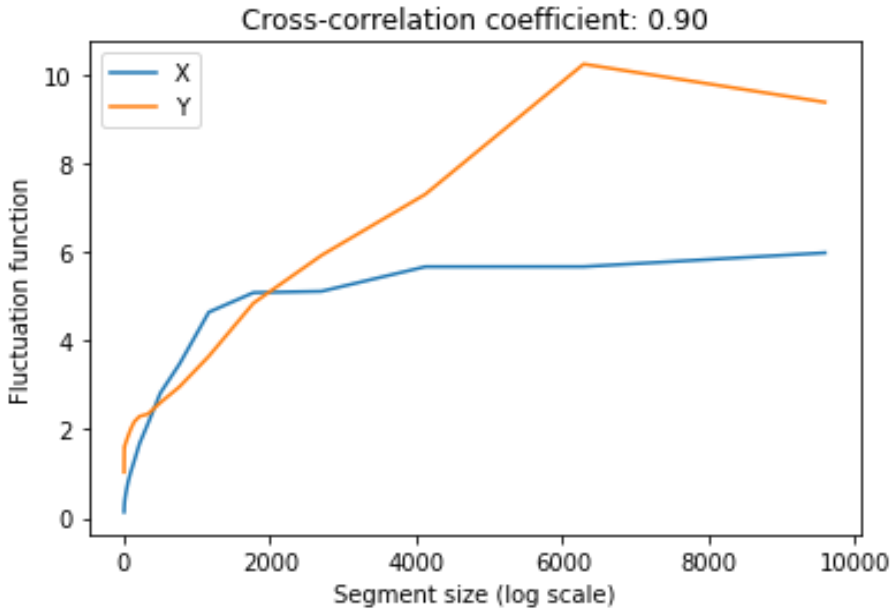

Fig.44. The Log-Log plot of the fluctuation function and scale of variable X (EEG) and Y(EMG) during arm flexion and extension under varying loads

In summary, the multifractal spectrum is a tool for analysing the scaling properties of complex systems, providing insights into the heterogeneity and self-similarity at multiple scales within a dataset. It is widely used in fields such as physics, mathematics, finance, geophysics, and image processing to study and understand the intricate nature of multifractal phenomena. This analysis provides valuable information about the organisation and distribution of complexity within the system, helping to uncover patterns, correlations, and underlying dynamics.

Mutual Information

Mutual information is a measure of the statistical dependence between two random variables or signals. It quantifies how much information is shared between the two signals. Specifically, it quantifies the extent to which the occurrence of one variable reduces the uncertainty about the other variable.[38]

Let's denote the two signals as X and Y. The mutual information between X and Y, denoted as I(X; Y), is calculated based on the probability distributions of X and Y. It can be expressed mathematically as:

$$I(X; Y) = \sum\sum P(x, y) \log (P(x, y) / (P(x)P(y))) \quad \text{Eq. [2]}$$

where:

- P(x, y) represents the joint probability distribution of X and Y, i.e., the probability that X takes the value x and Y takes the value y.

- P(x) and P(y) are the marginal probability distributions of X and Y, respectively, i.e., the probabilities of X taking the value x and Y taking the value y independently.

The mutual information measures the reduction in uncertainty about one signal (e.g., X) given the knowledge of the other signal (e.g., Y). It is zero if X and Y are independent, meaning that knowing one signal provides no information about the other. Higher values of mutual information indicate a stronger dependence between the signals, with a maximum value reached when X and Y are perfectly correlated. Mutual Information is a parameter that can also describe the underlying dynamics associated with simultaneous EEG and EMG signal generation schemes subject to a specific cognitive action. [43]

To calculate the Mutual Information (MI) between two signals x and y using nearest neighbours as suggested by Kraskov is given below:

1. Choose the number of nearest neighbours (K) for the calculation. This is a parameter that you need to define based on your specific analysis and dataset. A larger K captures more complex relationships but may introduce noise, while a smaller K may oversimplify the relationship.

2. For each point in signal x, find its K nearest neighbours in signal y using a distance metric such as Euclidean distance or cosine similarity.

3. Estimate the probability density of finding a neighbour in y given a point in x. This can be done by dividing the number of neighbours within a small distance (epsilon) from each point in x by the total number of neighbours considered.

4. Repeat step 2 and 3, but swap the roles of x and y. Find the K nearest neighbours for each point in y and estimate the probability density of finding a neighbour in x given a point in y.

5. Calculate the joint probability distribution between x and y by multiplying the densities obtained in steps 3 and 4. This represents the probability of finding a pair of points (one from x and one from y) within the considered distances.

6. Calculate the marginal probability distributions of x and y by summing the joint probabilities over the other variable. For example, to obtain the marginal distribution of x, sum the joint probabilities along the y-axis.

7. Compute the Mutual Information by summing the product of the joint probabilities and the logarithm of the ratio of joint and marginal probabilities. The formula for Mutual Information (MI) is:

$$MI(x, y) = \text{sum}(P(x, y) * \log(P(x, y) / (P(x) * P(y)))) \quad \text{Eq. [3]}$$

8. Repeat steps 1-7 for different values of K to assess the impact of different neighbourhood sizes on the MI calculation.

9. Finally, analyse and interpret the calculated Mutual Information to understand the dependence or independence between the signals x and y. Higher MI values indicate stronger dependencies, while lower values suggest independence.

It's important to note that estimating Mutual Information using nearest neighbours is just one approach among many [39], [44], [45]. There are alternative methods like histogram-based approaches or using different distance metrics that can be explored depending on the nature of data and the specific goals of analysis [46], [47].

Joint Entropy

Joint entropy is a measure of the amount of uncertainty or randomness in two jointly distributed random variables. It is commonly used in information theory and can be used to quantify the amount of information contained in the joint distribution. When we have two distributions, the joint entropy estimate provides a measure of the average amount of information that is needed to describe both distributions together. It measures the degree of uncertainty in both distributions combined.[48]

The joint entropy estimate is calculated as the negative sum of the probabilities of each pair of outcomes in the joint distribution, multiplied by their logarithm base 2. This formula is as follows:

$$H(X,Y) = - \sum p(x,y) \log_2 p(x,y) \qquad \text{Eq. [4]}$$

where X and Y are the two random variables, and p(x,y) is the joint probability mass function of X and Y.

A high joint entropy estimate indicates that the two distributions have a lot of randomness or uncertainty, while a low joint entropy estimate indicates that the two distributions are highly

correlated and have less randomness or uncertainty. Overall, the joint entropy estimate provides a useful measure of the amount of information contained in two distributions, and can be used in a variety of applications such as data compression, pattern recognition, and information retrieval [49].

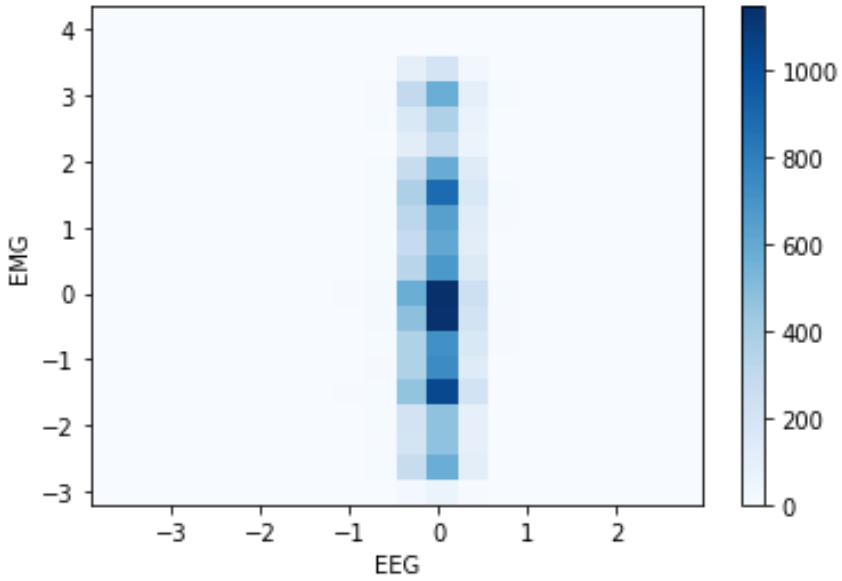

Fig.45 A joint histogram plot of EEG and EMG signals during weight lifting action

A joint histogram plot, as shown in fig.45 also known as a two-dimensional histogram or a density plot, displays the joint distribution of two variables x and y. Each variable is plotted on one of the axes, and the plot shows how often the two variables occur together at different values. Overall, a joint histogram plot can be a useful tool for understanding the relationship between two variables. By interpreting the shape, density, and outliers of the plot, you can gain insights into the patterns and trends in the data.

The steps of the algorithm used for estimating the joint Shannon entropy [50] between EEG and EMG signals is computed as follows: Estimating the joint probability density between two signals using Shannon entropy involves several steps.

Here's a high-level overview of the process:

1. Obtain the two signals: Collect or generate the two signals, which is one EEG channel and one EMG channel.

2. Discretize the signals: To apply Shannon entropy, you need to discretize the continuous signals into discrete values. This step involves dividing the range of each signal into a finite number of bins or quantization levels. The number of bins depends on the desired resolution and the characteristics of the signals.

3. Construct a joint probability matrix: Create a two-dimensional matrix representing the joint probability distribution between the discretized values of the two signals. The matrix will have dimensions corresponding to the number of bins used for each signal. Each cell in the matrix represents the probability of the two signals simultaneously taking on specific values.

4. Normalise the joint probability matrix: Normalise the joint probability matrix by dividing each cell's value by the total number of data points or samples used to construct the matrix. This normalisation ensures that the probabilities sum up to one, representing a valid probability distribution.

5. Calculate the Shannon entropy: Compute the Shannon entropy of the joint probability distribution using the normalised joint probability matrix. The formula for Shannon entropy is:

$$H(X, Y) = - \Sigma \Sigma P(x, y) \log2(P(x, y)) \quad \text{Eq. [5]}$$

Where P(x, y) represents the probability of the joint event (x, y) occurring.

Iterate over each cell of the joint probability matrix, calculating the product of P(x, y) and log2(P(x, y)) for each valid probability value, and sum up these products.

6. Interpret the Shannon entropy: The resulting Shannon entropy value represents the amount of information or uncertainty in the joint probability distribution. Higher entropy indicates more uncertainty or randomness, while lower entropy suggests more predictability or regularity in the relationship between the two signals. The above algorithm was implemented using *scipy* and *numpy* libraries in Python using Google Colab platform.

4.4.3. Results

The above analysis generates a vector of MFDXA, MI and JEn estimated for different patients at different loads in their arms starting from no load contraction up to 5 kg. In this section, we have compiled the results obtained from the above analysis into a classical feature set model with the loads as labels and the parameters as features. This was done to draw interrelationships between Load and Corticomuscular coherence and to observe the variation of the parameters along different loads as lifted by different subjects.

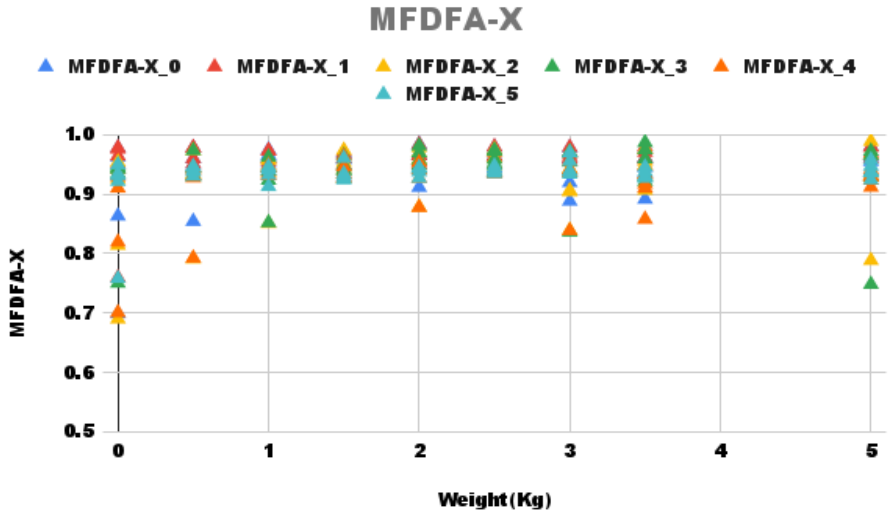

Fig.46. Variation of cross correlation coefficient of fluctuation function along with Weight lifted by 5 subjects

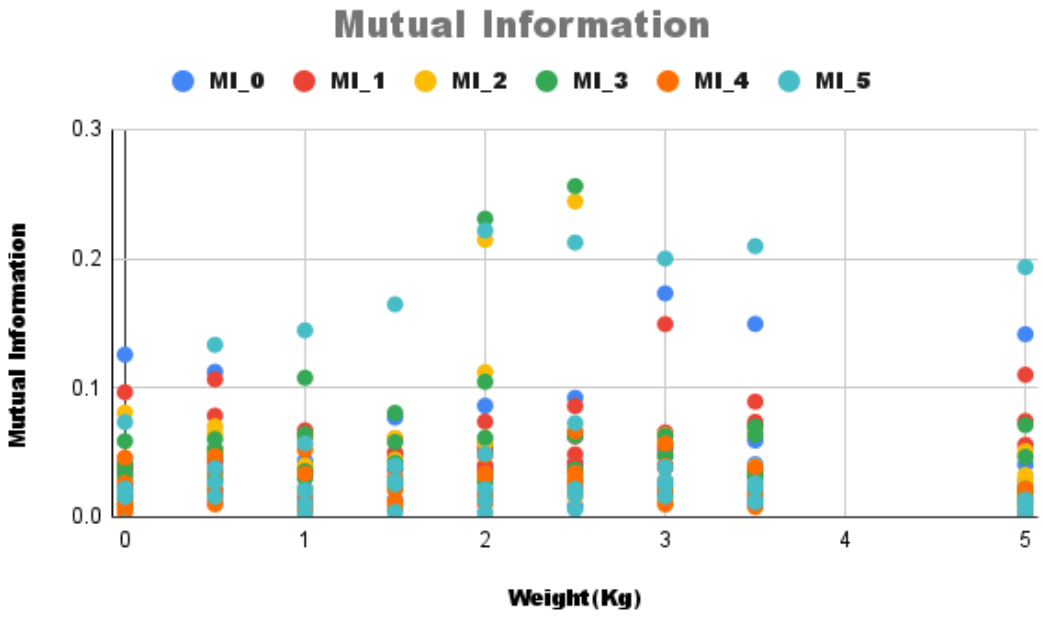

Fig.47. Variation of Mutual Information along with weights as lifted by 5 different subjects

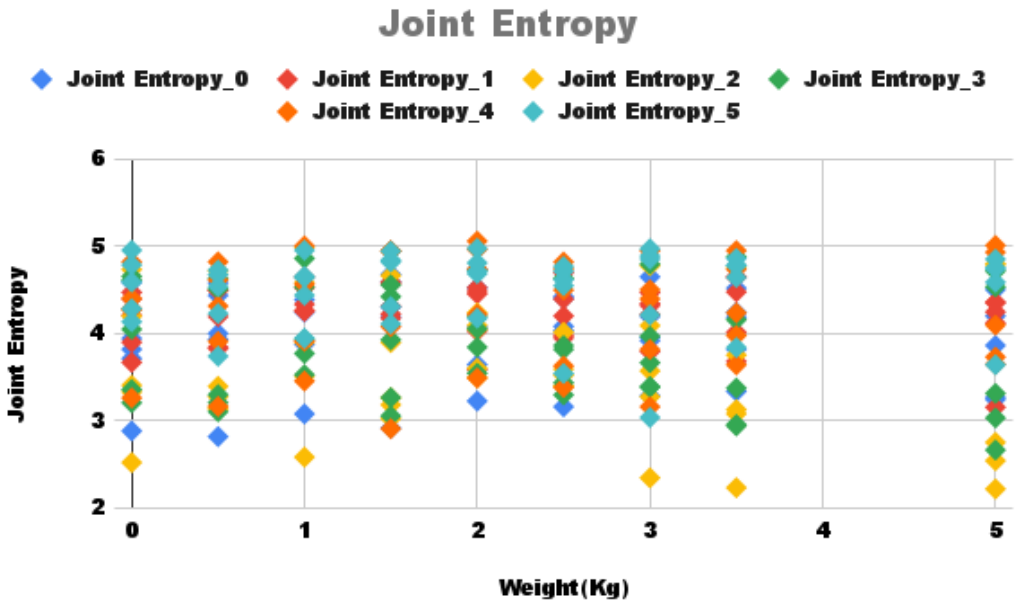

Fig.48. Variation of Joint Entropy values along with increasing load for 5 different subjects

In fig.46, fig.47 and fig.48 The variation of the Detrended Cross correlation coefficient, Mutual Information and Joint Entropy values are observed with respect to varying loads lifted by different subjects. The observation indicates that EEG and EMG are highly correlated during a specific cognitive action and can be measured using these parameters. The variation in the correlation coefficient between EEG and EMG at certain loads indicates that the parameters are sensitive to the loading conditions and correlation increases with increasing load and again falls back at the highest load for some subjects. This is an indication of the relationship between the EEG beta band and firing rate of the EMG motor neurons.

In order to investigate the significance of these parameters in estimating the relationship between weight and neuromuscular dynamics, we performed a one way ANOVA test in between groups to test the level of significance at $p \leq 0.01$. Firstly, we have selected all the three parameters for each cross-correlation channel of EEG and EMG. Secondly, we have clubbed all the channels used

for calculating MFDXA, MI and JEn respectively. Then we have performed the one way analysis of variance in between channels and in between parameters. The results of the F-statistic and p value is given in Table.4 and Table.5, where we can see that F-statistic value is higher than F-critical value and p value obtained is less than 0.01 in all the cases. The F-statistic value and a p-value of close to 0 indicate a highly significant result in the statistical analysis. The F-statistic is a measure of the ratio of the between-group variability to the within-group variability in an ANOVA test. With such a high F-statistic value and an extremely low p-value (close to zero), it suggests strong evidence against the null hypothesis. In other words, the probability of observing the data or more extreme data, assuming the null hypothesis is true, is virtually impossible. Therefore, we would reject the null hypothesis and conclude that there is a significant difference or relationship between the variables being analysed.

Table.6. One Way ANOVA table showing F and P value for interrelated variables for different channels

EEG(Cz-Ref) x M1	**EEG(Cz-Ref) x M2**	**EEG(C3-Cz) x M1**	**EEG(C3-Cz) x M2**	**EEG(C4-Cz) x M1**	**EEG(C4-Cz) x M2**
F-Statistic: 1910.6098 P-Value: 3.6234e-98	F-Statistic: 5985.2526 P-Value: 3.0768e-130	F-Statistic: 807.2409 P-Value: 9.4416e-75	F-Statistic: 1316.5199 P-Value: 6.3912e-88	F-Statistic: 1806.8327 P-Value: 1.2734e-96	F-Statistic: 3862.9597 P-Value: 7.3719e-118

Table.7. One Way ANOVA table showing F and P value for interrelated variables among all channels

MFDXA	**MI**	**JEn**
F-Statistic: 4.2387 P-Value: 0.001	F-Statistic: 3.0041 P-Value: 0.011	F-Statistic: 14.4312 P-Value: 1.6865e-12

4.4.4. Discussion

The interrelationship between CMC and the varying loads lifted by human arm are estimated using the MFDXA, MI and JEn as prospective descriptors of the brain and muscle coordination. The estimation of the parameters to obtain the crosscorrelation between EEG signal collected from cortical regions and EMG signals collected from the human arm muscles, proved to significantly enhance the quality of estimation of CMC compared to previous studies. Previous studies mostly focused on linear estimation of the crosscorrelation based on statistical analysis or cross spectral analysis at specific frequency bands, which failed to take into account the nonstationary and chaotic nature of the physiological signals. Previous studies have hinted that force is an important factor in estimation of the CMC magnitude along with a different paradigm as adopted by the researchers for measuring CMC. No study has been performed using Fractals and Entropy analysis techniques to estimate the CMC under different conditions. In this regard the present study addressed this research gap and attempted to quantify the CMC based on nonlinear dynamical systems analysis using EEG and EMG signal, which is a much cost effective and safer alternative to Magnetoencephalography (MEG) and other imaging methods. Here is the list of studies performed using EEG-EMG to estimate the CMC as shown in Table.6

From the above results in table.4 and table.5, we observe that MFDXA, MI and JEn are good descriptors of neuromuscular coordination as represented by the corticomuscular coherence estimation technique. This technique does not only capture the underlying dynamics of neuromuscular communication systems but is also sensitive to changes as evident by the experimental protocol. These results actually open a gateway towards understanding the concepts involved in quantification of corticomuscular coherence for the design of efficient and effective techniques to detect neuromuscular dysfunctionalities and also measure the progress of treatment or rehabilitation. From fig.46, fig.47 and fig.48 we can infer that, during no load contraction the uncertainty is very high because of the disorderness in motor unit action potential (MUAP) firing, but as and when weight is applied then the uncertainty tends to reduce owing to more ordered MUAP firing at higher weights. As soon as the subject is asked to lift 5Kg load on arms, then again, the uncertainty increases a bit for some subjects who felt fatigued in lifting such a high load.

Table.8. Comparison of CMC values between healthy subjects and patients as estimated with EEG-EMG signal coherence

Ref	Subjects	Inference
[51]	Normal: 7 Stroke: 5	Lower CMC observed in Stroke patients than healthy individuals
[52]	Normal: 24 Spinocerebellar ataxia (SCA): 19	Lower CMC observed with lower limb EMG in SCA patients than healthy patients
[53]	Normal: 18 Tremor: 18	CMC level dropped intermittently in case of CMC patients whereas it remained higher for healthy subjects
[54]	Normal: 15 Cerebral Palsy: 14	Low CMC in gamma band for Cerebral Palsy subjects in comparison to healthy individuals
[55]	Normal: 17 Amyotrophic Lateral Sclerosis: 17	Low CMC in beta band for ALS patients as compared to healthy subjects
[56]	Normal: 8 Stroke: 21	Lower CMC observed in case of Stroke patients than healthy individuals arm muscles.

The fatiguing of the muscles, again introduced disorderness in the system hence increasing uncertainty as seen from the lower values of MI and high value of JEn along with decrease in fractal cross correlation coefficient at 5Kg load. The uncertainty at no load and 5 kg load is clearly

evident from the results owing to higher disorderness when no external energy is applied. When energy is applied into the muscles in the form of load, then it becomes ordered, hence there is reduction in entropy and higher value of MI. The rate of information transfer between brain and muscles increases while loading of the muscles and also depicts a high degree of correlation.

The study has its own limitations pertaining to the smaller number of subjects involved in the study, and absence of any clinical data validation. The main objective of this study is to propose a method that can be implemented based on the theoretically rich concept of the nonlinear dynamical systems analysis which is best suited for nonstationary and stochastic bio signal processing. This motivated us to develop the methodology and validate it on the basis of our own designed experiments. The concept is thought to have immense potential if proper validation is done for the same using clinical data for its applicability in real life scenarios.

4.4.5. Conclusion

In the proposed methodology, we have presented an analysis technique based on nonlinear dynamical systems theory and validated it with an in-house experiment to quantify the corticomuscular coherence during weight lifting action. The experimental data was analysed to calculate the MFDXA, MI and JEn using preprocessed and segmented data. The parameters were investigated about their potential in describing the underlying dynamics associated with the neuromuscular coordination using simultaneously acquired EEG and EMG from different subjects. The study was conducted with an objective to quantify the corticomuscular coherence using the nonlinear cross correlation parameters. The results obtained after the analysis are significant enough in distinguishing the corticomuscular coherence calculated at different weights. The parameters are 99.99% statistically significant in distinguishing between variables and weights. With this observation, we can conclude that the above-mentioned parameters are reliable descriptors of Corticomuscular coherence and can be extended further in measuring the loss of coherence during any neuromuscular disorder like cerebral palsy, stroke rehabilitation, paralysis or any other cause related to loss of neuromuscular coordination. The method may be used as a

measurement tool for quantifying the degree of neuromuscular dysfunction in patients suffering from it, in a completely cost effective and non-invasive way. The algorithm may also be extended further using Artificial Intelligence and Machine Learning techniques for automated detection of corticomuscular coherence and provide quick and automated diagnosis info to the caregiver or subject. The degree of loss of coherence can be predicted by an AI model well trained with MFDXA, MI and JEn as features with other potential linear descriptors.

4.4.6. Future Scope

The results of the proposed CMC estimation technique are preliminary and indicate strong potential for diagnostic applications for patients suffering from various neuromuscular dysfunctions. The proposed methodology is supposed to work well in a clinical setting and further clinical validation with patient data is required. Artificial Intelligence and Machine Learning techniques can be applied here, but only with a much larger dataset. Overall, there is enough scope in this field of study as it is just in its infancy and has the potential to outperform many existing techniques to effectively measure, diagnose and treat patients suffering from various neuromuscular disorders.

References

[1] T. Mima, M. Hallett, and H. Shibasaki, 'Chapter 7 Coherence, cortico-muscular', in *Handbook of Clinical Neurophysiology*, M. Hallett, Ed., in Handbook of Clinical Neurophysiology, vol. 1. Elsevier, 2003, pp. 87–94. doi: 10.1016/S1567-4231(09)70155-8.

[2] P. Brown and P. Grosse, 'Chapter 57 EEG—EMG coherence in movement disorders', in *Supplements to Clinical Neurophysiology*, R. C. Reisin, M. R. Nuwer, M. Hallett, and C. Medina, Eds., in Advances in Clinical Neurophysiology, vol. 54. Elsevier, 2002, pp. 382–386. doi: 10.1016/S1567-424X(09)70477-5.

[3] X. Lou, S. Xiao, Y. Qi, X. Hu, Y. Wang, and X. Zheng, 'Corticomuscular Coherence Analysis on Hand Movement Distinction for Active Rehabilitation', *Comput. Math. Methods Med.*, vol. 2013, p. e908591, Apr. 2013, doi: 10.1155/2013/908591.

[4] K. Airaksinen *et al.*, ‘Cortico-muscular coherence parallels coherence of postural tremor and MEG during static muscle contraction’, *Neurosci. Lett.*, vol. 602, pp. 22–26, Aug. 2015, doi: 10.1016/j.neulet.2015.06.034.

[5] H. Maezawa, ‘Cortico-muscular communication for motor control of the tongue in humans: A review’, *J. Oral Biosci.*, vol. 58, no. 3, pp. 69–72, Aug. 2016, doi: 10.1016/j.job.2016.03.001.

[6] J. Liu, Y. Sheng, and H. Liu, ‘Corticomuscular Coherence and Its Applications: A Review’, *Front. Hum. Neurosci.*, vol. 13, 2019, Accessed: May 25, 2023. [Online]. Available: https://www.frontiersin.org/articles/10.3389/fnhum.2019.00100

[7] T. Mima, J. Steger, A. E. Schulman, C. Gerloff, and M. Hallett, ‘Electroencephalographic measurement of motor cortex control of muscle activity in humans’, *Clin. Neurophysiol.*, vol. 111, no. 2, pp. 326–337, Feb. 2000, doi: 10.1016/S1388-2457(99)00229-1.

[8] Task-dependent modulation of 15-30 Hz coherence between rectified EMGs from human hand and forearm muscles’, Accessed: May 25, 2023. [Online]. Available: https://physoc.onlinelibrary.wiley.com/doi/10.1111/j.1469-7793.1999.0559v.x

[9] S. Mehrkanoon, M. Breakspear, and T. W. Boonstra, ‘The reorganization of corticomuscular coherence during a transition between sensorimotor states’, *NeuroImage*, vol. 100, pp. 692–702, Oct. 2014, doi: 10.1016/j.neuroimage.2014.06.050.

[10] S.-C. Bao, W.-W. Wong, T. W. Leung, and K.-Y. Tong, ‘Low Gamma Band Cortico-muscular Coherence Inter-Hemisphere Difference following Chronic Stroke’, *Annu. Int. Conf. IEEE Eng. Med. Biol. Soc. IEEE Eng. Med. Biol. Soc. Annu. Int. Conf.*, vol. 2018, pp. 247–250, Jul. 2018, doi: 10.1109/EMBC.2018.8512208.

[11] A. Coffey *et al.*, ‘Altered supraspinal motor networks in survivors of poliomyelitis: A cortico-muscular coherence study’, *Clin. Neurophysiol.*, vol. 132, no. 1, pp. 106–113, Jan. 2021, doi: 10.1016/j.clinph.2020.10.011.

[12] J. Gross, J. Kujala, M. Hämäläinen, L. Timmermann, A. Schnitzler, and R. Salmelin, ‘Dynamic imaging of coherent sources: Studying neural interactions in the human brain’, *Proc. Natl. Acad. Sci.*, vol. 98, no. 2, pp. 694–699, Jan. 2001, doi: 10.1073/pnas.98.2.694.

[13] T. Mima and M. Hallett, ‘Electroencephalographic analysis of cortico-muscular coherence: reference effect, volume conduction and generator mechanism’, *Clin. Neurophysiol.*, vol. 110, no. 11, pp. 1892–1899, Nov. 1999, doi: 10.1016/S1388-2457(99)00238-2.

[14] P. Nijhuis, P. E. Keller, S. Nozaradan, and M. Varlet, ‘Dynamic modulation of cortico-muscular coupling during real and imagined sensorimotor synchronisation’, *NeuroImage*, vol. 238, p. 118209, Sep. 2021, doi: 10.1016/j.neuroimage.2021.118209.

[15] C. Micheli and C. Braun, ‘Enhancing the Signal of Corticomuscular Coherence’, *Comput. Math. Methods Med.*, vol. 2012, p. e451938, May 2012, doi: 10.1155/2012/451938.

[16] J.-P. Lachaux *et al.*, ‘Estimating the time-course of coherence between single-trial brain signals: an introduction to wavelet coherence’, *Neurophysiol. Clin. Neurophysiol.*, vol. 32, no. 3, pp. 157–174, Jun. 2002, doi: 10.1016/S0987-7053(02)00301-5.

[17] D. Pal and S. K. Mitra, ‘Oil price and automobile stock return co-movement: A wavelet coherence analysis’, *Econ. Model.*, vol. 76, pp. 172–181, Jan. 2019, doi: 10.1016/j.econmod.2018.07.028.

[18] X. Xi *et al.*, ‘Construction and analysis of cortical–muscular functional network based on EEG-EMG coherence using wavelet coherence’, *Neurocomputing*, vol. 438, pp. 248–258, May 2021, doi: 10.1016/j.neucom.2021.01.102.

[19] R. W. Thatcher, ‘Coherence, phase differences, phase shift, and phase lock in EEG/ERP analyses’, *Dev. Neuropsychol.*, vol. 37, no. 6, pp. 476–496, 2012, doi: 10.1080/87565641.2011.619241.

[20] B. Schelter, M. Winterhalder, J. Timmer, and J. Kurths, ‘PHASE SYNCHRONIZATION AND COHERENCE ANALYSIS: SENSITIVITY AND SPECIFICITY’, *Int. J. Bifurc. Chaos*, vol. 17, no. 10, pp. 3551–3556, Oct. 2007, doi: 10.1142/S0218127407019354.

[21] R. Kenville *et al.*, ‘Corticomuscular interactions during different movement periods in a multi-joint compound movement’, *Sci. Rep.*, vol. 10, no. 1, Art. no. 1, Mar. 2020, doi: 10.1038/s41598-020-61909-z.

[22] C. M. Gray, A. K. Engel, P. König, and W. Singer, ‘Synchronization of oscillatory neuronal responses in cat striate cortex: temporal properties’, *Vis. Neurosci.*, vol. 8, no. 4, pp. 337–

347, Apr. 1992, doi: 10.1017/s0952523800005071.

[23] A. B. Schwartz and J. L. Adams, ‘A method for detecting the time course of correlation between single-unit activity and EMG during a behavioral task’, *J. Neurosci. Methods*, vol. 58, no. 1, pp. 127–141, May 1995, doi: 10.1016/0165-0270(94)00167-F.

[24] B. Schack and W. Krause, ‘Dynamic power and coherence analysis of ultra short-term cognitive processes — A methodical study’, *Brain Topogr.*, vol. 8, no. 2, pp. 127–136, Dec. 1995, doi: 10.1007/BF01199776.

[25] S. J. Schiff, P. So, T. Chang, R. E. Burke, and T. Sauer, ‘Detecting dynamical interdependence and generalized synchrony through mutual prediction in a neural ensemble’, *Phys. Rev. E*, vol. 54, no. 6, pp. 6708–6724, Dec. 1996, doi: 10.1103/PhysRevE.54.6708.

[26] N. F. Rulkov, M. M. Sushchik, L. S. Tsimring, and H. D. I. Abarbanel, ‘Generalized synchronization of chaos in directionally coupled chaotic systems’, *Phys. Rev. E*, vol. 51, no. 2, pp. 980–994, Feb. 1995, doi: 10.1103/PhysRevE.51.980.

[27] N. M. Safri, N. Murayama, T. Igasaki, and Y. Hayashida, ‘Effects of visual stimulation on cortico-spinal coherence during isometric hand contraction in humans’, *Int. J. Psychophysiol.*, vol. 61, no. 2, pp. 288–293, Aug. 2006, doi: 10.1016/j.ijpsycho.2006.03.003.

[28] K. Airaksinen *et al.*, ‘Cortico-muscular coherence in advanced Parkinson’s disease with deep brain stimulation’, *Clin. Neurophysiol.*, vol. 126, no. 4, pp. 748–755, Apr. 2015, doi: 10.1016/j.clinph.2014.07.025.

[29] J. Hirschmann *et al.*, ‘Differential modulation of STN-cortical and cortico-muscular coherence by movement and levodopa in Parkinson’s disease’, *NeuroImage*, vol. 68, pp. 203–213, Mar. 2013, doi: 10.1016/j.neuroimage.2012.11.036.

[30] C. R. Forman, K. J. Jacobsen, A. N. Karabanov, J. B. Nielsen, and J. Lorentzen, ‘Corticomuscular coherence is reduced in relation to dorsiflexion fatigability to the same extent in adults with cerebral palsy as in neurologically intact adults’, *Eur. J. Appl. Physiol.*, vol. 122, no. 6, pp. 1459–1471, Jun. 2022, doi: 10.1007/s00421-022-04938-y.

[31] S. Franceschetti, E. Visani, F. Panzica, A. Coppola, P. Striano, and L. Canafoglia, 'Cortico-muscular coherence and brain networks in familial adult myoclonic epilepsy and progressive myoclonic epilepsy', *Clin. Neurophysiol.*, vol. 151, pp. 74–82, Jul. 2023, doi: 10.1016/j.clinph.2023.04.009.

[32] H. E. Rossiter *et al.*, 'Changes in the location of cortico-muscular coherence following stroke', *NeuroImage Clin.*, vol. 2, pp. 50–55, Jan. 2013, doi: 10.1016/j.nicl.2012.11.002.

[33] L.-L. H. Pan *et al.*, 'Effects of 8-week sensory electrical stimulation combined with motor training on EEG-EMG coherence and motor function in individuals with stroke', *Sci. Rep.*, vol. 8, no. 1, Art. no. 1, Jun. 2018, doi: 10.1038/s41598-018-27553-4.

[34] P. Belardinelli, L. Laer, E. Ortiz, C. Braun, and A. Gharabaghi, 'Plasticity of premotor cortico-muscular coherence in severely impaired stroke patients with hand paralysis', *NeuroImage Clin.*, vol. 14, pp. 726–733, Jan. 2017, doi: 10.1016/j.nicl.2017.03.005.

[35] V. de Seta *et al.*, 'Cortico-muscular coupling to control a hybrid brain-computer interface for upper limb motor rehabilitation: A pseudo-online study on stroke patients', *Front. Hum. Neurosci.*, vol. 16, 2022, Accessed: May 26, 2023. [Online]. Available: https://www.frontiersin.org/articles/10.3389/fnhum.2022.1016862

[36] F. Pichiorri *et al.*, 'Exploring high-density corticomuscular networks after stroke to enable a hybrid Brain-Computer Interface for hand motor rehabilitation', *J. NeuroEngineering Rehabil.*, vol. 20, no. 1, p. 5, Jan. 2023, doi: 10.1186/s12984-023-01127-6.

[37] W.-X. Zhou, 'Multifractal detrended cross-correlation analysis for two nonstationary signals', *Phys. Rev. E*, vol. 77, no. 6, p. 066211, Jun. 2008, doi: 10.1103/PhysRevE.77.066211.

[38] A. Kraskov, H. Stögbauer, and P. Grassberger, 'Estimating mutual information', *Phys. Rev. E*, vol. 69, no. 6, p. 066138, Jun. 2004, doi: 10.1103/PhysRevE.69.066138.

[39] A. Orlitsky, 'Information Theory', in *Encyclopedia of Physical Science and Technology (Third Edition)*, R. A. Meyers, Ed., New York: Academic Press, 2003, pp. 751–769. doi: 10.1016/B0-12-227410-5/00337-9.

[40] J. W. Kantelhardt, S. A. Zschiegner, E. Koscielny-Bunde, S. Havlin, A. Bunde, and H. E.

Stanley, ‘Multifractal detrended fluctuation analysis of nonstationary time series’, *Phys. Stat. Mech. Its Appl.*, vol. 316, no. 1, pp. 87–114, Dec. 2002, doi: 10.1016/S0378-4371(02)01383-3.

[41] S. Dutta, D. Ghosh, and S. Samanta, ‘Multifractal detrended cross-correlation analysis of gold price and SENSEX’, *Phys. Stat. Mech. Its Appl.*, vol. 413, pp. 195–204, Nov. 2014, doi: 10.1016/j.physa.2014.06.081.

[42] K. Pearson and F. Galton, ‘VII. Note on regression and inheritance in the case of two parents’, *Proc. R. Soc. Lond.*, vol. 58, no. 347–352, pp. 240–242, Jan. 1997, doi: 10.1098/rspl.1895.0041.

[43] S.-H. Jin, P. Lin, and M. Hallett, ‘Linear and nonlinear information flow based on time-delayed mutual information method and its application to corticomuscular interaction’, *Clin. Neurophysiol.*, vol. 121, no. 3, pp. 392–401, Mar. 2010, doi: 10.1016/j.clinph.2009.09.033.

[44] L. Paninski, ‘Estimation of Entropy and Mutual Information’, *Neural Comput.*, vol. 15, no. 6, pp. 1191–1253, Jun. 2003, doi: 10.1162/089976603321780272.

[45] B. Frénay, G. Doquire, and M. Verleysen, ‘Estimating mutual information for feature selection in the presence of label noise’, *Comput. Stat. Data Anal.*, vol. 71, pp. 832–848, Mar. 2014, doi: 10.1016/j.csda.2013.05.001.

[46] W. Li, H. Wang, and L. Zhuang, ‘GCNs–FSMI: EEG recognition of mental illness based on fine-grained signal features and graph mutual information maximization’, *Expert Syst. Appl.*, vol. 228, p. 120227, Oct. 2023, doi: 10.1016/j.eswa.2023.120227.

[47] P. Golub, A. Antalik, P. Beran, and J. Brabec, ‘Mutual information prediction for strongly correlated systems’, *Chem. Phys. Lett.*, vol. 813, p. 140297, Feb. 2023, doi: 10.1016/j.cplett.2023.140297.

[48] B. Chen, J. Wang, H. Zhao, and J. C. Principe, ‘Insights into Entropy as a Measure of Multivariate Variability’, *Entropy*, vol. 18, no. 5, Art. no. 5, May 2016, doi: 10.3390/e18050196.

[49] F. J. Valverde-Albacete and C. Peláez-Moreno, ‘The evaluation of data sources using

multivariate entropy tools', *Expert Syst. Appl.*, vol. 78, pp. 145–157, Jul. 2017, doi: 10.1016/j.eswa.2017.02.010.

[50] Y. Karaca and M. Moonis, 'Chapter 14 - Shannon entropy-based complexity quantification of nonlinear stochastic process: diagnostic and predictive spatiotemporal uncertainty of multiple sclerosis subgroups', in *Multi-Chaos, Fractal and Multi-Fractional Artificial Intelligence of Different Complex Systems*, Y. Karaca, D. Baleanu, Y.-D. Zhang, O. Gervasi, and M. Moonis, Eds., Academic Press, 2022, pp. 231–245. doi: 10.1016/B978-0-323-90032-4.00018-3.

[51] Y. Gao, L. Ren, R. Li, and Y. Zhang, 'Electroencephalogram–Electromyography Coupling Analysis in Stroke Based on Symbolic Transfer Entropy', *Front. Neurol.*, vol. 8, 2018, Accessed: Jul. 08, 2023. [Online]. Available: https://www.frontiersin.org/articles/10.3389/fneur.2017.00716

[52] L. Velázquez-Pérez *et al.*, 'Early corticospinal tract damage in prodromal SCA2 revealed by EEG-EMG and EMG-EMG coherence', *Clin. Neurophysiol. Off. J. Int. Fed. Clin. Neurophysiol.*, vol. 128, no. 12, pp. 2493–2502, Dec. 2017, doi: 10.1016/j.clinph.2017.10.009.

[53] S. Sharifi *et al.*, 'Intermittent cortical involvement in the preservation of tremor in essential tremor', *J. Neurophysiol.*, vol. 118, no. 5, pp. 2628–2635, Nov. 2017, doi: 10.1152/jn.00848.2016.

[54] I. Riquelme, I. Cifre, M. A. Muñoz, and P. Montoya, 'Altered corticomuscular coherence elicited by paced isotonic contractions in individuals with cerebral palsy: a case-control study', *J. Electromyogr. Kinesiol. Off. J. Int. Soc. Electrophysiol. Kinesiol.*, vol. 24, no. 6, pp. 928–933, Dec. 2014, doi: 10.1016/j.jelekin.2014.07.004.

[55] M. Proudfoot *et al.*, 'Impaired corticomuscular and interhemispheric cortical beta oscillation coupling in amyotrophic lateral sclerosis', *Clin. Neurophysiol.*, vol. 129, no. 7, pp. 1479–1489, Jul. 2018, doi: 10.1016/j.clinph.2018.03.019.

[56] Y. Fang *et al.*, 'Functional corticomuscular connection during reaching is weakened following stroke', *Clin. Neurophysiol.*, vol. 120, no. 5, pp. 994–1002, May 2009,

4.5. A Python based Support Vector Regression Model for prediction of Covid19 cases in India

The work presented here was published in Elsevier journal Chaos, Solitons & Fractals. The proposed work utilizes Support Vector Regression model to predict the number of total number of deaths, recovered cases, cumulative number of confirmed cases and number of daily cases. The data is collected for the time period of 1st March,2020 to 30th April,2020 (61 Days). The total number of cases as on 30th April is found to be 35043 confirmed cases with 1147 total deaths and 8889 recovered patients. The model has been developed in Python 3.6.3 to obtain the predicted values of aforementioned cases till 30th June,2020. The proposed methodology is based on prediction of values using support vector regression model with Radial Basis Function as the kernel and 10% confidence interval for the curve fitting. The data has been split into train and test set with test size 40% and training 60%. The model performance parameters are calculated as mean square error, root mean square error, regression score and percentage accuracy. The model has above 97% accuracy in predicting deaths, recovered, cumulative number of confirmed cases and 87% accuracy in predicting daily new cases. The results suggest a gaussian decrease of the number of cases and could take another 3 to 4 months to come down the minimum level with no new cases being reported. The method is very efficient and has higher accuracy than linear or polynomial regression.

4.5.1. Introduction

The spread of coronavirus disease 2019 (COVID-19) has become a global threat and the World Health Organization (WHO) declared COVID-19 a global pandemic on March 11, 2020**Invalid source specified.** . As of April 30, 2020, there were 3,359,055 confirmed cases and 238,999 deaths from COVID-19 worldwide**Invalid source specified.** (https://coronavirus.jhu.edu/data/new-cases). The COVID-19 pandemic has been greatly affecting people's lives and the world's economy. Among many infection related questions, governments and people are most concerned with (i) when will the COVID19 infection rate reach the maximum; (ii) how long the pandemic will take to stop spreading and (iii) What could be the total number of individuals that will eventually be infected (iv) what will be the toatl number of deaths**Invalid source specified.**. The questions are of primary concern in India also, a country with high population density and

economic diversity. The spread of the disease in India is considerably lower than that of China, USA and other European countries. India is under complete lockdown since 21st March,2020 and experts belief that this could be detrimental in mitigating the Covid19 spread among its citizens. Currently the development of vaccines is still in progress and there are no effective antiviral drugs for treating COVID-19 infections.As on April,30 the total number of COVID19 cases in India is 35043 and 1147 has died due to Severe Actue Respiratory Syndrome(SARS) (https://www.mohfw.gov.in/). The total number of COVID19 recoverd individuals in India is 8889 until date.

The lockdown is severely affecting the poor and migrant labours. Staying at home may not be a feasible option in the near future since a lot of people may die out of hunger and other ailments. Newsmedia reports all over the world is reporting about the crisis and how it is effecting the lives of people. Many research is being carried out at all levels to quickly gather information, develop mitigation tools and methods and implementation of the same. Therefore policy makers and authorities want to have an overall view of the current situation and want to visualize the extent at which it can spread in the near future for informed policy making and deciding the next course of action.

The paper here discusses about the proposed prediction model of COVID19 spread in India using Support Vector Regression implemented in Python.3.6. The steps of the model is discussed in the methodology section wih subsequent analysis. The results are shown and discussed. The autors conclude the overall purpose of the work in Conclusion.

4.5.2. Methodology

a. Preparation of the dataset

The .csv file of Novel Coronavirus 2019 dataset available at https://www.kaggle.com/sudalairajkumar/novel-corona-virus-2019-dataset is downloaded. A separate .csv file is is created from the global dataset only for India. The columns include Total Deaths, Total Recovered and Total number of confirmed covid19 patients on day to day basis from 1st March,2020 to 30th April,2020 (61 days). All the data is in cumulative form. From the

cumulative dataset, we have computed the difference time series to get the values based on daily new case basis.So we have now extended our dataset to have six columns 3 for cumulative cases and 3 for respective daily new cases of deaths, recovery or confirmed Covid19 individuals.

b. Data Preprocessing

In data preprocessing section, we have set the columns created above as the dependent variable column (y) and number of days starting from 1st March as the independent variable (X). X column is basically a numpy array of elements 1 to 61. The X and y is then reshaped to be column vector of size 61 (i.e. 61 rows, 1 column)

The dataset is split for Training (60%) and Test (40%) using train_test_split() function imported from class model_selection of sklearn python library.The training and testing variables are saved for further evaluation.

The training and testing variables of both X and y are standardized using StandardScaler() object imported from class preprocessing of sklearn python library. Separate objects have been created for standardization of X and y data. The fit_transform() function is used to fit the object into the data and transform the values of X and y in standard form ranging from -3 to +3. The scaled data is now fit for regression application.

c. Support Vector Regression

Support Vector Regression is a popular choice for prediction and curve fiiting for both linear and non linear regression types. SVR is based on the elements of Support Vector Machine(SVM), where support vectors are basically closer points towards the generated hyperplane in an n-dimensional feature space that distincly seggregates the data ponits about the hyperplane. More discussions on the SVR and SVM can be found on**Invalid source specified.Invalid source specified. Invalid source specified.**. The SVR model performs the fitting as shown in Fig.1. The generelized equation for hyperplane may be respesented as $y = wX + b$, where w is weights and b is the intercept at $X = 0$. The margin of tolerance is represented by epsilon ε. The SVR regression madel is imported from SVM class of sklearn python library.The regressor is fit on the training dataset. The model parameters as chosen here for analysis is shown below.

SVR(C=1.0, cache_size=200, coef0=0.0, degree=3, epsilon=0.1, gamma='auto', kernel='rbf', max_iter=-1, shrinking=True, tol=0.001, verbose=False)

d. Visulization

The regression fitting of the data with predicted values of the test data is plotted using scatter plot function imported from matplotlib python library. The actual points and the predicted points are shown in Fig.2 for all the respective conditions.**Invalid source specified.**

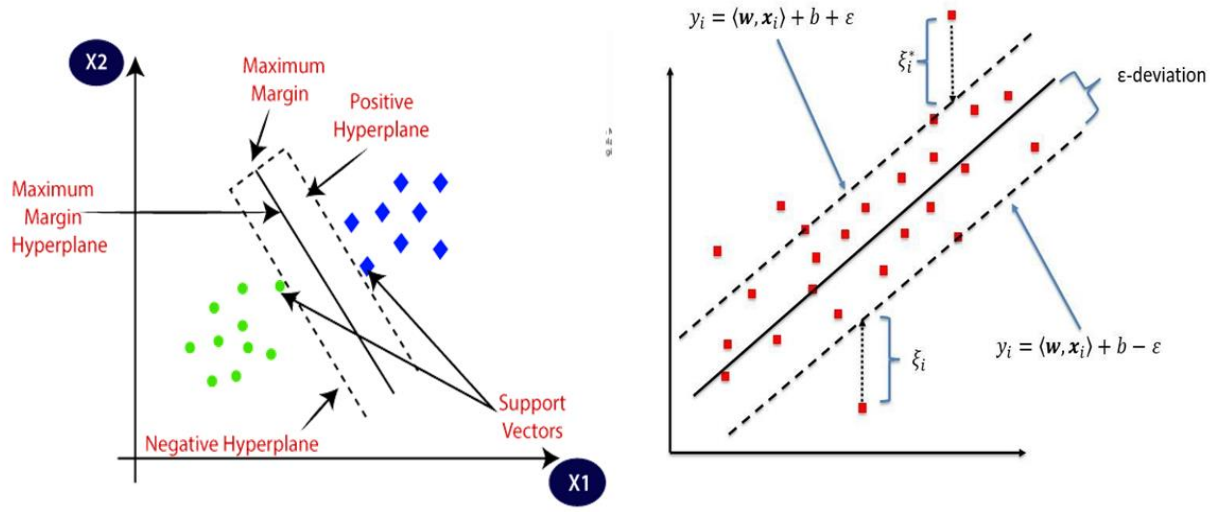

Fig.49. Support Vector Regression model for linear regression fitting where X1= X and X2 = y are the features and label in our case. [Image credit: *https://www.researchgate.net/figure/Schematic-of-the-one-dimensional-support-vector-regression-SVR-model-Only-the-points_fig5_320916953*]

e. Model Performance Evaluation

The model performance parameters are then evaluated to check for the reliability in predicting the outcome. The mean square error (MSE) , root mean sqaure error (RMSE), R^2 score and percentage accuracy are calculated and shown in Table.1.

f. Prediction

The prediction of the future values of the time series invloves few steps of data manipulation to obtain the cumulative trend so as to match the orignial dataset trend of the past. The past dataset is in cumulative form, but since we have implemented RBF kernel in our model, it is quite evident that the predicted time series would be decreasing gaussian trend. The decresing trend can be preserved by a transformation as discussed below. We have implemented few steps in the algorithm that could help us reach our objective.

Here we have obtained the predicted time series for each case seperately for 60 more days that start just after 30th April or 61st day from the starting. Therefore, we wish to merge the 60 days prediction with the past 61 days. The predicted column consits of decreasing values. So, we have computed the difference of the time series and then used absolute values of the difference time series. The difference time series gets inverted and gives us a rising trend, which saturates after certain values. Then we performed cumulative sum of the elements of the time series and added the max value of the the past time series to it. This helps us in preserving the trend and visualizing it in cumulative form. The plots of the past and forecasting values are shown in fig.3 and fig.4.

This transformation is not required for prediction of time series of daily new cases analysis.

All the necessary codes used in evaluation of the above mentioned steps is uploaded in GitHub repository for futher use and improvization. The link is https://github.com/DebanjanParbat/Support-Vector-Regression.

Table.7. The Support Vector Regression model performance parameters with RBF kernel and 10 % fitting confidence interval

Data	MSE	RMSE	Reg. Score	% Accuracy
Total Deaths	0.00849	0.092142	0.986812	99%
Total Recovered	0.030289	0.174036	0.973437	97%
Daily Confirmed	0.109448	0.330830	0.874900	87%
Cumulative Confirmed	0.012856	0.113386	0.988613	99%
Daily Deaths	0.130847	0.361727	0.821829	82%

4.5.3. Results and Discussion

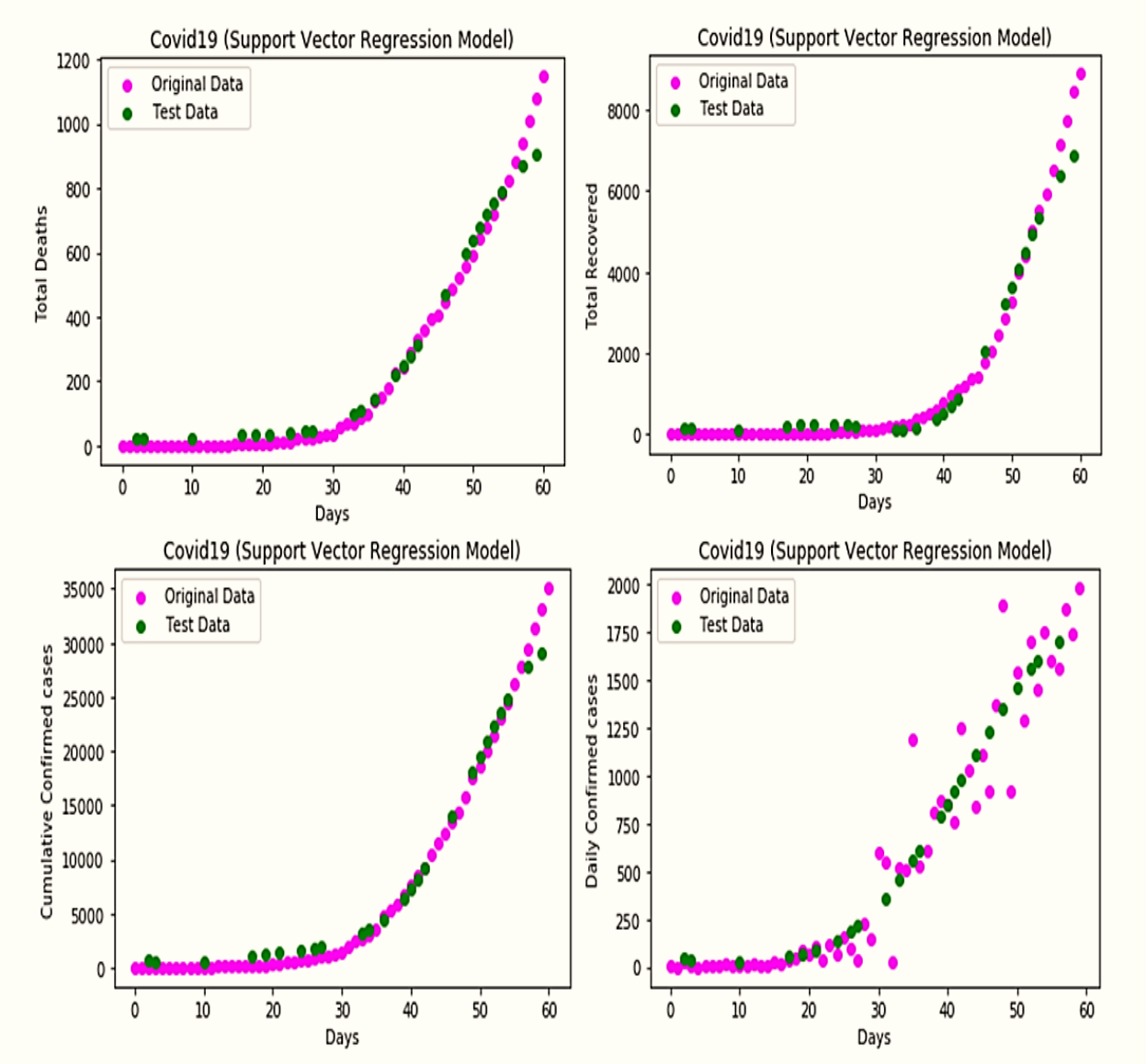

Fig.50. The figures shown here are the plots of regression fit with the data for total deaths, total recovered, cumulative confirmed cases and daily confirmed cases (in clockwise direction)

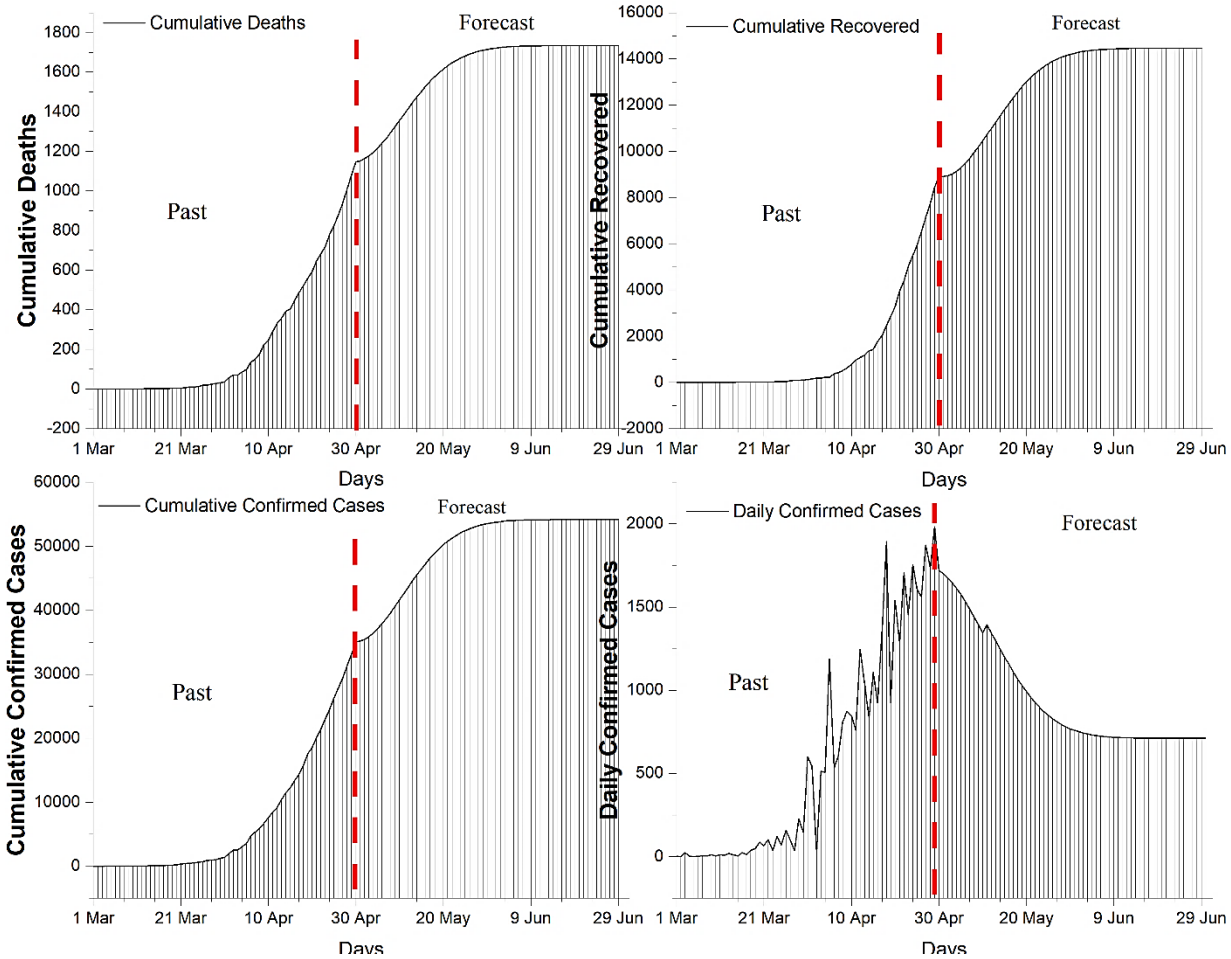

Fig.51. The past and forecast of the total deaths, total recovered, cumulative coinfirmed and daily confirmed cases of Covid19 patients in India. [Past : 1st Mar to 30th April ; Forecast : 1st May to 30th June]

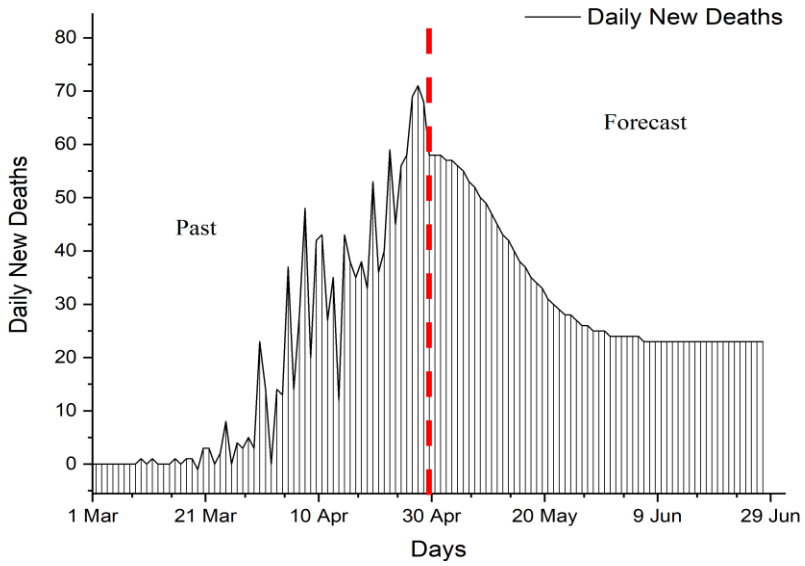

Fig.52. The past and forecast of the daily number of deaths

The results show that the model performed well in fitting the cumulative cases while a poor fiiting is observed in case of daily number of cases. The daily data show that, there are many spikes which reduces the accuracy of predictability of the model. The model predicts that the total numer of infected persons may cross the 55000 mark if the current rate of daily new cases prevail, by the second week of June. The total number of people that can die based on the recent trends predict that it can surpass 1600 mark within second week of June.

Moreover if more spikes are in daily deaths and daily new cases then the total number of infected person may rise and there could be more delay in attaining flatennig of the curve. The spikes induces non-stationarity in the dataset making it difficult for regression models to acccurately predict. But we can say, that if in near future the spikes are controlled with strict physical distancing and containment measures then the flattening of the curve can be achieved by the end of 2nd week of June.

4.5.Conclusion

The proposed methodolgy predicts the total number of COVID19 infected cases, total number of daily new cases, total number of deaths and total number of daily new deaths. The total number of recovered individuals is also predicted. Based on the recent trends, the future trends has been predicted using a robust machine learning model, the support vector regression. The SVR has been

reported to outperform the consistency in predictabilty with respect to other linear , plynomial and logistic regression models. The variabilty in the dataset is addressed by the proposed methodolgy. The model has above 97% accuracy in predicting deaths, recovered, cumulative number of confirmed cases and 87% accuracy in predicting daily new cases. The disease spread is significantly high and if proper containment measures with physical distancing and hygeinity is maintained then we can reduce the spikes in the dataset and hence lower the rate of progression.

References

[1] M. J. Frank and D. Badre, "How cognitive theory guides neuroscience," *Cognition,* vol. 135, pp. 14-20, 2015.

[2] R. D. Dias, M. A. Zenati, R. Stevens, J. M. Gabany and S. J. Yule, "Physiological synchronization and entropy as measures of team cognitive load," *Journal of Biomedical Informatics,* vol. 96, no. 103250, 2019.

[3] M. Mazher, A. A. Aziz and A. S. Malik, "An EEG-Based Cognitive Load Assessment in Multimedia Learning Using Feature Extraction and Partial Directed Coherence," *IEEE Access,* vol. 5, pp. 14819-14829, 2017.

[4] N. Kumar and J. Kumar, "Measurement of Cognitive Load in HCI Systems Using EEG Power Spectrum: An Experimental Study," in *Procedia Computer Science 84* , New Delhi, 2016.

[5] G. V. Tcheslavski, M. Vasefi and F. F. Gonen, "Response of a human visual system to continuous color variation: An EEG-based approach," *Biomedical Signal Processing and Control,* vol. 43, p. 130–137, 2018.

[6] A. P. Clark, A. P. Bontemps, B. D. Batky, E. K. Watts and R. T. Salekin, "Psychopathy and neurodynamic brain functioning: A review of EEG research," *Neuroscience and Biobehavioral Reviews,* vol. 103, p. 352–373, 2019.

[7] C. M. Michel and T. Koenig, "EEG microstates as a tool for studying the temporal dynamics of whole-brain neuronal networks: A review," *NeuroImage,* vol. 180, pp. 577-593, 2018.

[8] J. Cabral, M. L. Kringelbach and G. Deco, "Exploring the network dynamics underlying brain activity during rest," *Prog. Neurobiol,* vol. 114, pp. 102-131, 2014.

[9] B. L. Foster, B. J. He, C. J. Honey, K. Jerbi, A. Maier and Y. B. Saalmann, "Spontaneous neural dynamics and multi-scale network organization," *Front. Syst. Neurosci.,* vol. 10, p. 7, 2016.

[10] S. Perone and V. R. Simmering, "Applications of Dynamic Systems Theory to Cognition and Development: New Frontiers," in *Advanves in Child Development and Behavior,* Elesevier, 2017, pp. 43-80.

[11] K. Yufeng, H. Qi, L. Zhang, S. Chen, X. Jiao, P. Zhou, X. Zhao, BaikunWan and D. Ming, "Towards an effective cross-task mental workload recognition model using electroencephalography based on feature selection and support vector machine regression," *International Journal of Psychophysiology,* vol. 98, no. 2, p. 157–166, 2015.

[12] Y. Chen and T. D. Pham, "Sample entropy and regularity dimension in complexity analysis of cortical surface structure in early Alzheimer's disease and aging," *Journal of Neuroscience Methods,* vol. 215, no. 2, pp. 210-217, 2013.

[13] S. Kesic´ and S. Z. Spasic´, "Application of Higuchi's fractal dimension from basic to clinical neurophysiology: A review," *Computer methods and programs in Biomedicine,* pp. 55-70, 2016.

[14] W. Xingyuan and L. Chao, "Researches on chaos phenomenon of EEG dynamics model," *Applied Mathematics and Computation,* vol. 215, no. 2, pp. 30-41, 2006.

[15] R. Acharya, O. Fausta, N. Kannathala, T. Chuaa and S. Laxminarayan, "Non-linear analysis of EEG signals at various sleep stages," *Computer Methods and Programs in Biomedicine,* vol. 80, no. 1, pp. 37-45, 2005.

[16] G. Yina, G. R.Naik, H. Shuhua, A. Ajith and H. T.Nguyen, "Nonlinear multiscale maximal Lyapunov exponent for accurate myoelectric signal classification," *Applied Soft Computing ,* vol. 36, pp. 633-640, 2015.

[17] R. Chai, S. H. Ling, P. P. San, G. R. Naik, T. N. Nguyen, Y. Tran, A. Craig and H. T. Nguyen, "Improving EEG-based driver fatigue classification using sparse-deep belief networks," *Frontiers in neuroscience,* vol. 7, p. 103, 2017.

[18] A. Al-Ani, I. Koprinska and G. Naik, "Dynamically identifying relevant EEG channels by utilizing channels classification behaviour," *Expert Systems with Applications,* vol. 83, pp. 273-282, 2017.

[19] C. J. Stam, "Nonlinear dynamical analysis of EEG and MEG: Review of an emerging field," *Clinical Neurophysiology,* vol. 116, no. 10, p. 2266–2301, 2005.

[20] W. Klonowski, "Fractal analysis of electroencephalographic time series (EEG signals).," *The fractal geometry of the brain,* p. Springer413–429, 2016.

[21] E. Ruiz-Padial and A. J. Ibáñez-Molina, "Fractal dimension of EEG signals and heart dynamics in discrete emotional states," *Biological Pshycology,* pp. 42-48, 2018.

[22] L. Tang, H. Lv, F. Yang and L. Yu, "Complexity testing techniques for time series data : A comprehensive literaturer eview," *Chaos, Solitons and Fractals,* vol. 81, pp. 117-135, 2015.

[23] P. L. G. S. R. D. M. T. Thomas C Ferree, "Scalp elctrode impedance, infection risk, and EEG data quality," *Clinical Neurophysiology,* vol. 112, no. 3, pp. 536-544, 2001.

[24] S. Bhardwaj, P. Jadhav, B. Adapa, A. Acharyya and G. R. Naik, "Online and automated reliable system design to remove blink and muscle artifact in EEG," in *Conf Proc IEEE Eng. Med Biol Soc*, Milan, 2015.

[25] P. N. Jadhav, D. Shanamugan, A. Chourasia, A. R. Ghole, A. Acharyya and G. Naik, "Automated detection and correction of eye blink and muscular artifacts in EEG signal for analysis of Autism Spectrum Disorder," in *Conf Proc IEEE Eng Med Biol Soc.*, 2014.

[26] A. Subasi and M. I. Gursoy, "EEG signal classification using PCA, ICA, LDA and support vector machines," *Expert Systems with Applications,* vol. 37, no. 12, pp. 8659-66, 2010.

[27] H. Adelia, Z. Zhou and N. Dadmehr, "Analysis of EEG records in an epileptic patient using wavelet tranform," *Journal of Neuroscience Methods,* vol. 123, no. 1, pp. 69-87, 2003.

[28] A. Subasi, "EEG signal classification using wavelet feature extraction and a mixture of expert model," *Expert Systems with Applications,* vol. 32, no. 4, pp. 1084-93, 2007.

[29] M. Misiti, Y. Misiti, G. Oppenheim and J.-M. Poggi, Wavelet Toolbox MATLAB User's Guide, The MathWorks Inc., 1996.

[30] B. P. Marchant, "Time-Frequency analysis for biosystem engineering," *Biosystems Engineering,* vol. 85, no. 3, pp. 261-281, 2003.

[31] S. N. Sarbadhikari and K. Chakrabarty, "Chaos in the brain: a short review alluding to epilepsy, depression, exercise and lateralization," *Medical Engineering & Physics,* vol. 23, no. 7, pp. 445-455, 2001.

[32] M. H. Díaza, F. M.Córdova, L. Cañete, F. Palominos, F. Cifuentes, C. Sánchez and M. Herrera, "Order and Chaos in the Brain: Fractal Time Series Analysis of the EEG Activity During a Cognitive Problem Solving Task," in *Procedia Computer Science*, Rio de Janeiro, Brazil, 2015.

[33] M. Chakraborty and D. Parbat, "Fractals, chaos and entropy analysis to obtain parametric features of surface electromyography signals during dynamic contraction of biceps muscles under varying load," in *2nd International Conference for Convergence in Technology (I2CT)*, Mumbai, 2017.

[34] D. P. Subha, P. K. Joseph, R. Acharya and C. M. Lim, "EEG Signal Analysis: A Survey," *Journal of Medical Systems,* vol. 34, pp. 195-212, 2010.

[35] Y. Ma, W. Shi, C.-K. Peng and A. C.Yang, "Nonlinear dynamical analysis of sleep electroencephalography using fractal and entropy approaches," *Sleep Medicine Reviews,* vol. 37, pp. 1-9, 2017.

[36] T. F. Burns and R. Rajan, "Combining complexity measures of EEG data: multiplying measures reveal previously hidden information," *F1000Research,* vol. 4, p. 137, 2015.

[37] L. Zhenhu, W. Yinghua, S. Xue, L. Duan, V. L. J., S. J. W., H. Satoshi and L. Xiaoli, "EEG entropy measures in anesthesia," *Frontiers in Computational Neuroscience,* vol. 9, pp. 9-16, 2015.

[38] A. Wolf, J. B. Swift, H. L. Swinney and J. A. Vastano, "DETERMINING LYAPUNOV EXPONENTS FROM A TIME SERIES," *Physica D,* vol. 16, no. 3, pp. 285-317, 1985.

[39] J. C. Sprott, Chaoa and Time-Series Analysis, Oxford University Press, 2003.

[40] M. T. Rosenstein, J. J. Collins and C. J. D. Luca, "A practical method for calculating largest Lyapunov exponents," *Physica D Nonlinear Phenomenon,* vol. 65, no. 1-2, pp. 117-134, 1993.

[41] H. Kantz, "A robust method to estimate the maximal Lyapunov exponent of a time series," *Physics Letter A,* vol. 185, no. 1, pp. 77-87, 1994.

[42] A. Stefanski, "Estimation of the largest Lyapunov exponent in systems with impacts," *Chaos Solition Fractals,* vol. 78, p. 2443–2451, 2000.

[43] A. Stefanski and T. Kapitaniak, "Estimation of the dominant Lyapunov exponent of non-smooth systems on the basis of maps synchronization," *Chaos Solition Fractals,* vol. 15, no. 2, p. 233–244, 2003.

[44] J. Awrejcewicz, A. V. Krysko, N. P. Erofeev, V. Dobriyan, M. A. Barulina and V. A. Krysko, "Quantifying Chaos by Various Computational Methods. Part 1: Simple Systems," *Entropy,* vol. 20, no. 3, pp. 1-28, 2018.

[45] F. Takens, "Detecting strange attractors in turbulence," *Lect. Notes in Math,* vol. 898, p. 366, 1981.

[46] L. Cao, "Practical Method for determining minimum embedding dimension from a scalar time series," *Physica D,* vol. 110, no. 1-2, pp. 43-50, 1997.

[47] S. Sato, M. Sano and Y. Sawada, "Practical methods of measuring the generalized dimension and the largest Lyapunov exponent in high dimensional chaotic systems," *Prog.Theor.Phys,* vol. 77, no. 1, pp. 1-5, 1987.

[48] P. Paramanathan and R. Uthayakumar, "Application of fractal theory in analysis of human electrophysiological signals," *Computers in Biology and Medicine,* vol. 38, no. 3, pp. 372-378, 2008.

[49] C. Tricot, Curves and Fractal Dimension, New York: Springer, 1995.

[50] T. Higuchi, "Approach to an irregular time series on the basis of the fractal theory.," *Physica D,* vol. 31, no. 2, p. 277–283, 1988.

[51] M. Čukić, D. Pokrajac, M. Stokić, S. Simić, V. Radivojević and M. Ljubisavljević, "EEG machine learning with Higuchi's fractal dimension and Sample Entropy as features for successful detection of depression," *arXiv:1803.05985,* 2018.

[52] S. M. Pincus, "Approximate entropy as a measure of system complexity," *Proc Natl Acad Sci USA,* vol. 88, no. 2297-3301, pp. 2297-2301, 1991.

[53] A. Delgado-Bonal and A. Marshak, "Approximate Entropy and Sample Entropy: A Comprehensive Tutorial," *Entropy,* vol. 21, no. 6, p. 541, 2019.

[54] U. R. Acharya, S. V. Sree, S. Chattopadhyay, W. Yu and P. C. A. Ang, "Application of recurrence quantification analysis for the automated identification of epileptic EEG signals," *International Journal of Neural Systems,* vol. 21, no. 3, pp. 119-211, 2011.

[55] U. R. Acharyaa, F. Molinari, S. V. Sree, S. Chattopadhyay, K.-H. Ng and J. S. Suri, "Automated diagnosis of epileptic EEG using entropies," *Biomedical Signal Processing and Control,* vol. 7, no. 4, pp. 401-408, 2012.

[56] M. Li, W. Chen and T. Zhang, "Automatic epileptic EEG detection using DT-CWT-based non-linear features," *Biomedical Signal Processing and Control,* vol. 34, pp. 114-125, 2017.

[57] W. Chena, J. Zhuang, W. Yu and Z. Wang, "Measuring Complexity using FuzzyEn, ApEn, and SampEn," *Medical Engineering & Physics,* vol. 31, no. 1, pp. 61-68, 2009.

[58] J. S. Richman and J. R. Moorman, "Physiological time-series analysis using approximate entropy and sample entropy," *American Journal of Physiology,* vol. 278, no. 6, p. H2039–H2049., 2000.

[59] M. M. Rahman and S. A. Fattah, "An efficient feature extraction scheme for classification of mental tasks based on inter-channel correlation in wavelet domain utilizing EEG signal," *Biomedical Signal Processing and Control,* vol. 61, 2020.

[60] Y.-P. Lin, C.-H. Wang, T.-P. Jung, T.-L. Wu, S.-K. Jeng, J.-R. Duann and J.-H. Chen, "EEG-Based Emotion Recognition in Music Listening," *IEEE Transactions on Biomedical Engineering,* vol. 57, no. 7, pp. 1798-1806, 2010.

[61] F. Pedregosa, G. Varoquaux and A. Gramfort, "Scikit-learn: Machine Learning in {P}ython," *Journal of Machine Learning Research,* vol. 12, pp. 2825--2830, 2011.

Chapter 5 Brief Discussion

This chapter provides the key findings and highlights of the research undertaken regarding implementation of nonlinear timeseries analysis techniques for biomedical signals and systems.

To study the complexity changes during cognitive loading of the brain using Largest Lyapunov Exponent (LLE), Higuchi Fractal Dimension (HFD) and Sample Entropy (SampEn) as a multiparametric signature of cognitive processing.

These parameters were able to classify between different cognitive states, such as Emotion, Focus, Memory and Problem Solving with an accuracy of 99%.

The proposed method involves coarse graining a signal at different scales, using the popular multiscale entropy algorithms to detect apnea and normal events from single lead Electrocardiography (ECG), Instantaneous Heart Rate and ECG derived respiration.

A moderately accurate sleep apnea detection model with an accuracy ranging from 70% to 100% based on two different probabilistic thresholds of 50 % and 70% with reduction in false positive rate from 28% to 14 % for applications in development of AI based IoT connected smart wearable devices.

As the load increases, we observe a decrease in Entropy values, suggesting a trend towards greater system regularity and decreased unpredictability in the firing pattern of the MUAP. The alterations in Entropy play a significant role in defining the equilibrium between order and disorder within a system. Therefore, fluctuations in Entropy offer a means to assess the physical intricacy involved in weightlifting.

The proposed methodology introduces an analysis technique based on nonlinear dynamical systems theory to quantify corticomuscular coherence during weight lifting. An in-house experiment was conducted to validate this technique using simultaneously acquired EEG and EMG data from different subjects.

The results demonstrated that these parameters were highly statistically significant in distinguishing corticomuscular coherence at different weights with $p < 0.01$. This suggests that they are reliable descriptors of corticomuscular coherence and could potentially be used to assess

neuromuscular disorders such as cerebral palsy, stroke rehabilitation, paralysis, or other conditions associated with loss of neuromuscular coordination.

The proposed work utilizes support vector regression model to predict the number of total number of deaths, recovered cases, cumulative number of confirmed cases and number of daily cases.

The model has above 97% accuracy in predicting deaths, recovered, cumulative number of confirmed cases and 87% accuracy in predicting daily new cases.

Chapter 6 Conclusion

The author here would like to highlight that the thesis provides a validated methodology for using nonlinear time series analysis techniques for Biomedical Signals and Systems and AI based prediction and classification of interesting physiological phenomenon of human body. The research work delves into the realms of chaos theory to model the physiological changes as reflected in ECG, EEG and EMG signals while doing certain predefined tasks. The chaos theory determinants are obtained along with Fractal Dimension and Entropy. The study also captures the underlying system dynamics through the Multiscale analysis measures like Multiscale Entropy and its variants along with Multifractal Spectrum.

The above determinants were used to make different feature sets, across a wide variety of applications pertaining to Computer Aided Diagnosis, which were used to train various Machine Learning models to classify between normal and abnormal events. The performance of the models was found to very competitive with existing methods which were previously attempted by other researchers worldwide. The novelty lies in the fact that, such a large-scale in-depth analysis of various non linear dynamical parameters under one roof has not been attempted before as to the best of our knowledge. The idea of developing a powerful feature extractor for Biomedical Signals based on the concepts of Chaos, Fractals and Entropy to serve as efficient feature set for training a Machine Learning model to classify based on real life raw ECG, EEG and EMG signals. This may be further extended to study different other Biomedical Signals or different other disease conditions.

The tools and techniques discussed in the thesis may serve as theoretically accurate and computationally efficient set of algorithms which encompasses signal acquisition, signal cleaning, feature extraction, and to develop AI models to validate the significance of the features in accurately differentiating in between the classes. The models like sleep apnea detection, corticomuscular coherence estimation, cognitive stimulus modelling and muscle fatigue and coordination estimation have immense applications in the smart wearable devices having IoT connected AI interface. With the changing landscape of how health care is going to be provided is suggesting more and more studies like this could help the medical technology sector to grow and be a part of the digital health initiatives of various governments worldwide.

Chapter 7 Future Scope of Work

The work can be other extended by optimizing the proposed methodologies and algorithms on the pretext of developing applications which may have profound clinical significance. The study can be validated with a database comprising a large population so as to bring out the significance of this study. Moreover, different Artificial Intelligence and Machine Learning models along with Deep Learning models. The findings may be tested over clinical data, to properly validate the preliminary findings and trends.